EXPLORATORY STUDIES AND CHEMISTRY OF PHOTOGENERATED CARBANIONS AND CARBOCATIONS FROM DIBENZANNELATED SYSTEMS

By

Deepak Shukla
B.Sc.(Honours), Delhi University (India), 1983
M Sc., Indian Institute of Technology, Kanpur (India), 1985

A Dissertation Submitted In Partial Fulfilment
of the Requirements for the Degree
of

DOCTOR OF PHILOSOPHY

in the Department of Chemistry

We accept this dissertation as conforming to the required standard

Dr. P. C. Wan, Supervisor (Department of Chemistry)

Dr. T. M. Fyles, Department Member (Department of Chemistry)

Dr. A. McAuley, Department Member (Department of Chemistry)

Dr. J. N. Owens, Outside Member (Department of Biology)

Dr. A. C. Weedon, External Examiner (University of Western Ontario)

University of Victoria

Name Deepak Shukla

Dissertation Abstracts International is arranged by broad, general subject categories. Please select the one subject which most nearly describes the content of your dissertation. Enter the corresponding four-digit code in the spaces provided.

ORGANIC CHEMISTRY
SUBJECT TERM

0490
SUBJECT CODE

U·M·I

Subject Categories

THE HUMANITIES AND SOCIAL SCIENCES

COMMUNICATIONS AND THE ARTS
Architecture 0729
Art History 0377
Cinema 0900
Dance 0378
Fine Arts 0357
Information Science 0723
Journalism 0391
Library Science 0399
Mass Communications 0708
Music 0413
Speech Communication 0459
Theater 0465

EDUCATION
General 0515
Administration 0514
Adult and Continuing 0516
Agricultural 0517
Art 0273
Bilingual and Multicultural 0282
Business 0688
Community College 0275
Curriculum and Instruction 0727
Early Childhood 0518
Elementary 0524
Finance 0277
Guidance and Counseling 0519
Health 0680
Higher 0745
History of 0520
Home Economics 0278
Industrial 0521
Language and Literature 0279
Mathematics 0280
Music 0522
Philosophy of 0998
Physical 0523

Psychology 0525
Reading 0535
Religious 0527
Sciences 0714
Secondary 0533
Social Sciences 0534
Sociology of 0340
Special 0529
Teacher Training 0530
Technology 0710
Tests and Measurements 0288
Vocational 0747

LANGUAGE, LITERATURE AND LINGUISTICS
Language
- General 0679
- Ancient 0289
- Linguistics 0290
- Modern 0291

Literature
- General 0401
- Classical 0294
- Comparative 0295
- Medieval 0297
- Modern 0298
- African 0316
- American 0591
- Asian 0305
- Canadian (English) 0352
- Canadian (French) 0355
- English 0593
- Germanic 0311
- Latin American 0312
- Middle Eastern 0315
- Romance 0313
- Slavic and East European 0314

PHILOSOPHY, RELIGION AND THEOLOGY
Philosophy 0422
Religion
- General 0318
- Biblical Studies 0321
- Clergy 0319
- History of 0320
- Philosophy of 0322

Theology 0469

SOCIAL SCIENCES
American Studies 0323
Anthropology
- Archaeology 0324
- Cultural 0326
- Physical 0327

Business Administration
- General 0310
- Accounting 0272
- Banking 0770
- Management 0454
- Marketing 0338

Canadian Studies 0385
Economics
- General 0501
- Agricultural 0503
- Commerce-Business 0505
- Finance 0508
- History 0509
- Labor 0510
- Theory 0511

Folklore 0358
Geography 0366
Gerontology 0351
History
- General 0578
- Ancient 0579
- Medieval 0581
- Modern 0582
- Black 0328
- African 0331
- Asia, Australia and Oceania 0332
- Canadian 0334
- European 0335
- Latin American 0336
- Middle Eastern 0333
- United States 0337

History of Science 0585
Law 0398
Political Science
- General 0615
- International Law and Relations 0616
- Public Administration 0617

Recreation 0814
Social Work 0452
Sociology
- General 0626
- Criminology and Penology 0627
- Demography 0938
- Ethnic and Racial Studies 0631
- Individual and Family Studies 0628
- Industrial and Labor Relations 0629
- Public and Social Welfare 0630
- Social Structure and Development 0700
- Theory and Methods 0344

Transportation 0709
Urban and Regional Planning 0999
Women's Studies 0453

THE SCIENCES AND ENGINEERING

BIOLOGICAL SCIENCES
Agriculture
- General 0473
- Agronomy 0285
- Animal Culture and Nutrition 0475
- Animal Pathology 0476
- Food Science and Technology 0359
- Forestry and Wildlife 0478
- Plant Culture 0479
- Plant Pathology 0480
- Plant Physiology 0817
- Range Management 0777
- Wood Technology 0746

Biology
- General 0306
- Anatomy 0287
- Biostatistics 0308
- Botany 0309
- Cell 0379
- Ecology 0329
- Entomology 0353
- Genetics 0369
- Limnology 0793
- Microbiology 0410
- Molecular 0307
- Neuroscience 0317
- Oceanography 0416
- Physiology 0433
- Radiation 0821
- Veterinary Science 0778
- Zoology 0472

Biophysics
- General 0786
- Medical 0760

EARTH SCIENCES
Biogeochemistry 0425
Geochemistry 0996
Geodesy 0370
Geology 0372
Geophysics 0373
Hydrology 0388
Mineralogy 0411
Paleobotany 0345
Paleoecology 0426
Paleontology 0418
Paleozoology 0985
Palynology 0427
Physical Geography 0368
Physical Oceanography 0415

HEALTH AND ENVIRONMENTAL SCIENCES
Environmental Sciences 0768
Health Sciences
- General 0566
- Audiology 0300
- Chemotherapy 0992
- Dentistry 0567
- Education 0350
- Hospital Management 0769
- Human Development 0758
- Immunology 0982
- Medicine and Surgery 0564
- Mental Health 0347
- Nursing 0569
- Nutrition 0570
- Obstetrics and Gynecology 0380
- Occupational Health and Therapy 0354
- Ophthalmology 0381
- Pathology 0571
- Pharmacology 0419
- Pharmacy 0572
- Physical Therapy 0382
- Public Health 0573
- Radiology 0574
- Recreation 0575
- Speech Pathology 0460
- Toxicology 0383

Home Economics 0386

PHYSICAL SCIENCES
Pure Sciences
Chemistry
- General 0485
- Agricultural 0749
- Analytical 0486
- Biochemistry 0487
- Inorganic 0488
- Nuclear 0738
- Organic 0490
- Pharmaceutical 0491
- Physical 0494
- Polymer 0495
- Radiation 0754

Mathematics 0405
Physics
- General 0605
- Acoustics 0986
- Astronomy and Astrophysics 0606
- Atmospheric Science 0608
- Atomic 0748
- Electronics and Electricity 0607
- Elementary Particles and High Energy 0798
- Fluid and Plasma 0759
- Molecular 0609
- Nuclear 0610
- Optics 0752
- Radiation 0756
- Solid State 0611

Statistics 0463

Applied Sciences
Applied Mechanics 0346
Computer Science 0984
Engineering
- General 0537
- Aerospace 0538
- Agricultural 0539
- Automotive 0540
- Biomedical 0541
- Chemical 0542
- Civil 0543
- Electronics and Electrical 0544
- Heat and Thermodynamics 0348
- Hydraulic 0545
- Industrial 0546
- Marine 0547
- Materials Science 0794
- Mechanical 0548
- Metallurgy 0743
- Mining 0551
- Nuclear 0552
- Packaging 0549
- Petroleum 0765
- Sanitary and Municipal 0554
- System Science 0790

Geotechnology 0428
Operations Research 0796
Plastics Technology 0795
Textile Technology 0994

PSYCHOLOGY
General 0621
Behavioral 0384
Clinical 0622
Developmental 0620
Experimental 0623
Industrial 0624
Personality 0625
Physiological 0989
Psychobiology 0349
Psychometrics 0632
Social 0451

Supervisor: Dr. P. C. Wan

Abstract

Photochemical reactivity of several dibenzannelated systems has been investigated to demonstrate that the driving force inherent in many of their reactions is the attainment of a 4n π-electron system or intermediate in S_1. It has been shown that the inherent driving force for the benzylic C-H bond ionization in 9*H*-xanthene (**125**) and 9*H*-thioxanthene (**136**) is the formation of 8π-electron cyclically conjugated carbanion intermediates **130** and **137**, respectively, in S_1. Formation of deuterium incorporated products when **125** and **136** are photolyzed in NaOD-EtOD solutions and protium incorporation in products when photolysis of **123** and **134** is carried out in NaOH-EtOH is consistent with the intermediacy of carbanions in these reactions. Fluorescence quenching of **123** and **125** by ethanolamine in CH_3CN gave linear Stern-Volmer plots, with $k_q = (2.16 \pm 0.05) \times 10^7\ M^{-1}\ s^{-1}$ for **125** and $(1.12 \pm 0.05) \times 10^7\ M^{-1}\ s^{-1}$ for **123**, which corresponds to an isotope effect for quenching by ethanolamine, of $k_H/k_D = 1.92 \pm 0.04$. Enhanced stability of 8π carbanions in S_1 is further evidenced in the photodecarboxylation of xanthene-9-carboxylic acids (**142** and **145**) and thioxanthene-9-carboxylic acids (**147** and **148**) in aqueous solution. The intermediacy of carbanions has been demonstrated in the product studies carried out in 80% D_2O-CH_3CN solution. A mechanism has been proposed which involves heterolytic bond cleavage of the carboxylate ion in S_1 to give intermediate carbanions. Additional support for the excited state stability of 4n systems comes from the studies of **155**.

Photoexcitation of bent **155** results in its planarization to give planar **155** in S_1. The driving force for this change of conformation of **155** is believed to be the attainment of a conjugated 8π-electron internal cyclic array in S_1.

Photolysis of substituted suberenes in aqueous CH_3CN results in benzylic C-H bond cleavage in these systems in S_1 the efficiency of which is greatly affected by the nature of substituent present. Results obtained in this study are consistent with benzylic C-H bond cleavage, with H_2O acting as the base, to give intermediate carbanions in S_1. Quantum yields of exchange in L_2O-CH_3CN (L = H or D) and in a variety of other solvent mixtures have been measured.

The photochemistry of xanthenium (**99** and **114**) and thioxanthenium (**219**) cations has been studied in aqueous H_2SO_4 in the presence of di- and trimethoxybenzenes. It has been shown that the primary photochemical step is electron transfer from methoxybenzenes to singlet excited **99** and **114**. The radical intermediates thus generated subsequently react with O_2 to give peroxy compounds as final products.

These and other results of the photochemistry of dibenzannelated systems show that there is much interesting photochemistry to be discovered in these molecules.

Dr. P. C. Wan, Supervisor (Department of Chemistry)

Dr. T. M. Fyles, Department Member (Department of Chemistry)

Dr. A. McAuley, Department Member (Department of Chemistry)

Dr. J. N. Owens, Outside Member (Department of Biology)

Dr. A. C. Weedon, External Examiner (University of Western Ontario)

TABLE OF CONTENT

LIST OF TABLES

LIST OF FIGURES

Acknowledgements

I would like to express my greatest indebtedness to my supervisor Dr. Peter Wan for his thoughtful guidance and contributions to this work. He instilled in me the spirit of scientific inquiry, and has been a constant source of inspiration throughout the course of this work. I would also like to thank my colleagues, Dr. Erik Krogh, Dave Budac, Dr. Cai-Gu Huang, Xigen Xu, Wu Pin, Almira Blazek, Cheng Yang, Bing Guan, Geoff Zhang and Yijian Shi (Stone), who made my stay in Victoria such an unforgettable experience. I would also like to record my sense of appreciation for everyone in the Department of Chemistry for their friendship and generosity. My special thanks goes to Rita, my fiancée, for her encouragement, help, patience, and understanding.

Finally, it remains for me to thank the University of Victoria for giving me this opportunity and for financial assistance in the form of a University of Victoria Graduate Fellowship.

Dedicated To My Parents

CHAPTER ONE

INTRODUCTION

1.1 Prologue

Photochemical reactions are fundamentally different from ground state reactions since they involve the participation of an electronically excited state. As a consequence, photochemical reactions can occur via entirely different pathways from those encountered for ground state reactions. Consequently, the products formed in photochemical reactions often differ from ground state reactions, and can not usually be achieved even if ground state reactions were carried out at a temperature "equivalent" to the energy of the electronically excited state. The reason for this lies in the fact that the electronic configuration of an electronically excited molecule may never be achieved thermally, because in the latter case a variety of other reactions paths requiring much less energy are available, and these paths are utilized before the molecule can reach the desired state.[1]

The ground state electronic configuration of organic molecules consists of electrons in bonding molecular orbitals (MOs) with the antibonding MOs unoccupied. The absorption of light causes excitation of an electron from the highest occupied MO (HOMO) to the lowest unoccupied MO (LUMO), thereby creating an electronically excited state. Therefore, excited states of molecules possess excess energy which could be dissipated via a number of processes (radiative and non-radiative). Unimolecular processes such as bond

fragmentation and molecular isomerization are common. In the presence of an appropriate second molecule, bimolecular photochemical reactions, such as electron transfer to or from the excited species, can also occur. As this report mainly deals with excited state bond cleavage reactions, it is appropriate here to briefly dwell on the mechanistic possibilities for these processes.

The three most commonly cited bond fragmentation processes in the literature are (i) homolysis, where the bonding electron pair is equally apportioned between the two departing fragments; (ii) heterolysis, where the bonding electron pair remains with one fragment; and (iii) mesolytic cleavage, which involves the fragmentation of radical ions, formed as a result of electron transfer or charge transfer. The particular pathway followed by a given molecule is governed by a number of factors including the nature of the leaving group, the solvent, and the nature of the excited state (singlet versus triplet) from which the reaction is taking place.

Heterolytic bond cleavage reactions, in general, are not commonly encountered processes in organic photochemistry. This is mainly due to the fact that much of the earlier work in organic photochemistry was carried out in non-polar solvents where bond homolysis is energetically more favourable than bond heterolysis. Indeed it has been estimated[2] that in the absence of stabilizing solvent effects, heterolysis of a carbon-chlorine bond requires ≈170 kcal mol^{-1}, whereas the homolytic bond dissociation energy is about 80 kcal mol^{-1}. As a result much of the earlier work in the organic photochemical literature involved

intermediates derived from bond homolysis (radical and radical pairs) and electron transfer (radical ions). On the other hand, the situation changes when solvent effects are taken into consideration. In polar solvents, where ions and ion pairs can be solvated, heterolytic cleavage may become energetically favourable and photoactivation could lead to bond heterolysis rather than homolysis.

1.2 Photogeneration of Carbanions

1.2.1 *o*-Nitrobenzyl Carbanions

Nitrobenzyl carbanions were the first and at present the only kind of carbanion intermediates to be generated and spectroscopically observed in photochemical reactions. The mechanism of the overall C-H bond heterolysis, in the case of nitrotoluenes containing a nitro group *ortho* to the methyl group, is now well understood.[3-14] For example, photoexcitation of *o*-nitrotoluene (**1**) results in hydrogen transfer from the benzylic methyl group of **1** to the nitro group, to generate aciquinoid isomer **2** (Scheme **1.1**). The hydrogen transfer process is found to be reversible in the case of **1**, and the overall process does not result in any net chemical change. However, in aqueous solutions of pH > 3, deprotonation of the aciquinoid hydroxyl group (pK_a = 1-4)[9] competes effectively giving rise to *o*-nitrobenzyl carbanion (**3**), which in general are long-lived (> 100 μs) and have strong absorption in the visible region.[3-14] Irradiation of **1** in D_2O results in deuterium incorporation[9,15] at the benzylic carbon, consistent with the intermediacy of a carbanion.

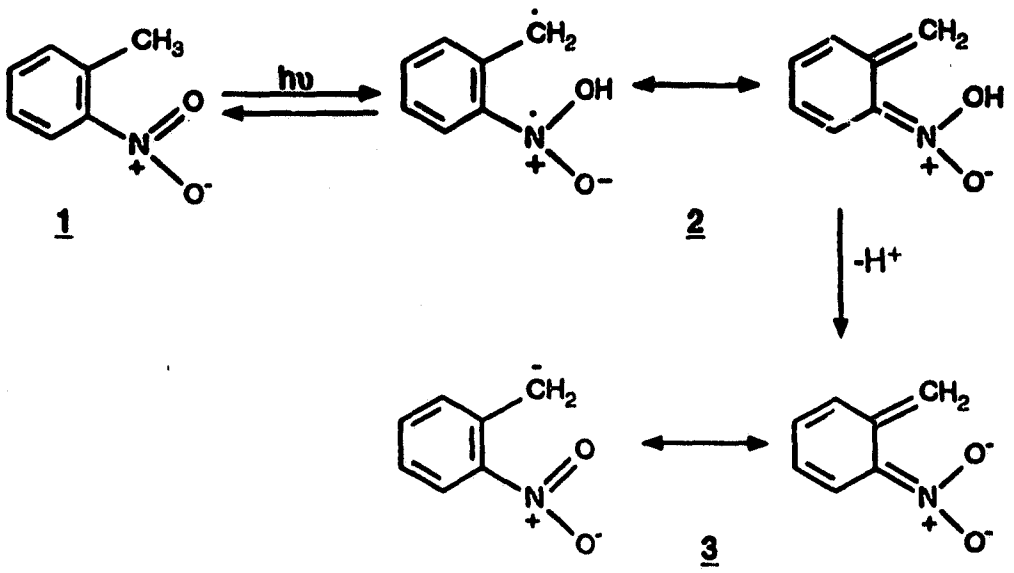

Scheme 1.1

Most of the studies in photogeneration of nitrobenzyl carbanions have concentrated on 2,4- and 2,6-dinitrotoluenes, which on irradiation generate long-lived carbanions in aqueous solutions. Atherton and Craig[11] have carried out detailed mechanistic studies of these systems using nano and picosecond laser flash photolysis (LFP) methods. Thus photoexcitation of 2,6-dinitrotoluene (4) in aqueous solutions results in the formation of the aciquinoid isomer 5 (λ_{max} = 400-420 nm) formed via initial intramolecular hydrogen transfer. The latter then undergoes deprotonation ($k_{(MeOH/OH^-)}$ = 5 x 10^4 s^{-1}) to give 2,6-dinitrobenzyl carbanion (6) (λ_{max} = 490-550 nm). This result was supported by McClelland and Steenken,[13] who by conductivity measurements have shown that photoexcited 4 undergoes rapid hydrogen transfer to form 5 as a nonconductive transient. The excited state responsible for the reaction has been shown to be the lowest n,π*

triplet state, which undergoes intramolecular hydrogen atom transfer with a very fast rate ($k = 0.5 \times 10^9\ s^{-1}$).

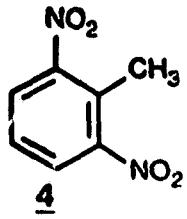

4

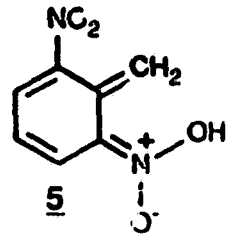

5

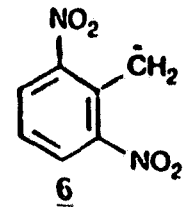

6

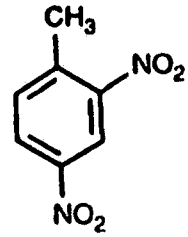

7

In the case of 2,4-dinitrotoluene (7), McClelland and Steenken[13] have shown that the assignment of the absorption due to 2,4-dinitrobenzyl carbanion is not straightforward due to large solvent-induced spectral shifts. In water, the carbanion exists in the hydrogen bonded form and exhibits λ_{max} at 350 and 500 nm whereas in CH_3CN, where the nature of solvated species is unspecified, it has λ_{max} at 400 and 600 nm. Similar spectral shifts have been reported for *p*-nitrobenzyl carbanion.[16]

1.2.2 Photodecarboxylation

Since the early report by Farkas and Wansbrough-Jones[17] in 1932 of the

photodecomposition of acetic acid in aqueous solution to yield methane and CO_2, photodecarboxylation (PDC) has been shown to occur for a variety of other carboxylic acids. The mechanisms of PDC have been extensively investigated and three primary mechanistic modes have been proposed based on the nature of the C-C bond cleavage step, viz., homolytic, mesolytic and heterolytic cleavages (*vide supra*). These mechanistic possibilities have been summarized in a recent review[18] and will not be dealt with in this report. However, PDC occuring via the heterolytic mode and where there is conclusive evidence for the involvement of carbanion intermediates is relevant to the present discussion and will be discussed in some detail below.

Arylacetic acids are the most commonly studied acids in PDC reactions[19-25] for the simple reason that the carbanion intermediates generated in these systems can be stabilized by the aryl group. The simplest arylacetic acid, viz., phenylacetic acid (**8**), has been studied by a number of groups. Thus photolysis of **8** in methanol results in the formation of bibenzyl and an unidentified polyacid (eq 1.1).[26] The process was shown to occur via a homolytic pathway but the

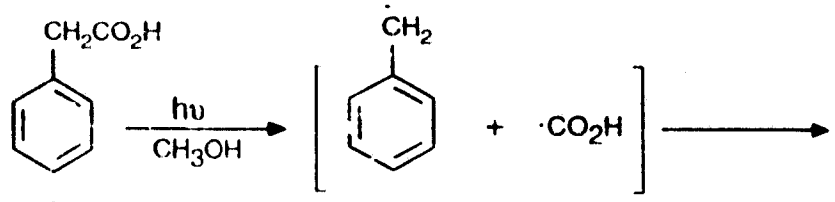

8 (1.1)

detailed quantitative studies were encumbered by low quantum efficiency (Φ < 0.03) of the process. However, other studies[21] have indicated that at least some portion of the PDC of 8 occurs via the heterolytic pathway (i.e., benzyl carbanion intermediate), by measuring the amount of deuterium incorporation in products obtained from photolysis in solvents such as MeOD and $(Me_2CH)_2O$-MeOD. Some deuterium incorporation was observed but it was noted that the major amount of PDC in 8 was via homolytic C-C bond cleavage. Substitution of a hydroxyl group or an equivalent electronegative substituent at the α-position to the carboxyl group of phenylacetic acid increases the propensity of these acids to photodecarboxylate via arylmethyl carbanion intermediates.[27] Wan and Xu[27] have shown that photolysis of mandelic acid (9) and α-hydroxy-2-naphthylacetic acid (10) in aqueous solutions results in PDC, to yield benzyl alcohol (11) and

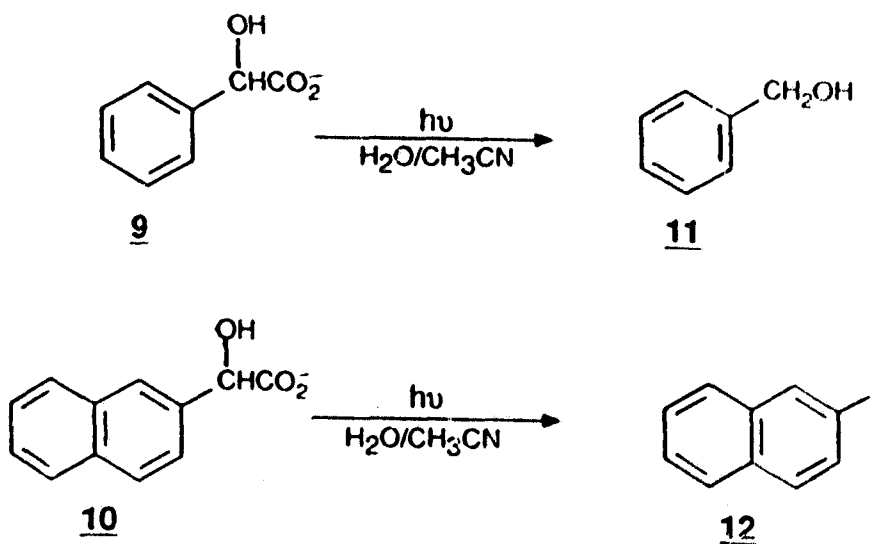

(1.2)

2-naphthylmethanol (**12**) (eq 1.2), respectively, with high quantum yields ($\Phi \approx 0.4$). On the other hand, the parent naphthylacetic acid (**13**) (with no substituent at the α-position), photodecarboxylates via a homolytic mechanism with a much lower quantum yield ($\Phi < 0.02$). The intermediacy of carbanions in the PDC of **9** and **10** was shown by the deuterium incorporation in products (viz., **11** and **12**) obtained from photolyses in D_2O. Further evidence for the involvement of a carbanion intermediate in these PDCs was in the low reactivity of α-hydroxy-3-methoxyphenylacetic acid (**14**) ($\Phi < 0.01$). Such low reactivity of **14** indicates

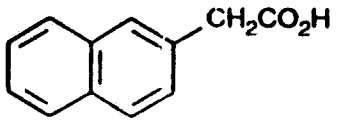

13

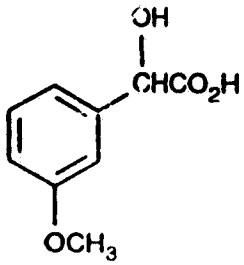

14

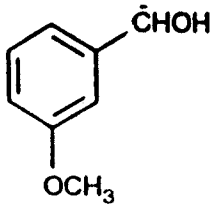

15

that the electron donating (in the excited state) *meta*-methoxy group destabilizes the intermediate α-hydroxyarylmethyl carbanion **15** formed after the loss of CO_2. It was also shown that the PDC does not take place at $pH < pK_a$, indicating that only the carboxylate ion was the reactive species. This was also confirmed by the lack of reactivity in the ester **16**.

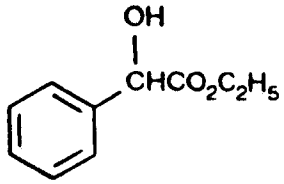

16

The *m*- and *p*-nitrophenylacetic acids (**17** and **18**) are, perhaps, the best characterized PDC reactions via carbanion intermediates.[16,19,22] Photolysis of **18** in aqueous solutions results in the formation of *p*-nitrotoluene (**20**) and *p,p'*-dinitrobibenzyl (**21**) (eq 1.3). Electron ejection from the carbanion **19** gives benzyl radical, which subsequently dimerizes to give **21**. Three LFP studies[16,19,22] of these

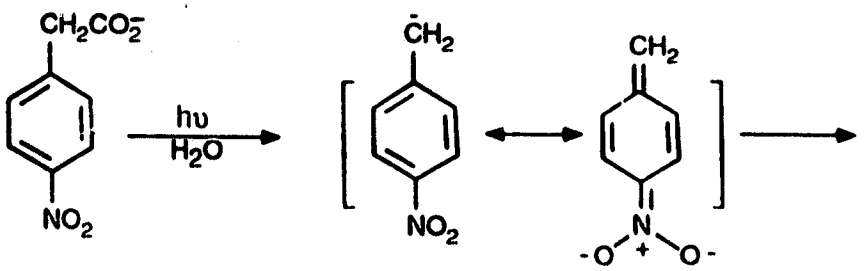

18 **19** (1.3)

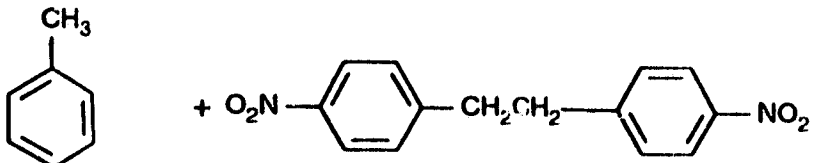

20 **21**

systems have been reported which give considerable insights into the mechanism of PDC. Employing conventional lamp flash photolysis, Margerum and Petrusis[19] reported, for the first time, the observation of a long-lived transient (τ = 53 s) at 358 nm which was assigned to the *p*-nitrobenzyl carbanion (**19**) derived from *p*-nitrophenyl acetate (**18**) in aqueous solution, with a high quantum yield of decarboxylation (Φ = 0.6). The *m*- isomer **17** also underwent an efficient decarboxylation but no transient assignable to the corresponding carbanion was observed, indicating that the corresponding *m*-nitrobenzyl carbanion was very

short-lived. More recent pico- and nanosecond LFP studies of **18** in aqueous

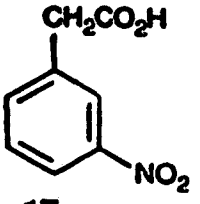

17

solution by Craig and coworkers[16,22] have provided a detailed mechanistic picture of PDC. It has been shown that PDC occurrs from the lowest triplet state, which in a primary adiabatic step generates **19** in its triplet state (λ_{max} ~ 290 nm; τ = 90 ns at pH > 5.0) (Scheme 1.2). The kinetics of the decay of triplet **19** has also been

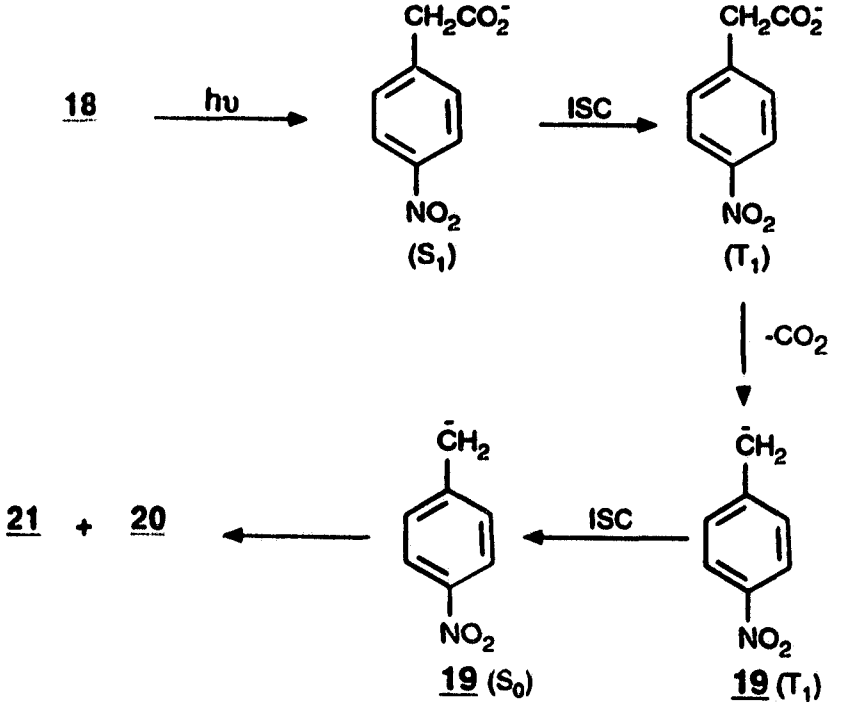

Scheme 1.2

studied in detail.[16] Wan and Muralidharan[33] have also proposed the involvement of nitrobenzyl carbanion intermediates from the triplet excited state in the photo-retro-Aldol type reactions of several nitrobenzyl derivatives and also in the PDC of 17 and 18 (*vide infra*).

Arylacetic acids such as 2-, 3- and 4-pyridylacetic acids (22) have been reported to undergo PDC via heterolytic cleavage. Stermitz and Huang[20,28] have shown that irradiation of these acids in aqueous solution results in efficient PDC (Φ = 0.20-0.50) to yield corresponding methylpyridines (eq 1.4). The reactions of these acids are most efficient at pH = pI (isoelectric point), indicating that the

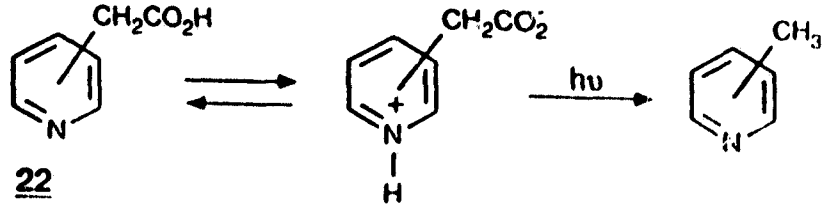

22 23 (1.4)

24

zwitterion 23 is the reactive species in the PDC. A discrete carbanion intermediate may not be involved in these reactions and a quinoid species (at least for the 2- and 4-isomers) of the type 24 might be involved in the reaction mechanism.

The PDC of benzoylformic acid (25) in aqueous solution (pH < 2.0) proceeds with high quantum efficiency to yield benzaldehyde (27).[29,30] The reaction is of interest because of its high quantum efficiency and lack of any side products. It has been suggested to be of possible use as an actinometer for 250-400 nm region.[29] Kuhn and Gorner[30], using LFP, have proposed that the excited triplet state of carboxylate 25 was the reactive state, which upon loss of CO_2 (in H_2O) gives the transient acyl anion 26, which subsequently undergoes protonation

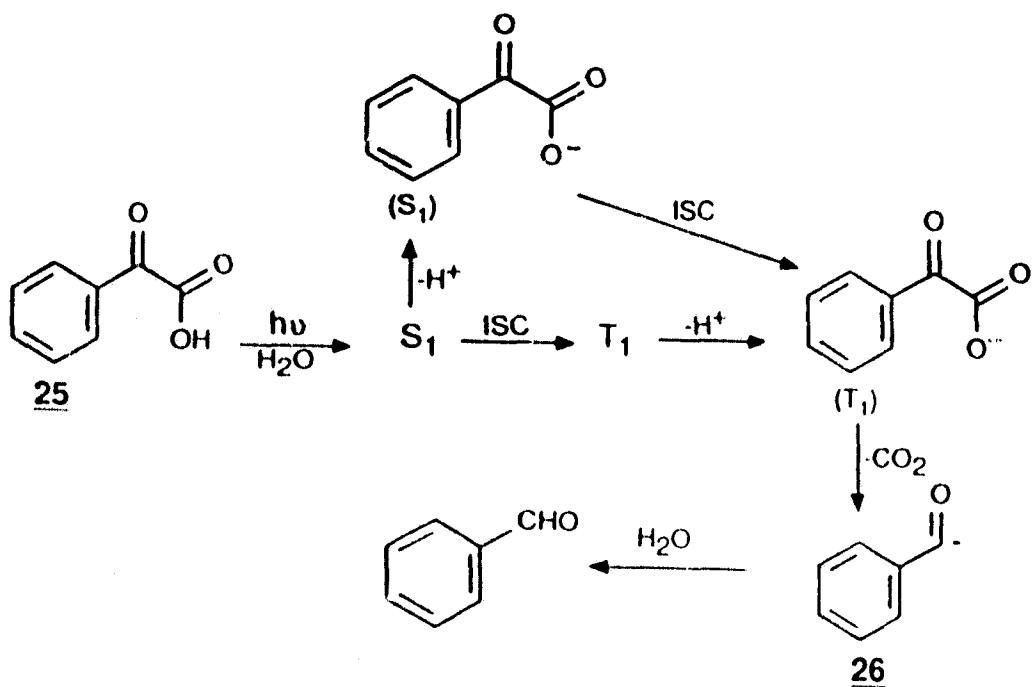

Scheme 1.3

to give benzaldehyde (27) (Scheme 1.3). However, there does not seem to be any apparent driving force for the triplet excited state (T_1) of carboxylate 25 to

decarboxylate, to produce a highly unfavourable species, viz., the acyl anion **26**. It is possible that the reaction mechanism in this case is analogous to the mechanism of PDC suggested for mandelic acid (**9**) (*vide supra*). Since slightly acidic solution is required for reaction of **25**, it is possible that the hydrated form of **25**, i.e., **27** is the actual reactive species. It must be noted that **27** is structurally

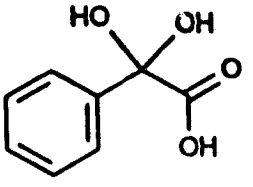

27

similar to mandelic acid (**9**), which has been shown to undergo facile PDC via a carbanion intermediate.

Wan and coworkers[31,32a,b] have demonstrated that the presence of a nitro substituent is not imperative to observe efficient PDC in diarylacetic acids. These authors have studied PDC in aqueous solutions of a series of compounds related to diphenylacetic acid (e.g., **28-31**), differing only in the structure of the central

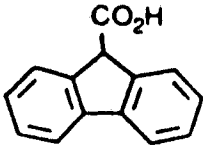

28

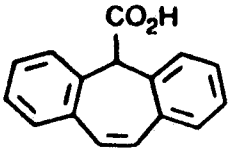

29

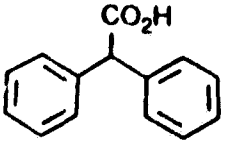

30

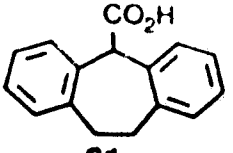

31

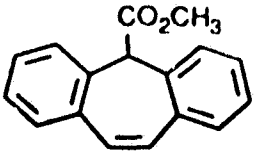

32

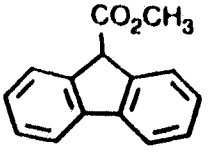

33

ring. Thus photolysis of 28 and 29 in deaerated 60% H_2O-CH_3CN at various pHs produced the corresponding hydrocarbons 36 and 37, respectively (eqs 1.5 and 1.6). Photolysis of esters 31 and 32 did not result in any reaction. It was also

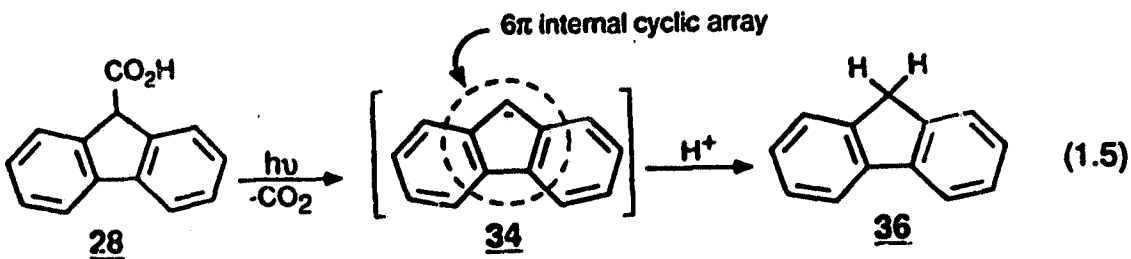

28 34 36 (1.5)

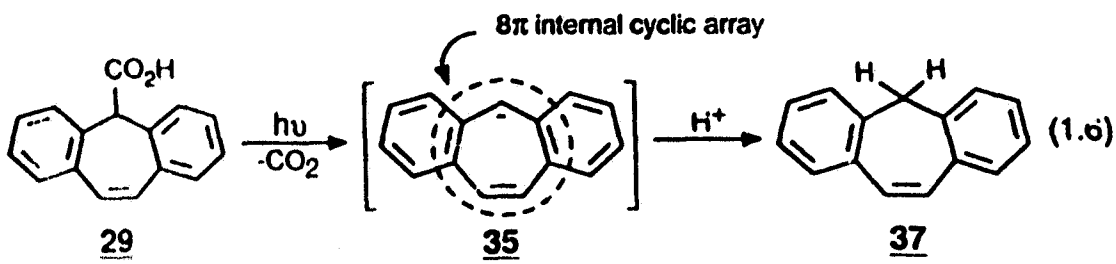

29 35 37 (1.6)

shown that PDC decreased at pH < pK_a of the acid, indicating that only carboxylate ion was the reactive species. Comparison of the ground state reactivity of these acids revealed that fluorene-9-carboxylic acid (28) was most easily decarboxylated via an aromatic 6π-electron 9-fluorenyl carbanion (34) intermediate, whereas suberene-5-carboxylic acid (29) was reluctant to decarboxylate even on prolonged reflux. This is not surprising since the ionic decarboxylation of 29 proceeds through an incipient 8π-electron (antiaromatic) carbanion intermediate 35, which would require a very high activation energy.

On the other hand, of all the systems investigated, **29** was the most reactive photochemically (Φ = 0.60; k(decarboxylation) = 6 x 10^9 s^{-1}), whereas **28** was the least reactive (Φ = 0.042; k(decarboxylation) = 8.8 x 10^6 s^{-1}). The intermediacy of carbanions in these PDCs was supported by the following facts: (i) the carboxylate ion is the more reactive than the acid form; (ii) deuterium incorporation in products when photolyses were carried out in D_2O; and (iii) lack of any radical-derived coupling products. It was further noted that the relative reactivity of **28** vs **29** was explicable in terms of the electron count in the central ring, called the internal cyclic array (ICA), of the carbanion intermediates derived from these systems (*vide infra*).

1.2.3 Photoretro-Aldol Reactions

Carbanions have been proposed as intermediates in several photoretro-Aldol reactions.[33-39] The retro-Aldol reaction is mechanistically akin to decarboxylation and, in general, exhibits base catalysis. Several appropriately substituted nitroaromatic compounds have been shown to undergo this type of reaction. Wan and Muralidharan[33] have shown that the photolysis of **38** in

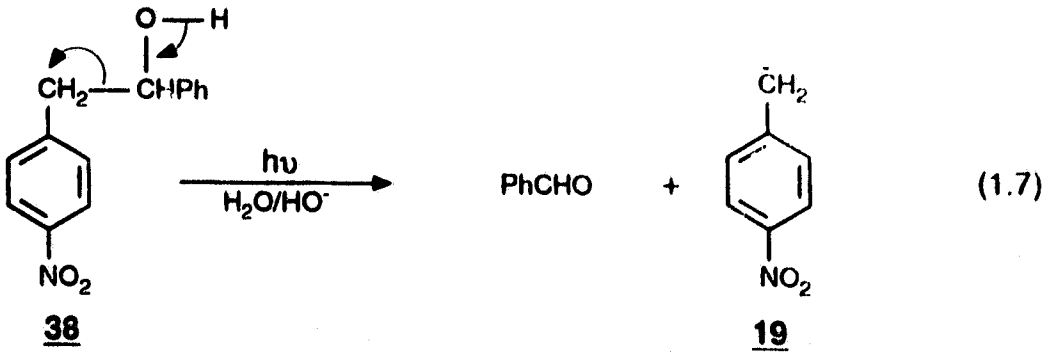

38 **19** (1.7)

aqueous solution results in the formation of *p*-nitrobenzyl carbanion **19** (eq 1.7). The proposed mechanism is similar to the PDC of *m*- and *p*-nitrophenylacetates (**17** and **18**) as discussed above and involves the excited triplet state mediated heterolytic cleavage of the benzylic bond as the primary photochemical step to produce the *p*-nitrobenzyl carbanion **19** (eq 1.7). Steenken and McClelland,[34] using LFP, have shown that the analogous reaction reported for the acetal **39** gave

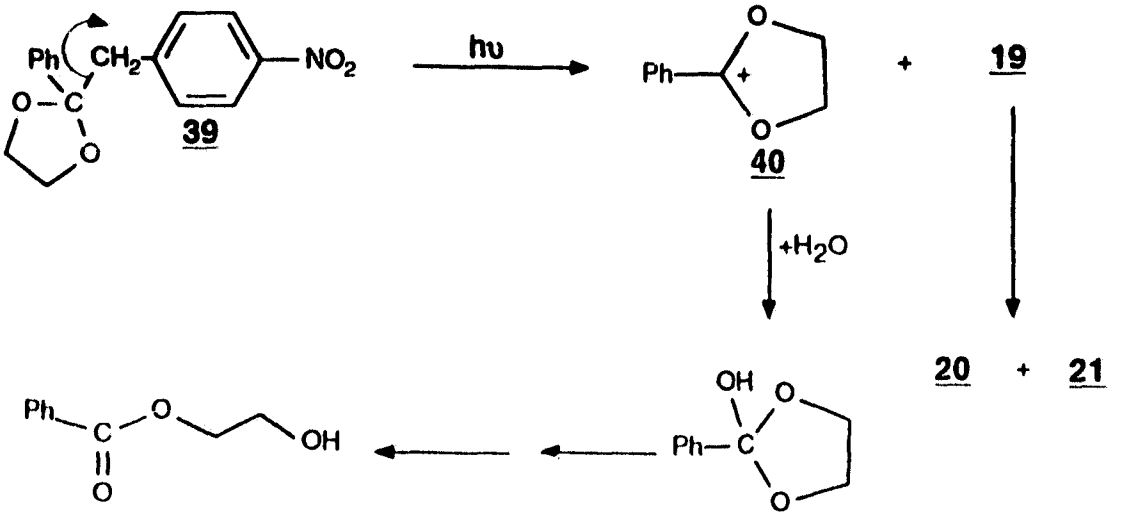

Scheme 1.4

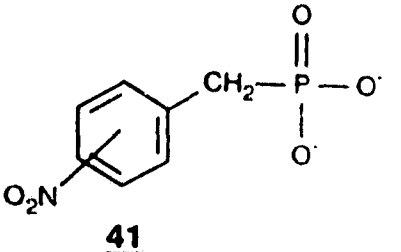

41

both *p*-nitrobenzyl carbanion (19; λ_{max} 355 nm) and the 2-phenyl-1,3-dioxolan-2-ylium ion (40) (λ_{max} 260 nm) (Scheme 1.4).[34] Related photoretro-Aldol reaction have also been observed for *m*- and *p*-nitrobenzylphosphonates 41.[35-37]

Wayner and Gravelle[38] have reported a photoretro-Aldol reaction for amine 42 in MeOH proceeding via the diphenylmethanyl carbanion 43 as the intermediate (eq 1.8). However, in cyclohexane the radical fragmentation pathway was found to be dominant. The triphenylmethyl carbanion has been photogenerated via a photoretro-Aldol reaction of 1,1,1-tripheny' phosphonate (44), which eliminates the metaphosphate ion on irradiation in basic solution.[39]

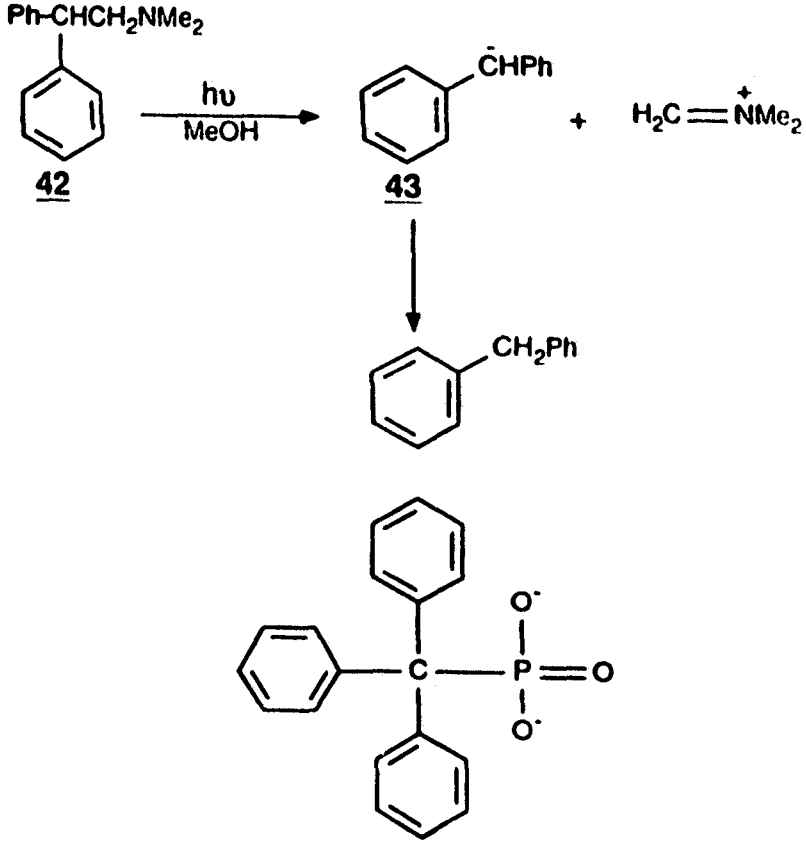

42 43 44 (1.8)

1.2.4 Excited State Carbon Acids

In the ground state carbanions are generated most commonly via deprotonation of the corresponding carbon acid precursor, by the action of a base of appropriate strength. A similar reaction for electronically excited states has not been very successful until very recently. Attempts have been made at deprotonating diarylmethanes such as fluorene (**36**) without any success.[6,40] Förster cycle calculations show that **36** and related compounds are much more acidic in S_1 ($pK(S_1)$ -8 to -12)[40] than in the ground state. However, photoexcitation of **36** and related hydrocarbons with a benzyl moiety in D_2O failed to result in

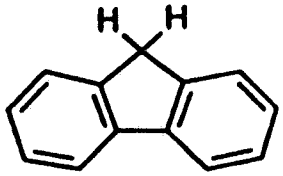

36

proton exchange, though a claim[41] has been made recently that **36** and two other derivatives undergo benzylic proton dissociation in S_1 in very basic medium. However, conclusive evidence such as deuterium exchange was not reported. It has been shown that the azulinium cation **45** is much more acidic in S_1 than in the ground state.[42] Thus flash photolysis of **45** (in strong acid) resulted in deprotonation of the excited state and transient formation of azulene (**46**) could be detected (eq 1.9). However, although this reaction is formally C-H deprotonation, it does not lead to or involve a carbanion intermediate.

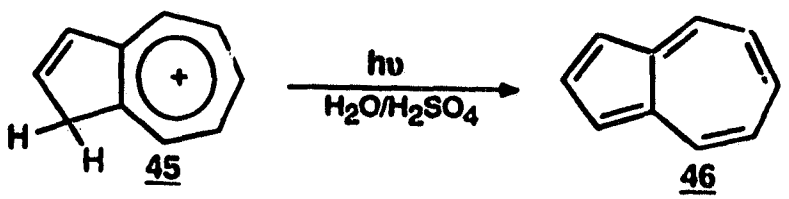

(1.9)

In the ground state, C-H deprotonations are typically very slow because of lack of hydrogen bonding to solvent and the substantial geometrical and solvation changes generally required on deprotonation of carbon acids.[43,44] If this also holds true for the excited state, such slow deprotonation rates would not be able to compete with the fast rates of decay generally available for S_1.

The cyclooctatetraene dianion (47) has been reported[45,46] to undergo facile protonation in the excited state in a medium where it could not be protonated in the ground state (eq 1.10). This result suggests that 47 is much more basic in the

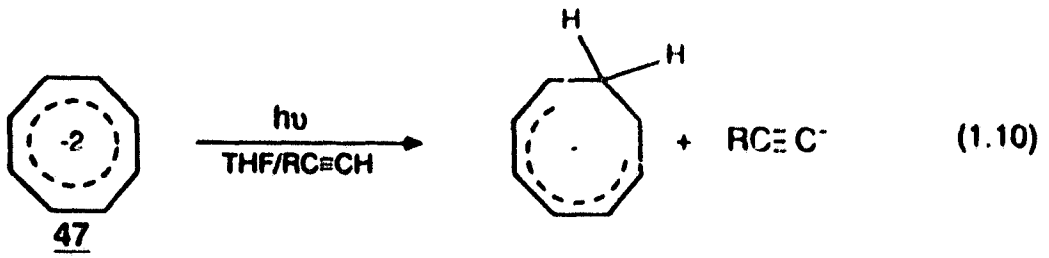

(1.10)

S_1 than in the ground state. It could also be interpreted as evidence that ground state carbanion systems containing 4n + 2 π-electrons (e.g., 47) are less favoured

in the excited state. The reverse reaction, i.e., photochemical deprotonation of a carbon acid to form the conjugate carbanion, has been shown to be unfavourable for systems such as fluorene (36) (*vide supra*). These results suggest that systems that generate 4n + 2 π-electron carbanions are less favoured on the excited state surface. Perhaps a hydrocarbon system which could generate a carbanion containing 4n π-electrons upon deprotonation would better be able to exhibit carbon acid behavior in the excited state. This is indeed the necessary requirement as was shown by the following studies.

The first example of an excited state carbon acid was reported by Wan and coworkers[47,48], who showed that suberene (37) is much more acidic in the S_1 state compared to the ground state ($pK(S_1) \sim -1$; $pK(S_0) \sim 31$-38). Thus, photolysis of suberene (37) in D_2O-CH_3CN resulted in exchange of the benzylic protons with deuteron ($\Phi = 0.030$) to give **37-*d*** (eq 1.11). Photolysis of 5,5-dideuterosuberene (**37-d_2**) in H_2O-CH_3CN resulted in exchange of the deuteron at the benzylic

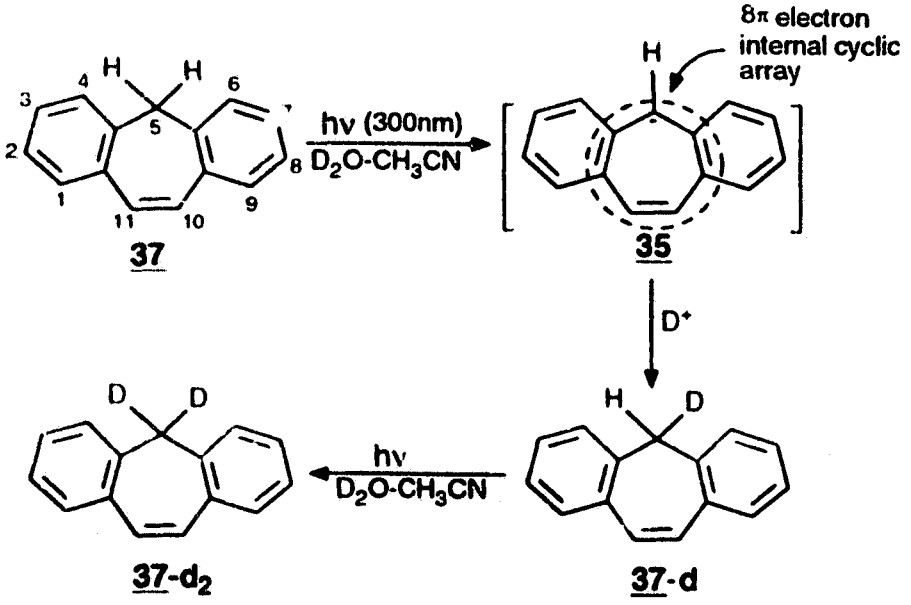

(1.11)

position (C-5) with the proton from the solvent (Φ = 0.035), also giving **37-*d***. The proposed mechanism of the reaction involves initial C-H bond heterolytic cleavage, with water acting as the general base, to generate the suberenyl carbanion (**35**), which undergoes reprotonation exclusively at the 5-position (eq 1.11). The mechanism is further supported by the fact that the fluorescence emission of **37** was efficiently quenched by H_2O in CH_3CN solution (k_q = 1.68 x 10^8 M^{-1} s^{-1}) and that the corresponding fluorescence quenching rate for 5,5-dideuterosuberene (**37-*d*$_2$**) was lower, giving a primary isotope effect (k_H/k_D) of 2.8. Since related compounds such as fluorene (**36**), diphenylmethane (**48**) and suberane (**49**) do not exhibit C-H bond cleavage in the S_1, it was proposed that the photogeneration of a 4n π-electron cyclically conjugated carbanion was a necessary requirement to observe carbon acid behavior in S_1.

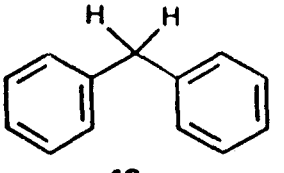

48

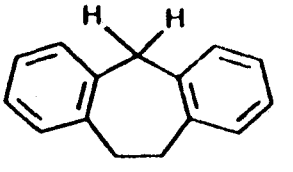

49

In a related study, Wan and co-workers[49] have shown that 5-suberenol (**50**) undergoes photoketonization to give dibenzosuberone (**52**) via a carbanion mechanism (eq 1.12). The key step in this reaction is C-H bond heterolysis on photoexcitation, to generate the 4n π-electron carbanion **51**. Intermediacy of this carbanion in the reaction was further confirmed by the photolysis of **50** in D_2O

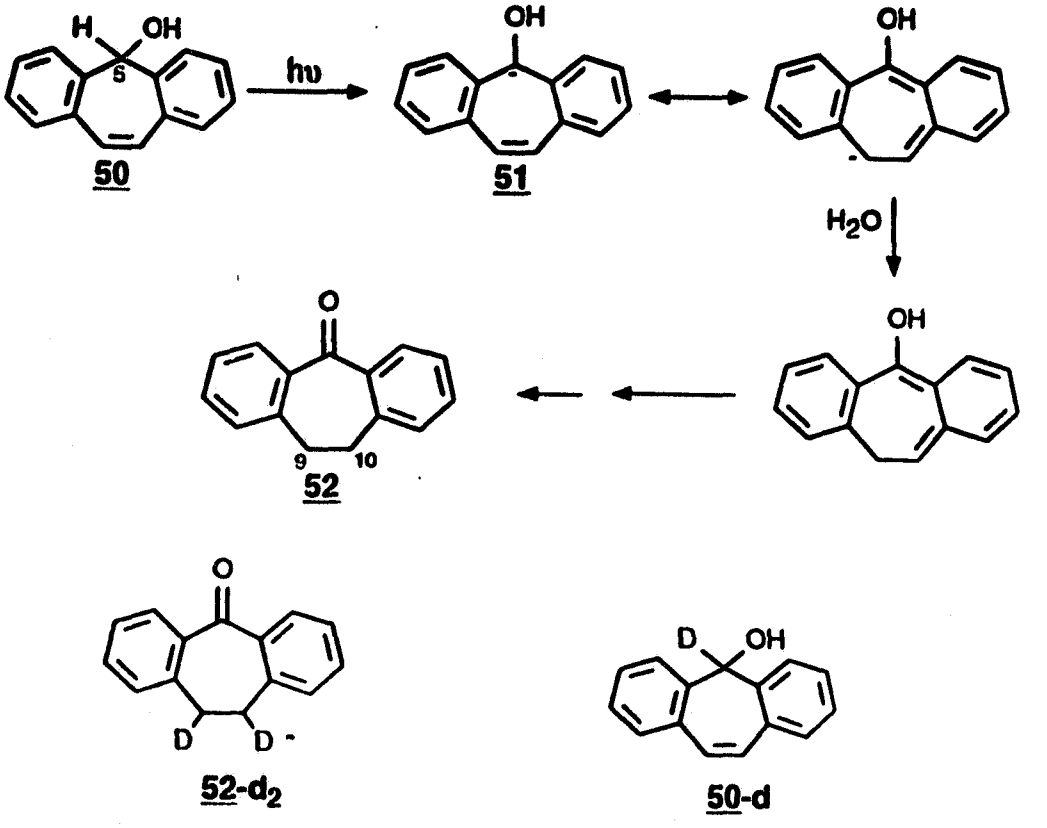

which resulted in the formation of 5-deuterio-5-suberenol (**50**-*d*), and dibenzosuberone (**52**-d_2) in which each of the 9- and 10-positions were monodeuterated. Fluorescence quenching rates of **50** and 5-deuterio-5-suberenol (**50**-*d*) by H_2O in CH_3CN again showed a substantial primary isotope effect (k_H/k_D = 2.9). These results support a mechanism in which H_2O deprotonates the benzylic C-H bond of **50** in the primary step to generate carbanion **51**.

These studies present compelling evidence that there is an enhanced driving force for the photogeneration of intermediates which contain cyclically

conjugated 4n π-electrons in the excited state, compared to systems which are not cyclically conjugated or generate 4n + 2 π-electron intermediates.

Wan, Yates and coworkers[50-52] have proposed that the photochemistry observed for *m*- and *p*-nitrobenzyl alcohols and related compounds may be rationalized by proposing that the primary photochemical step is benzylic C-H bond heterolytic cleavage from the triplet excited state, to generate a delocalized anion, which subsequently reacts to give the observed redox-type products. For example, in the reaction for *p*-nitrobenzyl alcohol (53), the initially generated carbanion 54 reacts via an overall redox reaction to give *p*-nitrosobenzaldehyde (55) (eq 1.13). The reaction was shown to be catalyzed by hydroxide ion

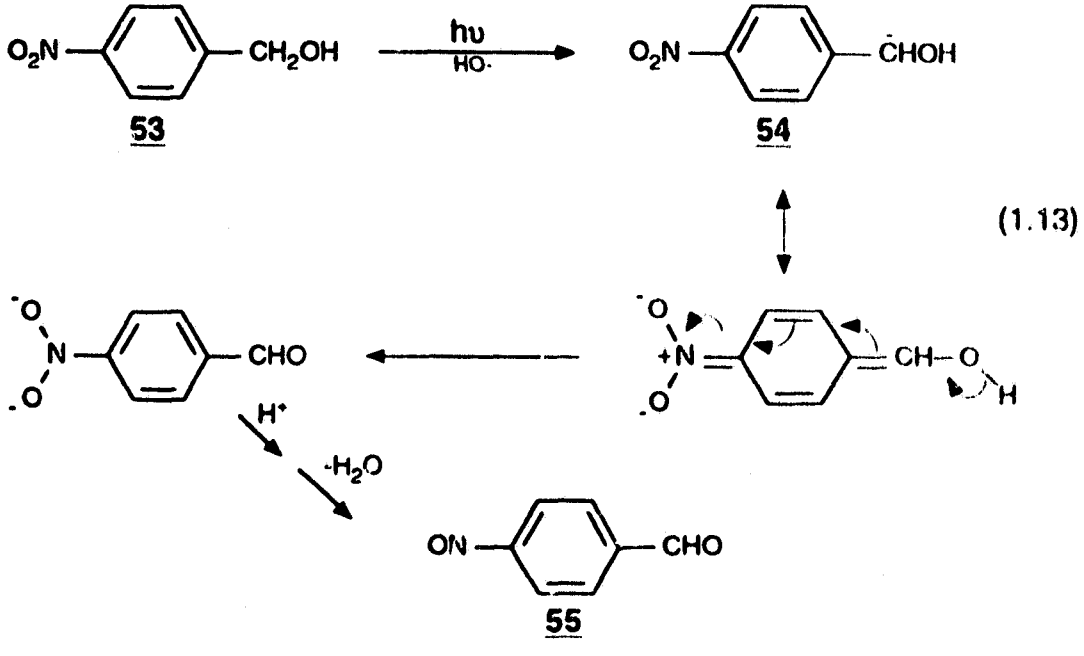

consistent with a carbanion mechanism. However, photolysis in $D_2O/^-OD$ resulted in no observable deuterium incorporation in the substrate, suggesting

that every photogenerated carbanion leads to the product. A significant primary α-deuterium (at the benzylic position) isotope effect ($\Phi_H/\Phi_D > 4$) was observed which is indicative of abstraction of these protons in the product forming step. The mechanism of reaction for *m*-nitrobenzyl alcohol is similar to that proposed for 53, i.e., initial formation of α-hydroxy-*m*-nitrobenzyl carbanion (56). However, simple redox chemistry was not observed and an electron transfer from the photogenerated carbanion to the substrate was proposed, giving rise to a more complex product mixture.[52,53]

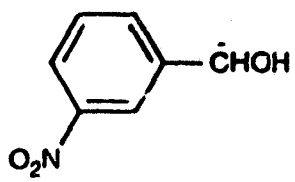

56

1.3 Photogeneration of Carbocations

Carbocations are important intermediates in organic chemistry, and as such have been extensively studied.[54,55] Their existence and role in a variety of ground state (thermal) reactions such as rearrangement, nucleophilic substitution and elimination are well established and a number of reviews dealing with different facets of ground state carbocation chemistry are now available.[54-57]

In recent years, the generation of carbocation intermediates by photochemical methods has attracted considerable attention.[58,59] In general the four most commonly employed methods to generate carbocation intermediates

are, (i) photoheterolysis or photosolvolysis, which involves formal heterolytic cleavage of a σ bond between a carbon atom and a hetero atom, such as oxygen, nitrogen, etc.; (ii) photoprotonation of a carbon-carbon double or triple bond; (iii) photoheterolysis of a radical cation; and (iv) light induced one electron oxidation of a radical (R·). The following discussion is not aimed to be an exhaustive account of carbocation photogeneration, since Cristol and Bindel's review[58] on the subject is still an authoritative source of information in this area. More recently Das[59] has reviewed the progress made in the photogeneration and study of transient carbocations and carbanions by laser flash photolysis methods.

1.3.1 Photosolvolysis

The photosolvolysis of organic molecules involves formal heterolytic cleavage of a σ bond, R-X, on irradiation. The carbocationic species thus generated can then be trapped by the nucleophilic solvent to give the solvolysis product (eq 1.14).

$$\text{R-X} \xrightarrow{h\upsilon} \text{R}^+ \ \text{X}^- \xrightarrow{\text{SolH}} \text{R-Sol} + \text{HX} \qquad (1.14)$$

One of the earliest examples of photogeneration of carbocation was reported by Lifschitz and Joffe in 1919.[60] Irradiation of triarylmethyl (TAM) leuco dye 57 in EtOH results in the efficient loss of cyanide ion to generate cation 58, which in the absence of light recombines with the cyanide ion to regenerate 57 (eq 1.15). This reaction was later shown to be highly solvent dependent, and in polar

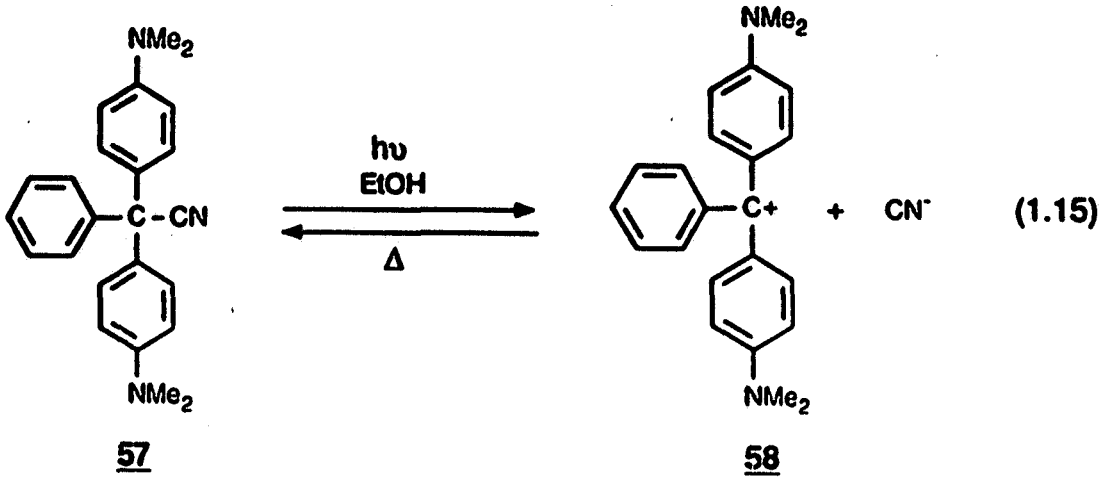

57 58 (1.15)

solvents (e.g., EtOH) the quantum efficiency of formation of 58 was close to unity.[61] Holmes[62a,b] later showed that photolysis of 57 in aqueous ethanol results in the formation of the corresponding solvolysis products 60a and 60b via a carbocation intermediate. Herz[63] in LFP studies of these systems showed that the S_1 state of 57 was the precursor to the cation 58. Triphenylmethane derivative 61 and other TAM derivatives have also been studied by picosecond LFP methods

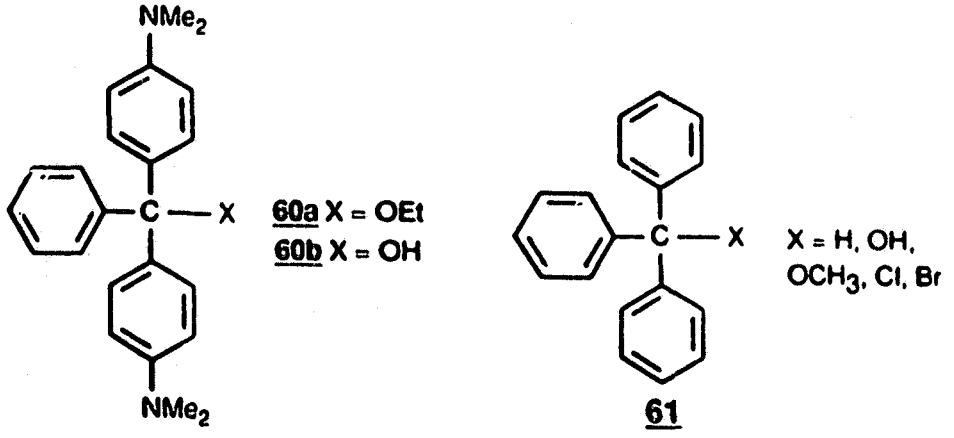

61

in both polar and non-polar solvents. In non-polar solvents like cyclohexane, homolytic bond cleavage generating radical intermediates is the common reaction pathway. However, in polar solvents like MeOH and CH_3CN heterolytic cleavage leading to carbocationic intermediates is the predominant pathway.[63] These studies also delineated the effect of leaving groups (e.g., Cl, OH, OCH_3 etc.) on the ease of photoheterolysis. For example, in **61**, photoheterolytic cleavage to form the corresponding carbocation for X = OH is much more faster than X = OCH_3; no carbocation formation occurs for X = H. These relative rates of heterolytic cleavages in **61** have been correlated[64] to the higher electron affinity of HO· (1.83 eV) compared to CH_3O· (1.57 eV) and H· (0.80 eV). Argument that the electron affinity of a leaving group is correlates with the ease with which it can undergo heterolytic cleavage in S_1 is strengthened by the fact that the $PhCH_2$-OCH_3 bond (68-70 kcal/mol) is actually weaker than the $PhCH_2$-OH bond (78 kcal/mol). Employing LFP, the temporal changes in hybridization (from sp^3 to sp^2) at the central carbon atom of TAM systems during carbocation formation in the S_1 state has also been studied.[65] However, in a later study Peters and Manring[63] showed that these results are attributable to solvents (EtOH and glycerol) used in the study and not due to changes in hybridization at the central carbon.

Using LFP studies Scaiano and coworkers[66] have shown that photolysis of phosphonium chloride **62** results in the formation of the corresponding

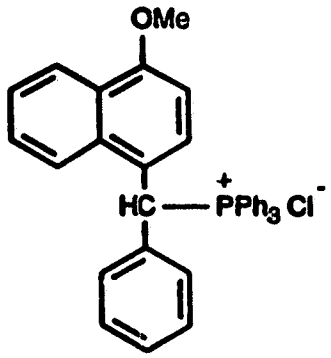

62

carbocation (λ_{max} ~360 and λ_{max} ~500 nm; τ = 2.5 μs). The bimolecular rate constants of reaction for the photochemically generated cation with added nucleophiles are near the diffusion controlled limit (e.g., $k(N_3^-) = 1.8 \times 10^{10}\ M^{-1}\ s^{-1}$ and $k(Cl^-) = 2.2 \times 10^{9}\ M^{-1}\ s^{-1}$).

McClelland, Steenken and coworkers[67,68] in extensive LFP studies of TAM and diarylmethyl systems in aqueous CH_3CN solution, have measured the quantum efficiencies of photohomolysis and photoheterolysis in these systems. In CH_3CN, the quantum yield for homolysis (Φ = 0.2-0.4) are shown to be essentially independent of the nature of substituent on the benzene ring, while the efficiency of heterolysis increases with increasing electron donating ability of the substituent ($\Phi < 0.07$ for CF_3 and $\Phi < 0.3$ for OMe). Furthermore, the yield of the photogenerated cation has been shown to correlate with the σ^+ value of the *para*-substituent and on the pK_R^+ value (*measure of cation stability in solution*) of the cation.[68] The efficiency and yield of cation formation has also been shown to depend on the nature of the leaving group. For example, in the halides, the

observed heterolysis to homolysis ratio correlates with the pK_a value of the conjugate acid HX and not with the electron affinity of the halide radical.[68]

1.3.2 Photosolvolysis of Benzyl Derivatives

Although the early work on the photosolvolysis of TAM derivatives generated considerable interest, it was not until many years later that photosolvolysis reactions were extended to simple organic compounds. In this respect, photosolvolyses of benzyl derivatives have been a subject of numerous studies.[58] The interest in these systems is partly due to the inherent simplicity of these systems and the significant contributions made by Zimmerman and coworkers[69,70] in the early 1960's. In their pioneering work Zimmerman and Sandel[69] correctly predicted the enhanced photoreactivity of *meta*-methoxybenzyl acetate (**63**) compared to the *para*- isomer **64**, by calculating the electron density distribution for the S_1. The *meta*- isomer **63** which is most resistant to solvolysis in the ground state has a quantum yield of photosolvolysis nearly ten times (Φ = 0.13) that of *para*- isomer **64** (Φ = 0.016). This reversal in reactivity was shown to be due to the enhanced electron density at *meta* position in **63** in the S_1 state. The placement of acetoxymethylene group at the *meta*- position thus leads to the loss of acetate ion following excitation. This so called "*meta*- electron transmission" effect was explained with the aid of non-Kekulé structure **65** (eq 1.16). The structure **65** could be envisioned as the excited state of the benzyl cation which could react with a nucleophile such as water to give benzyl alcohol

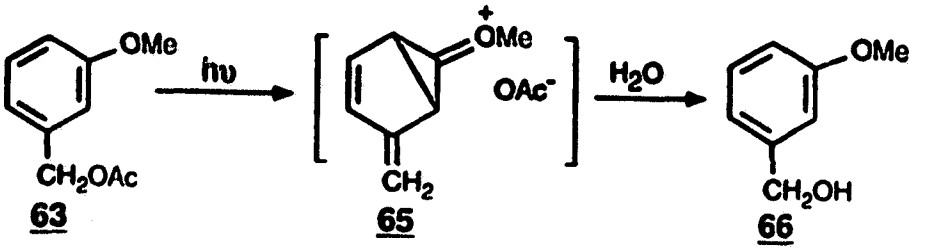

63 65 66 (1.16)

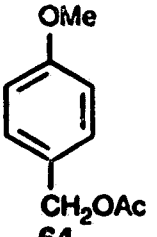

64

66. Besides solvolysis products, radical-derived products, via benzylic C-OAc bond homolysis, are also formed in these reactions.

Since the early reports by Zimmerman and coworkers[69,70], the involvement of carbocations in the photosolvolysis of benzyl compounds has been supported by several other studies. For example, Cristol and Schloemen[71] have shown that photosolvolysis of 67 results in the formation of isomeric deuterium labelled alcohols 68 and 69 (eq 1.17). The formation of 69 is envisioned as arising from the Wagner-Meerwein rearrangement of the initially formed carbocation 70, followed by solvolysis by water.

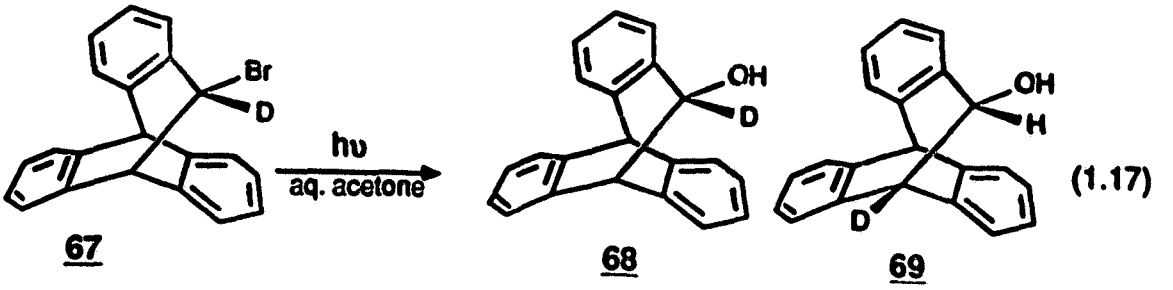

67 68 69 (1.17)

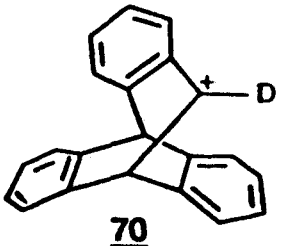

70

In the photosolvolysis of optically active (-)-1-phenylethyltrimethylammonium iodide (71) in water, McKenna and coworkers[72a,b] have shown that the recovered 71 undergoes little racemization, indicating that internal return in the initially formed ion-pair is not significant. Similarly, Jaeger[73a,b] has shown the involvement of carbocation in the photosolvolysis of 72.

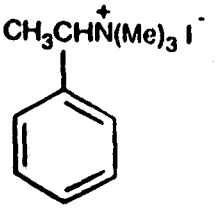

71

Photolysis of ^{18}O labelled 72 in aqueous methanol results in the formation of corresponding methyl ether. Besides solvolysis products, some radical derived products are also formed in this reaction. Interestingly, the recovered 72 shows complete scrambling of ^{18}O's, which by photolysis of optically active 73 is shown

to be via internal return of the initially formed ion-pair. Thus, photolysis of optically active **73** in aqueous methanol yields the corresponding completely racemized methyl ether. However, the recovered **73** shows ^{18}O scrambling, but no loss in optical activity. These results are consistent with the mechanism in which the initially formed ion-pair can either dissociate, to yield solvolysis product, or collapse to give back the ^{18}O scrambled **73** with total retention of configuration. The proposed unifying gross mechanism involving the benzyl cation is shown in Scheme 1.5.

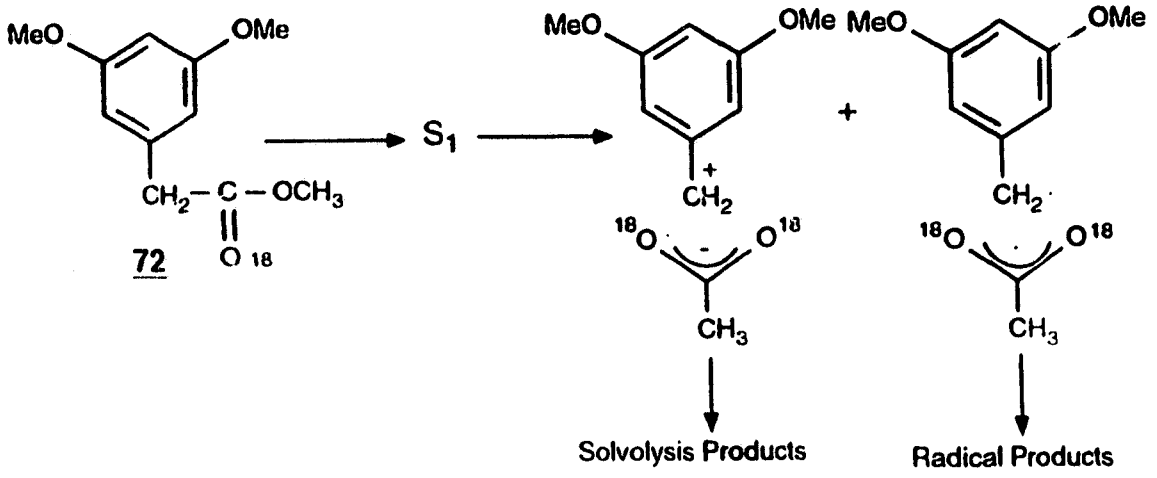

Scheme 1.5

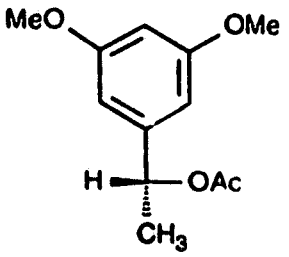

73

Photosolvolysis of benzyl compounds with a variety of leaving groups has been extensively investigated. For example, both benzylsulfonium tetrafluoroborate salt **74** and phenylethyltrimethylammonium salt **71** have been

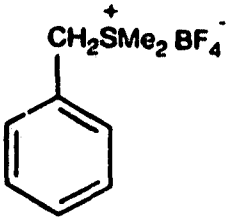

74

shown to undergo photosolvolysis in aqueous solution via the corresponding intermediate benzyl carbocations.[72,74,75] Furthermore, McKenna and coworkers[72,75] have demonstrated that the efficiency of photosolvolysis in **71** is greatly affected by the nature of the substituents present on the benzene ring. For example, the quantum yields of photosolvolyses of **71** remains more or less (Φ ~ 0.31 to 0.39) constant for a variety of substituents (for e.g., CH_3, OCH_3). However, for *meta*-cyano (CN) substitution the quantum yield is very low (Φ ~ 0.005), presumably due to the lower electron density at the carbon *meta*- to the CN group ("*meta* effect"). McKenna and coworkers[76] have also shown that benzyl halides (chloride, bromide and iodide) undergo photosolvolysis from both S_1 and T_1 states.

Arnold and coworkers[77] in the photosolvolysis of 1-naphthylmethyl derivatives **75** have developed a semi-quantitative scale of leaving group abilities of various groups in the excited state. The photosolvolysis of **75** in methanol

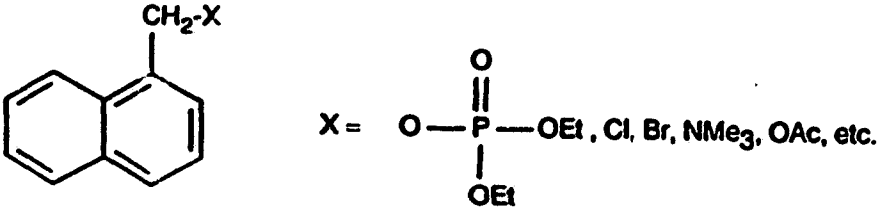

75

affords products derived both from heterolytic and homolytic cleavage of $NpCH_2$-X bond. The quantum yields of products derived from both heterolytic and homolytic cleavage are dependent on the nature of the leaving group (X). Using fluorescence quenching rates and quantum yields of solvolysis products, a scale of leaving group abilities of various groups has been proposed:

$$S(CH_3)_2 > Cl^- \approx N(CH_3)_2 \cdot O_2P(OEt)_2 > O_2CCH_3 > SO_2CH_3$$

The case for X = I has been omitted because a study by Schuster and coworkers[78] has shown that this substrate reacts by a pathway quite different from that of the other X groups and involves the radical anion of molecular iodine.

A considerable amount of work has been reported by Cristol and coworkers[79] and Morrison[80] on the photosolvolytic behavior of bridged systems such as 76 and 77. Photolysis of these systems in general gives both the

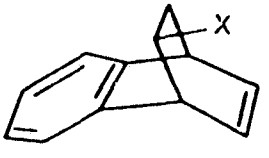

76

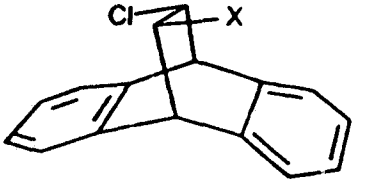

77

solvolysis and Wagner-Meerwien rearrangement products. A major part of this work on the photosolvolysis of these systems deals with the stereochemical requirements for both the leaving group and migrating group. Cristol and coworkers[79] have proposed a mechanism (Scheme 1.6) for the observed photobehaviour of these systems which involves initial electron transfer from the aromatic ring to the remote leaving group forming a zwitterionic biradical species. Loss of the leaving group from the zwitterionic biradical species then leads to the formation of cation biradical, which may then undergo rearrangement or decay to the bridged phenonium ion. A similar mechanism has also been proposed by Jaeger[81] to account for the products observed in the photosolvolysis of β-arylethyl (homobenzyl) system **78**. Irradiation of **78** in aqueous methanol results in the

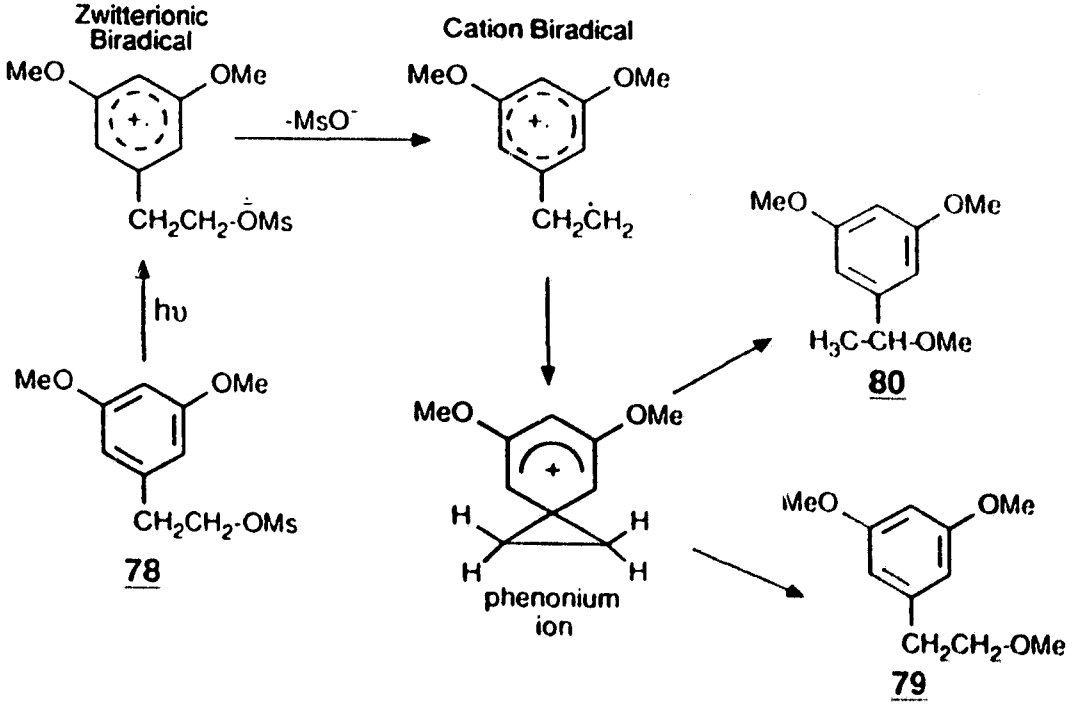

Scheme 1.6

the formation of photosolvolysis product 79, as well as a minor amount of the rearrangement product 80. The proposed mechanism which explains the formation of observed products is shown in Scheme 1.6. This mechanism is further supported by results of irradiation of α,α'-dideuterio analog of 78 which gives solvolysis products with completely scrambled deuteriums, and the recovered starting material with partial scrambling of deuteriums.[81]

Miller and coworkers[82] have reported an interesting case of photosolvolysis of 3,4-dichloroaniline (81) in water to yield 83 (eq 1.18). To rationalize the formation of 83, authors have proposed the intermediacy of aryl cation 82

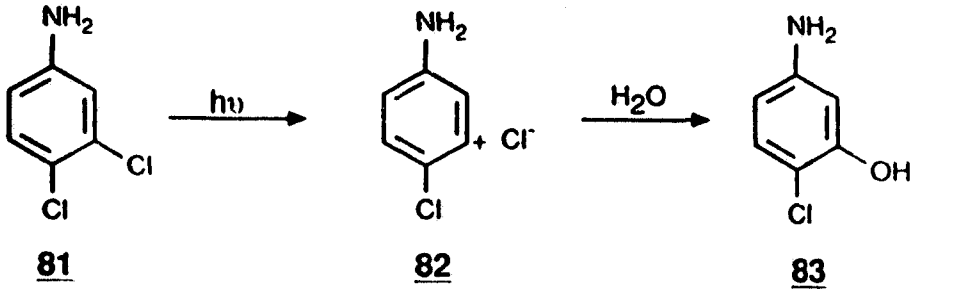

81 82 83 (1.18)

(eq 1.18). Due to large electron density at carbon *meta*- to the NH_2 group ("*meta*-effect"), the C-Cl bond is polarized in the excited state and cleaves heterolytically to yield cation 82, which is subsequently trapped by water to give 83.

1.3.3 Photodehydroxylation

The hydroxide ion (HO^-) is considered a very poor leaving group in the ground state solvolysis reactions. However, there are a number of examples

where it has been shown that HO^- behaves as a good leaving group in the photosolvolysis reactions.[83] The first example of a light induced heterolytic

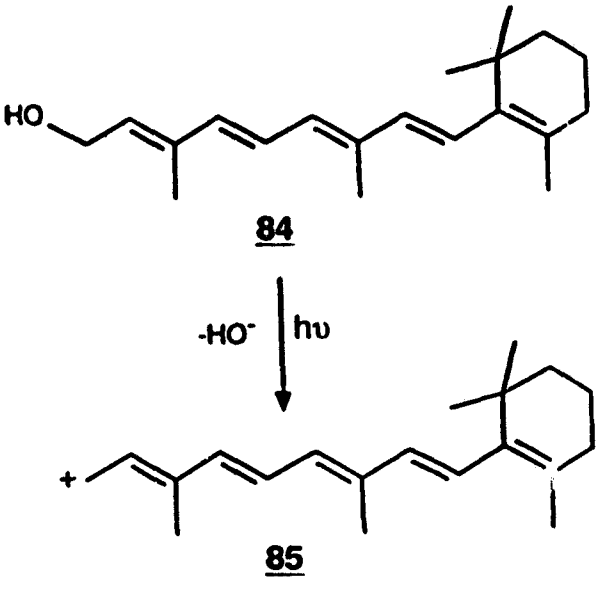

(1.19)

cleavage of a C-OH bond was reported for *all-trans*-retinol (84) by Rosenfeld and coworkers.[84] Nanosecond LFP of 84 at 337 nm results in the C-OH bond heterolytic cleavage in the S_1 state, thereby generating the retinylic cation 85 (λ_{max} 590 nm) (eq 1.19). A picosecond LFP study by Pienta and Kesseler[85] provides a more detailed mechanistic picture of this process. Laser excitation of 84 results in rapid formation of contact ion-pair over a picosecond time scale following the formation of the cation 85, and before the appearance of free ions observed over several nanoseconds.

Benzyl alcohol derivatives are by far the most widely studied systems in photodehydroxylation reactions. Lin and coworkers[86] first reported that

irradiation of bichromophoric benzyl alcohol **86** in methanol, results in the heterolytic C-OH bond cleavage generating the benzyl cation **87**, which undergoes fragmentation to yield alkene **88** and triarylmethyl cation **89** (eq 1.20).

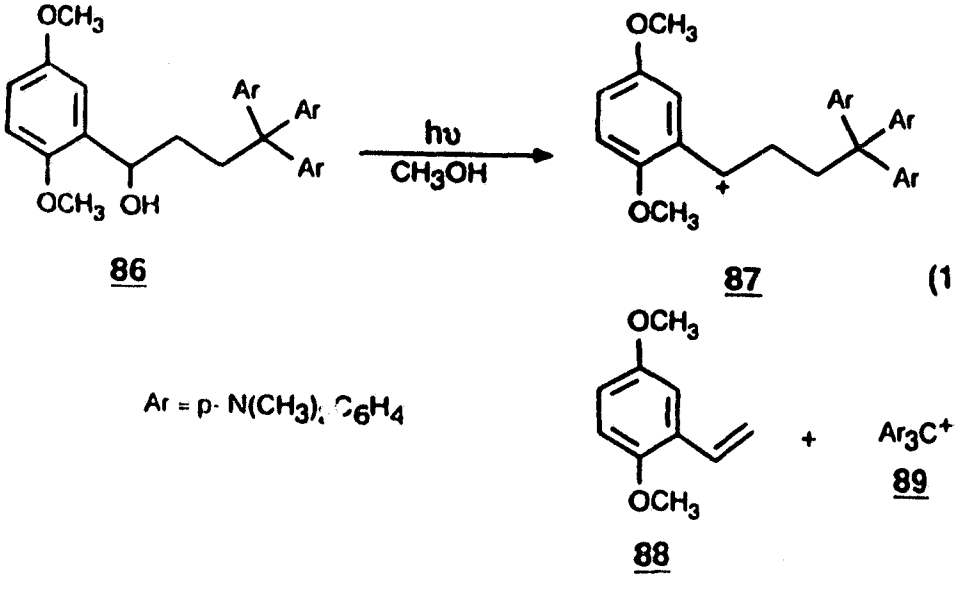

86 **87** (1.20)

88 **89**

Fragmentation of the cation **87** only occurs when the departing carbocation could be stabilized by one or more electron donating groups, such as dimethylaminophenyl groups in the cation **89**. It was further shown that irradiation of alcohols **90** and **91** does not result in any observable reaction suggesting that both an electron accepting (phenyl) and donating (dimethylamino) moieties are required to observe an efficient photodehydroxylation reaction. However, these donor and acceptor moieties do not necessarily have to be on the

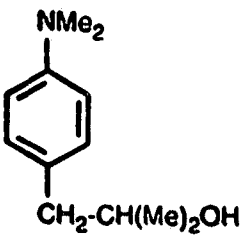

90

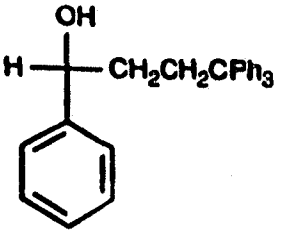

91

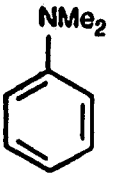

92

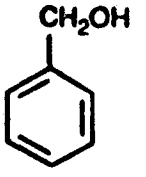

93

same molecule as shown by the efficient photosolvolysis of benzyl alcohol (93) in the presence of N,N-dimethylaniline (92). A charge transfer mechanism has been proposed to explain these observations (Scheme 1.7). In this mechanism,

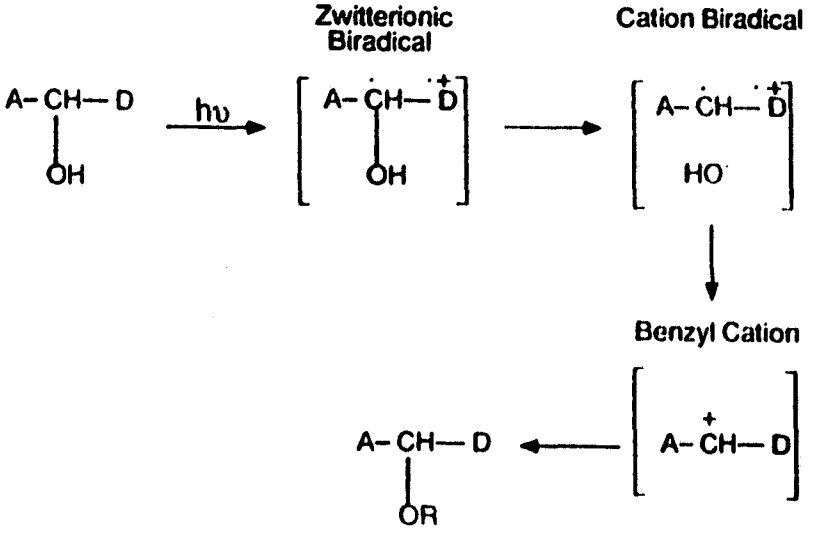

Scheme 1.7

photoexcitation results in the charge transfer from the electron donor (D) to the

acceptor (A) moiety. The radical anion thus formed presumably expels the hydroxide ion to give the benzyl radical, which is then reoxidised by the radical cation of the electron donor to give a ground state benzyl cation, which can undergo fragmentation or nucleophilic attack.

In recent years Wan and coworkers[87-91] have proposed an entirely different mechanism for the photosolvolysis of benzyl alcohols. Turro and Wan[91] have shown that the proton assisted photodehydroxylation of methoxy substituted benzyl alcohols in aqueous solution proceeds via a benzyl cation ($PhCH_2^+$) intermediate. For example, photolysis of *ortho*-methoxybenzyl alcohol (94) in aqueous methanol results in the formation of the corresponding methyl ether (eq 1.21). Small amounts (≤ 5%) of dimeric products 95 and 96, resulting from the

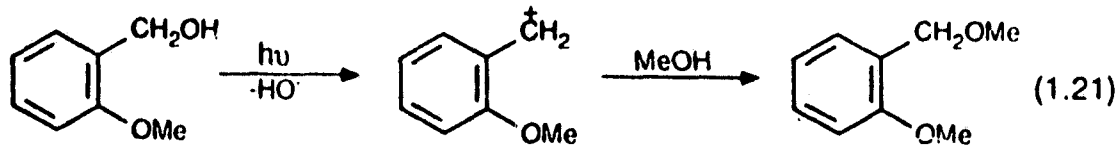

94 (1.21)

$ArCH_2CH_2Ar$ **95**

$ArCH_2OCH_2Ar$ **96**

benzylic C-OH bond homolysis, are also observed. This reaction has been shown to be acid catalyzed as the efficiency of formation of photosolvolysis products increases with decreasing pH.[91] Acid catalysis is further manifested in the fluorescence emission quenching of alcohol 94 by added acid, in the same pH

region where acid catalysis of photosolvolysis is observed. Comparison of fluorescence emission quenching rates showed that *ortho*-methoxybenzyl alcohol (94) is at least 3 times more reactive than the corresponding *meta*- isomer 97. Although this result is contrary to the predictions made by Zimmerman and Sandel[69,70], it must be noted that in the case of 94 and 97 photosolvolysis was

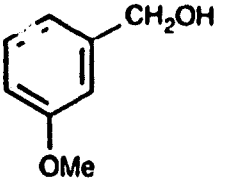

97

carried out in the presence of an added acid, which is the required catalyst to observe photodehydroxylation. A mechanism has been proposed in which the primary photochemical step involves proton assisted cleavage of the $ArCH_2$-OH bond to generate the $ArCH_2^+$ cation (Scheme 1.8). An alternative mechanism

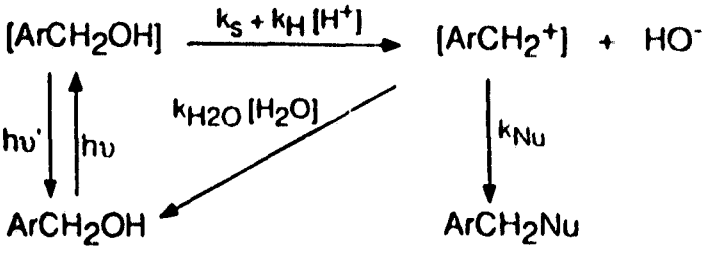

Scheme 1.8

involving the benzylic C-OH bond homolysis was ruled out since it could not fully account for the observed acid catalysis. Other studies[87-90] have been carried out which delineate the effect of substituents in photosolvolysis of benzyl

alcohols. The results obtained in these studies are in accord with the "*meta* electron transmission" effect proposed by Zimmerman and Sandel.[69,70]

In a study of structurally rigid benzyl alcohol derivatives, Wan and coworkers[92] have reported the adiabatic photodehydroxylation of 9-phenylxanthen-9-ol (98) to generate the 9-phenylxanthenium carbocation 99 in the S_1 state (Scheme 1.9). The adiabatic nature of this process was established by steady-state fluorescence studies. A single step water assisted photodehydroxylation mechanism has been proposed (Scheme 1.10). This

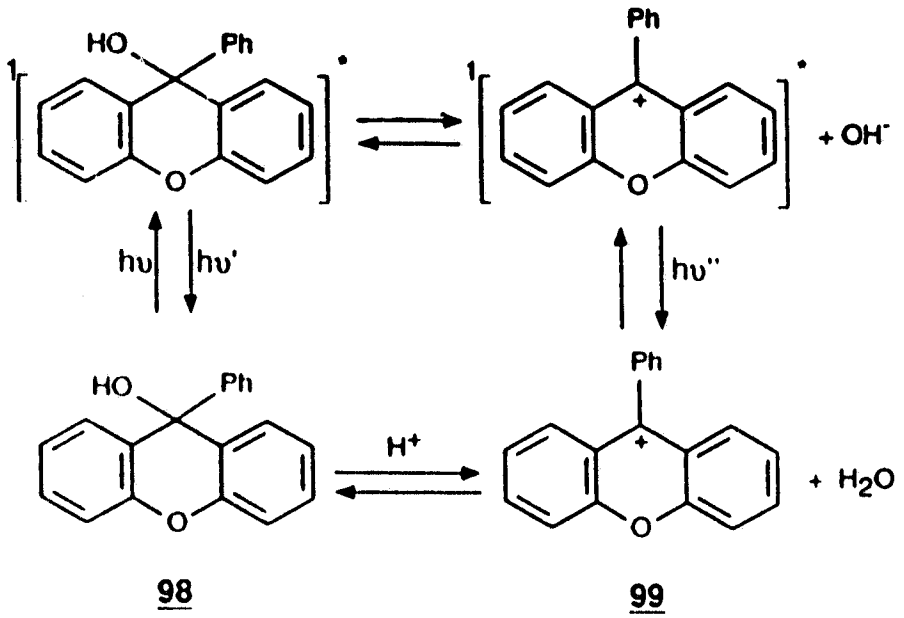

98 99

Scheme 1.9

mechanism is supported by the solvent isotope effect observed on the emission yields of 98 and 99 in H_2O and D_2O solutions. The emission yield (Φ_f) of 98 increases by ≈ 16% on going from 20% CH_3CN-H_2O to 20% CH_3CN-D_2O, whereas

the emission yield of cation 99 exhibits a concomitant decrease of similar extent. This is consistent with the water assisted dehydroxylation in the S_1 state. Recent LFP studies by Das and Minto,[93] McClelland and coworkers,[94] and Okuyama and coworkers[95] confirm that the primary photochemical step in photodehydroxylation of 98 is the loss of hydroxide ion. However, it is also shown that only a small fraction of the photodehydroxylation (≈ 1% in 1:1 H_2O-CH_3CN) occurs via the adiabatic route.

Other rigid benzylic alcohols have also been shown to undergo efficient photodehydroxylation. Wan and Krogh[96] have shown that 9-fluorenol (100) undergoes efficient photosolvolysis in aqueous methanol via the intermediate 9-fluorenyl cation 101, to give the corresponding methyl ether (eq 1.22). The LFP

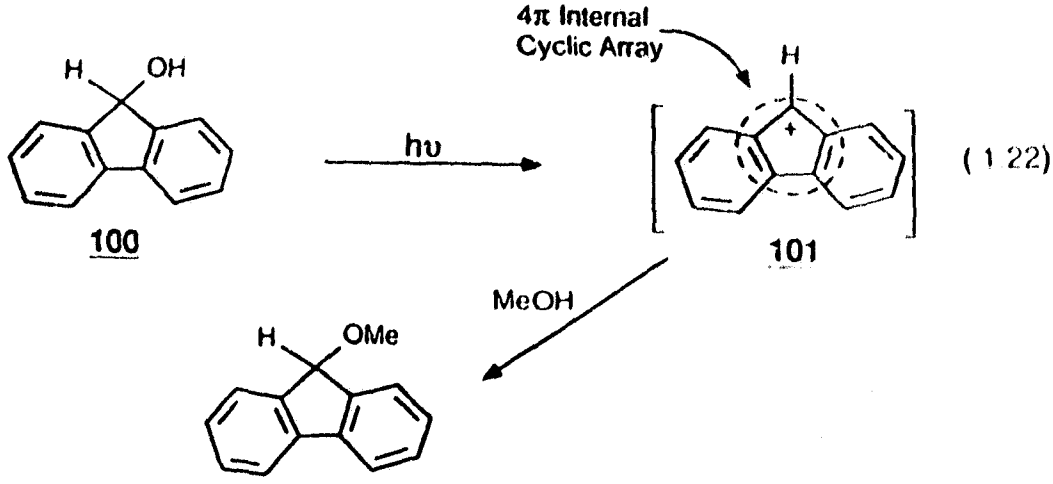

(1.22)

studies of 100 have shown that not only the cation 101, but radical 102 (via C-OH bond homolysis) is also formed in this reaction.[97,98] The propensity of 100 to

undergo efficient photosolvolysis is attributed to the formation of an antiaromatic 4π-electron 9-fluorenyl cation **101** which may possess an aromatic character on the excited state surface. This contention is further supported by the observed lower photochemical reactivity of several dibenzosuberenyl alcohols which form 6π (4n+

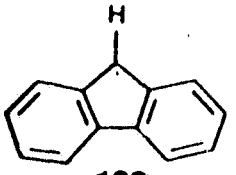

102

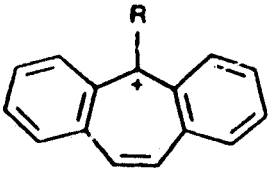

103

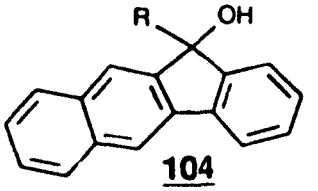

104

2) electron carbocations (e.g., **103**) under conditions where **100** and other 9-fluorenol derivatives (e.g., **104**)[99a,b] react much more efficiently.

1.3.4 Photoinduced Electron Transfer (PET) Reactions of Carbocations

The initial step of producing a photochemically excited state often provides the driving force for electron transfer reactions that are not thermodynamically favourable when both electron donor and electron acceptor are in the ground electronic state. Excitation of an electron from the HOMO to the LUMO reduces the ionization potential and increases the electronic affinity of a molecule, as shown in Fig 1.1. Thus, an electronically excited molecule can function both as a powerful one-electron reducing agent (electron donor, D) and a one-electron oxidizing agent (electron acceptor, A). The feasibility of PET reaction between an excited state donor and acceptor is dictated by overall change in free energy ΔG

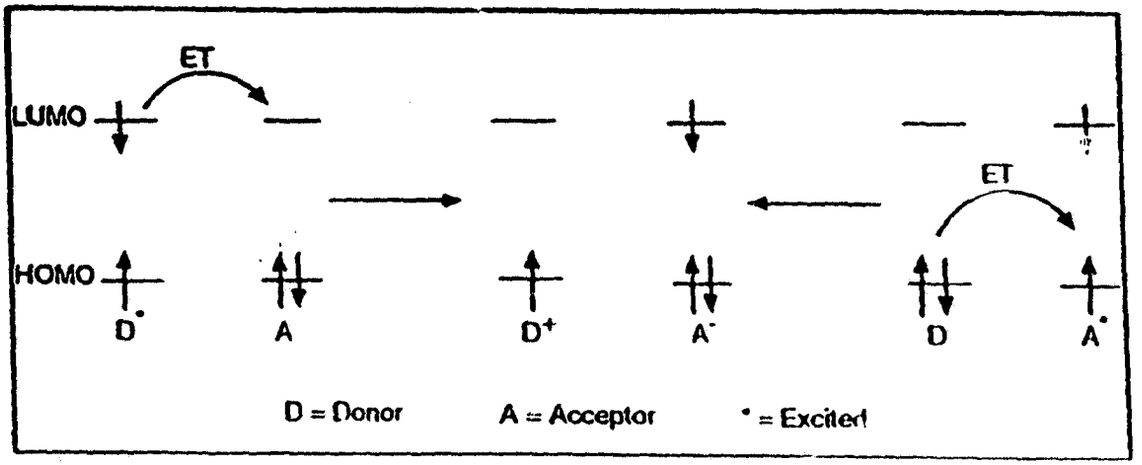

Figure 1.1 Electron transfer energetics of excited states

which accompanies the reaction. In polar solvents, it can be predicted on the basis of the simple equation derived by Weller and co-workers[100] (eq 1.23)

$$\Delta G \text{ (kcal/mol)} = 23.06\{E_{D/D^+} - E_{A^-/A} - e^2/a\chi\} - \Delta E_{0,0} \qquad (1.23)$$

where: E_{D/D^+} and $E_{A^-/A}$ are the oxidation and reduction potentials of the donor and acceptor respectively; $e^2/a\chi$ is the energy gained by bringing the two reacting species to the encounter distance in a medium of dielectric constant χ; and $\Delta E_{0,0}$ is the electronic excitation energy of the donor.

Once the electron transfer has taken place the subsequent ability of the intermediates, viz., radicals or radical ions, to undergo further chemistry depends on several factors including the lifetimes of the singlet contact or solvent

separated ion pairs, and the rate of back electron transfer.

Unlike the photochemistry of carbanions, which has been reasonably well-studied,[101] the photochemistry of carbocations has received considerably less attention. In the early 1970's van Tamelen and coworkers reported the steady state photolysis of several stabilized carbocations.[102] The reactions were often complex and very solvent dependent. Although no electron donors were deliberately added, the nature of the products occasionally suggested an electron transfer had taken place. For example, photolysis of triphenylcyclopropenium bromide (**105**) in 10% aqueous H_2SO_4 affords hexaphenylbenzene (**106**) in 50% yield (eq 1.24). The efficiency of this reaction increases when methanol is used as a co-solvent.

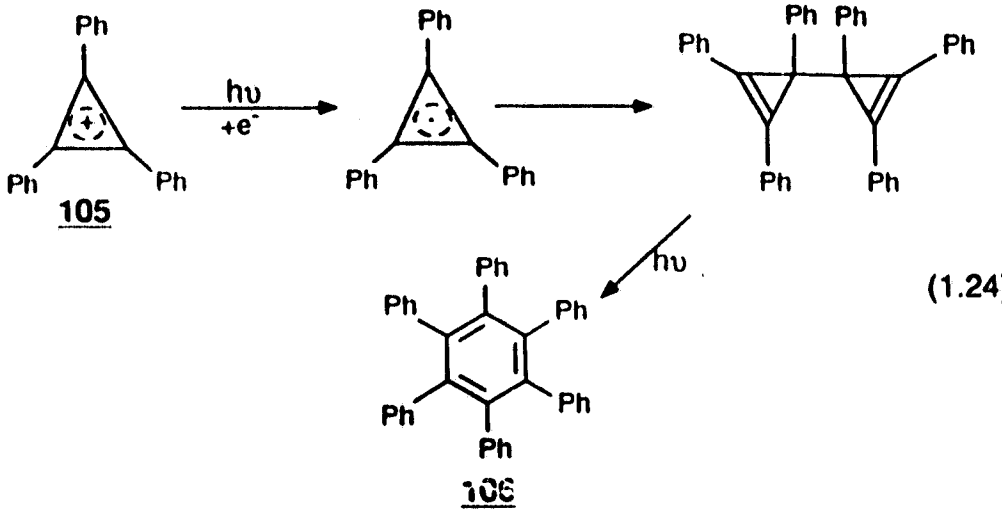

105 106 (1.24)

More recently, Al-Ekabi and coworkers[103] have reported that irradiation of 1,1'-(di-*p*-anisylmethyl)ethyl cation (**108**) in benzene-trifluoroacetic acid solution results in electron transfer from the neutral precursor **107** to the cation **109**

(Scheme 1.10). The quantum yields of the photoproducts are very low (Φ = 0.001), presumably due to an efficient back electron transfer process. The nature

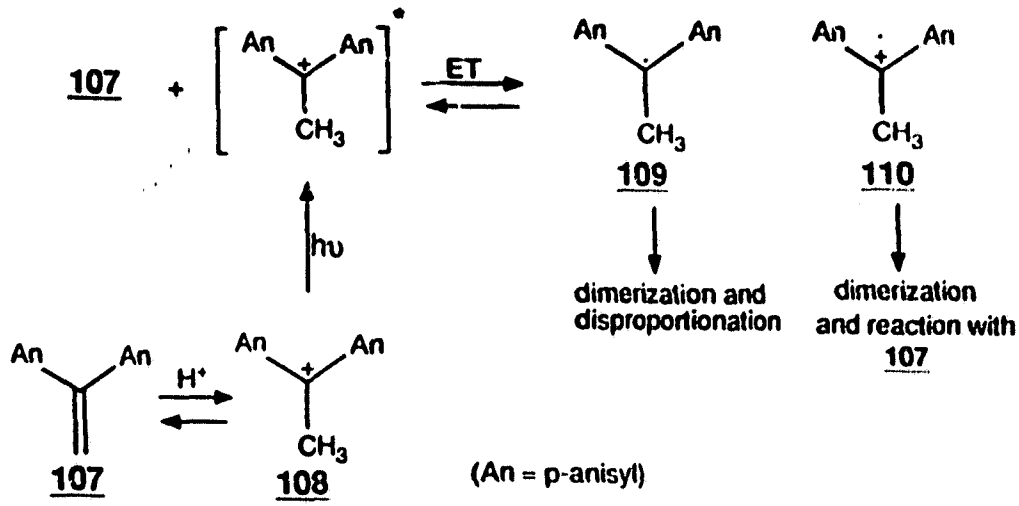

Scheme 1.10

of the final products strongly suggests the intermediacy of the radical **109** and the radical cation **110**. In the presence of a better electron donor such as 1,2,4-trimethoxybenzene (TMB), the yields of products derived from radical cation **110** is suppressed because of the competitive interception of the excited **108*** by the TMB. The presence of TMB also quenches the dimerization of radical **109**, indicating that the back electron transfer reaction is more facile with TMB than with **107**. The radical cation **110** has been directly observed in the course of microsecond flash photolysis studies. When dicyanoanthracene is used as the excited state electron acceptor in presence of **107**, same transient absorption assignable to **110** is observed. However, in the presence of TMB this transient is

completely quenched.[103]

Takahashi and coworkers[104] have studied the photochemistry of charge transfer (CT) complexes of the tropylium cation (111) and a series of substituted arenes in CH_3CN solutions. Photoexcitation of these CT complexes leads to an electron transfer from the arene donor to the tropylium cation acceptor (eq 1.25).

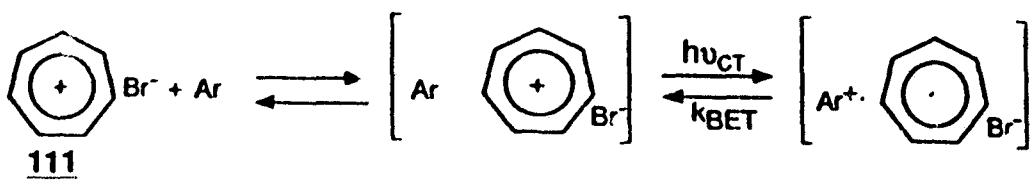

111

Ar = substituted benzenes, naphthalenes

The arene radical cations thus formed (within 30 ps laser pulse) have been detected by time resolved spectroscopic techniques. The subsequent decay of the radical cation and the concomitant regeneration of the ground state CT complex occurs with a rate constant, $k_{BET} > 4 \times 10^{10}\ s^{-1}$ (eq 1.25). No further chemical reactions are observed from the excited state CT complex because of short lifetime of the arene radical cation ($\tau \approx 15$ ps), and the fast rate (k_{BET}) of back electron transfer. Hence, prolonged photolysis of the CT complexes of substituted benzenes, naphthalenes, and anthracenes fails to yield any detectable photoproducts. However, unimolecular processes are quite rapid and can effectively compete with back electron transfer. For example, isomerization of hexamethyl Dewar benzene **112** is photoinduced via excited CT complex (eq 1.26).[104]

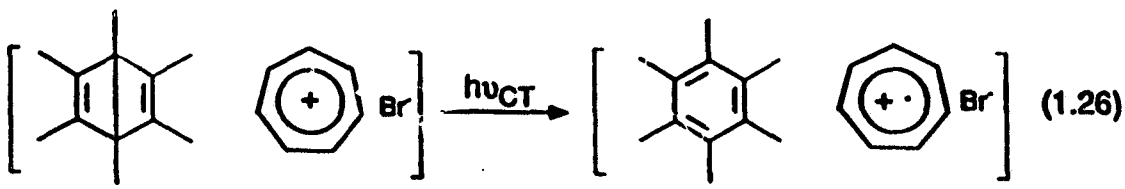

(1.26)

112

A number of xanthenium and thioxanthenium cations in their singlet excited states have been found to be efficiently quenched by a variety of aromatic donors.[105a] For example, the emission of 9-phenylxanthenium cation (**99**) is quenched by a number of electron donors with rates varying from 4.5×10^9 M^{-1} s^{-1} (for benzene) to 2.6×10^{10} M^{-1} s^{-1} (for anthracene). The products derived from

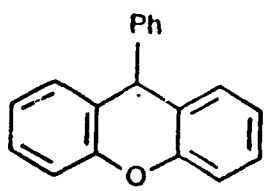

113

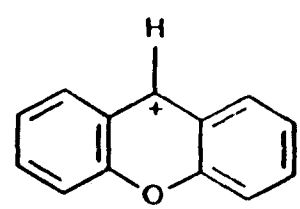

114

electron transfer, viz., arene radical cation and 9-phenylxanthenyl radical (**113**) have been detected by transient spectroscopic methods. Azarani and coworkers[106] have shown that the fluorescence quenching rates of dibenzosuberenyl (**103**), xanthenium (**114**) and 9-phenylxanthenium (**99**) cations by electron donors (e.g., substituted benzenes) can be correlated to their oxidation potentials. Johnston and coworkers[105b] have shown that the ground state of cation **115** acts as an

electron acceptor from the triplet of 1-methoxynaphthalene (116) ($k_q \sim 1 \times 10^9\ M^{-1}s^{-1}$ in trifluoroethanol). The transient absorption spectra resulting from LFP of 116 in the presence of the cation 115 shows the formation of the naphthalene radical cation $116^{+\cdot}$ and radical $115^{\cdot}$ (eq 1.27).

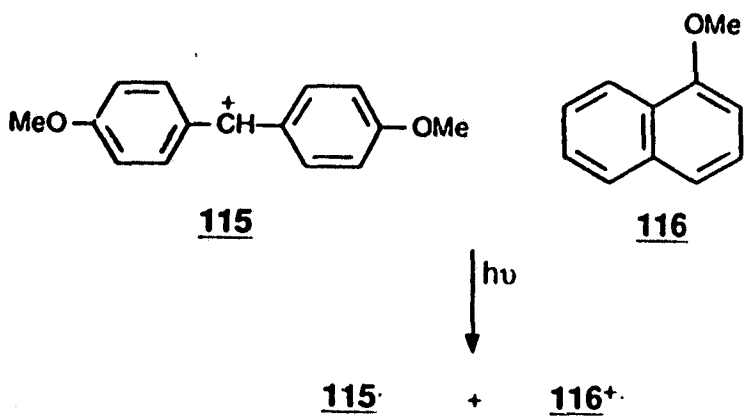

(1.27)

1.4 Excited States of Aromatic and Antiaromatic Systems

Since the discovery of benzene by Faraday[107] in 1825, the chemistry of aromatic compounds has attracted considerable attention. It was Kekulé who first proposed the term 'aromatic compounds' as a name for describing benzene and its derivatives because of their odour.[108] A variety of chemical and physical phenomena are interpreted as caused by, or directly related to, the aromatic nature of substances. The predisposition to electrophilic substitutions vs low proclivity towards addition reactions of benzene and the unusual tendency of a molecule to release a positive or negative group (for e.g., cyclopentadiene, cycloheptatriene) are some known examples of how significantly aromatic

character and the tendency of species to acquire such character influences chemical behaviour. Important physical properties, such as diamagnetic ring current and characteristic electronic transitions, as expressed by NMR and UV patterns, are also associated with the aromaticity in the molecule under consideration. However, an unambiguous criterion which could be used to classify particular compounds as aromatic or antiaromatic does not exist. The criteria based on the reactivity data characterizes the kinetic stability and are determined by the properties not only of the ground state of the molecule, but also those of the transition state of the reaction being considered. In their monograph "Facts and Theories of Aromaticity", Lewis and Peters[109] concluded on the basis of a detailed discussion of various interpretations of the term "aromaticity" that the most general definition reduces to the following: "an aromatic molecule is a molecule which resembles benzene".

The connection between electronic make-up of aromatic molecules and their unusual stability was noticed as early as 1922. It was suggested that a sextet of electrons in a molecule like benzene confer reduced unsaturation and a tendency to be inert. In 1928 the marked stability of the cyclopentadienide anion was attributed to the presence of a sextet of electrons. The first quantum mechanical explanation of the phenomenon of aromaticity was provided by Hückel's molecular orbital (HMO) theory in 1931.[110] Hückel predicted that a planar molecule containing a cyclic array of π electrons is stabilized when the bonding π-orbitals are completely filled with the electrons and, the non-bonding

and antibonding molecular orbitals are unoccupied. The fulfilment of these conditions leads to the familiar 4n + 2 (n = 0, 1, 2,..) rule for the number of π-electrons in an aromatic compound. Since each orbital can contain two electrons, only cyclic molecules having (4n + 2) π electrons (n = 0, 1, 2, ...) will have a closed shell configuration and therefore will be extra stable. This is analogous to the "closed shell" arrangement of electrons about atoms of the inert elements ($2n^2$ electrons) which exhibit marked stability. In contrast, cyclic conjugated systems with 4n π-electrons have an open shell electronic configuration and hence do not exhibit any extra stability. This Hückel 4n + 2 aromaticity rule has now been experimentally verified for a large number of neutral and charged cyclic systems.

The contribution of cyclic conjugation of electrons to the energy of a molecule is characterized by the Hückel resonance energy (RE), which in terms of the Hückel approximation is defined as the difference between the total π-electron energies of the conjugated molecule and a reference system consisting of same number of isolated double bonds. In aromatic systems, the cyclic π-electron delocalization reduces the energy content of the system relative to the corresponding model compound which lacks such cyclic delocalization. On the other hand, cyclic delocalization of π-electrons in 4n antiaromatic systems raises its energy compared to the reference compound which is not cyclically conjugated. The resonance energy has been shown to be an excellent aromaticity index for a number of monocyclic conjugated compounds. The RE as an index of aromaticity has also been used to predict the extent of aromaticity in a number

of conjugated heterocyclic systems such as **117** and **118**.[112]

117

118

Electronic excitation of aromatic as well as antiaromatic molecules results in redistribution of electrons which affects both their physical and chemical properties. One way to understand changes that accompany electronic excitation is to examine the nodal properties of the HOMO and the LUMO of the molecule. In aromatic (4n + 2) systems the nodal properties of molecular orbitals are such that the LUMO always contains one more nodal plane than the HOMO.[112] Thus when an electron is excited from the HOMO to the LUMO it results in the weakening of bonds (decrease in the net bond order). For example, the ring bond lengths of benzene increases from 1.393 Å to 1.434 Å in the S_1 state and the aromatic character (and RE) is significantly reduced.[113] On the contrary, in the antiaromatic systems containing 4n π-electrons, the HOMO and the LUMO have equal number of nodal planes. When the HOMO contributes local bonding between two neighbouring atoms, the LUMO provides antibonding of equal magnitude and vice versa. For example, in cyclobutadiene (**119**) the HOMO has bonding character between atoms 1 and 3, 2 and 4, whereas the LUMO has

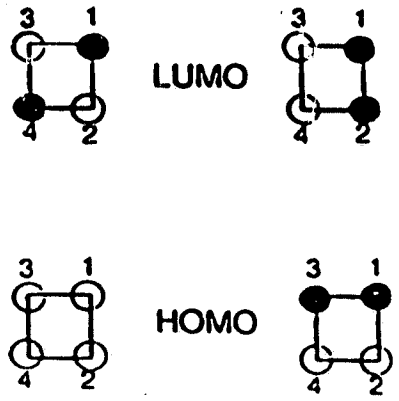

Figure 1.2 HOMO and LUMO characteristics of cyclobutadiene

antibonding character between these centres (Fig 1.2). Thus, excitation of an electron in **119** from the HOMO to the LUMO reduces the bond alternating effect of HOMO and the π-electrons evenly localize in the four membered ring. As a direct consequence of this uniform delocalization of π electrons in the entire ring, the aromatic character of **119** (and similar 4n systems) is enhanced in the excited state. This reversal of aromatic character of 4n + 2 vs 4n systems has also been predicted by a number of theoretical calculations. Aihara's calculation[114] of delocalization energies for a number of Hückel aromatic and antiaromatic systems show that excitation of an electron in a cyclic aromatic (4n+2) systems results in an overall decreased electron delocalization whereas electrons in antiaromatic (4n) systems on excitation become more delocalized. For example, the resonance energy of benzene (0.273 β) is greatly reduced in the excited state (-0.692 β); whereas the resonance energy of **119** increases on excitation (-1.226 β (T_1) to 0.305 β(S_1)).[114] Experimentally such a situation is best represented by a high reactivity

of benzene in the excited state forming benzvalene (120), Dewar benzene (121), and prismane (122) on irradiation, whreas 119 appears to be relatively stable,

120

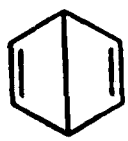

121

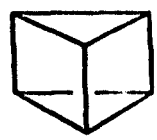

122

decomposing to acetylene on extended irradiation. Similar conclusions were reached by Jug and coworkers[115] in their calculations on the number of 4n + 2 and 4n π-electron systems at the SINDO1 level using the bond order as a measure of aromaticity. The bonds are significantly elongated and the bond alternation is increased in number of 6π electron systems in the excited S_1 and T_1 states, indicating aromatic character of these systems is reduced in the excited states. In contrast, the optimized geometries of some 4n π-electron systems in the excited states exhibit increased aromatic character as indicated by bond equalization or reduced bond alternation.

Chak and Dingle[116] have performed PPP π-SCF calculations on the cyclopentadienyl and cycloheptatrienyl systems as well as their dibenzo derivatives. The calculations on the dibenzo 4n π-systems indicate that the strong bond alternation in bond lengths and charge distribution in the ground state (S_0) becomes weaker in the S_1 state. For example, in 9-fluorenyl cation 101 most of the positive charge in S_0 tends to localize in the central five-membered

ring, and only a small amount is delocalized into benzene rings. However, calculations on the S_1 of **101** show the weakening of bond alternation indicating that there is enhanced charge delocalization of electrons. This is also supported by the observed efficient photosolvolysis of 9-fluorenol (**100**) in 1:1 MeOH-H_2O (*vide supra*), a medium in which diphenylmethanol (no cyclic delocalization of charge possible) does not show any reaction.[96] Similar calculations on the systems with aromatic electron count (4n+2), showed that they also experience extensive electron distribution in the S_1 state. For example, in 8π-electron dibenzosuberenyl carbanion **35**, the delocalization of electrons in the central seven member ring has been shown to be enhanced in the S_1 state, and hence **35** is predicted to be more stable in the S_1 state.[116] Experimentally this is manifested in the benzylic C-H bond cleavage of suberene **37** in the S_1 state to give intermediate carbanion **35**. In contrast fluorene (**36**) which forms 6π-electron 9-fluorenyl carbanion does not undergo C-H bond cleavage in the S_1 state (*vide supra*). The efficient PDC of suberene carboxylic acid (**29**) via 8π-electron suberenyl carbanion (**35**), compared to fluorene carboxylic acid (**28**) and diphenylcarboxylic acid (**30**), is also in accord with the enhanced stability of 8π carbanions in the excited state.

1.5 Proposed Research

It has been demonstrated that in dibenzannelated systems the photogeneration of carbocation and carbanion intermediates that consist of 4n π-electrons in an internal cyclic array (ICA) is favoured on the excited state

surface.[32,48,49,96] The facile photodecarboxylation of several dibenzannelated acetic acids (e.g., 29)[32] and unique carbon acid behaviour of suberene (37)[48] (*vide supra*), have been attributed to the photogeneration of a cyclically conjugated 8π (4n) electron carbanion intermediate in these reactions. The efficient photosolvolysis of fluorenols (e.g., 100) via 4π-electron carbocation intermediates[96] further supports this notion. In contrast, reactions that give rise to 4n + 2 π-electron intermediates (carbanions and carbocations) are less favoured in the excited states. Thus, assuming that the Hammond's postulate applies to the excited state surface, it would appear that the activation barrier ($\Delta G^{\ddagger}$) encountered for the formation of 4n π-electron intermediates on the excited surface is lower than for the corresponding 4n + 2 π-electron intermediates. In other words, reactions that give rise to cyclically conjugated 4n π-electron intermediates are favoured, because such species are more stabilized on the excited state surface relative to their 4n + 2 counterparts. There is some theoretical justification behind this proposal as well. Calculations carried out on a number of aromatic (4n +2) and antiaromatic (4n) systems have shown that excitation results in reversal of their respective stabilities.[112,114] That is, ground state stable aromatic (4n + 2) systems are destabilized, whereas antiaromatic (4n) systems are stabilized on the excited state surface (*vide supra*).

This argument is true only if the reaction which gives rise to such intermediates takes place (at least partially) on the excited state surface, that is, the reaction is *adiabatic*. However, so far there has been no proof for the

adiabaticity of such reactions and hence, no direct evidence for the formation of such 4n π-electron intermediates (carbanions or carbocations) on the excited state surface is available.

The present work is a continuing effort to obtain a better understanding of this unique phenomenon of enhanced reactivity of 4n systems on the excited state surface. In this dissertation, attempts will be made to show the generality of this process, and to address the question of structure-reactivity. The dibenzannelated systems **125**, **136**, **142** and **147** were chosen as progenitors of carbanion intermediates by way of C-H bond photoheterolysis and photodecarboxylation reactions. These systems are isoelectronic to suberene (**37**) and give rise to

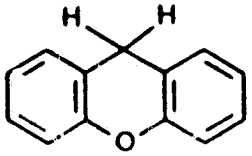

125

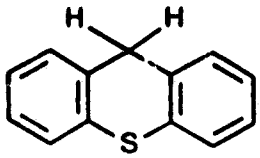

136

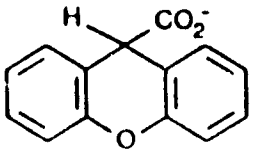

142

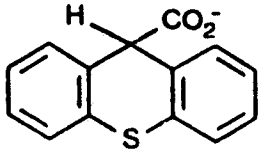

147

carbanion intermediates which consist of 8π-electrons in an ICA. However, carbanions derived from these systems (**125** or **136**) are expected to be less stable than the corresponding suberenyl carbanion (**35**), because the presence of bridge hetero atoms (O and S), which reduces the extent of negative charge delocalization (compared to the suberenyl carbanion **35**). This difference in

relative stabilities of carbanion intermediates should be manifested in reduced reactivity (carbon acid behaviour) of **125** and **136** compared to **37**. For similar reasons, the photodecarboxylation efficiencies of **142** and **147** are expected to be lower than that of **29**. The related isoelectronic system **140** is shown not to exhibit carbon acid behaviour in the excited state because of a competing electron transfer process. The mechanism of this process has been investigated in detail by employing LFP.

The enhanced stability of $4n\pi$ electron systems in the excited state is further manifested in the unprecedented photophysical properties of **155** discovered during the course of this work. The driving force behind the excited state planarization of **155** is shown to be the attainment of an 8π-electron ICA in S_1.

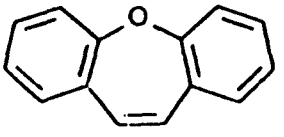

155

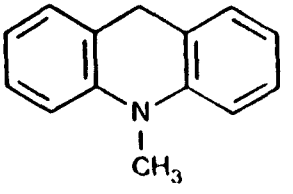

140

The question of structure-reactivity in the excited state carbon acid behaviour of suberene (**37**) is addressed by investigating the reactivity of various substituted suberenes. The substituted suberene derivatives **180**, **185** and **189** were synthesized to examine the effects of electron donating and electron withdrawing substituents on the efficiency of benzylic C-H bond ionization in S_1.

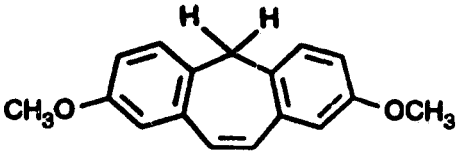

180

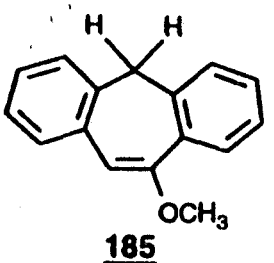

185

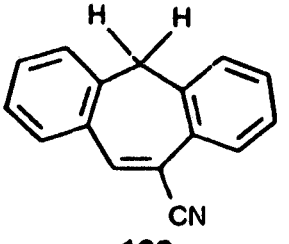

189

The results obtained in these studies support the intermediacy of 8π-electron suberenyl carbanions in these reactions. Highly annelated systems **193** and **196**

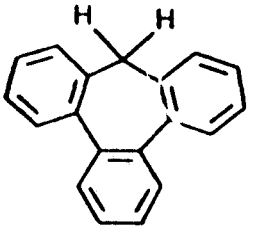

193

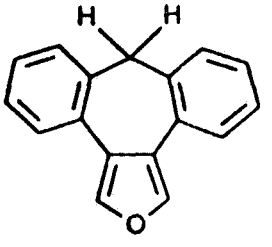

196

undergo C-H bond ionization in the S_1 only in the presence of an added base (e.g., ethanolamine). This difference in reactivity of **193** (or **196**) vs **37** underscores the differences in the stability of corresponding carbanion intermediates.

The second part of the dissertation deals with the photogeneration and

photochemistry of dibenzannelated carbocations. Previous studies have shown that, in the presence of a variety of electron donors, 9-phenylxanthenium cation (**99**) and 9-xanthenium cation (**114**) act as very good electron acceptors in the S_1 state. However, no attempts were made to identify the products that are formed once the electron transfer has taken place. In the present study it is shown that these cations, **99** and **114**, in the S_1 state accept an electron from di- and trimethoxybenzenes to give the corresponding radical intermediates. The radical intermediates subsequently react with oxygen present in the reaction mixtures to give dialkyl peroxy compounds as the final product.

Finally, it is shown that irradiation of 9-thioxanthenols (e.g., **226**, **228** etc.) in aqueous solution (pH 7) results in adiabatic photodehydroxylation to give

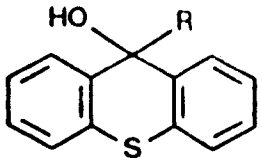

226 R = H **228** R = CH_3

220 R = Ph **229** R = CH_2Ph

the corresponding thioxanthenium carbocations in the S_1 state. The adiabaticity of the process is investigated by steady-state fluorescence studies. The reactivity of photogenerated thioxanthenium cations with added nucleophiles is also studied.

1.6 Experimental Approach

The rates of reaction of the various excited states either towards C-H

heterolytic cleavage, decarboxylation, electron transfer and dehydroxylation are of primary interest. Since these rate constants are not themselves directly measurable, use is made of directly measurable parameters, viz., the product quantum yields (Φ_p), fluorescence quantum yields (Φ_f) and fluorescence lifetimes (τ_f).

The results presented in this thesis were obtained in a systematic manner as follows. Initially, product studies were carried out to accumulate evidence for a working mechanism of the photoreaction being investigated. The photoproducts formed in a given reaction were identified and characterized by NMR, UV and GC/MS analyses. The product quantum yields, Φ_p, were determined to measure the efficiency of the photoreaction. The amount of photoproduct(s) formed was measured by GC-MS analyses or occasionally by ^{1}H NMR integrations. The light intensity at the wavelength of irradiation was monitored using chemical actinometry and quantified by either potassium ferrioxalate actinometry or GC/^{1}H NMR (in case of secondary photochemical actinometers). The mechanism was further probed by investigating the effect of solvent and isotopic substitution on the photoprocess. Whenever possible, steady-state fluorescence quenching studies were employed to measure the excited rate constants. The fluorescence lifetimes (τ_f) were measured by single photon counting. Finally, a mechanism of the photoprocess is proposed which is consistent with all the accumulated experimental data.

CHAPTER TWO

PHOTOGENERATION OF ANTIAROMATIC 8π CARBANIONS FROM OXYGEN AND SULFUR-CONTAINING DIBENZANNELATED SYSTEMS

2.1 Excited State Carbon Acid Behaviour of 9*H*-Xanthene (125) and 9*H*-Thioxanthene (136): Photogeneration of 8π-Electron Cyclically Conjugated Carbanions via Benzylic C-H Bond Heterolysis

2.1.1 Product Studies

2.1.1.1 Photolysis of 9*D*-Xanthene (123) in Aqueous Solution

Photolysis of a 10^{-3} M solution of 9*D*-xanthene (**123**) in 50% H_2O-CH_3CN at 300 nm (Rayonet RPR 100 photochemical reactor; ≈ 15-17 °C; Ar purged) for 1 hour did not result in any residual exchange of deuterium, and the starting material was recovered with some photodecomposition to give **126-129** (< 20%) (eq 2.3). However, photolysis of **123** in an aqueous NaOH solution resulted in the deuterium exchange at the benzylic position. Thus, photolysis of a 10^{-3} M solution of **123** in 50% 1M NaOH-EtOH (*ca.* 75 min), upon work up gave a mixture which was analyzed by ^{1}H NMR and GC/MS. The ^{1}H NMR (250 MHz) of the product mixture showed the appearance of a new unresolved triplet at δ 4.05 (J ≈ 1-2 Hz) (Figure 2.1). This peak was assigned to 9*D*,9*H*-xanthene (**124**) by comparison with the ^{1}H NMR spectra of an authentic sample. The aromatic proton signals did not change in the photolyzed sample. The amount of **124** formed was calculated to be ≈8%, by integrating the area under the peak at δ 4.05.

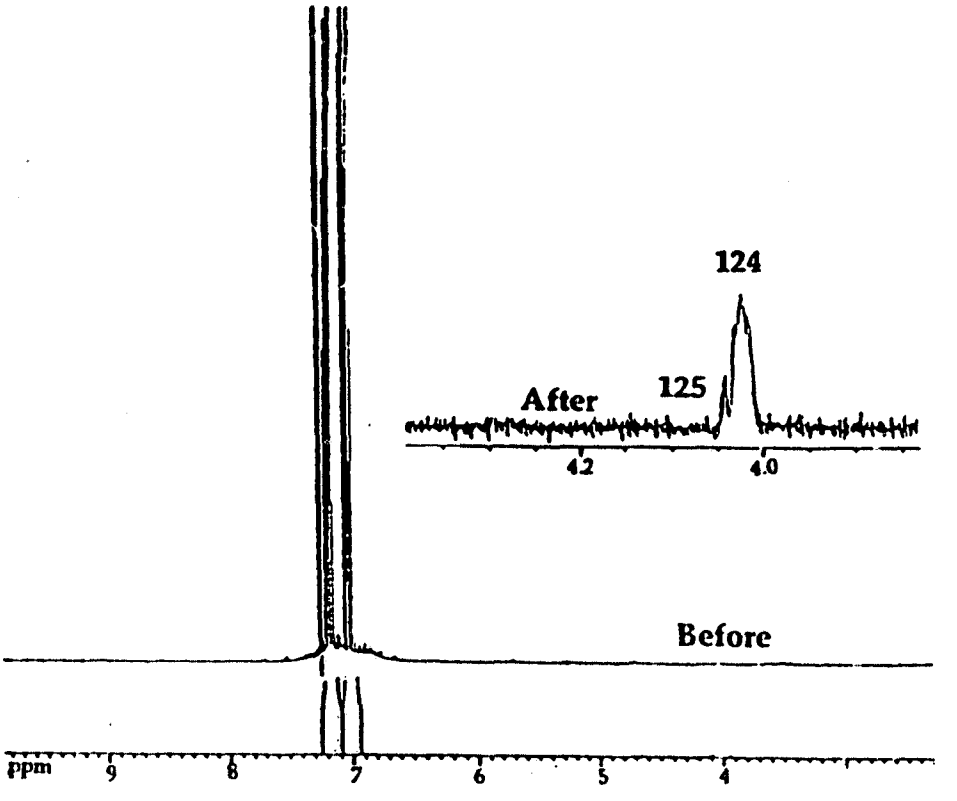

Figure 2.1 ^{1}H NMR (250 MHz) spectrum of **123** before and after (inset) photolysis in 50% 1 M NaOH-EtOH, showing formation of monodeuterated **124** and **125**.

However, the mass spectral analysis of the same product mixture showed the presence of both **124** (10%) and **125** (3%) (eq 2.1). It was not possible to

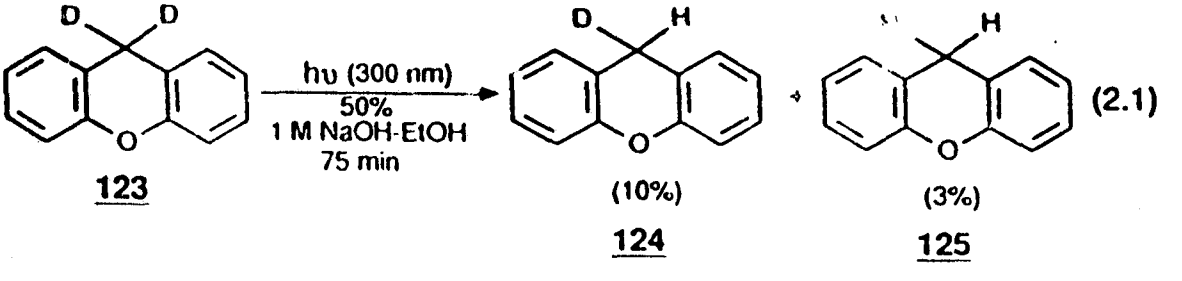

accurately determine the amount of **125** by ^{1}H NMR spectral analysis, because the triplet due to **124** at δ 4.05 overlaps the singlet due to **125** at δ ≈4.09 (Figure 2.1).

Photolysis of 9*H*-xanthene (125) in 50% 1 M NaOD-EtOD also resulted in the exchange of benzylic protons with the deuterons from the solvent to yield 124 (12%) and 123 (4%), as indicated by GC/MS analysis of the product mixture (eq 2.2).

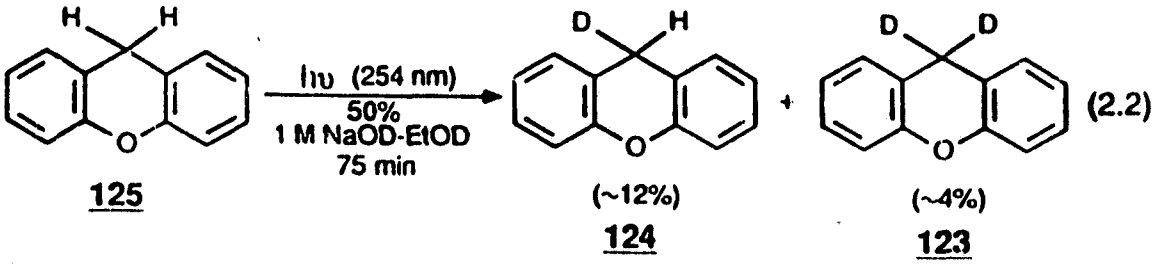

125 (~12%) **124** (~4%) **123**

The possibility that a residual amount of deuterium might be incorporated into the benzene ring positions **125** was examined by ^{2}H NMR. A solution of **125** in 50% 1 M NaOH-EtOH was irradiated for 1 hour and the reaction mixture, after work-up, was examined by ^{2}H NMR in CH_2Cl_2 with acetone-d_6 as internal standard. The spectrum of the product mixture showed a strong peak at $\delta \approx 4.1$, indicative of mono- and dideuteration (i.e., formation of **123** and **124**) at the benzylic position. No peak was observed in the aromatic region of the ^{2}H spectrum, clearly showing that the deuterium exchange takes place exclusively at the C-9 position of **125**.

The deuterium exchange of **123** with the solvent takes place only on irradiation. A control experiment where a solution of **123** in 50% 1 M NaOH-EtOH was left stirring in the dark for 1 hour did not result in deuterium exchange at the benzylic position. Increasing the concentration of NaOH (*ca.* 5 M) also did

not promote deuterium exchange in dark, and the unchanged starting material could be recovered after work-up.

The kinetics of exchange was followed by irradiating a solution of **123** in 50% 1 M NaOH-EtOH, and removing aliquots after set periods of time. The aliquots upon work-up were examined by ^{1}H NMR and GC/MS to determine the yields of products, viz., **124** and **125**, and starting material. The resulting plot of such an experiment is shown in Figure 2.2. It is clear from the plot that at short

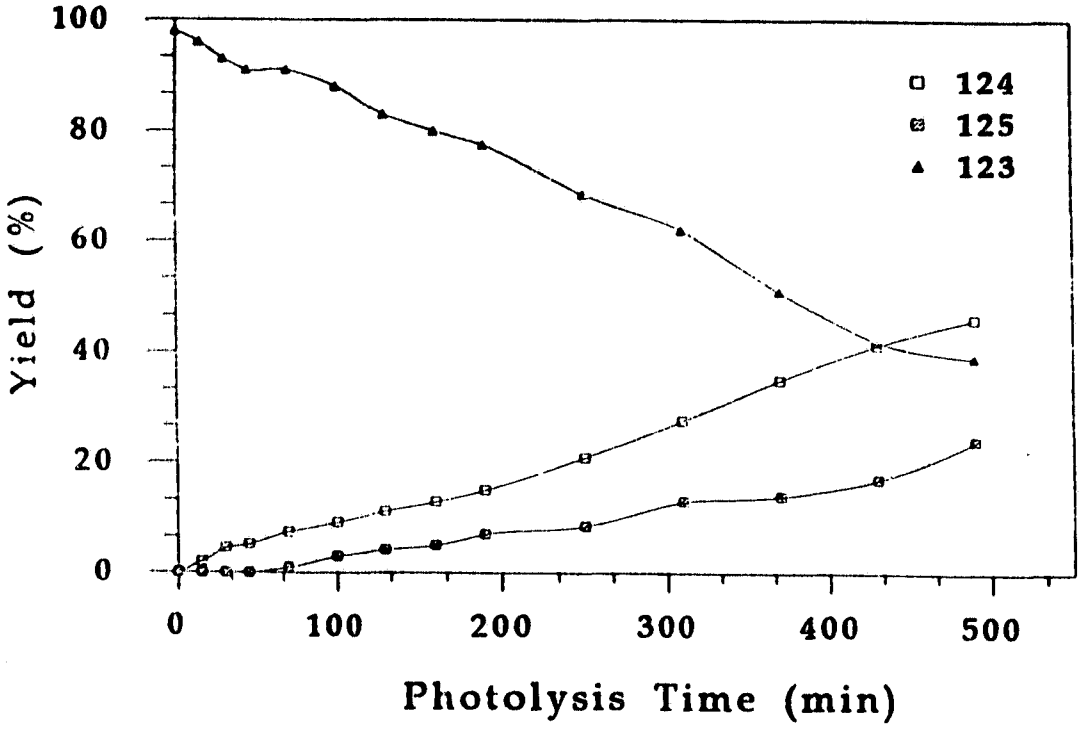

Figure 2.2 Plot of percent recovered **123** and yields of exchange photoproducts **124** and **125** vs photolysis time in 50% 1 M NaOH-EtOH.

photolysis times the only product observed is **124**, indicating that it is the primary photoproduct, which reacts via a secondary photoreaction to give **125**. This shows that the proton exchange in **123** is a sequential process.

Previous results obtained in our laboratories have shown that photolysis of **125** in 100% CH_3CN for 1-2 hours results in its photoisomerization to yield 6*H*-dibenzo[b,d]pyran (**126**) as a major product.[117] In addition to **126**, 2-benzylphenol (**127**), 9,9′-bisxanthene (**128**), and 2-(2′-hydroxyphenyl)benzyl (**129**) alcohol are also

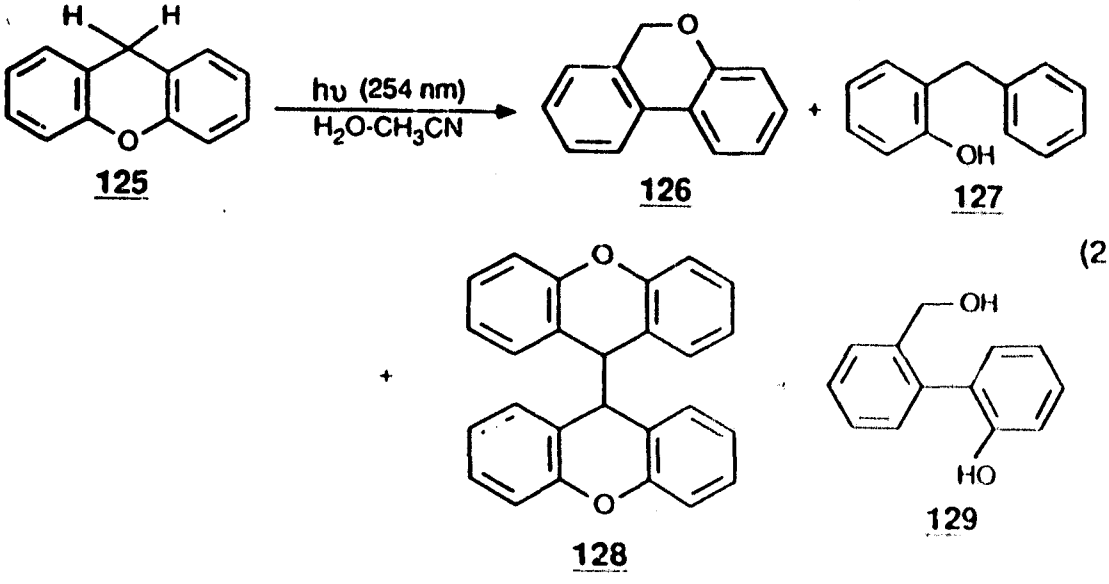

125 126 127 128 129 (2.3)

observed as minor products (eq 2.3). However, photolysis of **125** in 50% 1 M NaOH-EtOH for the same period of time did not give any isomerized product. This suggests that under these reaction conditions, benzylic proton exchange of **125** competes efficiently with its isomerization.

When **123** was photolyzed in 100% EtOH, in the absence of aqueous

NaOH, no protium incorporation at the benzylic position (to give **124**) was observed. This suggests that NaOH is the deprotonating base which abstracts deuteron from the excited **123** to form the intermediate 9-xanthenide carbanion (**130**), which is subsequently protonated by the solvent to give the overall

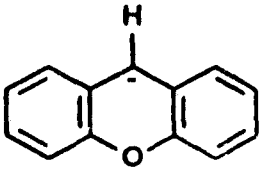

130

deuterium exchanged product **124**. The proposal that NaOH is the deprotonating base is further supported by the fact that when the concentration of NaOH in the photolyses of **123** in 50% NaOH-EtOH was increased, the yields of the exchanged products, viz., **124** and **125**, also increased (Table 2.1).

Table 2.1 Conversions to Exchange Photoproducts 124 and 125 in the Photolysis of 9*D*-Xanthene (123) in 50% NaOH-EtOH.

[NaOH][a]	% 124[b]	% 125[b]
1 M	10	3
2 M	16	5
3 M	23	7
4 M	33	11
5 M	40	14

a) A 10^{-3} M solution of **123** in 50% NaOH-EtOH photolysed at 300 nm for 75 min.
b) Product distribution analyzed by ^{1}H NMR (250 MHz) integration and GC/MS analyses; errors in calculated percentages are estimated to be ≤ 3%.

An alternative possibility which could account for the protium incorporation in **123** involves initial homolysis of the benzylic C-D bond to generate 9-xanthenyl radical (**131**), which subsequently abstracts hydrogen from

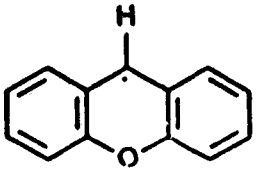

131

the solvent to give deuterium exchange product **124**. However, deuterium exchange via C-H(D) homolysis can be ruled out since no deuterium/protium incorporation is observed when **123**/**125** was photolyzed in 100% CH_3CN (or 100% 2-PrOH), a better hydrogen donating solvent than H_2O or EtOH. In addition, any photogenerated 9-xanthenyl radical (**131**) would be expected to dimerize efficiently to give **128**, which was not observed in these photolyses.

2.1.1.2 Photolysis of 123 in the Presence of Ethanolamine

Photolysis of a 10^{-3} M solution of **123** in 100% CH_3CN in the presence of 5.0 M ethanolamine (*ca.* 10 min) resulted in the formation of **125** (≥ 98%) as the only observable product by ^1H NMR. However, when a similar solution was irradiated for a shorter period of time (*ca.* 5.0 min) both **124** (≈60%) and **125** (≈24%) were observed in the ^1H NMR spectrum of the reaction mixture (eq 2.4). No deuterium exchange took place when a solution of **123** in 100% CH_3CN was irradiated (however efficient isomerization of **123** was observed (*vide supra*)),

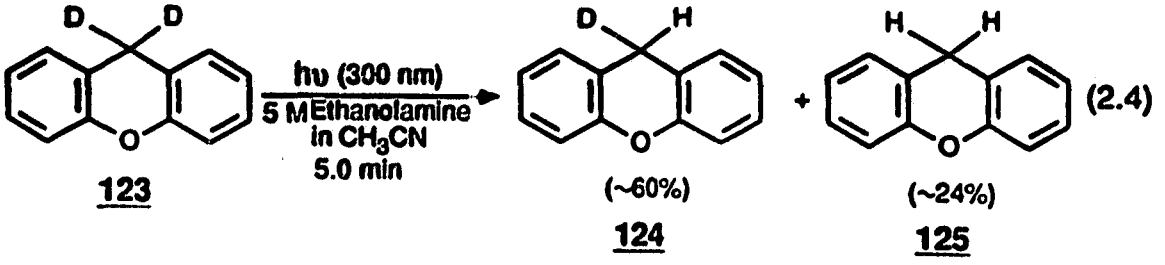

123 (~60%) 124 (~24%) 125

suggesting that ethanolamine acts as the deprotonating base. This is further supported by the increase in quantum yields (Φ's) of deuterium exchange (to give **124**) as the concentration of ethanolamine is increased (*vide infra*). Control experiments showed that deuterium exchange of **123** does not take place in the dark, clearly demonstrating that the observed deuterium exchange in the presence of ethanolamine is a photochemical process.

A comparison of the amounts of monodeuterium exchange product **124** formed in the photolyses of **123** in the presence of aqueous NaOH and ethanolamine indicates that ethanolamine in CH_3CN is a much better base at promoting deuterium exchange than aqueous NaOH in 95% EtOH. The possible reason(s) for these differences are not clear at this stage.

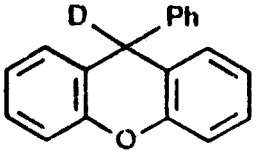

132

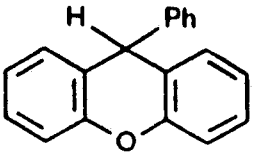

133

Photolyses of related system 9-phenyl-9*D*-xanthene (**132**) and 9-phenyl-9*H*-xanthene (**133**) were also carried out to investigate the effect of substituent on the

exchange process. However, photolysis of **133** in 50% NaOH-EtOH (*ca.* 2 h) or in the presence of ethanolamine in CH_3CN did not result in deuterium exchange at the benzylic position. Instead, efficient isomerization of **133** (possibly similar to the isomerization of **125** in 100% CH_3CN)[117] was observed. However, repeated attempts to determine the structure of the isomerized produ. were of no avail. Increasing the concentration of bases (NaOH or ethanolamine; *ca.* 5 M) also did not promote exchange in **133**, and only isomerization of **133** was observed.

2.1.1.3 Photolysis of 9*D*-Thioxanthene (134) in Aqueous Solution

Photolysis of 9*D*-thioxanthene (**134**) in 50% H_2O-CH_3CN (λ_{ex} = 300 nm) also did not result in deuterium exchange at the benzylic position. However, irradiation of a 10^{-3} M solution of **134** in 50% 1 M NaOH-EtOH (*ca.* 30 min) resulted in deuterium exchange at the benzylic position with the solvent. The ^{1}H NMR (250 MHz) spectrum of the reaction mixture showed the appearance of a new unresolved triplet at δ 3.82 (J ≈ 1-2 Hz) (Figure 2.3) due to monodeuterated **135** and a singlet at δ 3.85 due to 9*H*-thioxanthene (**136**) (eq 2.5). The

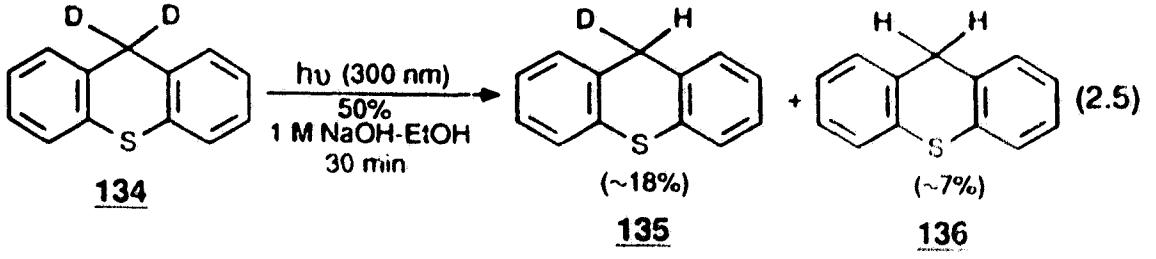

assignments of the photoproducts were based on the comparison with the ^{1}H NMR spectra of authentic materials. Based on the ^{1}H NMR integration the

amounts of **135** and **136** present in the reaction mixture were calculated to be ≈18% and ≈7% respectively, (eq 2.5). No reaction took place when **134** was photolyzed in 100% EtOH, and the starting material was recovered quantitatively. No deuterium exchange at the benzylic position of **134** takes place in the absence of irradiation, clearly showing that the deuterium exchange is a photochemical process.

Photolysis of 9*H*-thioxanthene (**136**) in 50% 1 M NaOD-EtOD also resulted in the formation of monodeuterated **135** (≈21%) and dideuterated **134** (≈9%) (eq 2.6). No deuterium incorporation takes place in the benzene ring proton

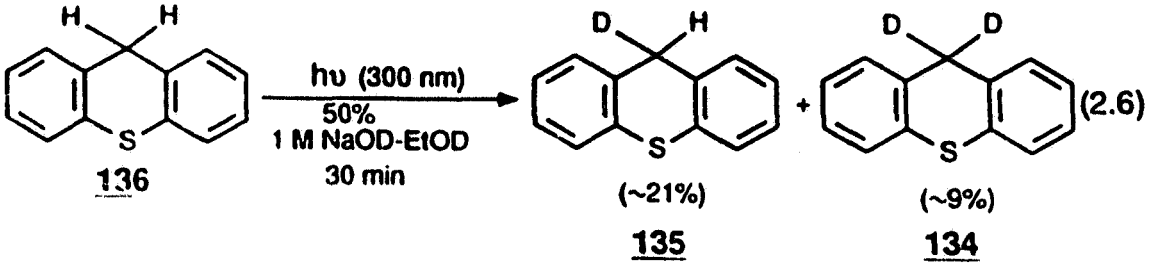

positions. The ^2H NMR (CH_2Cl_2 with acetone-d_6 as internal standard) of the reaction mixture showed a strong peak at $\delta \approx 3.85$, indicative of mono- and dideuteration at the benzylic position; no peak was observed in the aromatic region (between δ 7.0-7.5).

The extent of proton exchange in photolysis of **134** in 50% NaOH-EtOH increased with the increasing NaOH concentration. The results obtained in the photolysis of **134** at varying NaOH concentrations are presented in Table 2.2. The amount of exchange products formed (viz., **135** and **136**) were calculated by ^1H NMR and GC/MS analyses. In general, good agreements, between the ^1H NMR

and MS data, for the calculated percentages of **135** and **136** were observed.

Table 2.2 Conversions to Exchange Photoproducts 135 and 136 in the Photolysis of 9*D*-Thioxanthene (134) in 50% NaOH-EtOH.

[NaOH][a]	% 135[b]	% 136[b]
1 M	18	7
2 M	22	9
3 M	29	11
4 M	35	13
5 M	43	15

a) A 10^{-3} M solution of **134** in 50% NaOH-EtOH photolysed at 300 nm for 30 min each.
b) Product distribution analyzed by ^{1}H NMR (250 MHz) integration and GC/MS; errors in calculated percentages are estimated to be ≤ 3%.

The kinetics of exchange was followed by ^{1}H NMR using **134** as the starting material. Thus a solution of 250 mg of **134** in 50% 1 M NaOH-EtOH was irradiated and aliquots removed after set periods of irradiation, and yields of products **135**, **136** and starting material were calculated by ^{1}H NMR spectral analyses. The production of monodeuterated **135** and 9*H*-thioxanthene (**136**) with photolysis time was monitored by the growth of ^{1}H NMR peaks at δ 3.82 and 3.85 respectively (Figure 2.3). The resulting plot of percentages yields vs photolysis

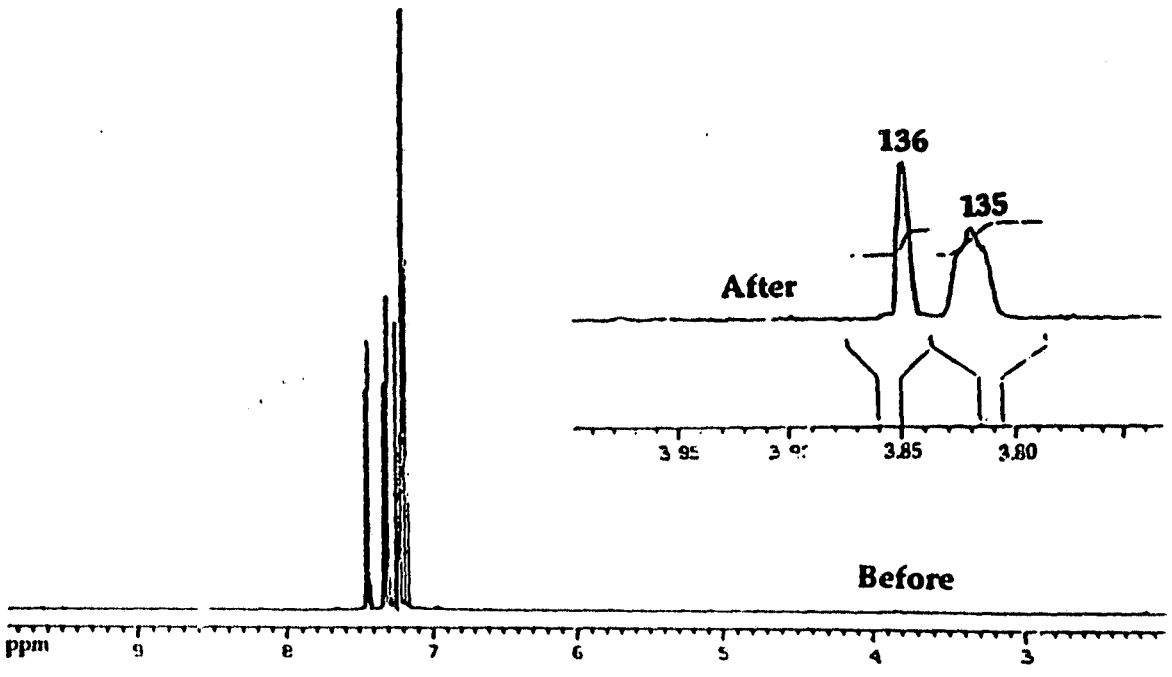

Figure 2.3 ^{1}H NMR (250 MHz) spectrum of **134** before and after (inset) photolysis in 50% 1 M NaOH-EtOH, showing formation of monodeuterated **135** and **136**.

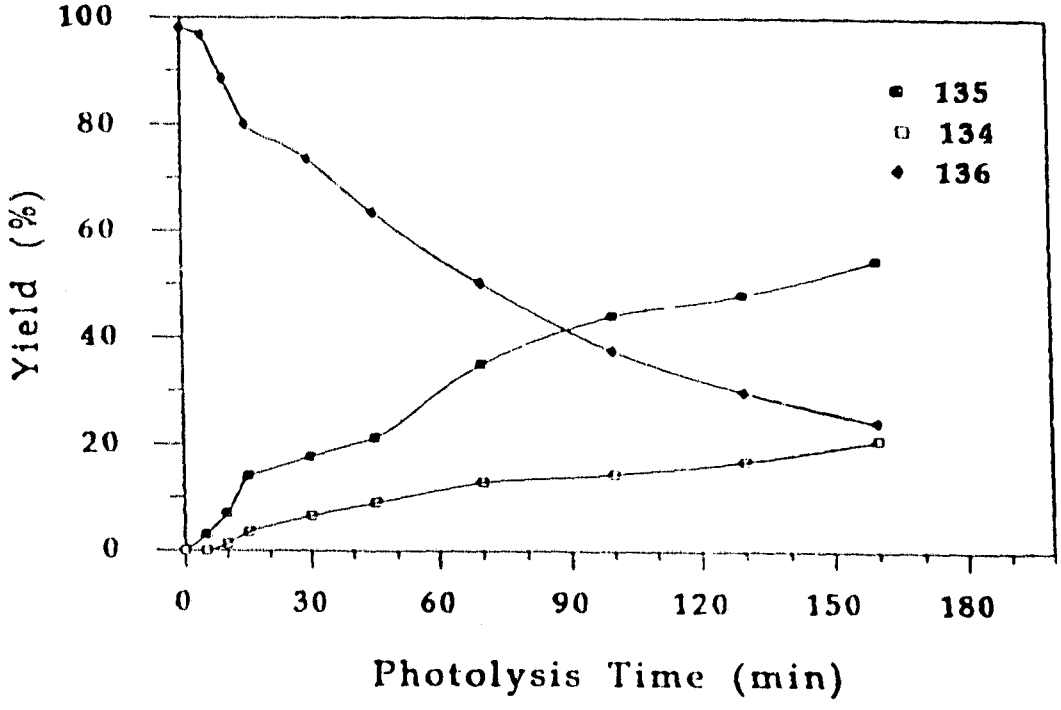

Figure 2.4 Plot of percent recovered **134** and yields of exchange photoproducts **135** and **136** vs photolysis time in 50% 1 M NaOH-EtOH.

time is shown in Figure 2.4. It is evident from this plot that the primary exchange product is monodeuterated **135**, which reacts via a secondary photoreaction to yield **136**.

The results obtained in the photochemical exchange studies of **134** (and **136**) strongly implicate the intermediacy of 9-thioxanthenide carbanion (**137**). The

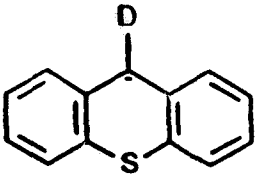

137

deuterium incorporation in **136** on photolysis in 50% NaOD-EtOD and protium incorporation in **134** on photolysis in 50% NaOH-EtOH are consistent with the 9-thioxanthenide carbanion (**137**) intermediate. Furthermore, the absence of protium/deuterium exchange when photolysis was carried out in 100% EtOH(D) suggests that NaOH(D) is the deprotonating base which abstracts proton (or deuterium) from the benzylic position of excited **136** to give the intermediate carbanion **137**. Increase in the exchange product (viz., **135** and **136**) yields with increasing NaOH concentration (Table 2.2) also supports the notion that NaOH is the deprotonating base.

2.1.1.4 Photolysis of 134 in the Presence of Ethanolamine

Photolysis of a 10^{-3} M solution of **134** in the presence of 0.5 M ethanolamine in CH_3CN (*ca.* 1 h) resulted in the formation of monodeuterated **135**

(≈11%) and **136** (≈4%) (eq 2.7). The reaction of **134** in the presence of

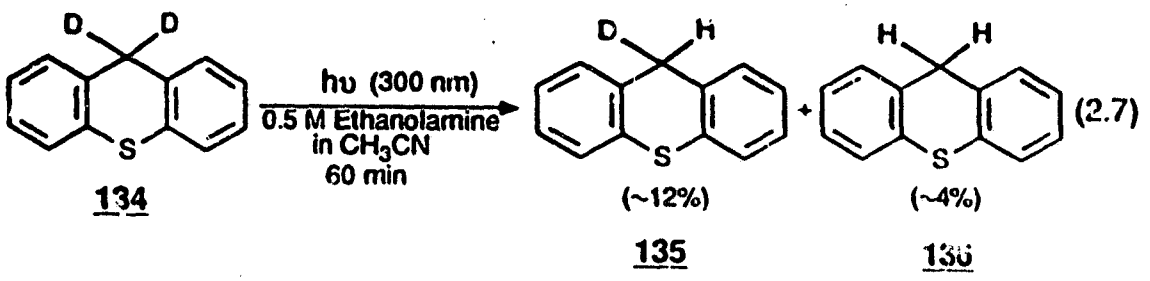

134 (~12%) **135** (~4%) **136**

ethanolamine was sluggish (unlike **123**) compared to its reaction in the presence of aqueous NaOH, as calculated by the amount of photoproducts (**135** and **136**) formed in these reactions. However, as the concentration of ethanolamine in CH_3CN was increased the yields of exchange products (**135** and **136**) increased, suggesting that ethanolamine was acting as the deprotonating base (*vide infra*).

Photolyses of related systems, 9-phenyl-9*D*-thioxanthene (**138**) and 9-phenyl-9*H*-thioxanthene (**139**) were also carried out. However, photolysis of **138**

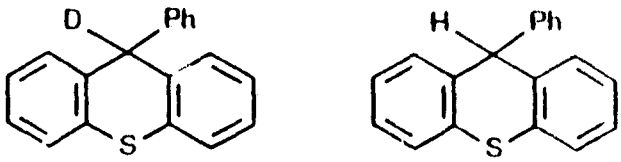

138 **139**

at various concentrations of NaOH and ethanolamine failed to result in any observable deuterium exchange. A possible reason for this behaviour could be the presence of phenyl group at the C-9 position which hinders the approach of the base thereby preventing it from abstracting the proton, which is the key step to observe exchange.

Photolysis of the isoelectronic system N-methylacridan (**140**) was also carried out to investigate the possibility of benzylic C-H bond heterolysis. However, photolysis of **140** in 50% D_2O-CH_3CN or in the presence of ethanolamine did not result in deuterium exchange at the benzylic position. Instead, a new product, viz., bis(N-methylacridyl) (**141**) was formed in these photolyses. Results of the photolyses of **140** and the mechanism of the formation of **141** will be discussed separately in detail (*vide infra*).

2.1.2 Quantum Yields

The efficiency with which the supplied light converts the starting material to product is measured by the quantum yield of product formation. The quantum yield (Φ) for formation of a particular product is given by eq 2.8.

$$\Phi = \text{moles of product formed/moles of light absorbed} \qquad (2.8)$$

Quantum yields (Φ's) for mono deuterium incorporation in **125** and **136** and mono protium incorporation in **123** and **134** were measured on an optical bench using the output of an Oriel 200-W Hg arc lamp with the monochromator set at λ_{ex} = 280 nm. Potassium ferrioxalate actinometry was employed to measure the lamp intensity at this excitation wavelength.[118] In general, 10^{-3}-10^{-4} M solutions of the substrates in an appropriate solvent mixture were irradiated with continuous purging with a stream of argon prior to and during the photolysis,

which served to deaerate as well as stir the reaction mixtures. The conversions to exchange products were kept between 15-20%, and the amount of deuterium incorporation in products was measured by GC/MS analyses.

Table 2.3 presents the Φ's of monodeuterium incorporation in **125** and **136** in 50% 1 M NaOL-EtOL (L = H and D) mixture. No deuterium incorporation

Table 2.3 Quantum Yields (Φ) of Formation of 124 and 135 on Photolysis in 50% NaOL-EtOL (L= H and D).

	Φ^c (124)	Φ^c (135)
Φ_H 50% 1 M NaOD-EtOD[a]	0.00019 ± 0.00004 (from **125**)	0.020 ± 0.005 (from **136**)
50% 1 M NaOH-EtOH[b] Φ_D	0.00021 ± 0.00002 (from **123**)	0.018 ± 0.004 (from **134**)
	Φ_H/Φ_D = 0.90 ± 0.10	Φ_H/Φ_D = 1.11 ± 0.05

a) Photolysis of 10^{-3} M solutions of **125** and **136**.
b) Photolysis of 10^{-3} M solutions of **123** and **134**.
c) Errors quoted are the standard deviation of three independent runs.

takes place in the absence of NaOL. In addition, the quantum yields for exchange (Φ's) obtained in NaOL-EtOL. (L = H or D) showed no significant isotope effect (Φ_H/Φ_D = 1.00 ± 0.10 (Table 2.3)), even though the initial process required for exchange involves C-H vs C-D bond cleavage. Quantum yields (Φ's) of protium incorporation in **123** and **134** in 50% NaOH-EtOH at various concentrations of NaOH were also measured and are presented in Table 2.4. Consistent with the

results of product studies, the Φ's of exchange photoproducts, viz., **124** and **135**, increase with the increasing concentration of NaOH.

Table 2.4 Quantum Yields (Φ) for Monoprotium Incorporation into 123 and 134 at Various Concentrations of NaOH in 50% NaOH-EtOH Solutions.[a,b]

[NaOH]	Φ[c] (123)	Φ[c] (134)
1 M NaOH	0.00021 ± 0.00002	0.018 ± 0.0005
2 M NaOH	0.00026 ± 0.00003	0.022 ± 0.002
3 M NaOH	0.00035 ± 0.00003	0.026 ± 0.003
4 M NaOH	0.00181 ± 0.00005	0.028 ± 0.003
5 M NaOH	0.00350 ± 0.0005	0.032 ± 0.002
50% H_2O-CH_3CN	0.00	0.00
100% EtOH	0.00	0.00

a) Determined by mass spectral analyses of 2-3 independent runs.
b) For solubility reasons 50% EtOH (v/v) used as co-solvent.
c) Errors quoted are standard deviations of 3 independent measurements.

Quantum yields (Φ's) of deuterium exchange for **123** and **134** were also measured in the presence of ethanolamine in dry CH_3CN. Table 2.5 presents the Φ's of monodeuterium exchange of **123** and **134** at various concentrations of ethanolamine. Comparisons of Φ's of monodeuterium incorporation from Tables

Table 2.5 Quantum Yields (Φ) for Monoprotium Incorporation into 123 and 134 at Various Concentrations of Ethanolamine.[a,b]

[Ethanolamine]	Φ^c (123)	Φ^c (134)
1 M	0.0074 ± 0.0002	0.0056 ± 0.0005
2 M	0.0098 ± 0.0004	0.0074 ± 0.0003
3 M	0.0141 ± 0.0002	0.0090 ± 0.0004
4 M	0.0173 ± 0.0002	0.0100 ± 0.0020
5 M	0.0193 ± 0.0003	0.0140 ± 0.0003
6 M	0.0240 ± 0.003	0.0173 ± 0.0004
100% CH_3CN	0.00	0.00

a) Determined by mass spectral analyses of 2-3 independent runs.
b) Ethanolamine solutions made in dry CH_3CN.
c) Errors quoted are standard deviations of 3 independent measurements.

2.4 and 2.5 reveals that ethanolamine (in CH_3CN) is a better base at promoting exchange of **123** than aqueous NaOH; whereas, in the case of **134** aqueous NaOH appears to be a better base at promoting exchange than ethanolamine. These results corroborate those obtained in the preparative scale photolyses of these compounds.

2.1.3 Steady-State Fluorescence and Lifetime Studies

Steady-state fluorescence quenching studies provide a crucial way to investigate the reactivity of excited singlet (S_1) states. For molecules with

fluorescent S_1, quenching is observed as a diminution of the intensity of light emission. A variety of processes can result in quenching including excited state reactions, energy transfer, complex formation, and collisional quenching. In the present context we are primarily concerned with quenching resulting from collisional encounters between the fluorophore and quencher, which is called collisional or dynamic quenching. Collisional quenching of fluorescence is described by the Stern-Volmer relationship[119] (eq 2.9).

$$F^0/F = 1 + k_q\tau_0[Q] = 1 + K_{SV}[Q] \qquad (2.9)$$

In eq 2.9, F^0 and F are the fluorescence intensities in the absence and presence of quencher, respectively, k_q is the bimolecular quenching constant, τ_0 is the lifetime of fluorophore in the absence of quencher, [Q] is the concentration of quencher, and $K_{SV} = k_q\tau_0$ is the Stern-Volmer quenching constant. A plot of F_0/F vs [Q] yields an intercept of one on the *y* axis and a slope equal to K_{SV}. Alternatively, since collisional quenching is a rate process which depopulates the S_1, the lifetimes of fluorophore in the absence (τ_0) and presence (τ) of quencher can be used to investigate the collisional quenching phenomenon. The Stern-Volmer equation which describes the lifetimes quenching is given by eq 2.10.

$$\tau_0/\tau = 1 + k_q\tau_0[Q] \qquad (2.10)$$

Eq 2.10 illustrates an important characteristic of collisional quenching, which is an equivalent decrease in fluorescence intensity and lifetime (eq 2.11),

$$F_0/F = \tau_0/\tau \qquad (2.11)$$

The decrease in lifetime occurs because quenching is an additional rate process which depopulates the S_1. The diminution in fluorescence intensity occurs because the quenching rate depopulates the S_1 without fluorescence emission. A good agreement between the quenching rates, k_qs, obtained by fluorescence intensity and lifetimes quenching methods is indicative of collisional or dynamic quenching. Sometimes fluorescence intensity diminution is also observed when the fluorophore and quencher form a complex in the ground state (called static quenching). Fluorescence quenching data, obtained by intensity measurement alone, can be explained by either dynamic or static processes. The measurements of fluorescence lifetimes is the most definitive method to distinguish between static and dynamic quenching. Static quenching removes a fraction of fluorophores from observation. The complexed fluorophores are nonfluorescent and the only observed fluorescence is from the uncomplexed fluorophore. The uncomplexed fraction of fluorophores is unperturbed, and hence the lifetime is τ_0. Therefore, for static quenching $\tau_0/\tau = 1$. In contrast, for dynamic quenching, $F_0/F = \tau_0/\tau$.[119]

In the present study the kinetics of proton/deuteron exchange was

investigated by both fluorescence emission intensity and lifetime quenching methods. The fluorescence emission and excitation spectra of **125** in dry CH_3CN are shown in Figure 2.5. Addition of ethanolamine quenched the emission

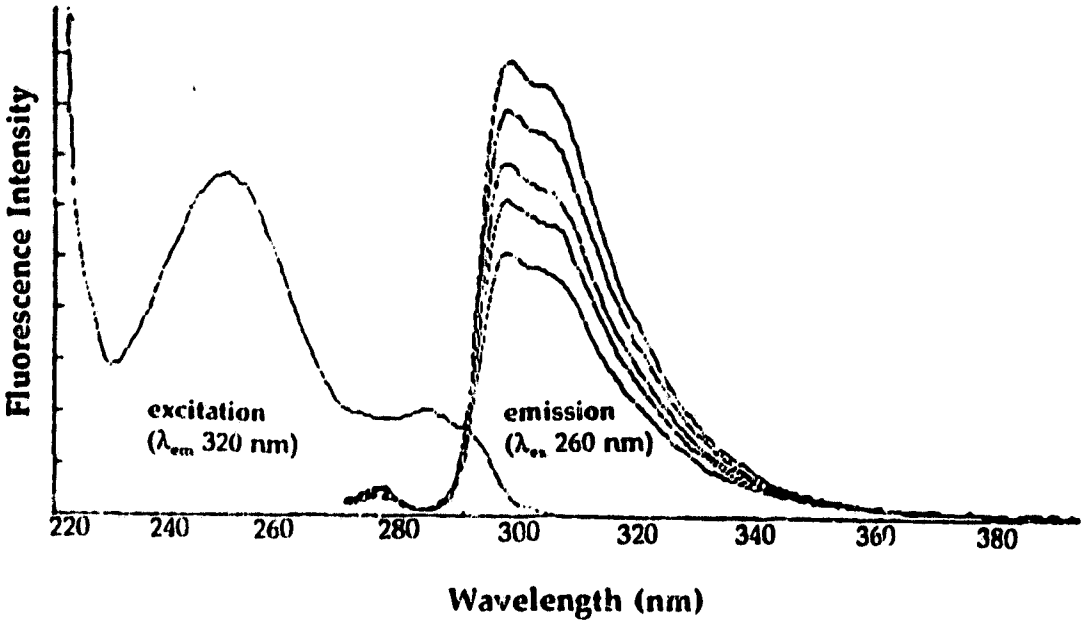

Figure 2.5 Fluorescence quenching of **125** in CH_3CN by added ethanolamine.

intensity of **125** in CH_3CN. The deuterated analogue **123** also displayed similar fluorescence emission quenching. However, the emission of 9-phenyl-9*H*-xanthene (**133**) in CH_3CN was not quenched by added ethanolamine. Stern-Volmer analyses of fluorescence emission quenching of **123** and **125** by ethanolamine resulted in good linear plots. The calculated steady-state fluorescence quenching rate constants (k_q) are shown in Table 2.7 (*vide infra*).

Fluorescence lifetimes (τ's) of **123** and **125** measured at different

Table 2.6 Lifetimes of 125 and 123 in CH_3CN at Various Concentrations of Ethanolamine.

[Ethanolamine][a]	Lifetimes (τ)[b]	
	125 (ns)	123 (ns)
100% CH_3CN	7.59 ± 0.03	7.72 ± 0.04
0.30 M	7.28 ± 0.02	7.56 ± 0.03
0.60 M	7.09 ± 0.03	7.41 ± 0.02
0.90 M	6.81 ± 0.04	7.25 ± 0.02
1.20 M	6.44 ± 0.04	7.05 ± 0.04
1.50 M	6.09 ± 0.05	6.77 ± 0.04
2.00 M	5.75 ± 0.04	6.53 ± 0.03

a) Freshly made ethanolamine solutions in dry CH_3CN.
b) Lifetimes (τ) obtained via Single Photon Counting; λ_{ex} 260 nm and λ_{em} 320 nm; all decays were single exponential with fitting parameter $\chi^2 \leq 1.30$.

ethanolamine concentrations in CH_3CN are presented in Table 2.6. It can be seen that lifetimes (τ's) of both **123** and **125** decrease with increasing ethanolamine concentration. However, the lifetime of **125** is quenched faster than the lifetime of **123**. A Stern-Volmer analysis of the lifetime quenching of **123** and **125** by ethanolamine resulted in good linear plots (Figure 2.6). The k_q's calculated from

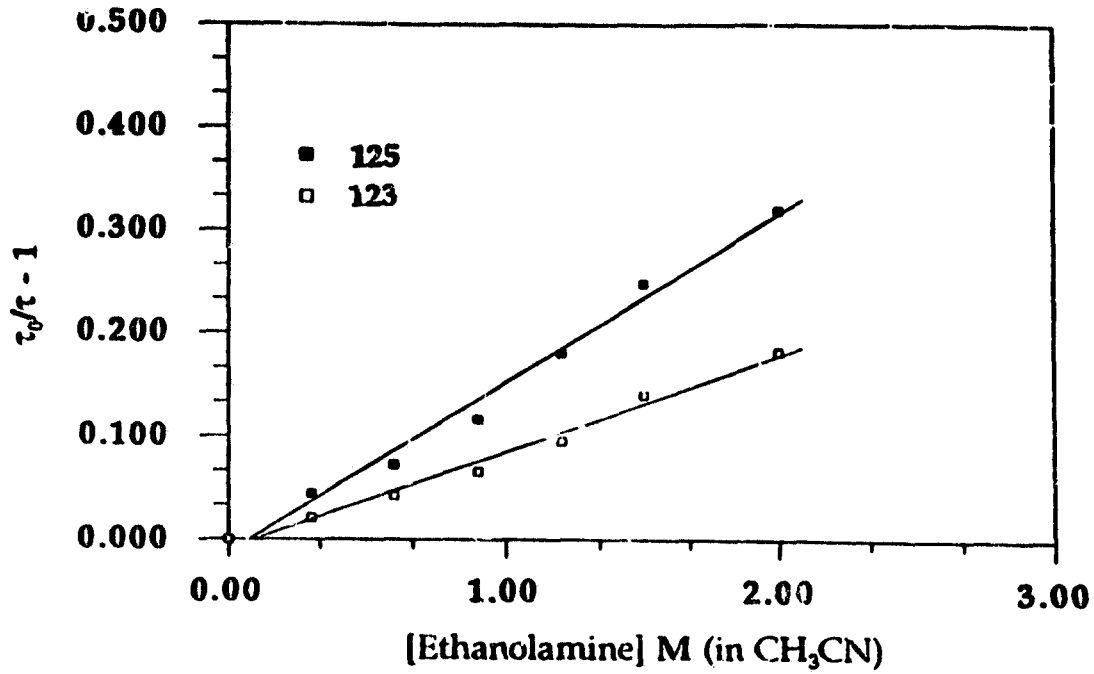

Figure 2.6 Representative Stern-Volmer plot of lifetime (τ) quenchings of **123** and **125** in CH_3CN by added ethanolamine.

Table 2.7 Fluorescence Quenching Rate Constants (k_q's) for 9*H*-Xanthene (125) and 9*D*-Xanthene (123) by Ethanolamine in CH_3CN.[a]

	k_q (M^{-1} s^{-1})	
	Steady-State[b]	Lifetimes[c]
123	(1.18 ± 0.04) x 10^7	(1.12 ± 0.05) x 10^7
125	(2.52 ± 0.05) x 10^7	(2.16 ± 0.05) x 10^7
k_H/k_D	2.18 ± 0.05	1.92 ± 0.04

a) By standard Stern-Volmer analyses of quenching.
b) Steady-state fluorescence spectra obtained by excitation of an argon purged (ca. 5.0 min) ≈10^{-7} M solutions of **123** and **125** at λ_{ex} = 260 nm.
c) Lifetimes (τ) obtained via single photon counting; λ_{ex} = 260 nm, λ_{em} = 320 nm; all decays were single exponential with fitting parameter $\chi^2 \leq 1.3$.

the Stern-Volmer analyses of lifetimes quenching of **123** and **125** by ethanolamine are presented in Table 2.7. It can be seen that there is a good agreement, within experimental errors, between the k_q's obtained by steady-state fluorescence quenching (k_q^{ss}) and lifetime quenching (k_q^{τ}) methods, indicating that the observed fluorescence quenching is a dynamic phenomenon (*vide supra*). A significant primary isotope effect, $(k_H/k_D)_q = 2.00 \pm 0.05$, is observed in the fluorescence quenching rates of **123** and **125** (Table 2.7). This result is consistent with C-L (L = H and D) bond heterolytic cleavage in the S_1 state with ethanolamine acting as the deprotonating base.

Attempts were also made to investigate the fluorescence quenching of **123** and **125** in 95% ethanol by aqueous NaOH. At low concentrations of NaOH (*ca.* 0.025 M) the emission of **123** in ethanol was quenched. However, at higher concentrations of NaOH the emission spectrum of **123** (and **125**) was distorted, which prevented a systematic fluorescence quenching study.

The fluorescence quenching studies of 9*H*-thioxanthene (**136**) (and **134**) were hampered due to its weak fluorescence ($\Phi_f = 0.020 \pm 0.005$ in CH_3CN; relative to suberene (**37**)[48] $\Phi_f = 0.86$). This is presumably due to the presence of the sulfur atom which promotes the intersystem crossing (ISC) rate of excited **136**. It is well known that presence of a heavy atom (e.g., sulfur) in molecules promotes the rate of ISC via spin-orbit interactions ("heavy atom effect").[120] The excitation and emission spectra of **136** in dry CH_3CN are presented in Figure 2.7.

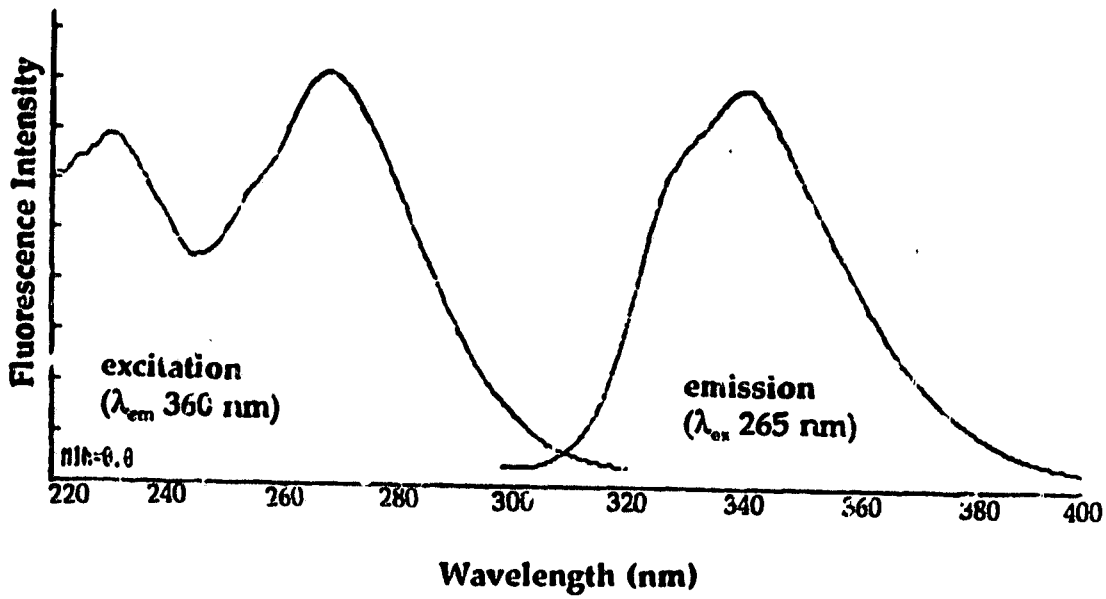

Figure 2.7 Excitation and emission spectra of 9*H*-thioxanthene (**136**) in CH_3CN.

Although fluorescence emission of **136** in CH_3CN was quenched by added ethanolamine, estimates of the quenching rate constant (k_q) from these data were not reproducible due to the weak fluorescence.

In previous studies[46] it has been shown that molecules like fluorene (**36**) and dibenzosuberane (**49**) (which do not undergo deuterium exchange at the benzylic position on irradiation in 50% D_2O-CH_3CN) do not exhibit fluorescence quenching by H_2O. In contrast, the fluorescence emission of suberene (**37**) in CH_3CN, which undergoes deuterium exchange via suberenyl carbanion (**35**) on irradiation in 50% D_2O-CH_3CN, is efficiently quenched by added H_2O (k_q = 1.71 ± 0.04 x 10^8 M^{-1} s^{-1}).[48] It has been proposed that the emission of suberene (**37**) is quenched via deprotonation of benzylic protons by H_2O in S_1.[48] In the present

study, the fluorescence emission of both 9*D*-xanthene (123) and 9*D*-thioxanthene (134) in CH_3CN are quenched by added ethanolamine - a solvent system in which these molecules exhibit deuterium exchange at the benzylic position (*vide supra*). That is, the singlet excited states of 123 and 134 are quenched via deprotonation of benzylic protons by ethanolamine. On the other hand, the 9-phenyl analogues, 132 and 138, which do not undergo deuterium exchange with ethanolamine, do not exhibit fluorescence quenching by added ethanolamine.

2.1.4 Mechanism of Exchange: Excited State Carbon Acids

In principle any organic compound that contains a C-H bond can function as a carbon acid in the classical sense by donating a proton to a suitable base.[121] However, deprotonation rates from C-H acids in the ground state are typically slow because of the lack of hydrogen bonding to the solvent and the substantial geometrical and solvation changes generally required on deprotonation of carbon acids.[43,44,121] If this holds true for electronically excited states as well, then such intrinsically slow rates for deprotonating C-H bonds would not compete favourably with the fast rates of decay intrinsic to an excited molecule.

Many organic molecules become more acidic or basic in the singlet excited state. This has been predicted based on Förster cycle calculations. The Förster cycle combines thermodynamic and spectroscopic data to predict the chemical equilibrium constants in the excited state.[122] For a simple deprotonation of the acid AH shown by the equilibrium of eq 2.12, it is possible to visualize both

ground and excited state process, as shown in Figure 2.8, with the appropriate energies connecting the various levels.

$$AH^* \rightleftharpoons A + H^+ \qquad (2.12)$$

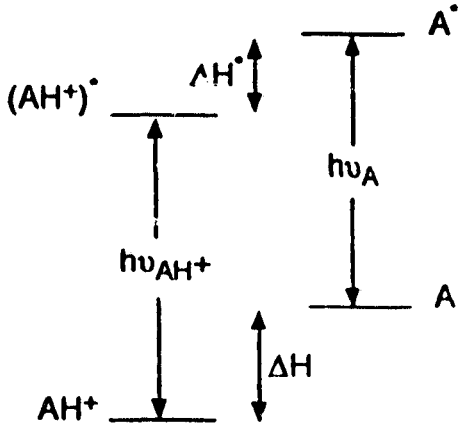

Figure 2.8 Förster cycle for the acid-base equilibrium given in equation 2.12.

The Förster cycle gives rise to eq 2.13,

$$\Delta H^* - \Delta H = N_A h(\nu_A + \nu_{AH^+}) \qquad (2.13)$$

where, ΔH^* and ΔH are the enthalpy changes in the excited and the ground states, ν_A and ν_{AH} are the frequencies of the lowest absorption bands of A and AH^+, h is the Planck's constant and N_a is the Avogadro number. Assuming,

$$\Delta H^* - \Delta H \sim \Delta G^{*0} - \Delta G^0 \qquad (2.14)$$

then,

$$\Delta pK = N_a h(\nu_A + \nu_{AH^+})/2.303RT \qquad (2.15)$$

The derivation of eq 2.15 assumes that: (a) the entropy of protonation, ΔS^0, is the same in the ground and excited states; (b) the 0-0 bands of either emission or absorption are accurately known.

Based on Förster cycle calculations, fluorene (**36**) ($pK(S_0)$ of benzylic protons ~21-23 in DMSO) has been predicted to become vastly more acidic in the S_1 state ($pK(S_1)$ = -8.5).[40] However, photoexcitation of fluorene (**36**) in D_2O does not result in deuterium exchange of the benzylic protons.[48] That is, fluorene (**36**) does not function as an excited state carbon acid. Failure to observe any proton exchange on excitation of **36** may be due to the intrinsically short lifetimes of the S_1, which competes favourably with the slow deprotonation rate of C-H bond. However, photoexcitation of suberene (**37**) ($pK(S_0)$ ~30; $pK(S_1)$ ≈ -7) in 50% D_2O-CH_3CN results in exchange of benzylic protons to give deuterium incorporated product (eq 1.11).[48] The proposed mechanism of the deuterium exchange involves benzylic C-H bond clevage in S_1 to give the intermediate suberenyl carbanion **35**,

which on subsequent deuteration from the solvent D_2O gives the overall exchange product. That is, suberene (37) acts like a carbon acid in the S_1 state.

The isoelectronic systems 9*H*-xanthene (125) and 9*H*-thioxanthene (134) also act as carbon acids in S_1. The results obtained in the product and steady-state fluorescence studies of 123 and 134 are suggestive of an ionic mechanism for the observed deuterium exchange from S_1. A mechanism consistent with all available data is presented in Scheme 2.1. In this mechanism, the base ethanolamine

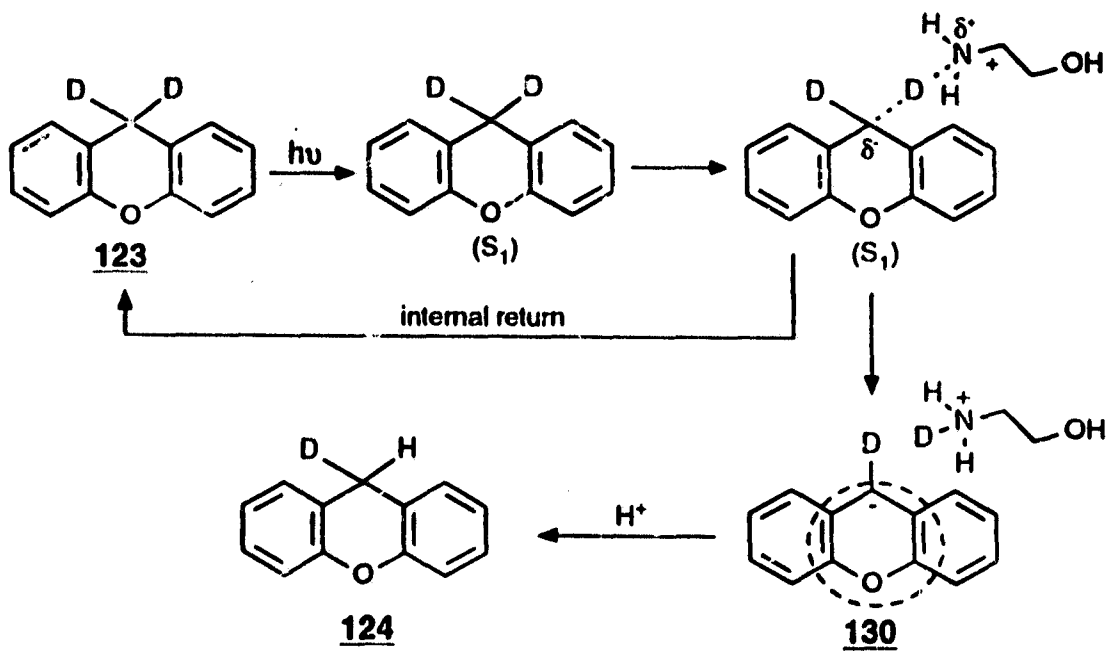

Scheme 2.1

abstracts the deuteron at the benzylic position of 123 in S_1 to give the intermediate

9-xanthenide carbanion (**130**). The carbanion **130** may be partially hydrogen bonded to the departing RNH_2D^+. Hence, the deuteron which is abstracted may rebond to the carbanion **130** thereby resulting in no net exchange (internal return). However, exchange of the departing deuteron with a proton from ethanolamine, and subsequent protonation of the carbanion **130** results in an overall exchange at the benzylic position of **123**, to give monodeuterated product (i.e., **124**).

The primary kinetic isotope effect, $(k_H/k_D)_q \approx 2.00$ (Table 2.7), observed in the fluorescence quenching rates of **123** and **125** respectively, by ethanolamine is consistent with the proposed ethanolamine assisted benzylic C-H vs C-D bond cleavage in the primary step in the S_1 state to give the intermediate carbanion **130**. Since internal return of abstracted deuteron or proton is possible, the isotope effect on the overall exchange quantum yields would be expected to be relatively small. This argument is supported by the following observations. The fluorescence quantum yield (Φ_f) of **123** in the nonreactive solvent CH_3CN is 0.23 ± 0.02 (relative to dibenzofuran). In the presence of 2.0 M ethanolamine the Φ_f of **123** in CH_3CN is quenched by ≈ 15% ($\Phi_f \approx 0.195$). However, the observed monodeuterium exchange quantum yield in this solvent is 0.0098 ± 0.0004. If it is assumed that the decrease in Φ_f is mostly due to the reaction of excited **123** via heterolytic deuteron abstraction from the benzylic C-D position, then out of about 35 deprotonated molecules only 10 exchange. This suggests that internal return of the deuteron is the major reaction pathway of carbanion **130** photogenerated via C-D ionization by ethanolamine.

The mechanism presented in Scheme 2.1 also explains the exchange in the presence of NaOH. The hydroxide ion abstracts deuteron from **123** in S_1 to give the intermediate 9-xanthenide carbanion (**130**) (which is possibly hydrogen bonded to the departing HOD), which is subsequently protonated by the solvent to give overall deuterium exchanged product, viz., **124** . Once again, internal return of the deuteron to the carbanion is a distinct possibility, in that case, no net exchange will result. The exchange quantum yields of **123** and **125** in NaOL-EtOL (L = H or D) (Table 2.3) do not exhibit isotope effect. Assuming the proposed carbanion mechanism in Scheme 2.1 is true, the primary isotope effect which arises from bond cleavage of C-H vs C-D is not manifested in exchange quantum yields ($\Phi_H/\Phi_D \approx 1.0 \pm 0.1$). This is not unexpected since the overall exchange requires the reprotonation of the photogenerated carbanion **130**. This second step has associated with it a primary isotope effect (protonation from L_2O) which compensates for the initial isotope effect. An estimate of the kinetic isotope effect using NaOH for the rates of C-D vs C-H bond cleavages in **123** and **125**, respectively, could not be made because of difficulties encountered in fluorescence quenching studies of these systems in ethanol in the presence of aqueous NaOH.

The mechanism shown in Scheme 2.1 also explains the observed proton (or deuteron) exchange in **134** in the presence of ethanolamine or NaOH. Consistent with the proposed ethanolamine assisted benzylic C-L (L = H and D) bond cleavage in S_1, the fluorescence of **134** in CH_3CN is quenched by added ethanolamine. However, an accurate estimate of fluorescence quenching rate

constants (and hence the kinetic isotope effect) is not available due to the weak fluorescence of 134 and 136.

The derivative 9-phenylxanthene (133), did not exhibit excited state carbon acid behaviour, possibly because of a competing isomerization process. Consistent with the lack of carbon acid behaviour, the fluorescence emission of 133 is not quenched by NaOH or ethanolamine. Similarly, 9-phenylthioxanthene (139) also does not exhibit C-H bond cleavage in S_1. However, no competing photoisomerization of 139 is observed. It is possible that the presence of the phenyl group in both 133 and 139 hinders the approach of the base thereby preventing it from abstracting the proton (or deuteron), the key step required to observe exchange.

2.1.5 Discussion: Stabilized 8π Carbanions in S_1

The enhanced carbon acid behaviour of suberene (37) in the excited state is of fundamental interest because in the ground state it is very difficult to deprotonate the same benzylic protons of 37 (pK ≥ 35), and requires the use of very strong bases (e.g., *n*-BuLi).[123] In contrast, 100% exchange of the dibenzylic protons of fluorene (36) with deuterons can be accomplished by refluxing in 50% D_2O-dioxane (pD ≈13).[48] The difference in the ground state reactivities of fluorene (36) vs suberene (37) is understandable in terms of the relative stabilities of respective carbanion intermediates. Deprotonation of Fluorene (36) in the ground state is energetically favourable because of the incipient formation of a highly

stabilized aromatic 6π-electron fluorenyl carbanion **34**, whereas suberene (**37**) gives rise to a highly destabilized antiaromatic 8π-electron suberenyl carbanion **35**. However, photoexcitation results in reversal of reactivities: **37** in S_1 undergoes facile benzylic C-H deprotonation to give the intermediate 8π-electron suberenyl carbanion **35**, whereas **36** is unreactive. Since related systems such as diphenylmethane (**48**) and dibenzosuberane (**49**), which cannot form cyclically conjugated carbanions, do not exhibit benzylic C-H bond deprotonation in S_1, it has been suggested that the excited state carbon acid behaviour of **37** is due to the enhanced stability of 8π-electron carbanion intermediate **35** in S_1.[48] Results obtained in other related studies also support the notion that formation of 4nπ-electron intermediates (carbanion and carbocations) is favoured in S_1.[32,49,96] The excited state carbon acid behaviour of 9*H*-xanthene (**125**) and 9*H*-thioxanthene (**136**) is also consistent with this notion. That is, the driving force behind the facile benzylic C-H bond ionization in **125** and **136** is the photogeneration of antiaromatic 8π-electron cyclically conjugated carbanions **130** and **137**, respectively. In the ground state, because of the antiaromatic nature of carbanions (8π-electrons in the central ring) **130** and **137**, these carbanions are difficult to form and strongly basic conditions are required to generate them. For example, 9-xanthenide (**130**) and 9-thioxanthenide (**137**) carbanions have been generated in the ground state via deprotonation of **125** ($pK(S_0) \approx 29$)[121] and **136** ($pK(S_0) \approx 30$)[121], respectively, by employing KNH_2 in liquid ammonia at -30 °C.[124a] The antiaromatic nature of carbanions **130** and **137** has been shown by the upfield

shift of the "benzenoid" protons in the ^{1}H NMR spectra.[124a-c] For example, the benzene ring protons of **125** appear in the aromatic region, δ 7-8, of the spectrum, whereas in the 9-xanthenide carbanion (**130**) these proton shift more upfield than could be accounted for by the presence of the negative charge (indicative of increased shielding) and appear between δ 5-6. Furthermore, the ^{13}C NMR spectral analyses of the 9-xanthenide carbanion (**130**) reveals that the negative charge is mostly localized at the carbanionic carbon (C-9), indicating that there is very little charge delocalization consistent with the antiaromatic nature of the species. In contrast, the negative charge in 9-thioxanthenide carbanion (**137**) is more delocalized primarily because of the ability of the bigger sulfur atom to stabilize the negative charge (*dπ-pπ* interaction).[124a]

In S_1, **125** and **136** are deprotonated under relatively mild reaction conditions to give intermediate carbanions **130** and **137**, respectively (*vide supra*). Based on Förster cycle calculations, the S_1 state of these molecules would be expected to be much more acidic (lower pK) than the S_0 state. Using Förster cycle calculations (eq 2.15), an estimate of $pK(S_1)$ of **125** was made. The main difficulty in using Förster cycle calculation for **125** lies in estimating the $\Delta E_{0,0}$ energy for the 9-xanthenide carbanion (**132**) because of its instability (*antiaromatic*). The 9-xanthenide carbanion (**130**) was generated under N_2 in dry THF using *n*-BuLi as the deprotonating base. The absorption spectrum of **130**, recorded immediately, showed a broad long wavelength band at $\lambda_{max} \approx 590$ nm. Based on this absorption band at 590 nm, our best estimate of $\Delta E_{0,0}$ for **130** is ≈44 kcal/mol.

Thus, using $pK(S_0)$[121] of 30 for **125**, the excited singlet state $pK(S_1) \approx -2$ for **125** was calculated. It is clear that based on this calculation, **125** is vastly more acidic in S_1 compared to the ground state. Fluorene (**36**; $pK(S_1) = -8.5$) and its derivatives have also been predicted to become highly acidic in S_1.[40] However, fluorene (**36**) does not undergo deuterium exchange on irradiation in D_2O. That is, kinetically it is not an excited state carbon acid although Förster cycle calculations predict it to be a very strong acid in S_1, if equilibrium can be attained. These observations are consistent with the proposal that only systems that give carbanions with 4n π-electrons in an internal cyclic array (e.g., **130**) have observable excited state carbon acid behaviour.[48]

To understand the enhanced reactivity of molecules that give rise to antiaromatic 4n π-electron carbanions in S_1, it is useful to invoke the same arguments that are used for ground state reactions. It is well known that transformations in the ground state that lead to the formation of the highly destabilized (higher ΔG^0) antiaromatic 4n π-electron intermediates have large activation barriers ($\Delta G^{\ddagger}$) compared to those that generate relatively stable aromatic 4n+2 π-electron intermediates. This argument is based on the Hammond postulate, which relates thermodynamic features of an elementary reaction to the structure and energy of the transition state, and hence kinetic behaviour.[128] This approach is presented diagrammatically in Figure 2.9.

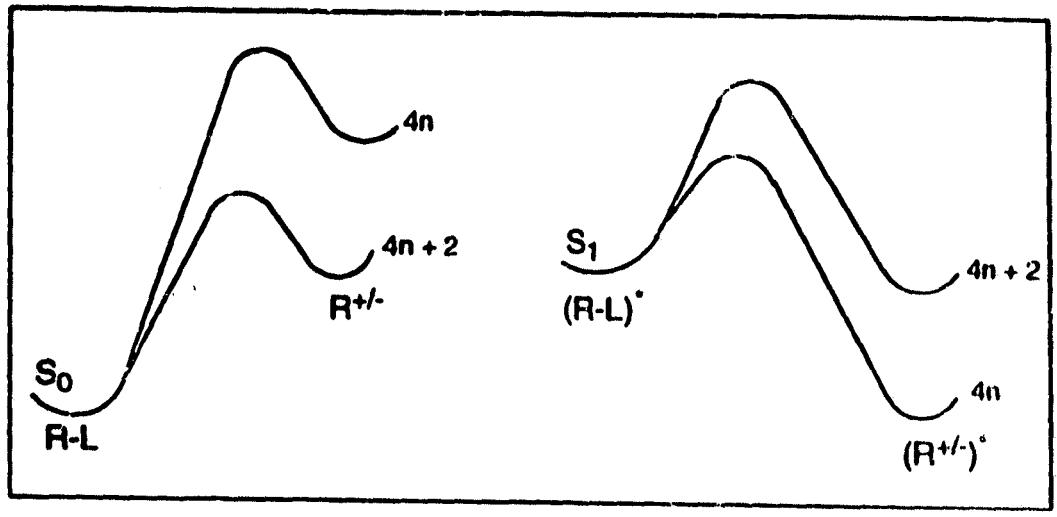

Figure 2.9 Illustration of the Hammond postulate as applied to S_0 and S_1 surfaces.

Previous studies have shown that photoreactions of dibenzannelated systems that give rise to intermediates containing 4n π-electrons ICA are favoured in the S_1 state, compared to their 4n+2 counterparts.[32,48,49,96,99,179] Photogeneration of 9-xanthenide (**130**) and 9-thioxanthenide (**137**) carbanions, both consisting of an 8π-electron ICA, is consistent with this notion. If the preferential formation of these carbanions, **130** and **137**, is taken to imply a lower activation barrier ($\Delta G^{\ddagger}$) on the S_1 surface, then extension of Hammond's postulate would suggest that in the S_1 state carbanions **130** and **137** are indeed more stabilized than their 4n+2 counterparts (e.g., the fluorenyl carbanion **34**). This argument is true assuming that, (a) the Hammond postulate applies to the S_1 surface and, (b) the C-H bond

cleavage takes place on the S_1 surface. There is no apparent reason to doubt the applicability of Hammond's postulate to the S_1 surface. However, there is no direct evidence for the adiabatic formation of carbanions **130** and **137** on the S_1 surface.

If the excited **125** and **134** funnel down from the S_1 to the S_0 potential energy surface, rather than proceeding on to react completely on the S_1 surface, then an enhanced stability of 8π carbanions **130** and **137** is not required to explain the enhanced reactivity of **125** and **134**, compared to fluorene (**36**), on photoexcitation (Figure 2.10a). Instead, it could be envisaged that C-H bond photoionization of **125** (or **134**) to give the intermediate carbanions **130** (or **137**) is preferred simply because the higher thermal activation barriers (to form these carbanions) brings the S_0 and the S_1 surfaces much closer together and hence increases the rate of internal conversion (diabatic return) (Figure 2.10a). In such a case the preferential formation of **130** or **137** is not due to the low activation barrier encountered on the S_1 surface, but rather due to small S_0-S_1 gap at some point on the reaction coordinate. However, since the transition state for formation of carbanions **130** and **137** occurs late on the S_0 surface (endothermic reaction) and rather early on the S_1 surface (exothermic reaction), it is not clear why internal conversion from S_1 to S_0 should occur prior to the activated complex formation on S_1. In order for diabatic return to the S_0 surface to be product forming, it must occur late enough to intercept the S_0 transition state. Thus as long as internal

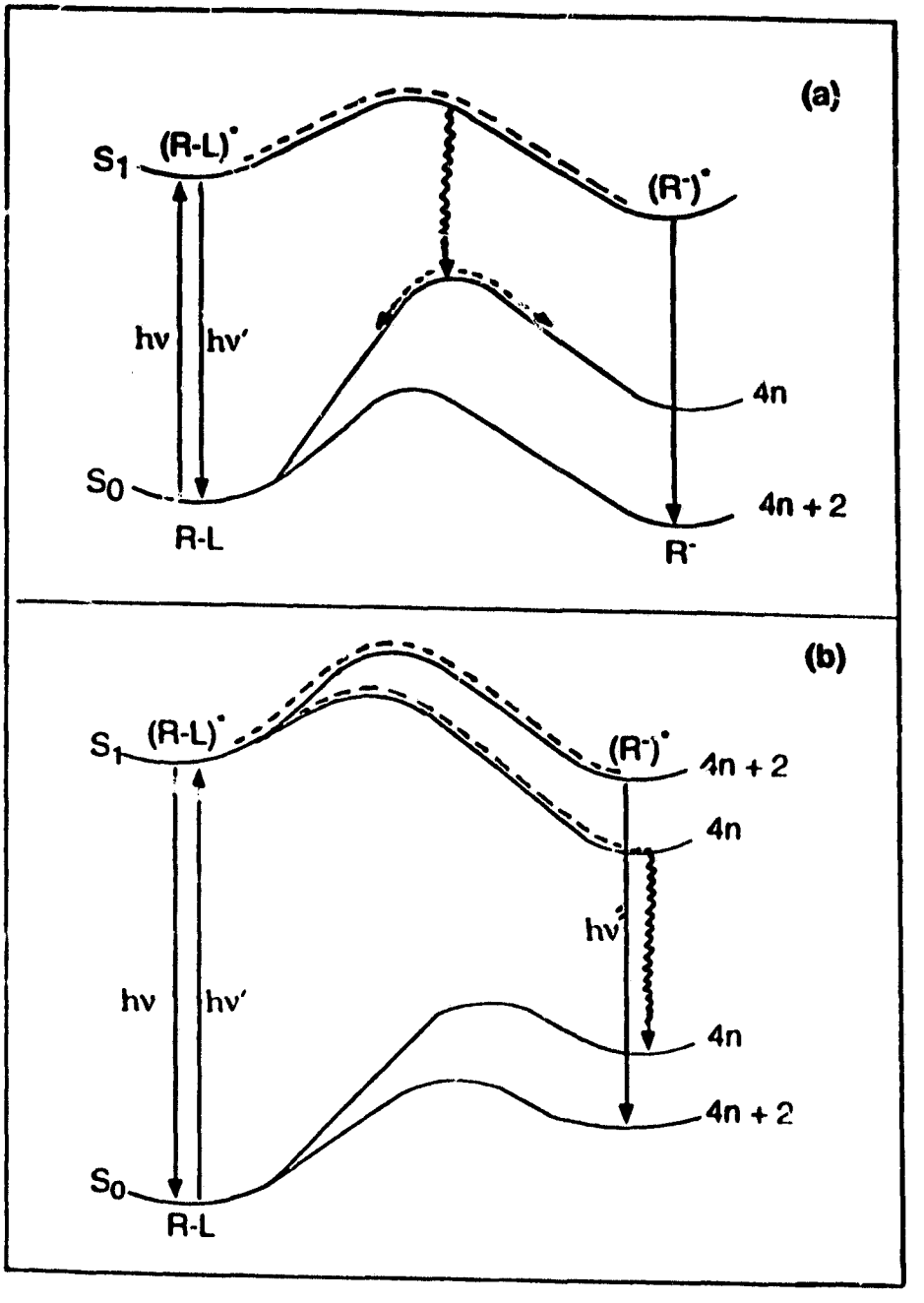

Figure 2.10 Generalized potential energy surface for two possibilities for excited state carbon acid dissociations, (a) Diabatic Process: internal return to the S_0 surface; (b) Adiabatic Process: excited state cleavage step followed by deactivation to the ground state ionic intermediates.

conversion to S_0 follows the rate limiting cleavage step, the excited state reactivity will reflect the S_1 energy barrier.

On the other hand if the reaction is adiabatic in nature, then the C-H bond photoionization step occur on the S_1 surface and the intermediate carbanions **130** and **137** are formed on the S_1 surface (Figure 2.10b). In this case, deactivation to the S_0 occurs at the carbanion stage. Interactions of these carbanions with the solvent molecules then deactivates them to the S_0 surface, and the rest of the reaction then proceeds along the S_0 surface. However, fluorescence emission from such photogenerated 4n (8π) carbanions has not been observed. In contrast, photochemical reactions which give rise to 4n+2 π-electron carbocation intermediates (e.g., **99**) have been shown to be adiabatic, by observation of their fluorescence emission.[92] This difference in emissive behaviour of 4n vs 4n+2 systems is understandable if the energy differences between S_0-S_1 for the two systems is taken into consideration. The S_0-S_1 energy gap for 4n+2 systems is larger compared to the 4n systems. For example, the 9-fluorenyl carbanion (**34**; 6π-electrons, 4n+2 system) is known to be fluorescent,[32c] and has a S_0-S_1 gap of 54-56 kcal mol^{-1}. Unfortunately, electronic spectra of antiaromatic ions are less well defined. Calculations carried out by Jug and Padma Malar[112] and Aihara[114] suggest that antiaromatic (4n) systems have low lying excited states. For example, in the case of the suberenyl carbanion (**35**) it has been estimated that the energy difference between S_0 and S_1 is at least 20 kcal mol^{-1} smaller than the gap for the corresponding 4n+2 ion.[32b] Hence, although no emission from the photogenerated

carbanions **130** or **137** has been observed, their efficient formation would suggest that these antiaromatic carbanions are indeed more stabilized in the excited state and can be generated adiabatically.

The excited state benzylic C-H deprotonation of **125** and **134** is clearly supported by both product and fluorescence quenching studies. It seems reasonable that the measured k_q's for fluorescence quenching of **123** and **125** by ethanolamine can be equated to the rates (k_H) of benzylic C-L (L = H or D) bond ionization in S_1 with ethanolamine acting as the base. These C-H bond ionization rates for **125** are an order of magnitude smaller than those obtained for suberene (**37**). This difference in reactivity of **125** vs **37** may be reflective of the relative stabilities of the intermediate 8π-electron carbanions **130** and **35**. In terms of resonance energy, in the ground state, it is well known that aromatic systems with a hetero atom (e.g., pyridine) are not as stable as their hydrocarbon analogue (e.g., benzene).[125] In the present context, the negative charge in the 9-xanthenide carbanion (**130**) cannot be delocalized as much as it can be compared to the corresponding suberenyl carbanion **35**. Because of the reduced negative charge delocalization, **130** would be expected to be less stable than **35**. This difference in stabilities of these carbanions (**130** vs **35**) is reflected in the reduced carbon acidity of **125** compared to **37**.

Dewar-Zimmerman[126a,b] and Woodward-Hoffmann[126d] rules predict that photochemical pericyclic reactions take place preferentially through excited forms of antiaromatic transition states. That is, an antiaromatic cyclic transition state is

more stable in the excited state than the corresponding aromatic transition state.[126c] Although the reaction investigated (C-H bond ionization) in the present study is not formally a pericyclic reaction, these rules still work in predicting the outcome of these reactions. That is, there is an inherent stabilizing effect of a 4n array of electrons on the excited state surface, analogous to the aromatic stabilization associated with 4n + 2 systems in the ground state. Further support for this proposal comes from the following photodecarboxylation studies of xanthene and thioxanthene carboxylic acid derivatives in aqueous solution (*vide infra*).

2.2 Photodecarboxylation of Xanthene and Thioxanthene Carboxylic Acids in Aqueous Solution: Photogeneration of 8π Electron Carbanion Intermediates

2.2.1 Product Studies

Photolysis of the diaryl acetic acids (Rayonet RPR 100 reactor; 254 nm lamps; quartz vessel; solution cooled with a cold finger to ~15 °C; argon-purged solutions; photolysis time 1-10 min.) were carried out using ~10^{-3} M solutions of substrates dissolved in 200 mL aqueous CH_3CN (typically 80% (v/v) H_2O-CH_3CN), and the pH adjusted using a pH meter, to ≥ 8 by adding an appropriate amount of a stock NaOH solution. Photolysis of all diarylacetic acids resulted in the formation of the corresponding decarboxylated products in moderately high yields. Photolysis in D_2O-CH_3CN resulted in the formation of the corresponding monodeuterated products, whereas photolysis in 100% CH_3CN resulted in no

reaction.

2.2.1.1 Photolysis of Xanthene-9-Carboxylic Acid (142)

Photolysis of an argon purged solution of **142** in 80% H_2O-CH_3CN (pH ≥ 8) for 10 min resulted in efficient decarboxylation to yield 9*H*-xanthene (**125**) and

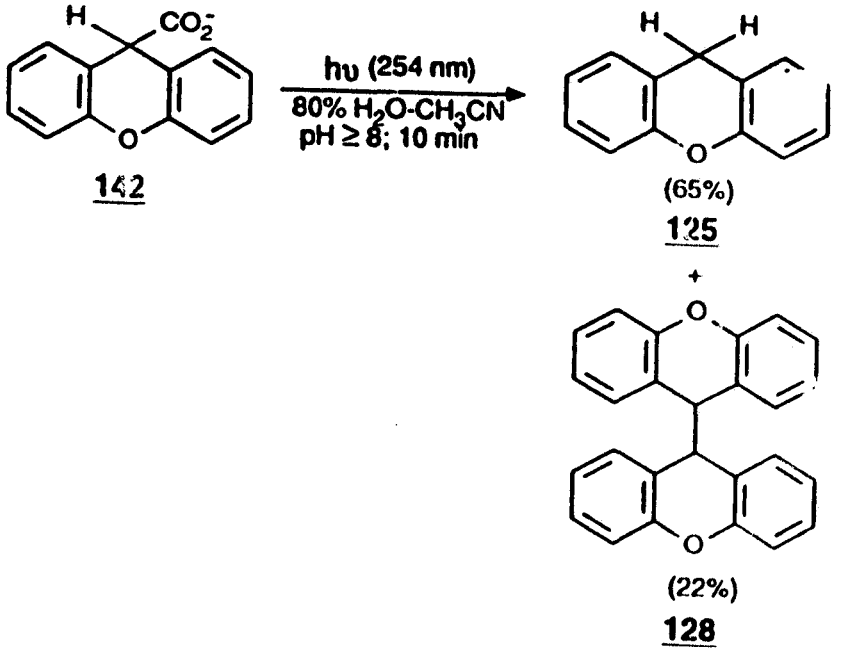

(2.16)

9,9′-bisxanthene (**128**) (eq 2.16) as indicated by ^{1}H NMR spectral analysis of the reaction mixture. The assignments of the photoproducts were based on comparison with the ^{1}H NMR spectra of the authentic samples.

In a previous study it has been shown that photolysis of **125** in aqueous CH_3CN solution in the presence of *p*-nitrobenzoic acid resulted in the formation of **128**.[117] The proposed mechanism of this dimerization involves electron transfer from **125** to *p*-nitrobenzoic acid to form the radical cation **125**$^{+\cdot}$, followed by

deprotonation, to give xanthenyl radical **131**, which subsequently dimerizes to form **128** (eq 2.17). To test for the possibility that **128** of eq 2.16 might be formed

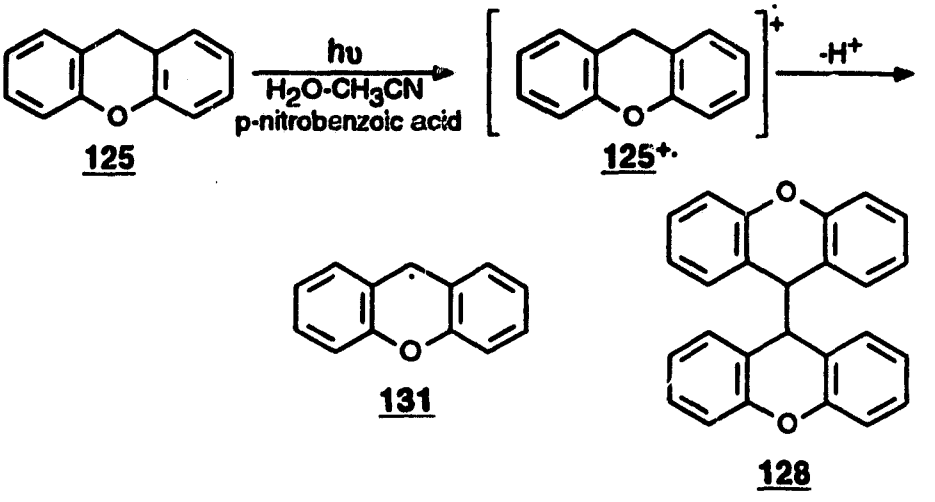

(2.17)

via secondary photolysis of **125**, a solution of **125** in 80% H_2O-CH_3CN (pH ≈ 9) was photolyzed for the same duration as used for **142** (*ca.*10 min). Dimer **128** was not formed under these reaction conditions, ruling out the possibility that **128** was formed via secondary photolysis of **125**. Furthermore, a kinetic study found that both **125** and **128** were present even at short photolysis times(*ca.* 30 seconds) (Figure 2.11). These results clearly demonstrate that both **125** and **128** are primary photoproducts of **142**.

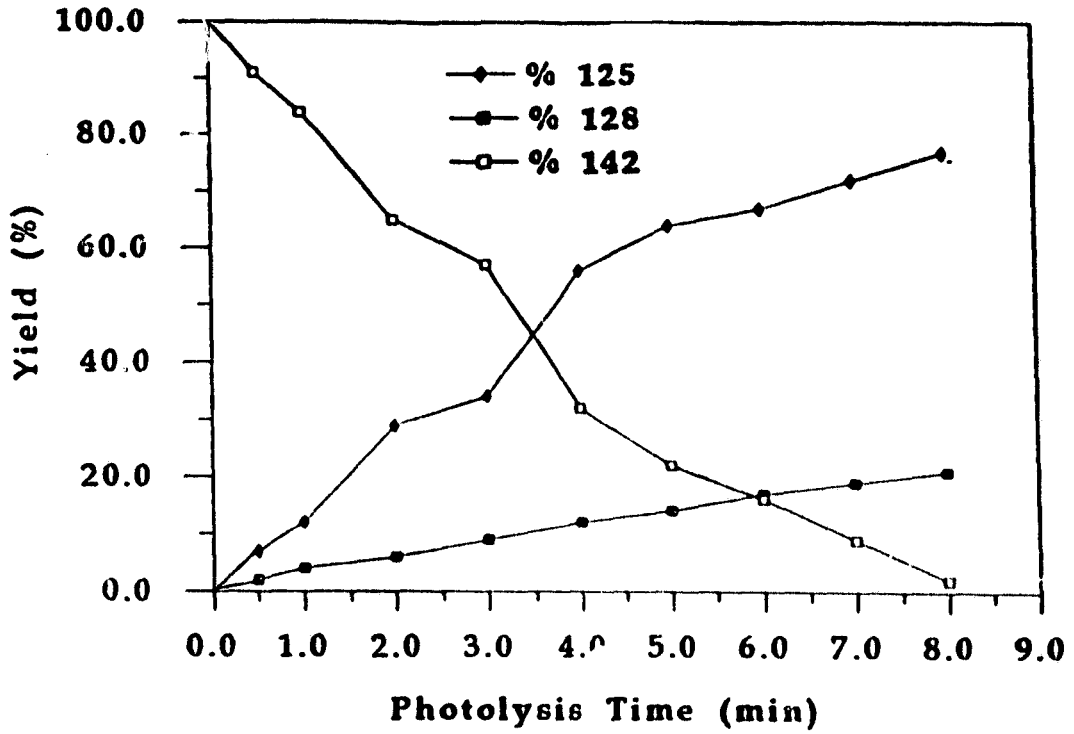

Figure 2.11 Plot of yields of photoproducts **125** and **128** vs photolysis time in 80% H_2O-CH_3CN (pH ≈7).

When the photolysis of **142** was carried out in 80% D_2O-CH_3CN solution (pD ≈ 8), it resulted in the formation of 9*D*,9*H*-xanthene (**124**) and **128** (eq 2.18). The ^1H NMR and mass spectral analyses of the photoproducts indicated that no deuterium was incorporated in 9,9'-bisxanthene (**128**). To rule out the possibility that the proton at C_9 of **142** was undergoing photoexchange with the solvent D_2O prior to the decarboxylation, 9-deuterio-9-xanthenecarboxylic acid (**143**) was photolyzed in 80% H_2O-CH_3CN. The recovered **143** showed no sign of having exchanged at this position at these short irradiation times. Furthermore, photolysis of **125** in 80% D_2O-CH_3CN did not result in deuterium exchange at

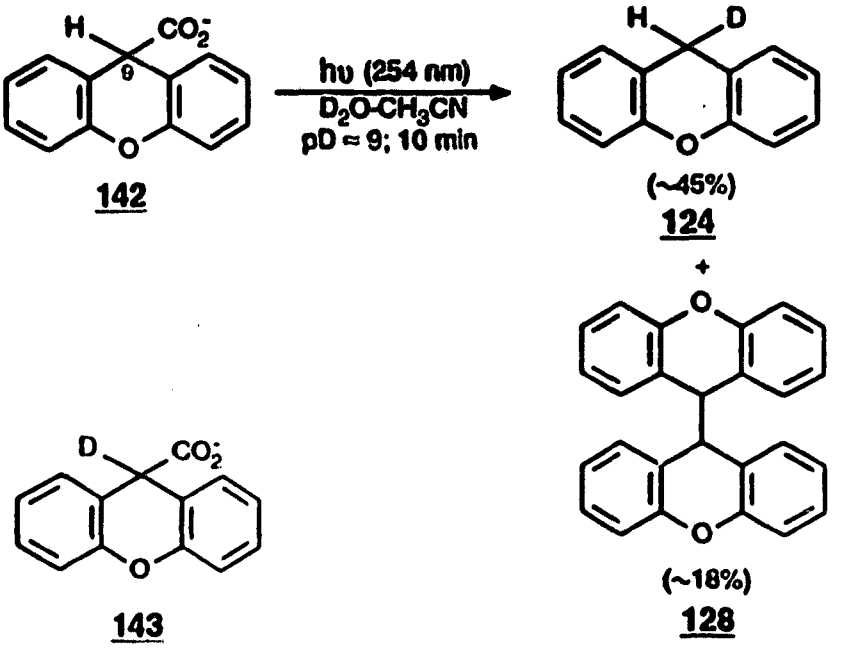

(2.18)

the benzylic position (a reaction that has been observed in more basic solution, *vide supra*). This rules out the possibility that deuterated **124** could have arisen from secondary photolysis of **125**. A dark reaction of **142** carried out in 80% D_2O-CH_3CN (pD ≈ 10) for 30 min did not result in any decarboxylation or proton exchange at the C_9 position with solvent D_2O. These results clearly indicate that the deuterium incorporated in **124** is via photodecarboxylation of **142**. This strongly implicates the intermediacy of 9-xanthenide carbanion (**130**). However, formation of 9,9'-bisxanthene (**128**) is consistent with the intermediacy of the 9-xanthenyl radical (**131**). Since it was shown above that both **124** and **128** are primary photoproducts (Fig. 2.11), it is possible that both C-C bond homolysis (to give radical **131**) and heterolysis (to give carbanion **130**) takes place on irradiation of **142**. One possible way to check for this possibility is to investigate the effect

of solvent on the photodecarboxylation of **142**. Solvent effects on reactions can be used to distinguish between ionic and radical mechanisms. Whereas reactions proceeding through ionic intermediates are greatly affected by the nature of solvent, radical reactions are generally unaffected. Hence, if C-C bond homolysis is taking place then photolysis of **142** in 100% CH_3CN should result in the exclusive formation of **128**. However, photolysis of **142** in 100% CH_3CN did not result in any observable reaction (eq 2.19), indicating that photodecarboxylation

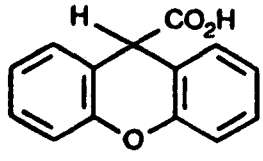

142

$$\xrightarrow[100\%\ CH_3CN]{h\upsilon\ (254\ nm)} \text{no reaction} \qquad (2.19)$$

of **142** via C-C bond homolysis does not take place. Alternatively, the radical **131** could arise via electron ejection from the intermediate carbanion **130** (Scheme 2.2). Carbanions are known to be good electron sources.[101e] In a related study it has been shown that photolysis of **142** in the presence of *p*-nitrobenzoic acid results in the formation of *p*-nitrobenzoate (PNB) radical dianion, as detected by ESR spectroscopy. The formation of PNB radical dianion is presumed to be via electron transfer from the photogenerated **130** to the *p*-nitrobenzoate. No ESR signal due to PNB radical anion was observed in the dark or on photolysis of PNB alone. These results support the notion that **130** is the precursor to both radical **131** and **125**.

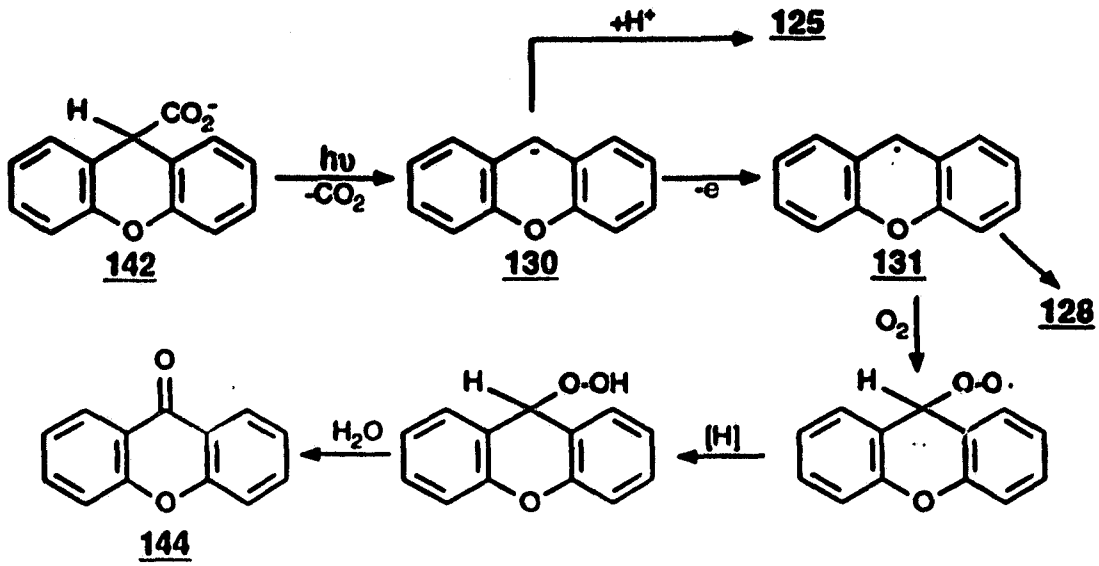

Scheme 2.2

Photolysis of **142** in oxygen saturated solutions under conditions where extensive decarboxylations occurred resulted in formation of **125**, **128** and 9-xanthone (**144**) (eq 2.20). Products obtained on photolysis under argon and under

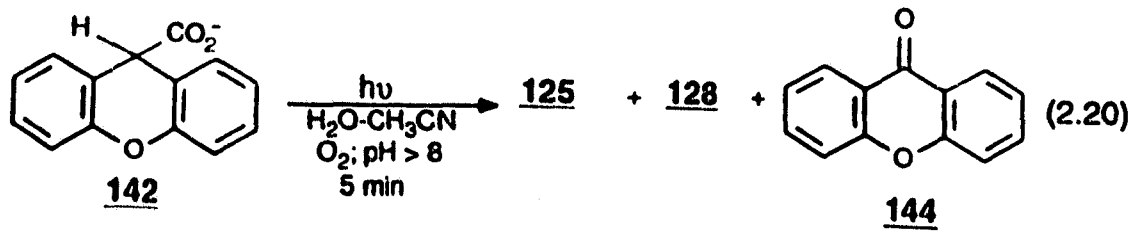

oxygen are presented in Table 2.8. Control experiments in which both **125** and **128** were independently photolyzed in O_2 saturated aqueous CH_3CN solutions (*ca.* 90 min) resulted in only trace amounts (< 1%) of **144**. Thus, photooxygenation

Table 2.8 Conversions and Product Distributions in the Photolysis of 9H-Xanthene-9-Carboxylic Acid (142) in O_2 and Ar Saturated 80% H_2O-CH_3CN (pH ~8) Solutions.[a]

	% 125	% 128	% 144
O_2[b] Saturated	~ 63%	~ 4%	~ 11%
Ar[b] Saturated	~ 63%	~ 11%	~ 4%

a) Product distribution analyzed by ^1H NMR integration.
b) ~ 80 mg of substrate dissolved in 80% H_2O-CH_3CN (200 mL; pH ~ 8) solution and irradiated with continuous bubbling of O_2 or Ar, at λ_{ex} 254 nm for 5.0 min.

of the initially formed photoproducts, viz., **125** and **128**, can be ruled out. It is evident from Table 2.8 that the conversion to **125** in both photolyses (in presence and absence of O_2) remains unaffected, whereas the amount of **144** formed in O_2 saturated solution is approximately equal to the amount of **128** formed in argon saturated solution. These observations suggest that both **128** and **144** have a common precursor, viz., 9-xanthenyl radical (**131**). In the absence of oxygen most of the radical **131** formed dimerizes to give **128**. However, in the presence of oxygen the bimolecular trapping of the 9-xanthenyl radical (**131**) by oxygen leads to the hydroperoxide which is known to break down to yield the ketone **144** (Scheme 2.2).

Table 2.9 summarizes the results obtained in photolysis of **142** in aqueous solutions of varying acidities. In general, both aryl and diarylacetic acids

decarboxylate only in their carboxylate ion forms.[19,27,33] Consistent with this

Table 2.9 Photoproduct Distribution in the Photolysis of Xanthene-9-Carboxylic Acid (142) in 80% H_2O-CH_3CN at Various pHs.

pH[a]	% 125[b]	% 128[b]	% 142[b]
1.0	0.00	0.00	100
3.0	23	7	70
4.0	63	12	24
7.0	61	15	24
8.0	63	15	22
10.0	65	16	18
12.0	64	14	21
100% CH_3CN	0.00	0.00	100%

a) pH of the aqueous portion of the solution; each solution contained ~75 mg of the substrate dissolved in 80% H_2O-CH_3CN (200 mL); pH of the solution was adjusted using a pH meter with dropwise addition of a standard solution of HCl or NaOH; λ_{ex} 254 nm; photolysis time 5.0 min.
b) Product distribution analyzed by ^1H NMR integration; errors in percentage conversions are estimated to be ± 8-10% of the quoted values.

prediction, **142** failed to photodecarboxylate at pH < pK_a (pK_a of **142** ≈ 4), indicating that only the carboxylate ion of **142** is the reactive species. The lack of reactivity of **142** in 100% CH_3CN is also consistent with this observation.

Preparative scale photolysis were also carried out with 9-phenylxanthene-9-carboxylic acid (**145**), to investigate the effect of the phenyl group on the

efficiency of the photodecarboxylation. Thus, photolysis of **145** in 80% H_2O-CH_3CN (pH ≥ 8) resulted in efficient reaction, to give 9-phenyl-9*H*-xanthene

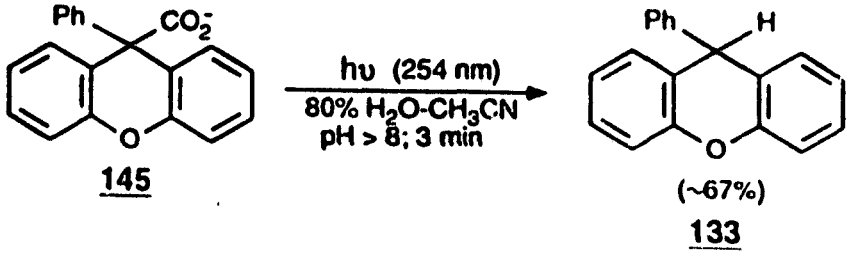

(2.21)

(**133**) as the only photoproduct (eq 2.21). A photolysis of **145** in 80% D_2O-CH_3CN (pD ≈ 9) resulted in the formation of deuterated **132** (eq 2.22). These results are consistent with the intermediacy of the 9-phenylxanthenide carbanion (**140**). No

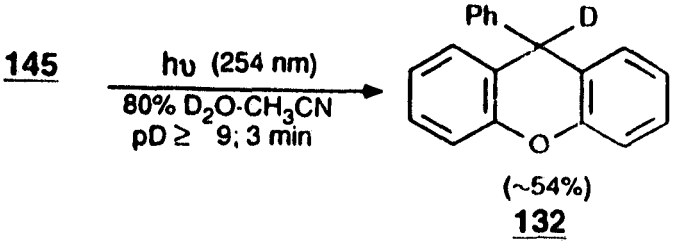

(2.22)

radical derived products were isolated in these photolyses. When **145** was photolyzed in oxygen saturated aqueous CH_3CN solution, only **133** was observed. Table 2.10 summarizes the results of photolyses of **145** in solutions of various pHs (pK_a of **145** ≈ 4.5).

Table 2.10 Conversions to 133 in the Photolysis of 9-Phenylxanthene-9-Carboxylic Acid (145) in 80% H_2O-CH_3CN Solutions of Various pHs.

pH[a]	% 133[b]	% 145[b]
1.0	0.00	100
2.0	0.00	100
4.0	5	12
7.0	21	78
8.0	23	77
10.0	30	70
12.0	33	66
100% CH_3CN	0.00	0.00

a) Quoted pH is of the aqueous portion of the solvent system; each solution contained 75 mg of **145** dissolved in 80% H_2O-CH_3CN (200 mL) and pH adjusted using a pH meter with dropwise addition of a standard solution of HCl or NaOH; λ_{ex} 254 nm; photolysis time *ca.* 2.0 min.
b) Conversion to product calculated by ^1H NMR integration using suberene (**37**) as external standard; errors in percentage conversions are estimated to be ± 10% of the quoted values.

A preliminary comparison of the relative reactivity of **142** and **145**, based on the conversion to the respective photoproducts **125** and **133**, shows that the presence of the bulky phenyl group at C-9 does not have any significant effect on the photodecarboxylation efficiency. This result is interesting considering the fact that photodecarboxylation of **145** generates a tertiary triphenylmethane carbanion, viz., **146**, whereas **142** gives a secondary carbanion, viz., **130**. Thermally, the formation of a tertiary carbanion is energetically less favourable compared to a

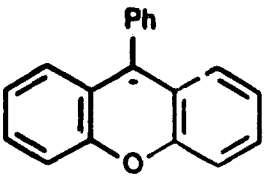

146

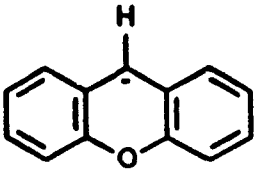

130

secondary carbanion, because of the lower stability of the former.[127]

2.2.1.2 Photolysis of Thioxanthene-9-carboxylic Acid (147)

Photolysis of **147** in 80% H_2O-CH_3CN (pH ≥ 8) led cleanly to the formation of 9*H*-thioxanthene (**136**) (eq 2.23). However, the yields of photoproduct **136** were

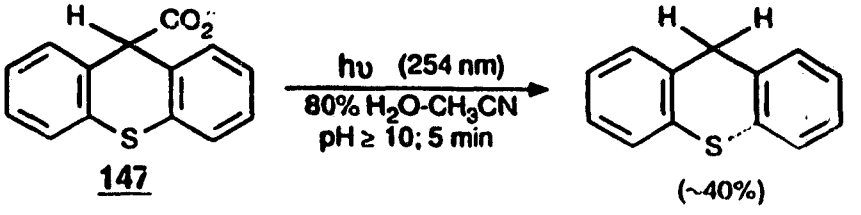

147 136 (2.23)

significantly lower than those obtained from **142** under similar reaction conditions.

Photolysis of **147** in a 80% D_2O-ACN (pD ≥ 9) resulted in clean formation

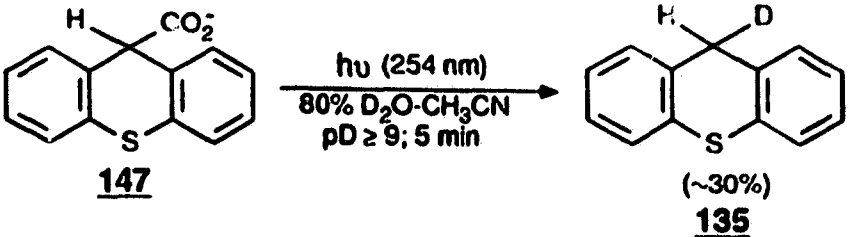

147 135 (2.24)

of the corresponding mono-deuterated product **135** (eq 2.24).

It was shown earlier that photolysis of **136** in basic solution results in deuterium exchange at the benzylic position, to give monodeuterated **135** (*vide supra*). However, photolysis of **136** under conditions employed for the photodecarboxylation did not result in any observable deuterium exchange at the benzylic position. This precludes the possibility that the observed deuterium incorporation in **135** could have resulted from a secondary photolysis of **136**. Photolysis of **147** in 100% CH_3CN did not lead to any product and the unchanged starting material was recovered (eq 2.25). In addition, no radical derived products

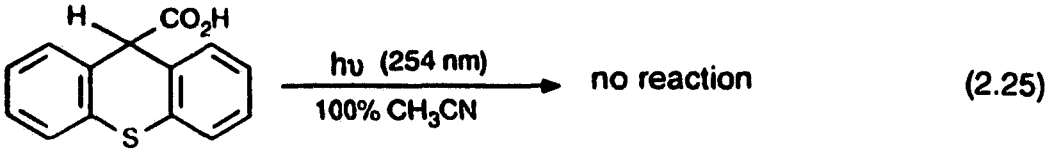

147 (2.25)

were observed on photolyses of **147** in aqueous solution. Photolysis in O_2 saturated aqueous solution also resulted in the formation of **136** as the only product.

The deuterium incorporation in photoproduct (viz., **135**) on photolysis of

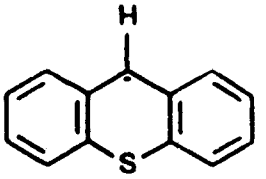

137

147 in D_2O and the absence of radical derived product(s) strongly implicates the

intermediacy of the 9-thioxanthenide carbanion (137). Furthermore, the lack of reactivity in aqueous solutions of pH's < pK_a (estimated pK_a of 147 ≈ 3.3) indicates that only the carboxylate ion is the reactive species.

Photolysis of 9-phenylthioxanthen-9-carboxylic acid (148) in 80% H_2O-CH_3CN (pH ≥ 8) solution also resulted in the formation of corresponding decarboxylated product 139 (eq 2.26). The presence of the phenyl group had no

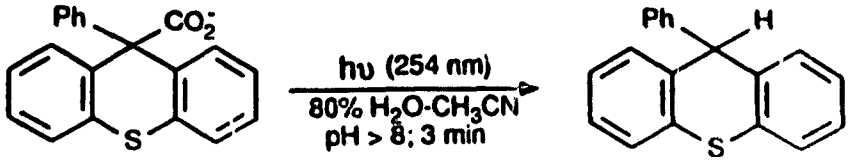

148 (~55%) 139 (2.26)

apparent effect on the reactivity of 148 as it decarboxylated with similar facility as the parent system 147. Consistent with the intermediacy of carbanion 149 in

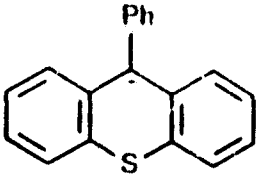

149

the photodecarboxylation, photolysis in 80% D_2O-CH_3CN (pD ≈ 9) resulted in the formation of deuterated 138 (eq 2.27).

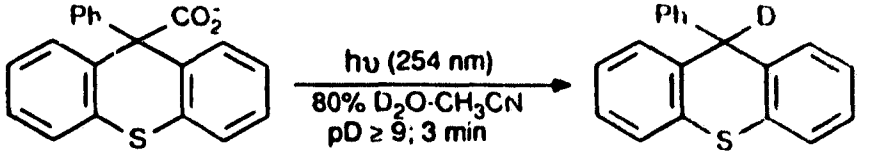

148 (~48%) 138 (2.27)

Photolyses of esters **150, 151, 152** and **153** in 80% H_2O-CH_3CN, conditions under which the corresponding acids react extensively, did not result in any

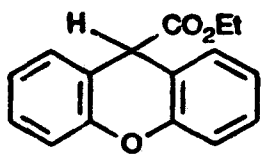

150

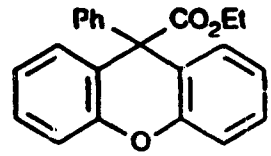

151

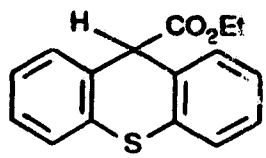

152

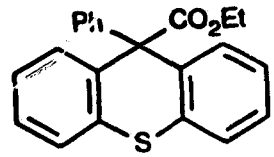

153

observable reaction, and the starting materials were recovered unchanged. This is consistent with the notion that only the carboxylate ion is the reactive species.

2.2.2 Product Quantum Yields

Quantum yields for photodecarboxylation (Φ_P's) of **142, 145, 147** and **148** were measured in deaerated 80% H_2O-CH_3CN solutions at various pH's. The solvent isotope effect and the effect of solvent on the efficiency of photodecarboxylation were also investigated in quantitative detail.

2.2.2.1 Quantum Yields at pH 7

The quantum yields (Φ_P's) for the photodecarboxylation (formation of product) were measured in aqueous solution (pH 7 buffer) using 20% (v/v) CH_3CN as cosolvent (Table 2.11). The measurements for all the acids were

carried out on an optical bench (λ_{max} = 280 nm) under a fine stream of argon, which served to deaerate and stir the solutions (*ca.* ≈ 1 x 10^{-3} M). Potassium ferrioxalate was employed to monitor the light intensity.[118] Conversions of the diarylacetic acids to the corresponding photoproducts were determined by GC analyses employing appropriate external standards. The GC results were corrected for differences in the detector response of the photoproduct and the external standard in each case. In the case of **142**, Φ_P refers to the formation of **125** (and **124**) only, since dimer **128** was not readily analyzable because of its long retention time on GC column.

Table 2.11 Product Quantum Yields (Φ_P)[a] for Photodecarboxylation of Diarylacetic Acids in 80% L_2O-CH_3CN (L = H or D) at pH 7/pD ~8.

	Φ_P (142)[d]	Φ_F (145)	Φ_P (147)	Φ_P (148)
H_2O (pH = 7)[b]	0.30 ± 0.03	0.28 ± 0.03	0.18 ± 0.02	0.22 ± 0.02
D_2O (pD ≈ 8)[c]	0.24 ± 0.004	0.22 ± 0.02	0.14 ± 0.02	0.17 ± 0.03

a) Quantum Yields (Φ_P) refers to the photoproduct formation, measured by GC using an appropriate external standard; the mass balance in each case was > 90%; the errors quoted are the standard deviations of 2-3 independent measurements.
b) 20% CH_3CN as co-solvent; pH 7 phosphate buffer used; λ_{ex} = 280 nm; Ar purged.
c) 20% CH_3CN used as co-solvent; pD adjusted by addition of standard 1 M NaOD solution; Ar purged.
d) In the case of **142**, Φ_P refers to the formation of **123** and **124** only; Φ for the formation of dimer **128** was not directly measureable because of its long retention time on GC column.

2.2.2.2 Solvent and pH Effects

The photodecarboxylation efficiency of all the acids displayed considerable solvent and pH dependency. In 100% CH_3CN none of the acids studied showed any reactivity. In general, the acids were less reactive in acidic solutions. These results are consistent with the preparative scale product studies described earlier.

Table 2.12 Product Quantum Yields (Φ_P's) for Photodecarboxylation of Diarylacetic Acids in Aqueous Solutions[a] at Various pHs.

pH[b]	Φ_P[c]			
	142[d]	145	147	148
1.0	0.00	0.00	0.00	0.00
2.0	0.00	0.00	0.00	0.00
4.0	0.074	0.060	0.038	0.046
9.0	0.33	0.30	0.20	0.23
10.0	0.33	0.32	0.22	0.26
12.0	0.34	0.33	0.23	0.26

a) 20% (v/v) CH_3CN used as co-solvent; Argon purged; λ_{ex} = 280 nm.
b) Standard buffer solutions used to get the desired pH; solutions of pH 10 and 12 prepared using a pH meter with dropwise addition of a standard solution of NaOH.
c) Φ_P's measured by GC using appropriate external standard in each case; the mass balance was > 90% in each case; the errors in the measurements are ± 10% of the quoted values.
d) Φ_P refers to the formation of 125 only.

The quantum yields of photodecarboxylation (Φ_P; product formation) of diarylacetic acids at various pH's are presented in Table 2.12. A cursory comparisons of Φ_P's reveals that xanthene carboxylic acids (**142** and **145**) photodecarboxylate more efficiently than the corresponding thioxanthene carboxylic acids (**147** and **148**) at all pHs.

2.2.2.3 Solvent Isotope Effects

Quantum yields (Φ_P's) of diarylacetic acids were also measured in D_2O (20% CH_3CN co-solvent) to measure the solvent isotope effect. The solutions were adjusted to pD ≥ 8 by adding NaOD (Table 2.13). Comparison of quantum yields (Φ_P's) obtained in H_2O and D_2O shows that product yields are lower in D_2O, corresponding to a normal solvent isotope effect, $\Phi_{H2O}/\Phi_{D2O} \approx 1.2\text{-}1.3$, and are consistent with a solvent assisted heterolytic mechanism of photodecarboxylation.

Table 2.13 Solvent Isotope Effect on Photodecarboxylation Quantum Yields of the Diarylacetic Acids.[a]

Φ_{H2O}/Φ_{D2O}	**142**	**145**	**147**	**148**
	1.25 ± 0.03	1.27 ± 0.03	1.28 ± 0.04	1.30 ± 0.05

a) Reactions carried out with 20% (v/v) CH_3CN cosolvent at pH 7 or pD ≥ 8.

2.2.3 Steady-State Fluorescence Studies

2.2.3.1 General Spectral Characteristics

The fluorescence emission spectra of carboxylic acids **142** and **145** had a similar appearance to the spectra of the corresponding xanthene chromophore. However, their fluorescence quantum yields ((Φ_f of **142** and **145**) in CH_3CN were considerably lower. The reason for this could be the presence of the carboxyl group which opens up additional radiationless decay pathways. Fluorescence emissions of **147** and **148** were extremely weak (Φ_f = 0.0001 in CH_3CN relative to biphenyl ether (Φ_f = 0.03 in cyclohexane)[135]), possibly due to the presence of sulfur atom, which promotes the rate of intersystem crossing, thereby reducing the fluorescence emission ("heavy atom effect").[120] Because of this no attempts were made to study their fluorescence behaviour as probe of mechanism.

2.2.3.2 Solvent and pH Effects on Fluorescence Quantum Yields

The fluorescence behaviour of acids **142** and **145** was strongly solvent and pH dependent. The parent acid **142** was moderately fluorescent in 100% CH_3CN (Φ_f = 0.022 ± 0.005, relative to biphenyl ether (Φ_f = 0.03 in cyclohexane)[135]), whereas the corresponding 9-phenyl analogue **145** was weakly fluorescent (Φ_f = 0.0082 ± 0.0005, relative to biphenyl ether). The weak emitting behaviour of **145** is probably due to the presence of phenyl group which opens up additional deactivation pathways competing with fluorescence.

It has been observed that the carboxylate forms of arylacetic acids are more

fluorescent than their protonated counterparts.[27,32a,b] However, in the present study the carboxylate form of the acids was found to be less fluorescent than their protonated counterparts which was consistent with their photoreactivity. For example, the fluorescence quantum yield of **142** in 100% CH_3CN was $\Phi_f = 0.022 \pm 0.002$, a solvent in which it does not exhibit any reactivity ($\Phi_P = 0.00$), whereas in 80% H_2O-CH_3CN (pH 7.0), a solvent system in which **142** efficiently photodecarboxylates (Φ_P at pH 7 = 0.30), the Φ_f was ≈ 0.0062.

The fluorescence emission intensities of **142** and **145** were progressively quenched as the pH of the aqueous portion in 80% H_2O-CH_3CN was increased, following an opposite trend in their photochemical reactivity. The pH dependence of fluorescence quantum yields (Φ_f) and product quantum yields (Φ_p) of **142** and **145** are presented in Figures 2.12 and 2.13, respectively. The drop in fluorescence intensity at higher pH's is due to the enhanced reactivity of the carboxylate ion form (higher Φ_P's) which provides an additional deactivational pathway for S_1 of the acids. These results are consistent with the results obtained in product studies; that is, only the carboxylate ion form is reactive.

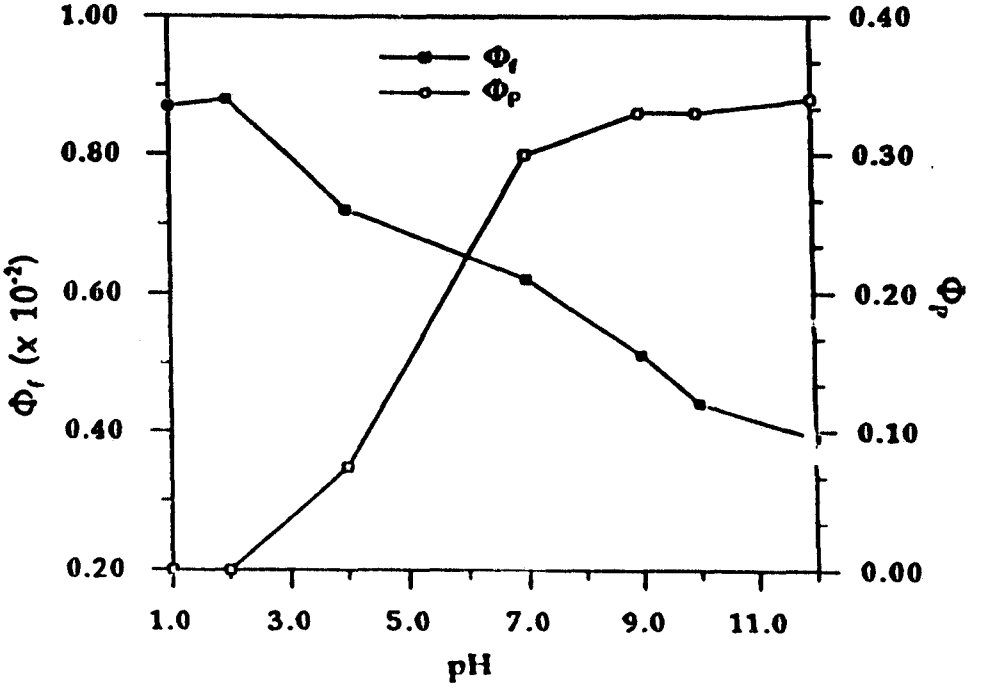

Figure 2.12 Fluorescence (Φ_f) and product (Φ_p) quantum yields for **142** as a function of the pH of the aqueous portion in 80% H_2O-CH_3CN.

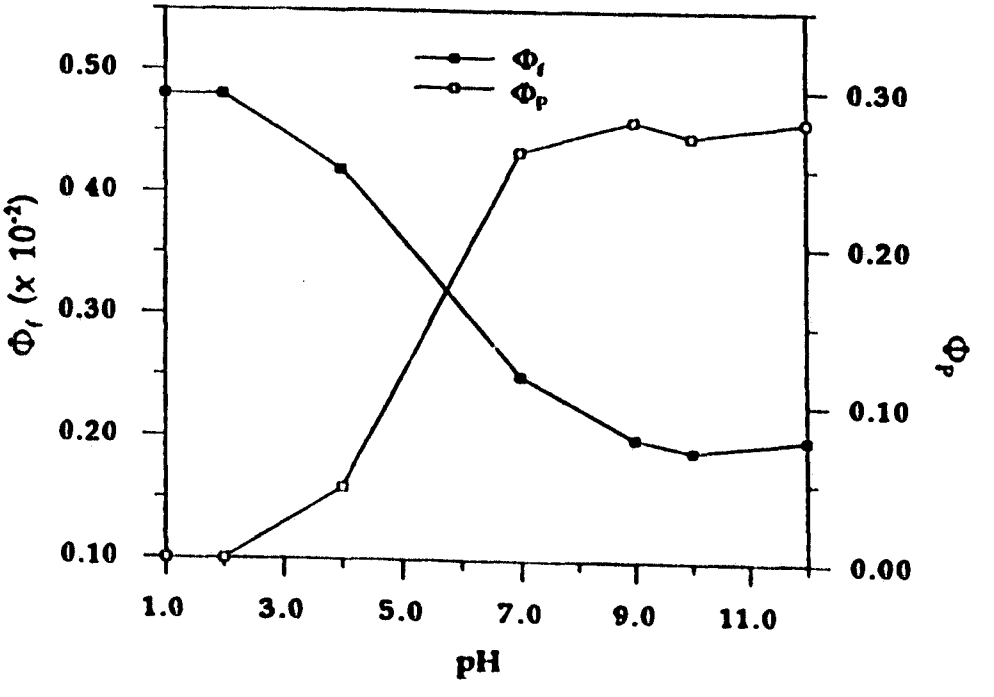

Figure 2.13 Fluorescence (Φ_f) and product (Φ_p) quantum yields for **145** as a function of the pH of the aqueous portion in 80% H_2O-CH_3CN.

2.2.4 Mechanism of Photodecarboxylation: Photogeneration of 8π-Electron Cyclically Conjugated Carbanions

The mechanism of photodecarboxylation of carboxylic acids and esters has been a subject of numerous studies. The generality of this process is now well established and a variety of mechanisms have been proposed.[18] For instance Miller and coworkers have outlined 25 possible cleavage modes for the carboxyl group.[24] Most of these possible modes could be eliminated in the present study on the basis of the results obtained in this work. However, there still remain three possible primary photochemical pathways which can account for the observed results in the present study (eqs 2.28-2.30).

$$R\text{-}CO_2^{\bullet} \xrightarrow{k_{dc}} R^- + CO_2 \qquad (2.28)$$

$$R\text{-}CO_2^{\bullet} \xrightarrow{k_h} R^{\bullet} + CO_2^{\bullet-} \xrightarrow{k_{ET}} R^- + CO_2 \qquad (2.29)$$

$$R\text{-}CO_2^{\bullet} \xrightarrow[-e^-]{k_{ee}} R\text{-}CO_2^{\bullet} \xrightarrow{k'_h} R^{\bullet} + CO_2 \qquad (2.30)$$

In the first (eq 2.28) and the simplest mechanism, photoexcitation of the carboxylate ion results in the loss of CO_2 via heterolytic C-C bond cleavage from S_1 to give the corresponding carbanion. The second process (eq 2.29) involves homolytic C-C bond fragmentation of the carboxylate, to generate the alkyl radical and the carbon dioxide radical anion. This initially formed radical-radical anion

pair then undergoes electron transfer, to generate the alkyl carbanion. Although the exact redox potentials of the various couples are not known for the xanthene and thioxanthene systems, electron transfer (k_{ET}) would form ground state antiaromatic carbanions, viz., **130** and **137**, respectively, and should not be favoured. Furthermore, the lack (*except in the case of* **142**) of radical derived products as well as observed solvent isotope effects are inconsistent with this mechanism (eq 2.29). The final possible mechanism (eq 2.30) for photodecarboxylation involves electron ejection from the excited carboxylate ion, followed by homolytic C-C bond cleavage to yield the corresponding radical intermediates. If these radicals are to be converted into the carbanions, as the product studies require, they must recapture the initially ejected electron, which is not reasonable since solvated electrons are efficiently scavenged by oxygen and other dissolved impurities or solutes.

Previous results obtained in our laboratories have clearly demonstrated that dibenzannelated acetic acids undergo photodecarboxylation from S_1 via eq 2.28, the details of which are shown in Scheme 2.3.[32] In this simple mechanism photoexcitation of the carboxylate ion leads to the loss of CO_2 from S_1 in a heterolytic manner, to generate the corresponding carbanion. The intermediate carbanions produced in the decarboxylation step are many orders of magnitude more basic than H_2O, and are protonated promptly or even concertedly with their formation, to give the hydrocarbon photoproducts. In the present study, the following observations support this ionic mechanism: (1) The incorporation of

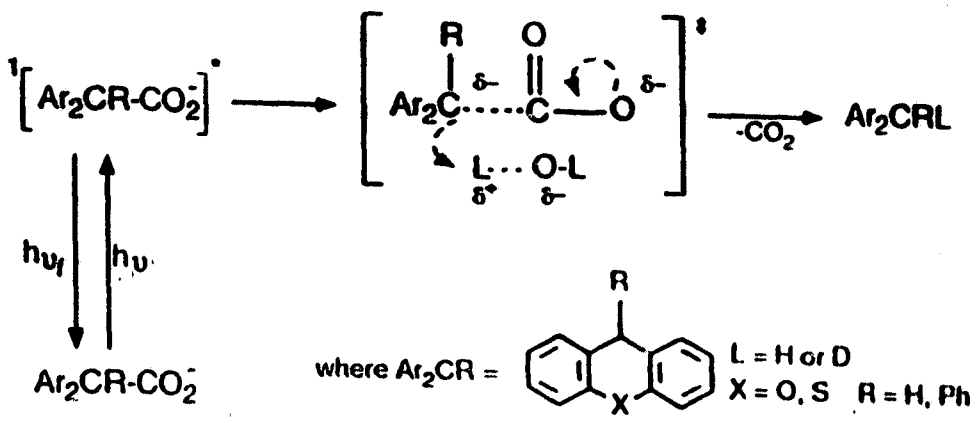

Scheme 2.3

deuterium in the photoproducts when the reactions are carried out in D_2O is consistent with the intermediacy of carbanions. The general lack of radical coupling products, further supports an ionic mechanism for photodecarboxylation. The only exception to this is **142**, which gave a radical coupling product, viz., 9,9'-bisxanthene (**128**). However, this does not imply that radical **131** is formed via a primary C-C bond homolysis of the carboxylate ion. Product studies of **142** indicate that **131** is formed via electron ejection from the initially generated 9-xanthenide carbanion **130**. This is further supported by the fact that when **142** is photolyzed in the presence of an electron acceptor *p*-nitrobenzoic acid (PNB), formation of PNB radical dianion has been detected by ESR spectroscopy, which is indicative of an electron transfer reaction.[31] No ESR signals are observed in the dark or on photolysis of PNB alone. The propensity of **130** to act as an one

electron reducing agent is compatible with it being a "π-excessive" antiaromatic system. (2) Fluorescence emissions of **142** and **145** display a strong dependence on the pH of solution, which is consistent with an ionic mechanism of photodecarboxylation via the carboxylate form. (3) Solvent isotope effects observed in the product quantum yields (Φ_P) when photolyses of these acids were carried out in H_2O and D_2O are consistent with the proposed ionic mechanism.

In the transition state the excited carboxylate ion is surrounded by water molecules which assist the photodecarboxylation, by stabilizing the developing negative charge at the carbon center via hydrogen bonding interactions. The solvent isotope effects (Φ_H/Φ_D; Table 2.13) observed in product quantum yields also suggest that heterolytic C-C bond cleavage step is associated with solvent interactions in the transition state. However, these interaction between the excited carboxylate ion and the solvent are probably not very strong ("loose transition state") since the observed solvent isotope effects are not very large ($\Phi_H/\Phi_D \approx 1.30$).

In ionic ground state decarboxylation reactions it is recognized that electron withdrawing groups that can stabilize the intermediate carbanions accelerate the reaction. However, Wan and Krogh[32a,b] have shown that the presence of such groups is not necessary to observe efficient photodecarboxylation in diarylacetic acids. In a study of series of compounds related to diphenylacetic acid (e.g., **28-31**), differing only in the structure of the central ring, Wan and Krogh[32a,b] have shown that in the ground state fluorene-9-carboxylic acid (**28**) is most easily decarboxylated whereas suberene-5-carboxylic acid (**29**) is reluctant to

decarboxylate even on prolonged reflux. This is not surprising since ionic decarboxylation of 29 would form an 8π-electron (antiaromatic) carbanion intermediate 34, which requires a very high activation energy. However, photochemically, 29 is the most reactive (Φ = 0.60; k(decarboxylation) = 6 x 10^9 s^{-1}), whereas 28 is the least reactive (Φ = 0.042; k(decarboxylation) = 8.8 x 10^6 s^{-1}) acid. The unconjugated systems 30 and 31 are about an order of magnitude more reactive than 28.

An estimate of the rate constant (k_{dc}) for photodecarboxylation, assuming the applicability of mechanism shown in Scheme 2.3, can be made by combining the product quantum yields (Φ_P) and fluorescence lifetimes (τ_f) (in 80% H_2O-CH_3CN) according to equation 2.31. These rate constants for 142 and 145 are

$$\Phi_P = k_{dc}\tau \text{ or } k_{dc} = \Phi_P/\tau \qquad (2.31)$$

presented in Table 2.14. Estimate of the photodecarboxylation rate constants of

Table 2.14 Rate Constants for Photodecarboxylation (k_{dc}) of 142 and 145 in 80% H_2O-CH_3CN (pH 7).

	τ (ns)[a]	k_{dc} (s^{-1})
142	0.40 ± 0.05	7.5 x 10^8
145	0.35 ± 0.05	8.0 x 10^8
29[a]	< 0.10[b]	~6.0 x 10^9

a) Lifetimes measured in 80% H_2O-CH_3CN via single photon counting.
b) Taken from ref. 32a.

147 and **148** could not be made because their short fluorescence lifetimes in aqueous solution($\tau < 0.1$ ns) could not be measured with the instrument available.

Comparison of these k_{dc}'s for **142** and **145** shows that presence of phenyl group has no significant effect on the photodecarboxylation rate. However, these rates are approximately an order of magnitude lower than for of suberene carboxylic acid[32a,b] (**29**; $k_{dc} = 6 \times 10^9\ s^{-1}$).

Attainment of a 4nπ-electron internal cyclic array (4n) in S_1 is not restricted to only charged intermediates. In the next section, photophysical studies of dibenz[b,f]oxepin (**155**) show that photoexcitation of this non-planar molecule in S_0 results in a planar fluorescent S_1 state. The driving force behind this conformational change is believed to be the attainment of a 8π-electron ICA in S_1 (*vide infra*).

2.3 Conformational Studies of Dibenz[b,f]oxepin (155) and Related Systems by Steady-State Fluorescence Spectrophotometry: Evidence for an Excited State 8π Internal Cyclic Array[129a]

2.3.1 Syntheses

2.3.1.1 Dibenz[b,f]oxepin (155)

The strategy utilized in the synthesis of dibenz[b,f]oxepin (**155**) is shown

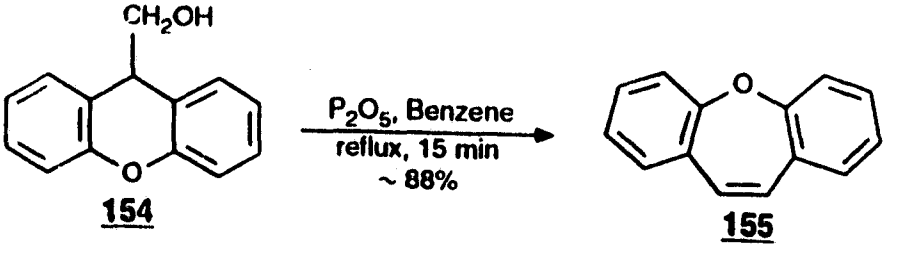

154 **155** (2.32)

in eq 2.32.[130] An acid catalyzed rearrangement of xanthene-9-methanol (154) with phosphorus pentoxide (P_2O_5) in boiling benzene readily afforded 155 in ~ 85% yield. Purification of the crude material by recrystallization from 95% EtOH afforded pure 155.

2.3.1.2 10,11-Dihydrodibenz[b,f]oxepin (156)

Reduction of 155 over 5% palladium-on-charcoal catalyst gave 10,11-dihydrodibenz[b,f]oxepin (156) in ~ 90% yield (eq 2.33).[130] The crude material was

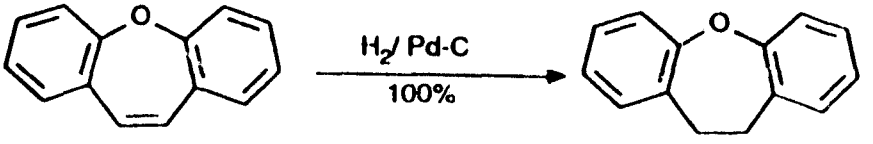

155 156 (2.33)

purified by distillation to afford pure 156 as a colourless viscous oil.

2.3.1.3 10-Hydroxy-dihydrodibenz[b,f]oxepin (157)

Following the general procedure of Zweifel and Brown[131] treatment of 155 with a solution of BH_3 in dry THF followed by oxidation with H_2O_2 in the

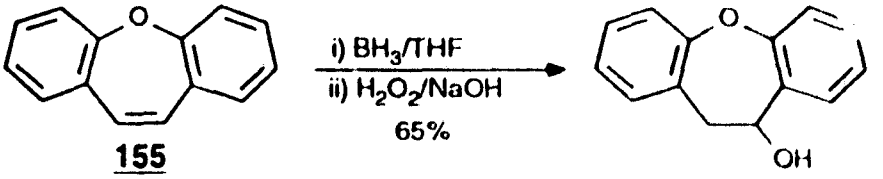

155 157 (2.34)

presence of 3 M NaOH afforded the crude **157** in ~ 72% yield (eq 2.34). The crude material was purified by bulb-to-bulb distillation to obtain pure **157** as a colourless viscous oil.

2.3.1.4 10-Hydroxysuberane (158)

Treatment of suberene (**37**) with BH_3 in dry THF followed by oxidation with H_2O_2/NaOH afforded the crude **158** as an oil (eq 2.35). The crude oil

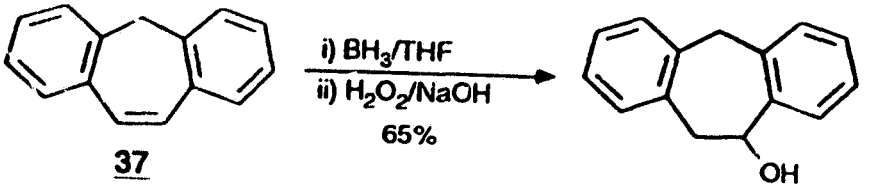

37 **158** (2.35)

could not be purified by bulb-to-bulb distillation because of its facile thermal dehydration to give starting material, viz., suberene (**37**). Column chromatography (neutral Al_2O_3; CH_2Cl_2) was employed to obtain pure **158**.

2.3.1.5 Dibenz[b,f]thiepin (160)

Treatment of thioxanthene-9-methanol (**159**) with P_2O_5 in boiling benzene readily afforded dibenz[b,f]thiepin (**160**) in ~43% yield (eq 2.36). The crude

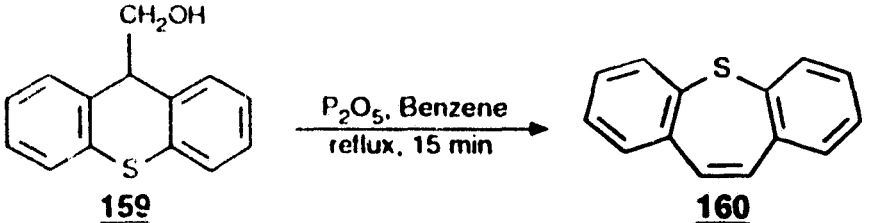

159 **160** (2.36)

material was purified by recrystallization from 95% EtOH and characterized by ^{1}H NMR (250 MHz) and mass spectrometry.

2.3.1.6 Dibenzocycloöctatetraene (163)

The synthesis of dibenzcycloöctatetraene (163) was achieved by the Wittig condensation of *o*-phthaldehyde (162) with the bis-phosphonium salt 161 in DMF using LiOEt as the base (eq 2.37).[132]

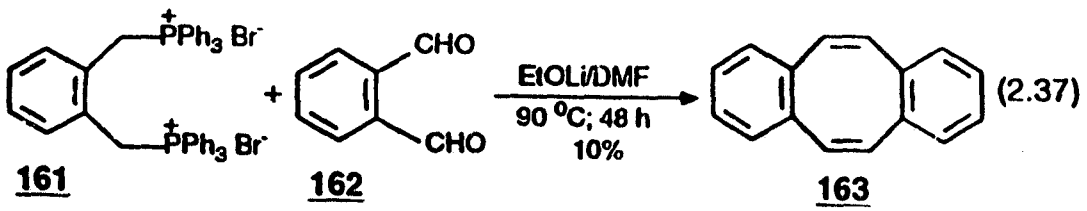

2.3.2 Product Studies

2.3.2.1 Photolysis of 10,11-Dihydrodibenz[b,f]oxepin (156)

When a 10^{-3} M solution of 156 in 100% CH_3CN was photolyzed at 254 nm (Ar purged; ~ 14 °C; 15-30 min) the colour of the reaction mixture changed immediately (*ca.* 1 min) to yellow. After 10 min of photolysis the CH_3CN was evaporated to obtain a yellow mixture. The ^{1}H NMR (90 MHz) spectrum of the product mixture, besides showing signals due to starting material 156, showed appearance of new signals between δ 7-6 and δ 2-4, indicating the formation of photoproduct(s). Thin layer chromatographic analysis of the product mixture

(silica plates; CH_2Cl_2) also showed the presence of several new spots, only one which was a significant (R_f = 0.14). Separation of this spot from the product mixture by preparative scale thin layer chromatography afforded a yellow solid. The ^1H NMR (250 MHz) spectrum of the isolated product showed complex sets of multiplets between δ 2-4 and δ 6-7, along with signals due to aromatic protons between δ 7.1-8.2 (*see Experimental*). The ^{13}C NMR spectrum (*see Experimental*) showed the presence of 28 distinct carbons. It was not possible to assign a structure to this product with any degree of confidence due to the complex nature of the ^1H and ^{13}C spectra. Attempts were made to solve the structure of the product by X-ray crystallography. The solid was crystallized from CH_2Cl_2/hexanes to give pale yellowish crystals. The ^1H and ^{13}C NMR of this

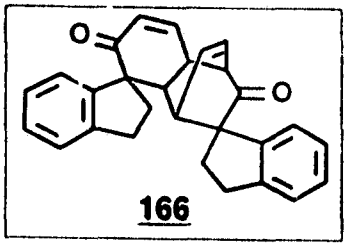

166

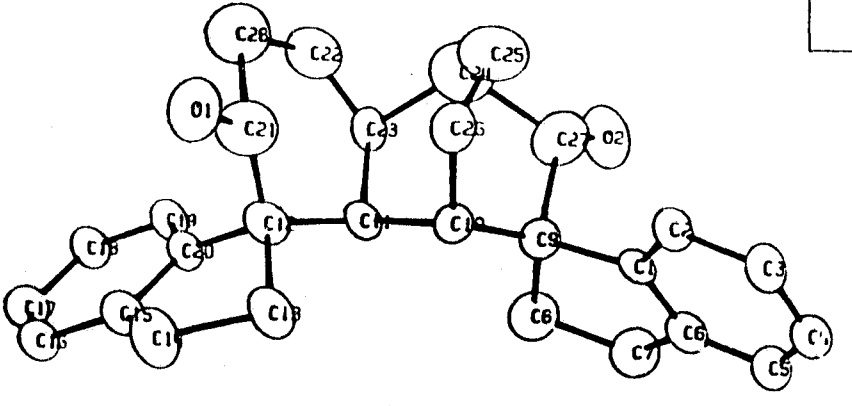

Figure 2.14 X-Ray crystal structure (preliminary) of **166**.

material were identical to the spectra observed before re-crystallization. A preliminary X-ray crystal structure showed the material to be a spiro adduct **166** (Figure 2.14). Difficulties were encountered in refining the structure to acceptable limits. Work will continue by other members of the group to improve this.

Previous studies of 9*H*-xanthene (**125**) photochemistry have shown that irradiation of **125** in aqueous CH_3CN solution results in its photoisomerization to yield the 6*H*-dibenzo[b,d]pyran (**126**).[117] The proposed mechanism of this isomerization involves initial aryl-oxygen bond homolysis from S_1, to give a biradical (Scheme 2.4). Trivial recombination of the biradical gives back

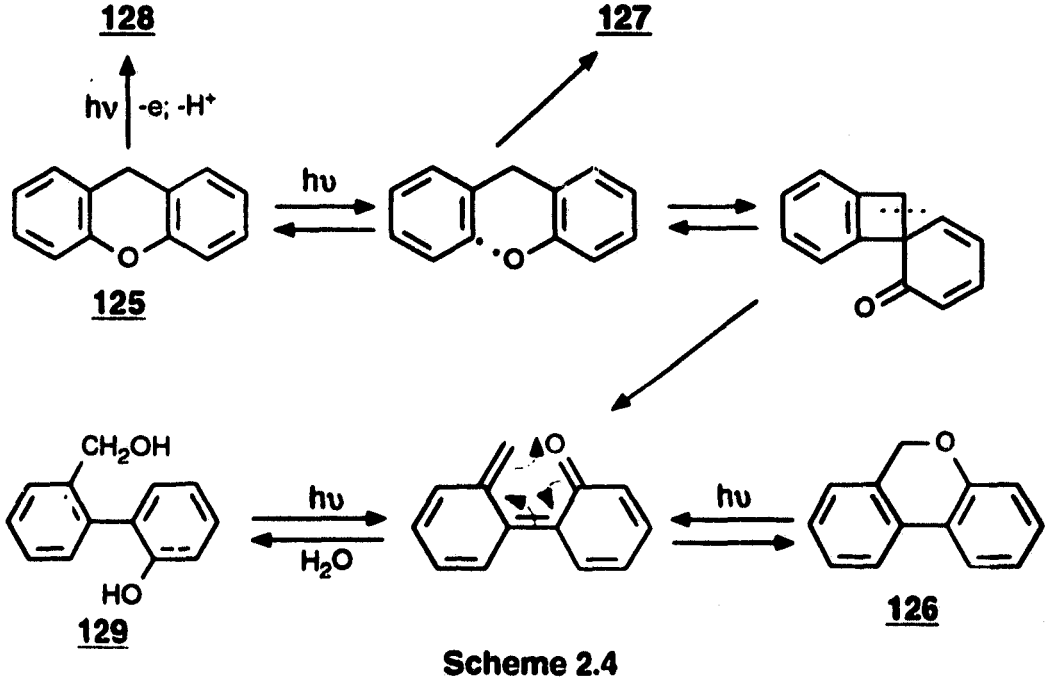

Scheme 2.4

9*H*-xanthene (**125**). However, recombination of the biradical at the ipso benzylic position (ortho to the phenol) gives a spiro ketone intermediate. Subsequent

homolysis of C-C bond of the spiro ketone shown gives a biphenyl *o*-quinone methide, which undergoes electrocyclic ring closure to give the observed pyran **126** (Scheme 2.4).[117] The high reactivity of the spiro ketone is obviously due to the presence of a highly strained fused four-membered ring in the molecule. The formation of **166** can also be explained by invoking a similar mechanism for **156**. That is, photoexcitation of **156** results in aryl-oxygen bond homolysis, to generate biradical **164** (eq 2.38). Subsequent coupling of biradical **164** by ipso attack of the

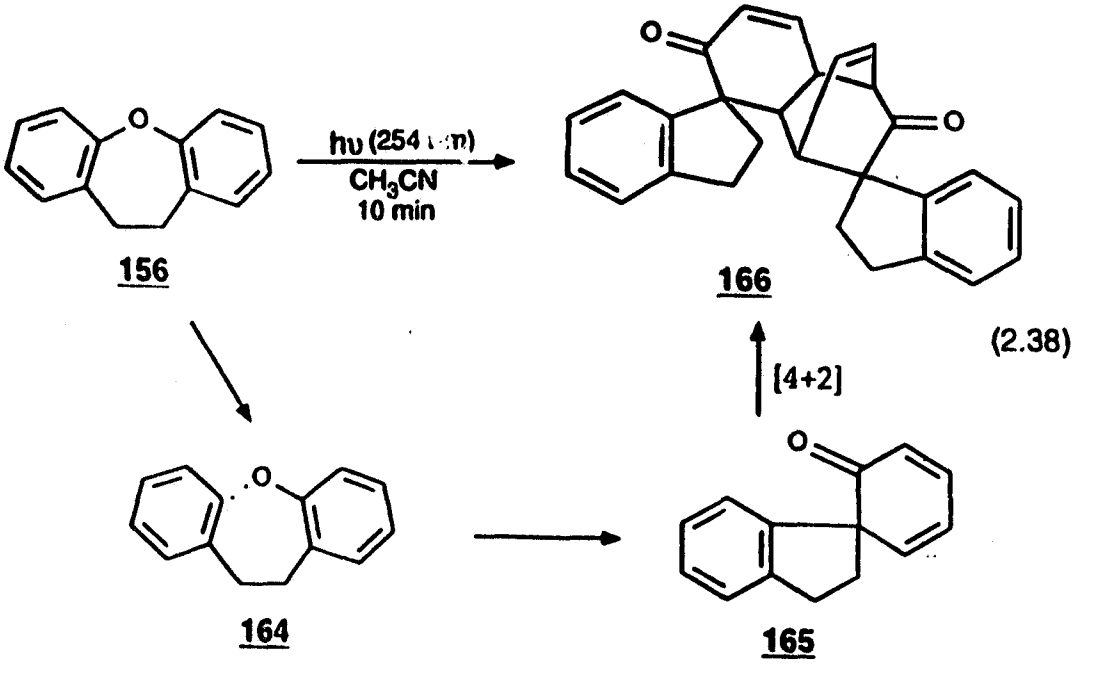

(2.38)

phenyl radical to the *ortho* position of the phenoxyl ring forms the spiro ketone **165**. Thermal [4+2] cycloaddition reaction of **165** with a second molecule yields the observed adduct **166**. This cycloaddition of **165** was unexpected; repeated attempts to isolate only the spiro ketone **165** were of no avail. However, based

on the structure of the final product **166** it is clear that **165** was formed. Thus, although **165** does not fragment as observed for the cyclobutene analog (*vide supra*), the presence of the cyclohexadienyl system makes it exceptionally reactive towards [4+2] cycloaddition.

2.3.2.2 Photolysis of Dibenz[b,f]oxepin (155)

Photolysis of a solution of **155** in 100% CH_3CN at 300 nm for 30 min did not result in any observable reaction. Even at longer irradiation times (*ca.* 60-90 min), **155** remained photochemically inert. This was surprising because under similar reaction conditions **156** reacted extensively to form the adduct **166**. Although the extended conjugation present in **155** (*cis*-stilbene like chromophore) lowers its S_1 energy relative to **156**, the complete lack of aryl-oxygen bond homolysis was unexpected. Steady-state fluorescence studies of **155** provided some remarkable insights of the nature of the excited state of **155** (*vide infra*).

2.3.2.3 Photolysis of Dibenz[b,f]oxepin (155) in the Presence of Et_3N

Photolysis of a 10^{-3} M solution of suberene (**37**) in the presence of ~ 5 M

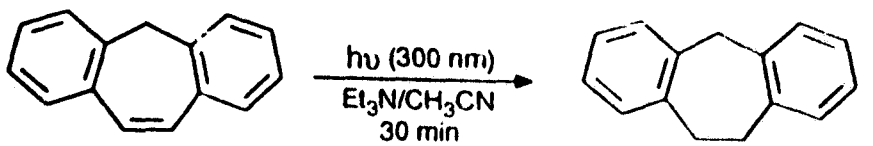

37 (87%) **49** (2.39)

Et_3N in CH_3CN (λ_{ex} = 300 nm; Ar purged; 30 min) resulted in the reduction of the

vinylic C=C bond to yield suberane (49) (ca. ≈ 87%) (eq 2.39). The mechanism of this reduction is believed to be via an initial electron transfer from Et_3N to photoexcited 37, to form the radical-ion pair (167) (Scheme 2.5).[133] Subsequent hydrogen abstraction by the radical anion followed by protonation (or *vice versa*) results in the overall reduction of the C=C bond, to give 49. A similar photolysis

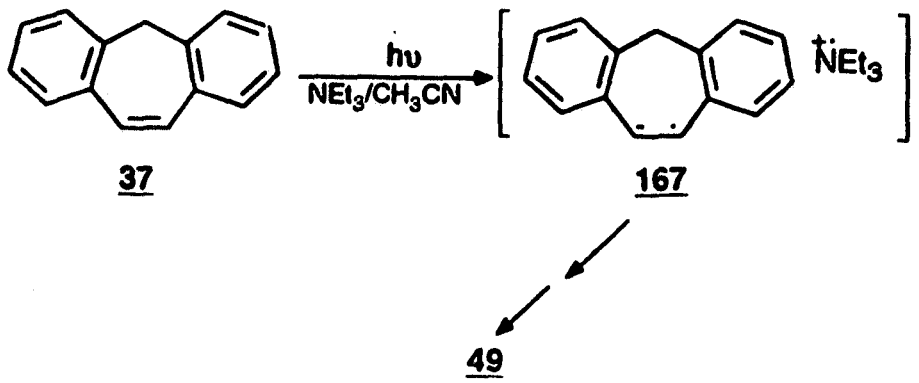

Scheme 2.5

of 155 in a solution of ~ 5 M Et_3N in CH_3CN resulted in a substantially lower yield of the corresponding reduced product 156 (ca. ≈ 27%)

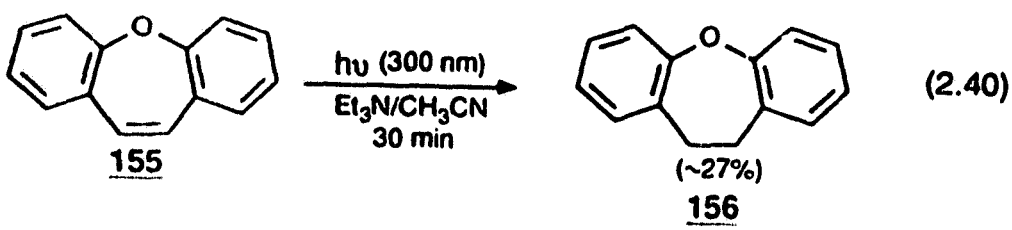

(2.40)

(eq 2.40). This suggests that the vinylic C=C bond of 155 is less prone to photoreduction compared to that in 37. The lower photoreactivity of the vinylic

C=C of 155 was further evidenced in photohydration reactions of 37 and 155 in aqueous acid discussed below.

2.3.2.4 Photolysis of 155 and 37 in Aqueous Acid

Photolysis of 155 in 50% CH_3CN-10% (w/w) H_2SO_4 at 300 nm (*ca.* 30 min) resulted in very inefficient photohydration of the C=C bond, to yield 157 (< 2%, by ^1H NMR integration) (eq 2.41). However, a similar photolysis of 37 resulted in an efficient reaction, to yield 158 (29%) (eq 2.42). Although, the reasons for

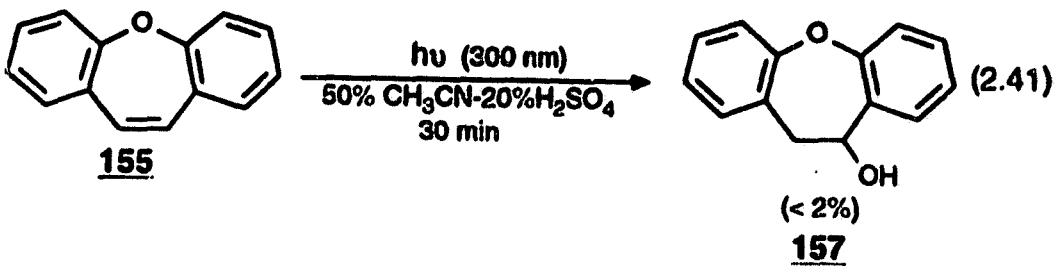

155 157 (2.41)

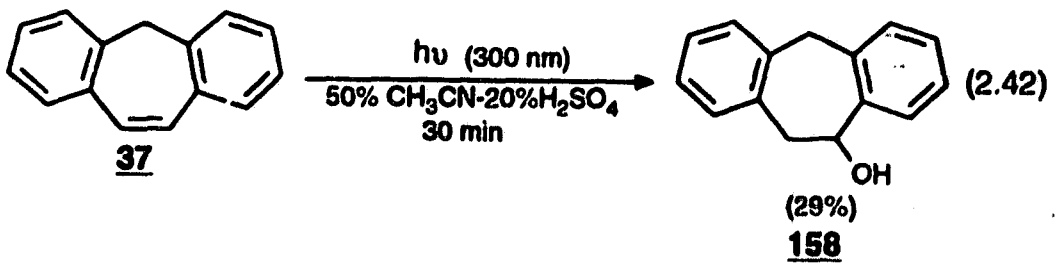

37 158 (2.42)

the lower reactivity of 155 vs 37 are not clear at this stage, it is clear that the vinylic C=C bond of 155 behaves differently compared to its counterpart in 37.

2.3.2.5 Photolysis of 157 and 158 in Aqueous Acid

Photolysis of **157** in 50% CH_3CN-20% H_2SO_4 at 254 nm (*ca.* 30 min) resulted in the efficient formation of **155** (*ca.* 50%, by ^1H NMR integration) (eq 2.43). A similar photolysis of **158** resulted in a much lower yield of **37** (~ 9%) (eq 2.44).

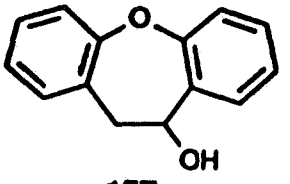

157

$h\upsilon$ (254 nm), 50% CH_3CN- 20% H_2SO_4, 30 min → **155** (50%) (2.43)

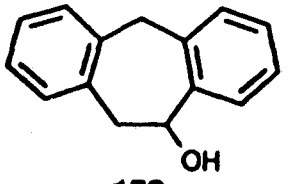

158

$h\upsilon$ (254 nm), 50% CH_3CN- 20% H_2SO_4, 30 min → **37** (~9%) (2.44)

In contrast, thermal acid catalyzed dehydration of **158** was very efficient to yield **37** (*ca.* 100%) (eq 2.45) whereas, it was difficult to dehydrate **157**, even in refluxing aqueous acid (*ca.* 50% CH_3CN-20% (w/w) H_2SO_4 solution) (eq 2.46).

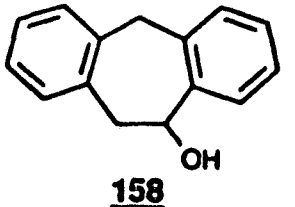

158

Δ, 10% H_2SO_4, 10 min → **37** (100%) (2.45)

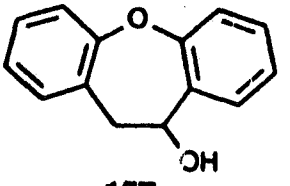

157

Δ, 20% H_2SO_4, 2 h → no reaction (2.46)

Photochemical dehydration of **157** (to give **155**) was so favourable that it could be readily achieved even in dilute acid solutions. Thus, photolysis of **157** in 50% CH_3OH-H_2O (pH ~ 1) resulted in the formation of **155** (≈ 45%) as the only product. In contrast, photolysis of **158** under similar conditions resulted in the formation of the corresponding methyl ether **168** (≈ 30%) (eq 2.47). These results

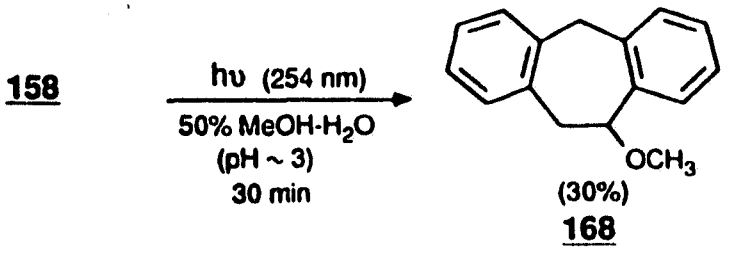

(2.47)

suggest that there is an enhanced driving force for the formation of the vinylic C=C in **155** on photolysis which is absent in **37**. Conversely, it is photochemically difficult to remove the vinylic C=C of **155** compared to **37**.

2.3.3 Steady-state and Transient Fluorescence Studies

The fluorescence and absorption characteristics of an aromatic molecule can often provide qualitative information concerning the conformation of the molecule in the ground and first excited states.[134] The theoretical basis for such studies lies in the Franck-Condon (FC) principle. The basis of which lies in the fact that electronic motion (≈ 10^{-15} sec) is much faster than the nuclear motion (≈ 10^{-13} to 10^{-11} sec). Thus immediately after excitation, the excited state of the molecule retains the ground state geometry and solvent cage. This is called the FC excited state. From this state, the molecule can rapidly (10^{-14} to 10^{-13} sec) lose excess vibrational

energy by thermal relaxation and end up in the lowest vibrational level (v_0) of S_1. Fluorescent molecules in solution usually have a singlet lifetimes of 10^{-9} to 10^{-6} s.

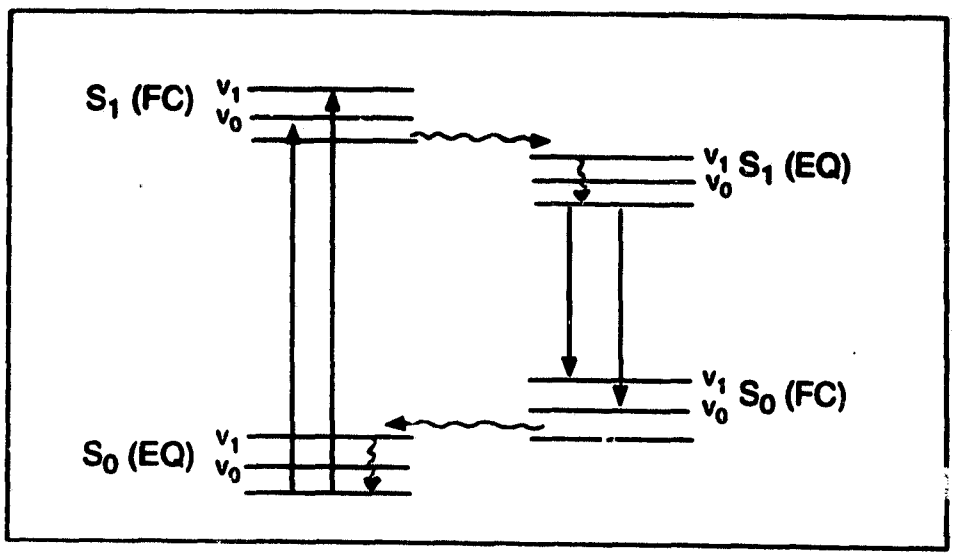

Figure 2.15 Four-state diagram illustrating the Franck-Condon principle.

Since solvent relaxation and changes in molecular geometry are governed by the speed of nuclear motion (10^{-13} to 10^{-15} sec), there is usually sufficient time for the excited state molecule to acquire a geometry and solvent cage more compatible with its electron density distribution. This lower energy state is called the equilibrium (EQ) excited state and it lies lower in energy than the FC excited state owing to the stabilization resulting from the change in geometry and solvent cage. Emission from the EQ excited state produces the FC ground state which has the

same geometry and solvent cage as the EQ excited state. Subsequently, thermal relaxation occurs and the molecule reaches the lower energy EQ ground state. These processes are diagrammatically presented in Figure 2.15.[134a] The emitting EQ excited state always lies lower in energy from the FC excited state. Therefore, amount of energy lost between the absorption and emission processes is related to the extent of geometrical and solvation changes that accompany the excitation process, and is known as the Stokes loss. As the difference in S_0 and S_1 geometries and solvation becomes greater, so does the extent of Stokes loss. Rigid molecules (e.g., anthracene) undergo little geometrical and solvation changes on excitation and exhibit small Stokes loss. These systems exhibit a mirror image relationship between their absorption and emission spectra. The presence of a mirror image relationship between the absorption and emission spectra indicates that the vibrational level spacings in the FC and EQ states of such molecules are similar. In contrast, if a molecule undergoes a large geometrical change on photoexcitation, a large Stokes loss and absence of mirror image relationship between the absorption and emission spectra are usually observed.[134b]

The fluorescence excitation and emission spectra of **156** in cyclohexane is shown in Figure 2.16. The broad structureless excitation spectrum was identical to its absorption spectrum. The emission spectrum of **156** (λ_{max} = 300 nm) was also structureless and showed no significant Stokes shift (Figure 2.16). In contrast,

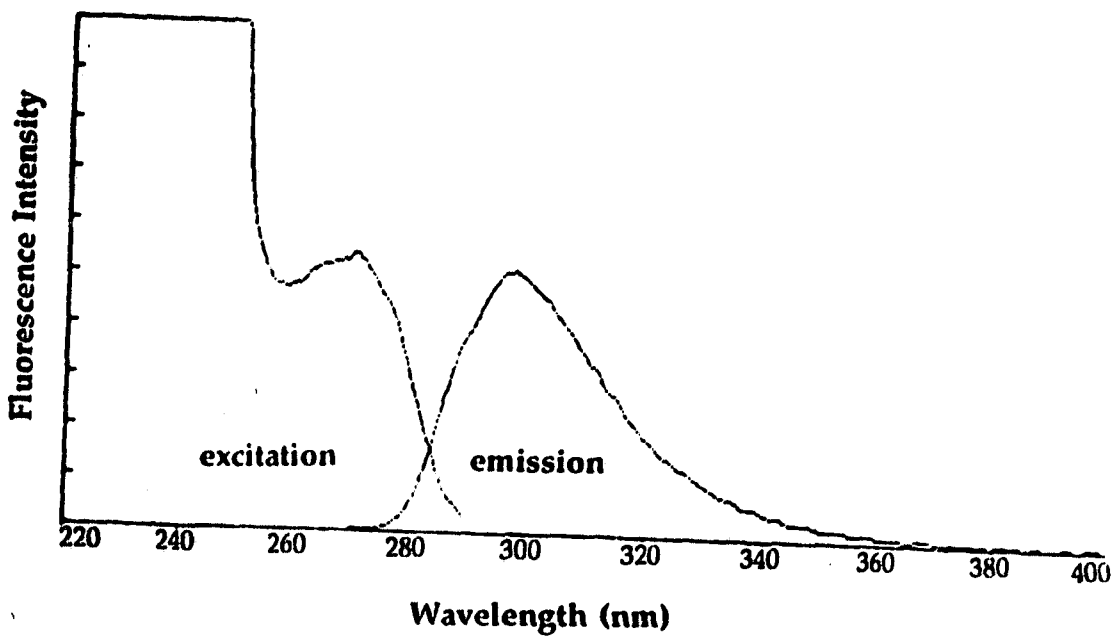

Figure 2.16 Fluorescence excitation and emission spectra of dihydrodibenz[b,f]oxepin (**156**) in CH_3CN.

the emission spectrum of **155** (λ_{max} = 478 nm in cyclohexane) was highly Stokes shifted (4720 cm^{-1}; Stokes-shift was calculated according to the definition given by Berlman[135]) and showed well defined vibronic structure (progression ≈1500 cm^{-1}) (Figure 2.17). The structureless excitation spectrum of **155** was essentially identical to its absorption spectrum. The shape and vibronic structure in the emission spectrum of **155** were not affected by the polarity of the solvent, suggesting that the observed Stokes-shift is not due to solvation changes experienced by **155** in the S_1 state. In fact, albeit a little more diffused, the vibronic structure was evident even in H_2O. Some photophysical parameters for

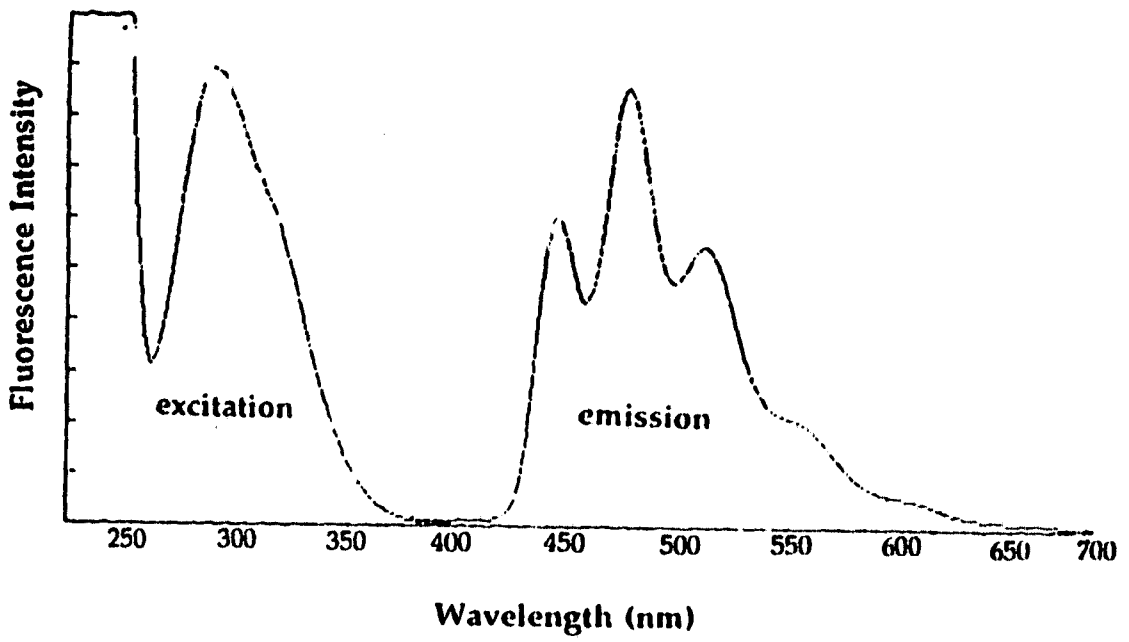

Figure 2.17 Fluorescence excitation and emission spectra of dibenz[b,f]oxepin (**155**) in CH_3CN.

155 and related systems are presented in Table 2.15.

Table 2.15 Photophysical Parameters for 155, 156 and 160 in CH_3CN.

Compound	Φ_f	τ_f^d (ns)
155	0.14 ± 0.02[a]	8.36 ± 0.04
156	0.08 ± 0.03[b]	2.50 ± 0.03
160	0.0012 ± 0.0002[c]	< 0.2

a) Measured relative to quinine bisulfate (Φ_f = 0.55 in 1 N H_2SO_4)[177].
b) Measured relative to xanthene (**125**) (Φ_f = 0.24 in CH_3CN; *vide supra*).
c) Measured relative to **155**.
d) Measured by single photon counting; all good first order decays; **155**: λ_{ex} 290 nm/λ_{em} 490 nm; **156**: λ_{ex} 260 nm/λ_{em} 320 nm; **160**: λ_{ex} 300 nm/λ_{em} 550 nm.

The emission spectrum of the related system dibenz[b,f]thiepin (**160**) also

displayed a similar large Stokes-shift. However, vibronic structure in the

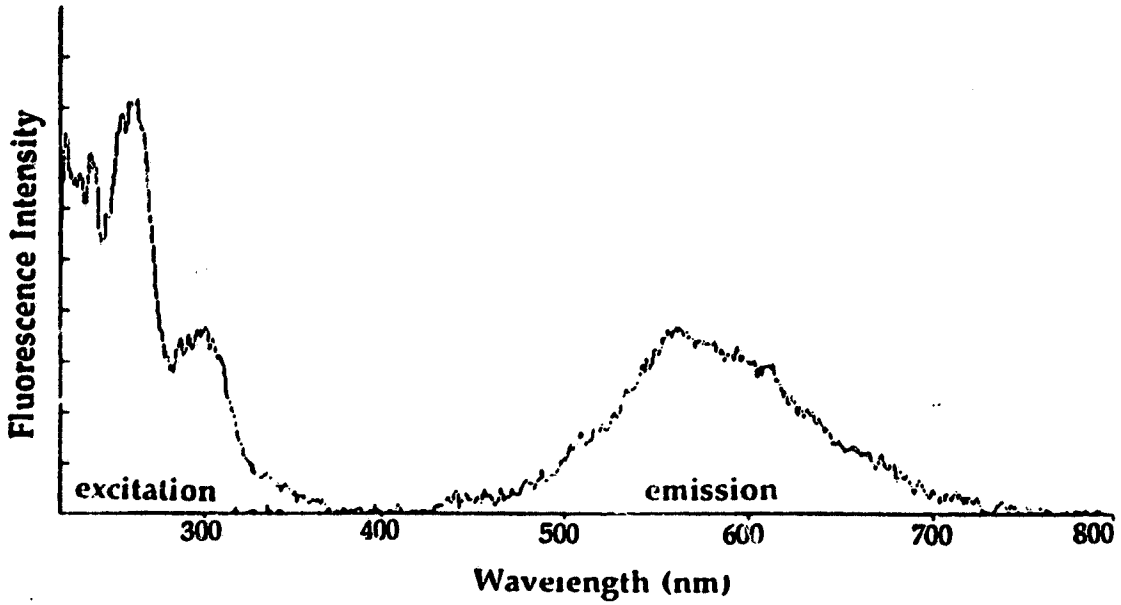

Figure 2.18 Fluorescence excitation and emission spectra of dibenz[b,f]thiapin (**160**) in CH_3CN.

emission of **160** was not evident (Figure 2.18). Its weak emission is probably due to the presence of the sulfur atom which increases the rate of intersystem crossing to the triplet state ("heavy atom effect").[120]

Suberene (**37**) also possesses the *cis*-stilbine chromophore like **155** and **160** but lacks possible conjugation through the methylene carbon. The emission spectrum of suberene[48] does not exhibit the large Stokes shift or enhanced vibronic structure observed for **155**. However, suberene is highly fluorescent (Φ_f = 0.86 ± 0.05; τ_f = 5.04 ± 0.04 (in CH_3CN))[48], which is a general characteristic of

"locked" stilbenes.[120]

The spectral characteristics of **155** suggest that its excited state geometry is different from that in the ground state. The ground state structure, as determined by X-ray crystallography,[136] resembles that of a "butterfly" (saddle-shaped), with its "wings" highly bent backwards (Bent **155**). Non-planar **155** is torsionally free around aryl-O and aryl-CH bonds and can therefore acquire a number of different conformations which are all energetically very similar. At room temperature, the S_0 state of **155** can thus be visualized as an ensemble of all such possible conformers. Since the energy difference between these various conformations is very small, electronic transition from S_0 results in a structureless absorption spectrum. On the other hand, transitions originating from a planar electronic state should produce highly structured spectra,[134] because planar rigid molecules do not have rotational freedom possessed by non-planar molecules. As a consequence the vibrational levels of planar molecule in a given electronic state are discrete. The highly structured emission spectrum of **155** indicates that the geometry of S_1 is planar and rigid.

A change from a non-planar S_0 state to a more planar fluorescent S_1 state has been well documented for biphenyl and related compounds.[134,135] The rationale commonly accepted for this behaviour of biphenyl is that there is enhanced double bond character in the bond joining the two phenyl rings in S_1 which is absent in S_0.[127] A similar geometrical change is proposed to occur on photoexcitation of **155**. That is, bent **155** in S_0 becomes planar **155** in S_1. The high

degree of non-planarity of **155** in the ground state is not surprising since simple

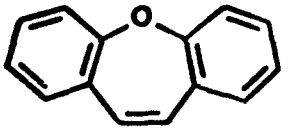

Planar **155**

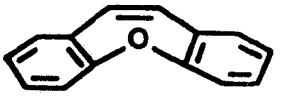

Bent **155**

Hückel-type arguments would predict that a planar structure would be unfavourable due to the antiaromatic nature of a planar 8π-electron cyclic array in the internal ring. More sophisticated MO calculations confirm this.[138] However, fluorescence studies indicate that the EQ excited state geometry of **155** is that of a rigid planar system (Planar **155**), allowing for complete conjugation of the internal cyclic array. Indeed, the emission of **155**, with its associated fine structure, could be mistaken for the fluorescence emission of anthracene (which has a similar overall appearance but is about 80 nm blue-shifted), a classic example of a strongly emitting rigidly planar (in both S_0 and S_1) aromatic molecule.[135]

Another possibility for the observed emission spectrum of **155** which was

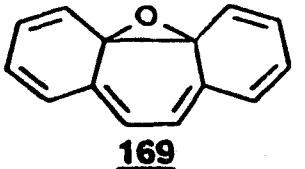

169

considered but ruled out is the formation of the valence isomer **169** via electrocyclic 6π ring closure. Adiabatic extrusion of the oxygen atom in a subsequent step then forms phenanthrene in S_1. However, the known fluorescence emission of phenanthrene is ≈ 110 nm blue-shifted compared to that observed for **155**. On the other hand, the observed emission might be due to the valence isomer **169** itself. This is unlikely since this would be equally possible in the case of suberene (**37**). However, **37** does not show any spectral characteristics that are observed for **155**. The fluorescence spectra of two related systems **163** and iminostilbene (**170**) were also studied. The absorption and emission

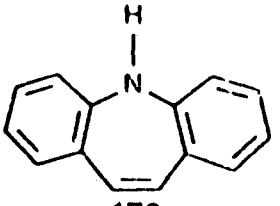

170

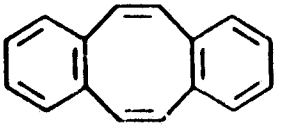

163

spectra of **163** were found to be structureless and did not exhibit a significant Stokes loss. These spectral characteristics suggest that **163** does not undergo geometrical changes (i.e., does not become planar) in S_1. This is presumably due to the unfavourable interactions experienced by the *peri* hydrogens preventing **163** from acquiring a planar structure. Emission studies of **170** proved to be extremely difficult because of its very weak emission. However, no significant Stokes loss was observed in the emission spectrum.

Corroborating chemical evidence for the above proposal of a "stabilized" planar geometry of **155** in S_1 comes from the reactivity data obtained in product

studies. Resistance of the vinylic C=C bond of **155** compared to **37** to undergo photoreduction (by Et_3N) and photohydration points towards the special nature of this bond in **155**. Thermal acid-catalyzed dehydration of **158** to form **37** is readily achievable (eq 2.45), whereas **157** is inert to dehydration, even in refluxing aqueous acid (eq 2.46). On the other hand, photodehydration of **157** to form **155** in 50% H_2O-MeOH is readily accomplished even in dilute acid solutions (pH 1-3), whereas **158** results largely in the formation of the corresponding methyl ether **168** (eq 2.47), indicating that there is an enhanced driving force for formation of **155** in the excited state which is absent in **158**.

The results of π-SCF PPP calculations[129b] of planar **155** in both S_1 and S_0 show that there is a greater degree of delocalization of the oxygen lone pair to the rest of the π-system in S_1 than in S_0. Moreover, the electron density from the oxygen is distributed more in the central ring in S_1 than in S_0, consistent with the proposal that there is an inherent driving force for this ring to achieve delocalization of 8π electrons (which is achieved only when **155** becomes planar in S_1).

These results unambiguously support the proposal that photoexcitation of bent **155** results in a planar fluorescent state. The energetics of this process are illustrated in Figure 2.18. The potential energy curves in Figure 2.18 show that a large energy barrier exists for the planarization of bent **155** in S_0. In S_1, bent **155** undergoes fast torsional twisting to acquire the planar fluorescent S_1(EQ) conformation. Emission from planar **155** produces the S_0(FC) which has the same

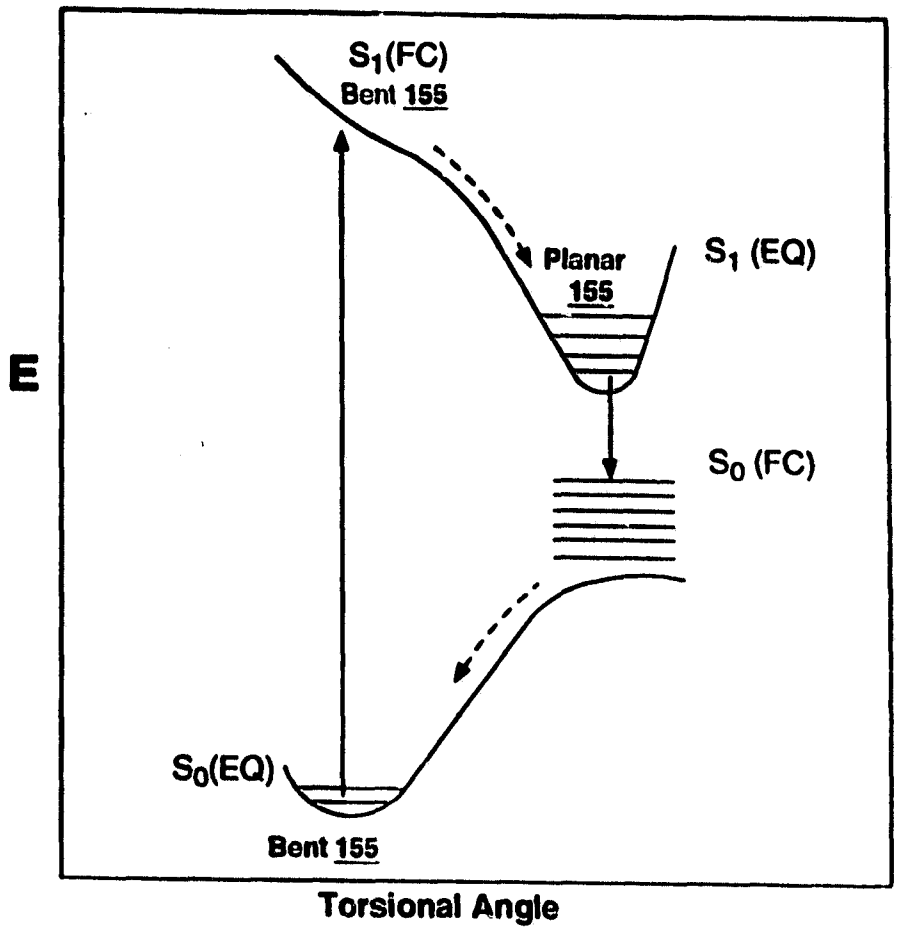

Figure 2.18 Potential energy surface for torsional twisting of **155** in S_0 and S_1 (energies not drawn to scale).

geometry as the S_1(EQ). Since no emission from the bent **155** (S_1(FC)) was observed, it suggests that there is no (or very small) energy barrier for the planarization of **155** on S_1 surface.

It was pointed out earlier that photolysis of N-methylacridan (**140**) in 50% H_2O-CH_3CN resulted in its dimerization, to form **141**. This process was investigated in more detail and is presented below.

2.4 Photoionization of N-methylacridan (140) in Aqueous Solution[139]

2.4.1 Product Studies

N-methylacridan (140) was prepared from $NaBH_4$ reduction of N-methylacridinium iodide, adapted from the reported procedure of Colter and coworkers[140] (eq 2.48). The crude white crystalline material was

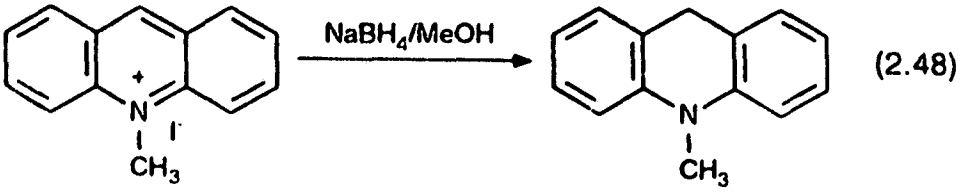

(2.48)

140

recrystallized several times from 95% EtOH until GC analysis showed no detectable traces of impurities.

Photolysis of **140** in 50% H_2O-CH_3CN at 254 nm (*ca.* 10-60 min) yielded very small amounts (< 5%) of 9,9'-bis(N-methylacridyl) (**141**), as detected by ^1H NMR of the product mixture. The solution after photolysis was of deep orange colour. However, photolysis of the above solution at 300 nm for the same length of time resulted in efficient formation of an off-white precipitate. Analysis of the ^1H NMR spectrum of the product mixture obtained in the 300 nm photolysis showed a much higher yield (≈ 50%) of **141** (by ^1H NMR integration) (eq 2.49).

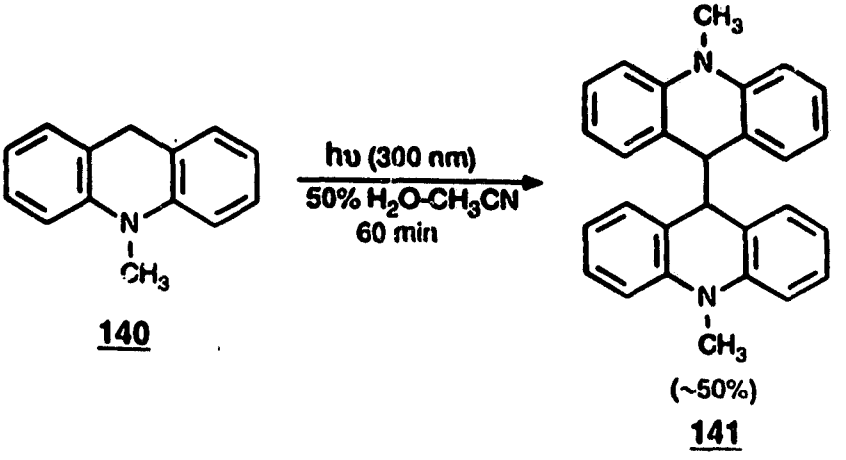

(2.48)

The pronounced change in the yield of **141** by simply changing the wavelength of irradiation from 254 nm to 300 nm was not expected since organic compounds in solution generally do not exhibit wavelength-dependent photochemistry.

Photolysis of **140** in 50% H_2O-CH_3CN (Ar purged) also leads to the formation of trace amounts of N-methylacridone (**171**) and N-methylacridinium ion (**172**) (*vide infra*), in addition to **141**, which is the only observable product by ^1H NMR. Both of **171** and **172** have intense ($\varepsilon \geq 40{,}000\ M^{-1}\ cm^{-1}$) absorption at ≈

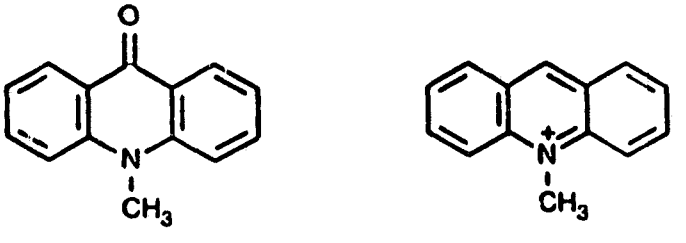

254 nm where **140** has very little absorption (its λ_{max} is at 286 nm). The observed "low" reactivity of **140** at 254 nm is therefore due to preferential absorption of

light by traces of **170** and **172** which are formed in the course of photolysis. The situation is very different at 300 nm. Here, both **171** and **172** have much lower molar extinction coefficients (ε) and all the light is absorbed by **140** (λ_{max} ~ 286 nm).

To investigate the effect of solvent polarity, photolysis of **140** was carried out in several polar and non-polar solvents. Yields of **141** obtained on photolysis of **140** at 300 nm in a variety of solvents are shown in Table 2.16. It is evident

Table 2.16 Yields of 141 on Photolysis of 140 under argon in Various Solvents.[a]

Solvent	% Yield of 141[b]
100% CH_3CN	9 ± 2
100% Et_2O	4 ± 2
95% EtOH	9 ± 2
100% hexane	5 ± 2
50% H_2O-CH_3CN	18 ± 3

a) A solution 50 mg of **140** in 100 mL of solvent irradiated for 15 min at 300 nm.
b) Due to the fact that **141** has a very long retention time on the GC column, yields were calculated by ^{1}H NMR integration of the product mixture after work-up.

that the yields of **141** are enhanced in more polar solvents, and are especially favourable in H_2O-CH_3CN.

In a related study Fukuzumi and coworkers[141] have shown that photolysis

of **140** in the presence of O_2 results in the formation of N-methylacridinium ion (**172**). The key step in the proposed mechanism of this reaction involves electron transfer from the photoexcited **140** to O_2, to generate a radical cation/anion pair ($140^{+\cdot}/O_2^{-\cdot}$). Subsequent transformation of this species depended on whether the solvent was pure CH_3CN or aqueous CH_3CN with added H^+, but in each case involving the formation of *N*-methylacridan radical (**140**$^{\cdot}$) from the decomposition of $140^{+\cdot}/O_2^{-\cdot}$.[141] In the present study photolysis of an O_2 purged solution of **140** in 50% H_2O-CH_3CN also resulted in the formation of **172**. However, **140** was found to be reactive even in the absence of O_2, in both 100% CH_3CN and aqueous CH_3CN solutions. Results of the photolyses of **140** in the presence and absence of oxygen and/or water are shown in Table 2.17.

Table 2.17 Yields of Products from Photolysis of 140 under Various Conditions at 300 nm.[a]

Solvent	Product (% yield)
100% CH_3CN (O_2 purged)	**171** (≈ 55%)[b]
50% H_2O-CH_3CN (O_2 purged)	**172**[c]
50% H_2O-CH_3CN (Ar purged)	**141** (≈ 50%)[b,d]

a) ~100 mg of **140** in 200 mL of solvent irradiated at 300 nm for 30 min.
b) Product identified by comparison with ^1H NMR of authentic sample; yields calculated by integration of appropriate peaks.
c) Detected by UV-Vis absorption spectrum by comparison to an authentic sample; yield not quantified but **172** is the only product observed under these conditions ($\Phi = 0.022 \pm 0.004$ using 10^{-3} M of **140** with $\lambda_{ex} = 302$ nm; oxygenated 50% H_2O-CH_3CN; steady-state irradiation); no **141** formed according to ^1H NMR of reaction mixture.
d) Photolysis was done for 120 min, because the formation of precipitate of **141** blocks light.

2.4.2 Quantum Yields for Formation of 141 in Various Solvents

Since **141** was not readily analyzable using GC because of its long retention time and possible decomposition on the column, quantum yields for the loss of substrate **140** (Φ_L) were measured instead (Table 2.18), using 9*H*-xanthene (**125**)

Table 2.18 Quantum Yields for Loss (Φ_L) of 140 and Fluorescence Lifetimes (τ) in Deaerated Solvents.

Solvent	Φ_L[a]	τ ns[b]
100% Et_2O	0.0060 ± 0.0006	3.7 ± 0.2
100% Hexane	0.0060 ± 0.0006	4.3 ± 0.2
100% CH_3CN	0.022 ± 0.002	7.0 ± 0.2
95% EtOH	0.0080 ± 0.0005	5.6 ± 0.2
50% H_2O-CH_3CN	0.085 ± 0.004	6.5 ± 0.2
100% H_2O[c]		3.0 ± 0.2

a) Measured by GC using **125** as external standard; λ_{ex} = 302 nm.
b) Measured by single photon counting; λ_{ex} 300 nm/λ_{em} 360 nm; all decays were single exponential ($\chi^2 \leq 1.30$).
c) < 2% CH_3CN used as a cosolvent.

as external standard. The GC results were corrected for differences in the detector response of xanthene (**125**) and the starting material **140**. Because **141** was the only isolable product in these experiments, where mass balances were excellent (> 90%), Φ_L when divided by a factor of two should be a good measure of the quantum yield for formation of **141**. Products **171** and **172** were formed in only trace amounts (< 1%) in argon purged solutions. The higher Φ_L in 50% H_2O-

CH_3CN compared to 100% CH_3CN, 95% EtOH and the other solvents used is consistent with the results of the product studies followed by ^1H NMR.

2.4.3 Steady-State and Transient Fluorescence Measurements

As has been already stated, photolysis of N-methylacridan (**140**) in 50% H_2O-CH_3CN at 254 nm results in the formation of trace amounts of N-methylacridone (**171**) and N-methylacrdinium ion (**172**). These compounds have higher ε at 254 nm than **140**, and once formed then absorb light preferentially, slowing down the reaction of **140**. However, **171** and **172** could not be detected by ^1H NMR of the reaction mixture. Steady-state fluorescence studies of the photolysis of **140** conclusively demonstrate that trace amounts of **171** and **172** are indeed formed on irradiation at 254 nm. Fluorescence spectra of **140** were recorded using 10^{-4} M deaerated 50% H_2O-CH_3CN solutions at excitation wavelengths of 254 and 300 nm. Excitation of **140** at 254 nm gave an intense emission centered at 480 nm and two much weaker emissions centered at 425 nm and 360 nm. The emission at 480 nm was assigned to N-methylacridinium ion (**172**) by comparison with the emission spectrum of the authentic material. This emission band increased in intensity as more and more of **172** is formed with increasing photolysis time. The weak emission bands at 425 nm and 360 nm were assigned to N-methylacridone (**171**) and N-methylacridan (**140**), respectively, by comparison with the emission spectra of the authentic samples. However, when **140** was excited at 300 nm only one emission band at 360 nm (due to **140**) was

observed. The intense emission observed from **172** on excitation at 254 nm is due to the fact that this ion has an intense absorption at this wavelength as well as being a strongly emitting chromophore. Ketone **171** also has an intense absorption here but it is not formed to the same extent as **172** in aqueous CH_3CN solutions (*vide supra*). These steady-state fluorescence measurements clearly demonstrate the formation of both **171** and **172** on photolysis of **140** in deaerated aqueous CH_3CN.

Fluorescence lifetimes of **140** were measured using single photon counting (λ_{ex} = 300 nm; λ_{em} = 360 nm) using deoxygenated solutions. Lifetimes of **140** in various solvents are shown in Table 2.18. All observed decays were single exponential. A decrease in lifetime (τ) is observed going from 100% CH_3CN to 100% H_2O with a concomitant increase in Φ_L. However, lifetimes of **140** in both 100% Et_2O and 100% hexane are shorter than expected based on the measured Φ_L in these two solvents. Hence, it seems that there is no simple correlation between fluorescence lifetime and the quantum efficiency of formation of **141** in a given solvent. Using fluorescence quenching data, Fukuzumi and coworkers[141] have found that the photoredox chemistry of **140** (in the presence of O_2) originates from S_1. The lifetime data in the present study are not completely consistent with S_1 reactivity but does not rule out S_1 reaction either. To investigate the nature of the excited state (S_1 vs T_1) involved in the reaction of **140** triplet quenching experiments were carried out.

2.4.4 Triplet Quenching of 140

The excited state responsible for a photochemical reaction is often, though not always, either the lowest excited singlet state (S_1) or the lowest triplet state (T_1) of a molecule. To find out which is involved, sensitization and quenching methods are employed. Most studies use triplet sensitizers or triplet quenchers, partly because the results of such studies are more easily interpreted than those involving the use of singlet sensitizers and quenchers.[142]

Triplet quenching experiments involve selectively exciting the molecule in presence of an appropriate triplet (T_1) quencher. The logic of triplet quenching is that if the quencher inhibits the reaction, then reaction is deduced to occur from T_1. A negative result implies that reaction occurs from S_1. In the choice of a suitable triplet quencher it is imperative that the T_1 energy of the quencher must be lower than the T_1 energy of the molecule under investigation for efficient energy transfer to take place. Furthermore, the quencher must not have a significant absorption in a region of the spectrum where the molecule is being excited.[142]

The triplet energy of 140 has not been measured. However, it would be expected to be close to that of N,N-dimethylaniline (173) and diphenylamine (174)

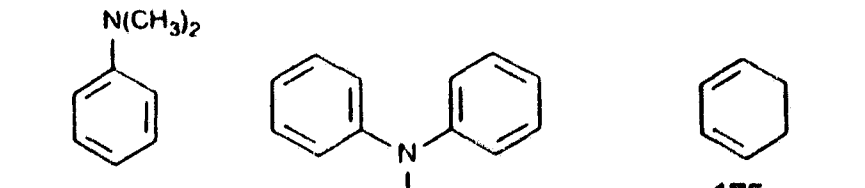

173 $E_T \approx 72{\cdot}75$ kcal mol^{-1}

174

175 $E_T \approx 53$ kcal mol^{-1}

(E_T's ≈ 72-75 kcal mol^{-1})[143], if not lower. Use of 1,3-cyclohexadiene (175) (E_T ≈ 53 kcal mol^{-1}) as triplet quencher would be appropriate.[142] Since the triplet lifetime of 140 was found to be ≥ 2 μs from laser flash photolysis experiments (*vide infra*) use of a 10^{-3} M solution of triplet quencher should quench all triplet states and hence also reaction of 140 to form 141 if the triplet state was indeed responsible for the observed chemistry. Photolysis of a 10^{-3} M solution of 140 in the presence of 0.003 M solution of 1,3-cyclohexadiene (175) in 100 mL CH_3CN at 300 nm gave the same yield of 141 as without added quencher. This shows that the lowest triplet is not the reactive state in the reaction of 140.

2.4.5 Mechanism of Photodimerization of 140

Extensive studies by Fukuzumi and coworkers[144] have shown that 140 is a modest reducing agent, in both ground and excited states. For example, photolysis of 140 in the presence of phenacyl bromide results in the formation of N-methylacridinium bromide and acetophenone via an overall redox process initiated by light.[144a] This same reaction could be sensitized with $[Ru(bpy)_3]^{+2}$ by irradiation at 452 nm, where 140 does not absorb.[144a] Use of photoexcited benzophenone with 140 has been reported by Peters and coworkers[145] to result in electron transfer from 140 to triplet benzophenone, to generate the corresponding radical anion/radical cation pair which subsequently collapse to the radical pair after proton transfer from 140^{+} to benzophenone radical anion. In all these studies, 140 has been used for redox or photoredox chemistry in conjunction with

an electron acceptor of some kind. However, results obtained in the present study clearly show that **140** is reactive even in the absence of any added electron acceptor, to produce **141** in modest yields.

The formation of **141** suggests the intermediacy of *N*-methylacridan radical (**140**·). Based on the knowledge of redox behaviour of **140**,[144,145] one can envision that the photoexcitation of **140** results in the one-electron transfer (solvent acting as an electron sink) to generate the *N*-methylacridan radical cation (**140**$^{+}$·) which upon deprotonation gives the radical **140**·. A working mechanism for the formation of **141** is presented in the Scheme 2.6.

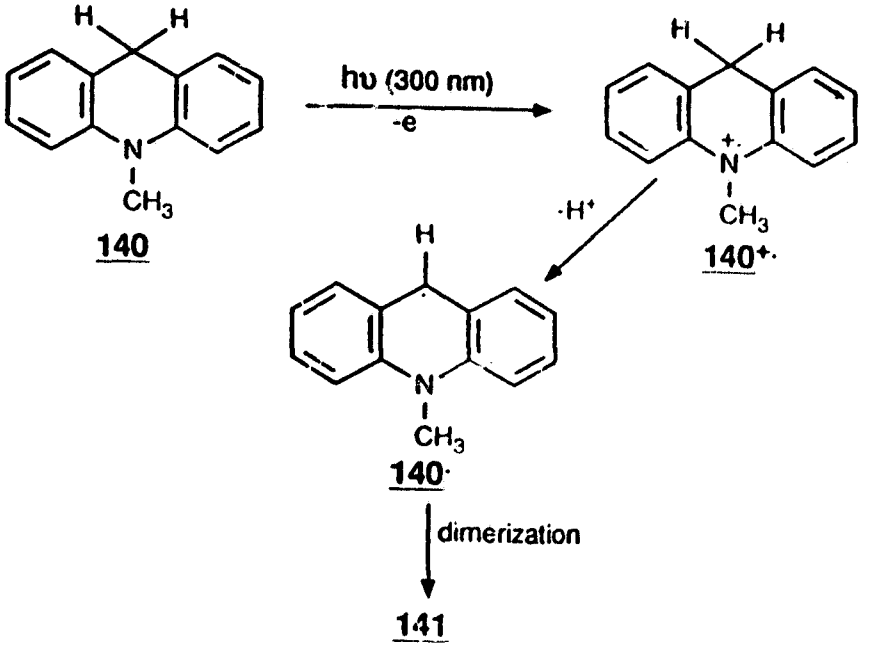

Scheme 2.6

To investigate the details of this proposed mechanism (Scheme 2.6) laser flash photolysis studies of **140**, in collaboration with Dr. L. J. Johnston (National Research Council (NRC) at Ottawa) were carried out at NRC.

Laser excitation of **140** at λ_{ex} = 308 nm in CH_3CN gave a transient species absorbing at λ_{max} = 520 nm ($\tau \approx 3$ μs). This transient was assigned to the triplet-triplet (T_1-T_1) absorption of **140** based on its efficient reaction with 1,3-cyclohexadiene (175; 1.2 x 10^{10} M^{-1} s^{-1}) and oxygen. A similar laser excitation of **140** in aqueous CH_3CN gave two transient species, absorbing between 600-700 nm and at λ_{max} 355 nm. The transient absorbing between 600-700 nm decayed in 70 μs, leaving a species with a sharp absorption at 355 nm and a weak shoulder at ≈ 420 nm. The 420 nm band was assigned to the *N*-methylacridinium ion (**172**), based on comparison with the spectrum of an authentic sample. The transient species absorbing in long wavelength region between 600-700 nm region also had a UV band at ≈ 330 nm ($\tau \approx 50$ μs). This transient (between 600-700 nm) was not affected by oxygen or 1,3-cyclohexadiene and was assigned to *N*-methylacridan radical cation (**140**$^{+\cdot}$), based on the comparison with the previously reported spectrum for **140**$^{+\cdot}$ by Peters and coworkers[145], and to the reported transient spectrum of diphenylamine radical cation[146]. The transient due to **140**$^{+\cdot}$ (λ_{max} 630 nm) was quenched by bases such as hydroxide (k(HO^-) = 2 x 10^7 M^{-1} s^{-1}) and pyridine (k = 7.3 x 10^5 M^{-1} s^{-1}). The rate constant obtained for the reaction of pyridine with **140**$^{+\cdot}$ was in good agreement with that obtained for deprotonation of **140**$^{+\cdot}$ in CH_3CN (+ 0.6 M Et_4N^+ BF_4^-) from simulation of electrochemical data

($k = 3.1 \times 10^6\ M^{-1}\ s^{-1}$)[147]. Time resolved conductance measurements further confirmed the formation of an ionic species, viz., $140^{+\cdot}$.

The laser flash photolysis experiments of **140** in aqueous CH_3CN showed that the transient signals due to T_1 (λ_{max} = 520 nm) and $140^{+\cdot}$ (λ_{max} = 630 nm) were formed rapidly within the duration of the laser pulse. However, the signal due to cation **172** (λ_{max} 420 nm) showed readily resolvable growth over a time-scale which agreed with the decay of $140^{+\cdot}$ (λ_{max} 630 nm), suggesting that the radical cation $140^{+\cdot}$ was the precursor of cation **172**.

Two laser experiments in which triplet **140** was generated in aqueous CH_3CN and then re-excited ≈ 100 ns later with a 530 nm Nd:YAG laser pulse, indicated that the photoionization of **140** can occur from a triplet state. However, the lowest energy triplet was not responsible for the one laser photoionization of **140** since all the radical cation $140^{+\cdot}$ was formed within the duration of the laser pulse, whereas the triplet absorption decayed over a period of several microseconds.

Laser excitation of **140** in aqueous CH_3CN in the presence of 0.038 M NaOH, shortened the lifetime of the radical cation $140^{+\cdot}$ ($\tau \approx 1.5$ μs), and showed the formation of a new species absorbing at λ_{max} 510 nm. However, this species was not particularly long lived (5-10 μs) and was not easily separable from the T_1 of **140**, which also absorbs in the 500 nm region. However, when the experiment was repeated in the presence of both hydroxide (to reduce $140^{+\cdot}$ lifetime) and 0.0025 M 1,3-cyclohexadiene (**175**) (to quench T_1 of **140**), the transient

species absorbing at λ_{max} = 510 nm was clearly observed. This transient was assigned to **140**$^{\cdot}$ based on comparison with the reported spectrum.[148,151] Furthermore, in the presence of hydroxide the rate of growth of signal due to **140**$^{\cdot}$ at 510 nm agreed well with the rate of decay of **140**$^{+\cdot}$ indicating that it was the precursor of radical **140**$^{\cdot}$.

In the absence of added base the kinetics of decay of **140**$^{+\cdot}$ agreed well with those for the growth of cation **172**. However, the lifetime of radical **140**$^{\cdot}$ was substantially shorter than that of **140**$^{+\cdot}$ under these conditions, suggesting either **140**$^{\cdot}$ or **140**$^{+\cdot}$ could be the precursor for cation **172**. In the presence of base and diene (to quench T_1), the growth of signal due to cation **172** occurred more slowly than the decay of **140**$^{+\cdot}$ but was in reasonable agreement with the decay of radical **140**$^{\cdot}$ monitored at 510 nm. Addition of small amounts of air to the sample resulted in a more rapid decay of the radical and a concomitant increase in the rate of production of cation **172**. However, addition of air did not decrease the yield of **172**; similarly, either oxygen or nitrogen purged samples gave the same yield of **172**. These results indicate that most of cation **172** is formed from radical **140**$^{\cdot}$, at least under these conditions.

The results of laser flash photolysis experiments demonstrate that excitation of **140** in aqueous CH_3CN results in its photoionization from S_1, to generate N-methylacridyl radical cation (**140**$^{+\cdot}$), which on subsequent deprotonation generates N-methylacridyl radical (**140**$^{\cdot}$), which dimerizes to give **141**. The detailed mechanism of photodimerization of **140** is presented in Scheme 2.7.

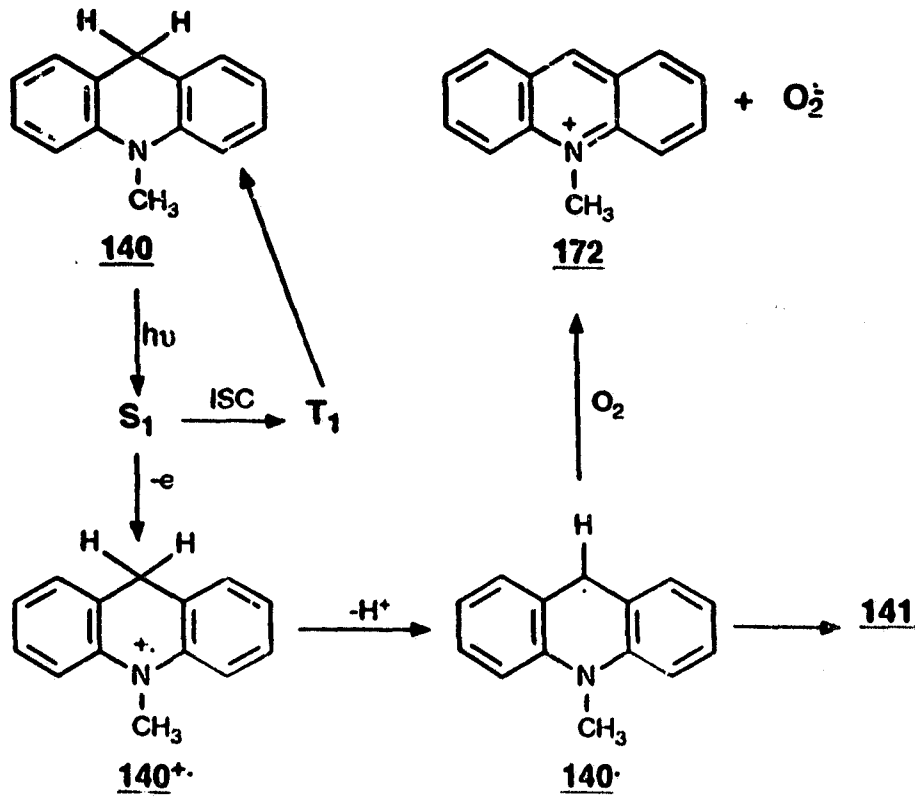

Scheme 2.7

In this mechanism photoionization of **140** from S_1, results in the formation of *N*-methylacridan radical cation (**140**$^{+\cdot}$). The major reaction pathway for **140**$^{+\cdot}$ is deprotonation, to give the corresponding radical **140**$^{\cdot}$; the intermediacy of **140**$^{\cdot}$ is demonstrated by both isolation of dimerization product **141** in preparative scale product studies and its direct detection in the laser flash photolysis experiments.

Intersystem crossing to T_1 of **140** does occur but leads to no chemistry. The lifetime of **140**$^{+\cdot}$ is shortened in the presence of added hydroxide which is consistent with the enhancement in deprotonation of **140**$^{+\cdot}$ to form **140**$^{\cdot}$. However, no overall increase in the yield of **141** was observed on increasing the pH suggesting that the product-limiting step is ionization of **140** which is probably irreversible. The radical **140**$^{\cdot}$ can be trapped by residual oxygen present in the solution (to give cation **172**) which competes with its dimerization. This notion is not unreasonable since, the product studies have shown that photolysis of **140** in oxygen purged solution results in the exclusive formation of **172**.

CHAPTER THREE

EXCITED STATE CARBON ACID BEHAVIOUR OF SUBSTITUTED SUBERENES: PHOTOGENERATION OF CYCLICALLY CONJUGATED 8π ELECTRON CARBANIONS

3.1 Syntheses

3.1.1 2,8-Dimethoxysuberene (180)

2,8-Dimethoxysuberene (**180**) was synthesized according to the method outlined in Scheme 3.1. The ketone **178** was synthesized following reported procedures[149] via the Parham cyclization[150] of the lithium salt of carboxylic acid **177** generated in situ by the treatment of **176** with one equivalent of *n*-BuLi followed by the addition of CO_2 (g) at -100 °C. Treatment of **177** with *n*-BuLi at -100 °C induced halogen-metal exchange followed by cyclization to yield the desired ketone **178**. The double bond of **179** was introduced by treating it with NBS to give corresponding 10-bromo substituted ketone which upon dehydrobromination with 2,4,6-collidine afforded the ketone **179**. Reduction of ketone **179** with the mixed hydride reagent[151] $LiAlH_4/AlCl_3$ in dry THF afforded 2,8-dimethoxysuberene (**180**) which was purified by recrystallization from $EtOH/H_2O$. The ^1H NMR and mass spectral analyses were consistent with the structure of **180**. The corresponding dideuterated **181** was similarly prepared by reducing ketone **179** with $LiAlD_4/AlCl_3$ in dry THF. The mass spectrum and ^1H NMR of **181** were consistent with the incorporation of two deuteriums at the indicated bibenzylic position.

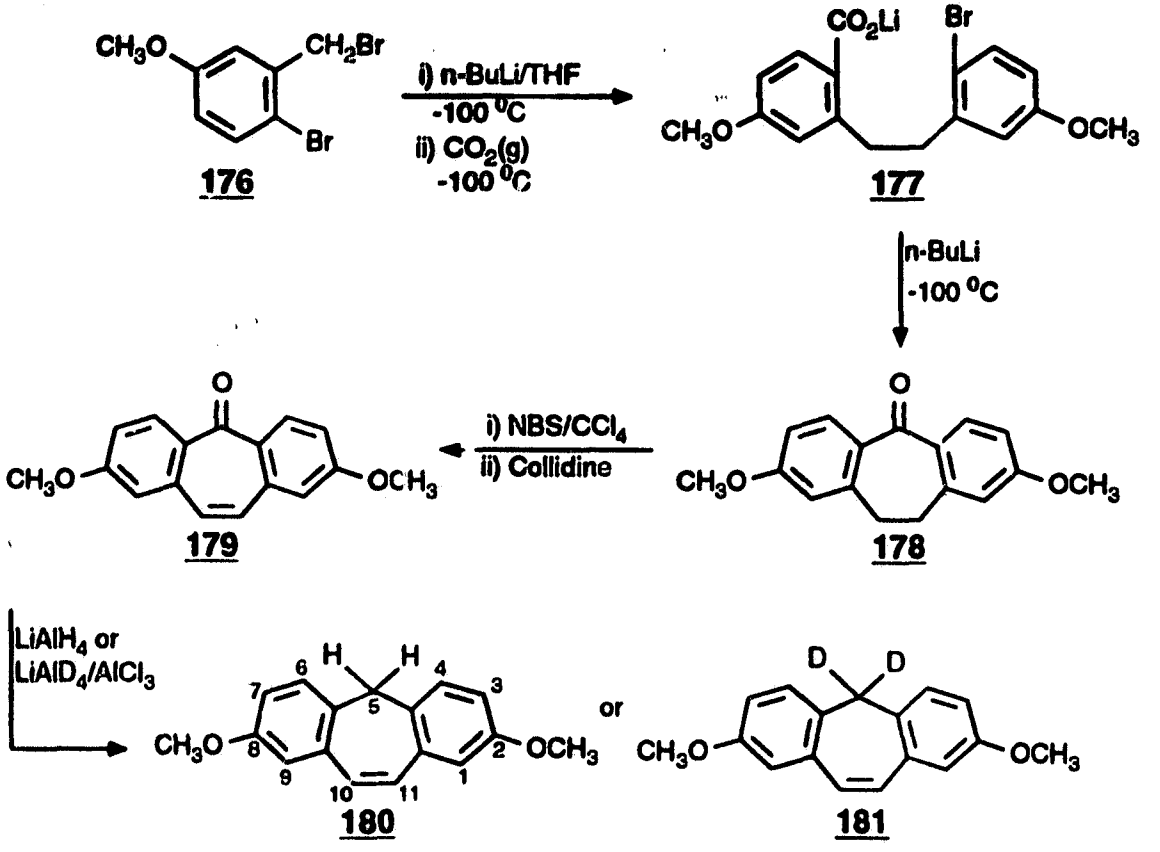

Scheme 3.1

3.1.2 10-Methoxysuberene (185)

10-Methoxysuberene (185) was synthesized by following Scheme 3.2. Dehydrobromination of 182 to give 183 had been earlier accomplished by using NaOH/MeOH[152], but it was found to result in low yields of 183. Treatment of 185 in refluxing 3 M methanolic solution of KOH for one hour was found to result in much higher yields (*ca.* > 90%) of 183. Subsequent reflux of 183 in methanolic KOH solution (*ca.* 3 M) for 4 hours, followed by cooling the reaction

mixture to -4 °C (18 h) afforded 10-methoxysuberone **184** as a yellow crystalline solid. Reduction of ketone **184** with $LiAlH_4/AlCl_3$ in dry THF afforded the

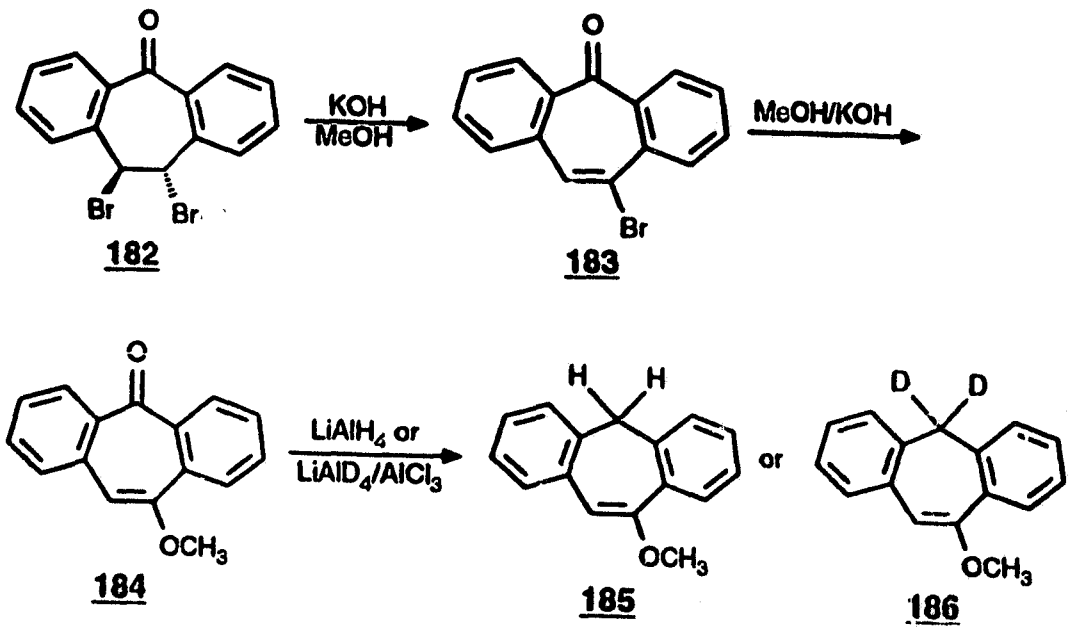

182 **183** **184** **185** **186**

Scheme 3.2

crude **185** which was purified by recrystallization from methanol. The ^1H NMR and mass spectral analyses of **185** were consistent with the indicated structure. The corresponding dideuterated **186** was similarly prepared by reducing **184** with $LiAlD_4/AlCl_3$ in dry THF. The ^1H NMR spectrum of **186** was similar to **185** except for the absence of the bibenzylic protons. The mass spectral analysis of **186** also indicated the presence of two deuteriums in the molecule.

3.1.3 10-Bromosuberene (187)

10-Bromosuberene (187) was prepared by reducing ketone 183 with $LiAlH_4/AlCl_3$ in dry THF (eq 3.1). The crude 187 was purified by column

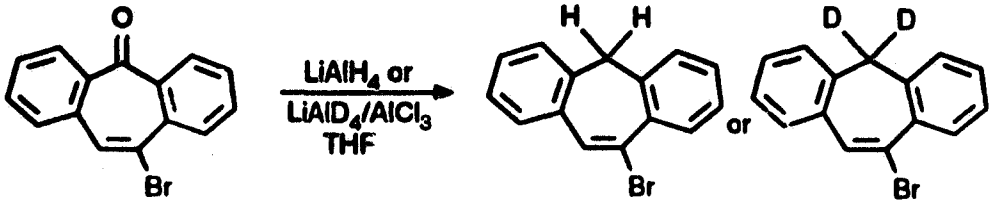

183 187 188 (3.1)

chromatography (silica gel; CH_2Cl_2) and recrystallized from petroleum ether. The ^1H NMR and mass spectrum of 187 were consistent with its indicated structure. The corresponding dideuterated 188 was similarly prepared by the reduction of 183 by $LiAlD_4/AlCl_3$ in dry THF and characterized by ^1H NMR and mass spectral analysis.

3.1.4 10-Cyanosuberene (189)

The strategy utilized for the synthesis of 10-cyanosuberene (189) is shown

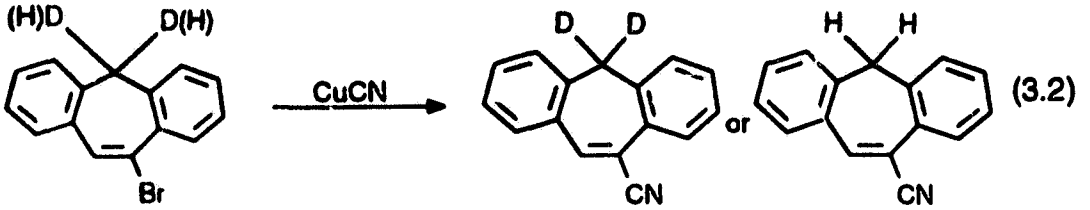

188 (187) 190 189 (3.2)

in eq 3.2. Treatment of the 10-bromosuberene (187) with CuCN in refluxing 1-

methyl-2-pyrrolidone[153] afforded a white solid which on further purification by column chromatography (silica gel; hexanes) and recrystallization from 100% EtOH afforded pure **189**. The ^{1}H NMR and mass spectrum of **189** were consistent with its indicated structure. The corresponding dideuterated **190** was similarly prepared by treating **188** with CuCN.

3.1.5 Tribenzosuberene (193)

Tribenzosuberene (**193**) was synthesized according to Scheme 3.3. Treatment of ketone **183** with potassium t-butoxide in the presence of furan afforded the adduct **191**.[152] Deoxygenation of **191** with $Fe_2(CO)_9$[154] in refluxing benzene yielded tribenzosuberenone (**192**) as a yellow crystalline solid. Reduction

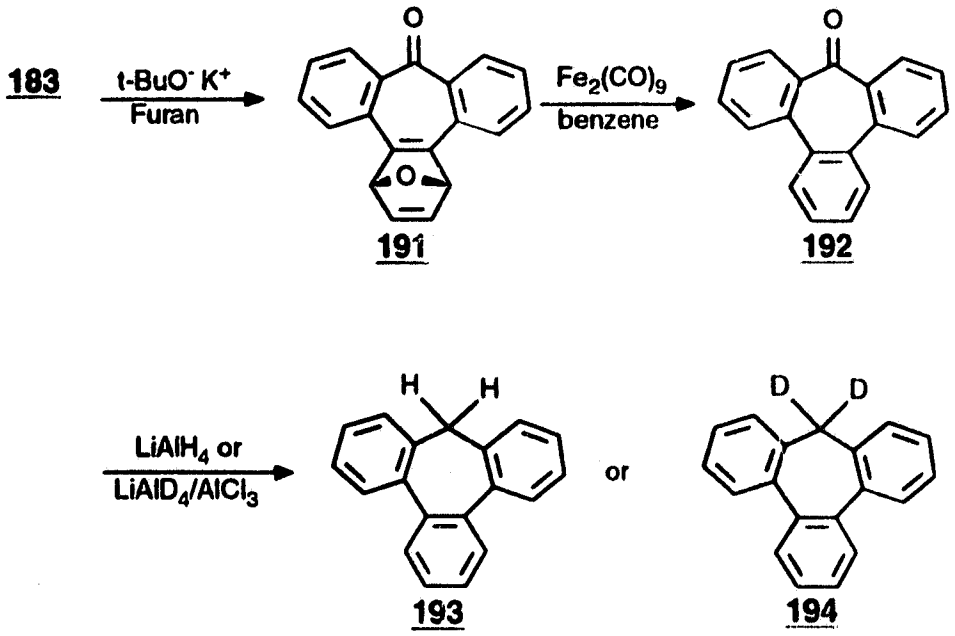

Scheme 3.3

of 192 with $LiAlH_4/AlCl_3$ in THF afforded the crude tribenzosuberene (193), which was purified by column chromatography (silica gel; CH_2Cl_2) and recrystallized from $EtOH/H_2O$. The mass spectral and ^1H NMR analyses of 193 were consistent with its indicated structure of 193. The dideuterated analogue194 was similarly prepared by reduction of ketone 192 with $LiAlD_4/AlCl_3$.

3.1.6 8*H*-Furo[3,4d]dibenzo[b,f]suberene (196)

Treatment of adduct 191 with 3,6-di(pyridin-2′-yl)-*s*-tetrazine[155] (TZ) in $CHCl_3$ afforded ketone 195 in > 98% yield. Ketone 195 was reduced with $LiAlH_4/AlCl_3$ in THF to afford the target molecule 196 (Scheme 3.4). The

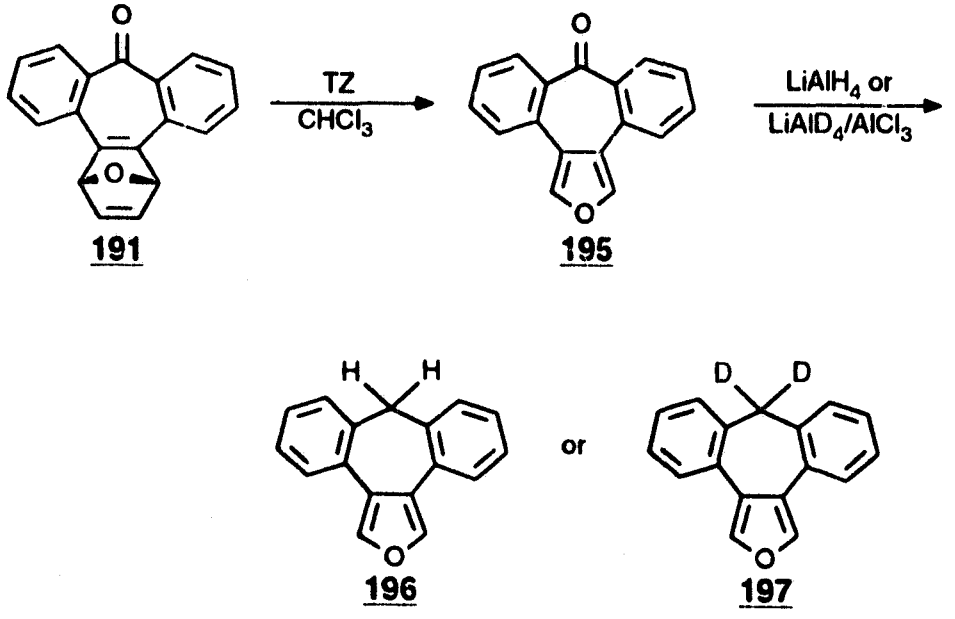

Scheme 3.4

^{1}H NMR analysis and mass spectrum of **196** were consistent with its indicated structure. The dideuterated **197** was similarly prepared by reduction of ketone **195** with $LiAlD_4/AlCl_3$.

3.1.7 3,4-Benzotropilidene (201) and 1,2-Benzotropilidine (202).

3,4-Benzotropilidene (**201**) was made from 1-benzosuberone (**198**) using the procedure of Burdett and coworkers[156]. Treatment of **198** with NBS in refluxing CCl_4 afforded **199** which on refluxing with 2,4,6-collidine yielded **200**. In subsequent steps **200** was converted to the corresponding tosylhydrazone, followed by treatment with MeLi in dry THF afforded **201** as an oil which was purified by distillation under reduced pressure to obtain pure **201** (Scheme 3.5).

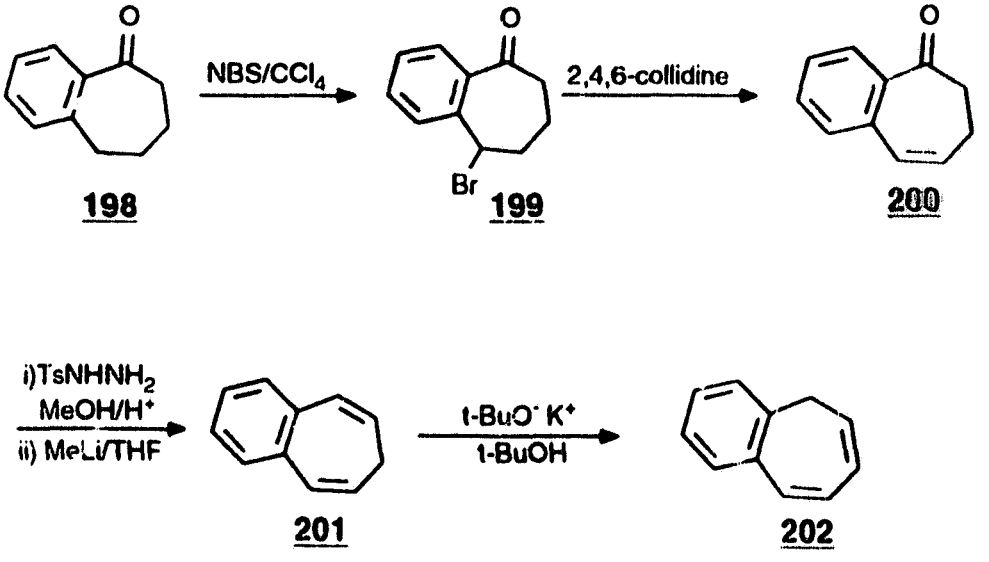

Scheme 3.5

Conversion of **201** to the isomer 1,2-benzotropilidine (**202**) was accomplished by

isomerization with potassium *t*-butoxide (Scheme 3.5).[157]

3.2 Product Studies

3.2.1 Photolysis of 2,8-Dimethoxysuberene (180)

Photolysis of 180 in 50% D_2O-CH_3CN for 2 hours gave a reaction mixture which showed the appearance of a new unresolved triplet at δ 3.58 (J ≈ 1-2 Hz) along with a decrease in signal intensity (relative to the vinyl protons) of the methylene signal of 180 at δ 3.60. The appearance of the triplet at δ 3.58 is consistent with the formation of 203 (≈ 25% based on ^1H NMR integration) in which the monobenzylic proton is coupled to the geminal deuterium. The aromatic and vinyl signals in the photolyzed sample remain unchanged. However, GC/MS analysis of the product mixture indicated formation of both 203 (~21%) and 181 (~3%) (eq 3.3).

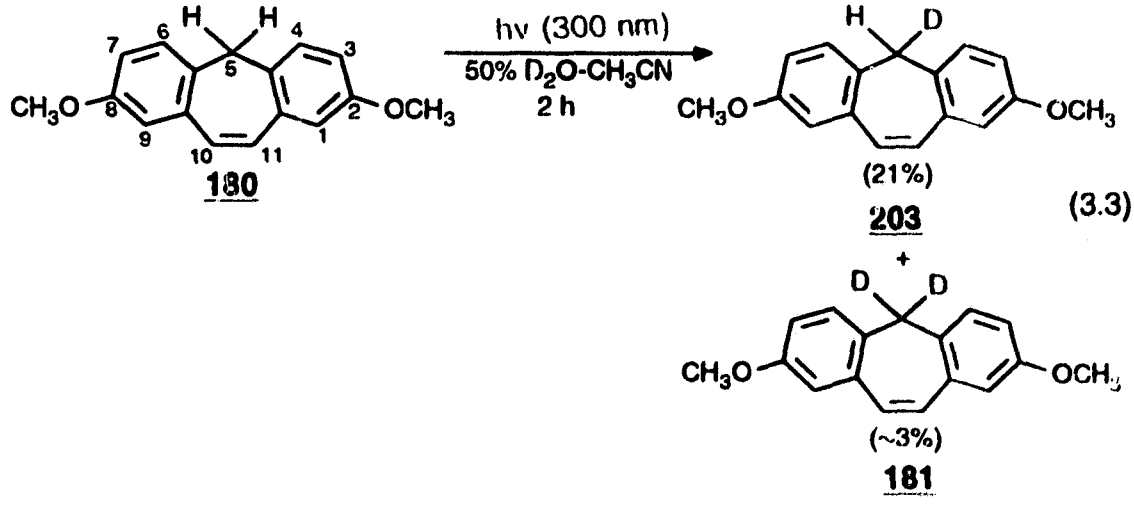

(3.3)

Previous results have demonstrated that photolysis of suberene (37) in 50% D_2O-CH_3CN results in deuterium incorporation at the 5-position to form

monodeuterated **37-*d*** (eq 1.11).[48] The ^1H and ^{13}C NMR spectra of the photoproducts obtained in the photolysis of **37** clearly showed that the deuteriums were incorporated at the benzylic position (C-5 position). The possibility that a residual amount of deuterium might be incorporated into other positions, viz., the vinylic or benzene ring positions, was ruled out since the ^2H NMR of the photoproducts showed < 2% deuterium incorporation at other positions of **37**. Results obtained in the photolysis of **180** were consistent with these findings. That is, ^2H NMR of the product mixture obtained after photolysis of **180** showed a strong signal at δ 3.60, indicating the formation of **203** and **181**, with no signals between δ 5.0-8.0.

Deuterium incorporation in **180** takes place only on irradiation. A solution of **180** in 50% D_2O-CH_3CN (pD 7-14) left stirring in the dark (at ≈ 22 ± 2 °C) for 2 hours did not result in deuterium incorporation.

Photolysis of dideuterated **181** in 50% H_2O-CH_3CN (*ca.* 2 h) at 300 nm also resulted in the formation of **203** (12%) and **180** (2%) (eq 3.4). In general, good agreement was observed between the calculated amounts of deuterium exchange by ^1H NMR and GC/MS. The kinetics of deuterium exchange was followed by

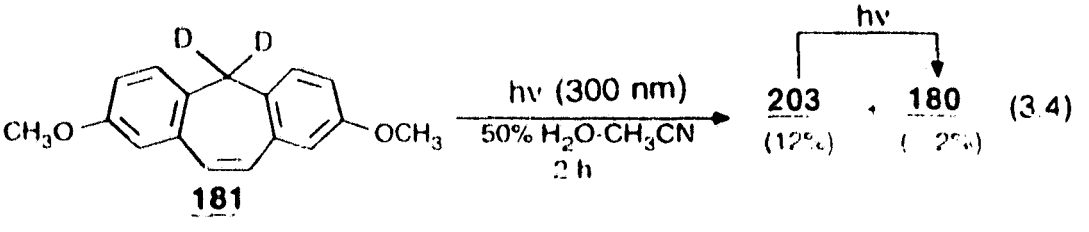

(3.4)

irradiating ~ 60 mg of **181** in 50% H_2O-CH_3CN and removing aliquots after set period of times. These aliquots were then examined by GC/MS (after work-up) to determine the yields of **203** and **180**. The results are presented in Figure 3.1. It is evident from the plot that the initially exchanged product is **203** (primary photoproduct), which subsequently reacts via a secondary photoreaction to give **181**.

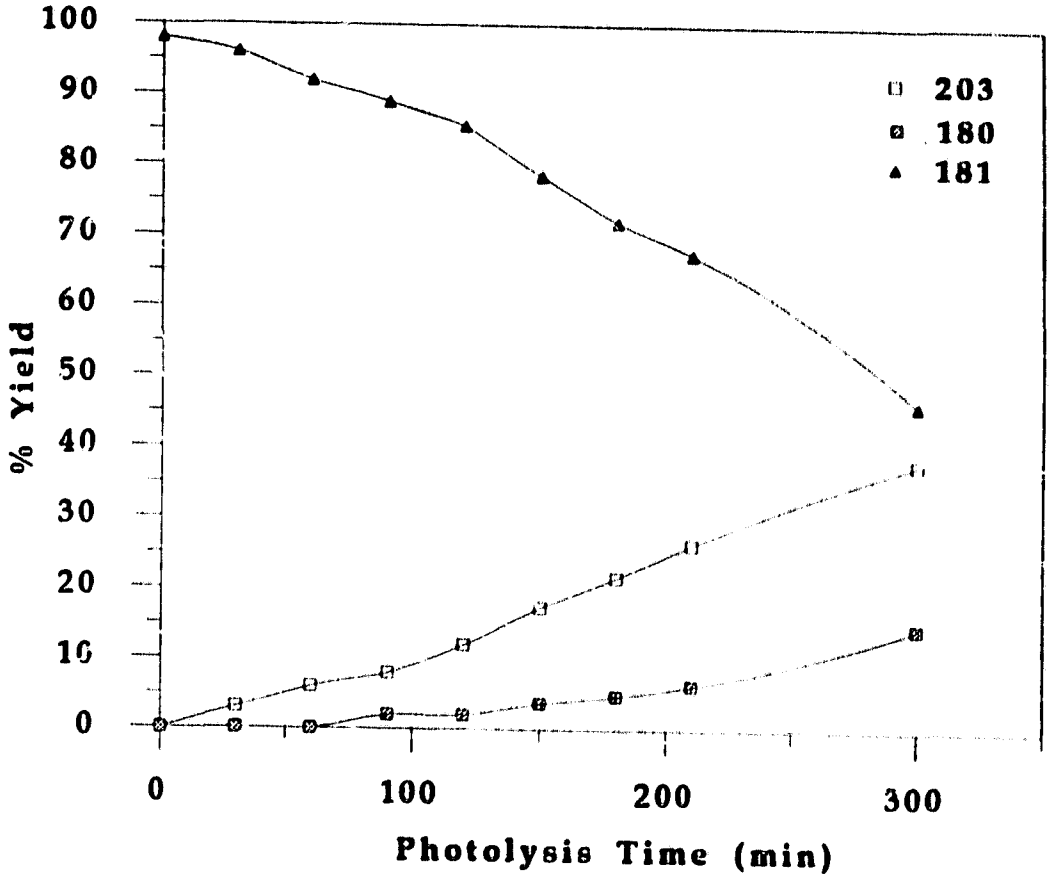

Figure 3.1 Plot of percent recovered **181** and yields of exchange photoproducts **203** and **181** vs photolysis time in 50% H_2O-CH_3CN.

Deuterium incorporation in **180** on irradiation in 50% D_2O-CH_3CN, and protium incorporation in **181** on photolysis in 50% H_2O-CH_3CN is consistent with the intermediacy of carbanion **204**. That is, photoexcitation of **180** results in the benzylic C-H bond ionization, with H_2O acting as the deprotonating base, to give the intermediate 8π-electron carbanion **204**. The photogenerated carbanion **204** is subsequently deuterated by the solvent to give overall exchange product (viz., **203**). Another mechanistic possibility that might explain the deuterium incorporation in **180** involves the initial homolysis of the benzylic C-H bond to

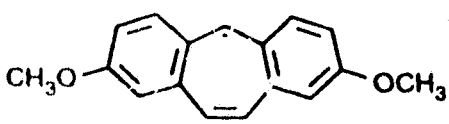

204

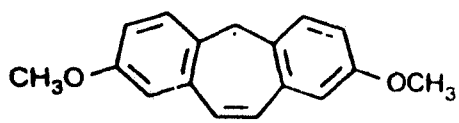

205

generate radical **205** which subsequently abstracts deuteron from the solvent. However, this possibility can be ruled out since when **180** was photolyzed in 100% CD_3CN no deuterium incorporated product was isolated. If radical **205** was indeed formed then it should have abstracted deuterium from CD_3CN, which is a better deuterium source than D_2O. In addition, if any radical were formed it would be expected to dimerize efficiently, to give the corresponding dimer of **180**, which was not observed.

To investigate the qualitative effect of methoxy groups in **180** on the efficiency of C-H bond heterolysis, photolysis of **180** and **37** was carried out under

identical conditions. Thus, photolysis of suberene (37) in 50% D_2O-CH_3CN resulted in substantially higher amounts of deuterium incorporated products, viz., 37-*d* (53%) and 37-*d*$_2$ (~2%), compared to a similar photolysis of 180 which resulted in significantly lower amounts of deuterium incorporated products, viz., 203 (~12%) and 181 (~3%). This result is in accord with the intermediacy of carbanion 204 in the deuterium exchange reaction of 180. The presence of methoxy groups destabilizes the negative charge of the incipient carbanion 204 in the transition state which retards the C-H bond photoheterolysis in 180. The effects of other substituents on the efficiency of excited state C-H bond ionization in suberene were also investigated, and are described below.

3.2.2 Photolyses of 10-Methoxysuberene (185) and 10-Cyanosuberene (189)

Photolysis of 185 in 50% D_2O-CH_3CN resulted in the formation of monodeuterated 206 (9%) (eq 3.5) as indicated by GC/MS analysis of the reaction mixture. At such short photolysis time (*ca.* 5 min) no dideuterated 186 was

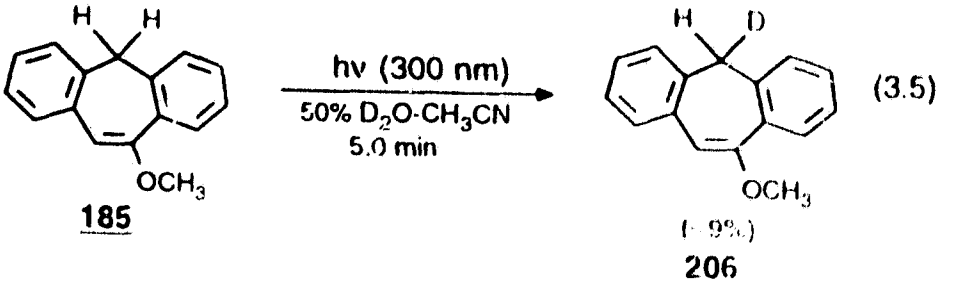

(3.5)

observed. Thermally, 185 in aqueous CH_3CN solution undergoes hydrolysis to yield 207 (eq 3.6). Because of this competing thermal reaction photolysis of 185

for longer durations could not be carried out. Consistent with the intermediacy

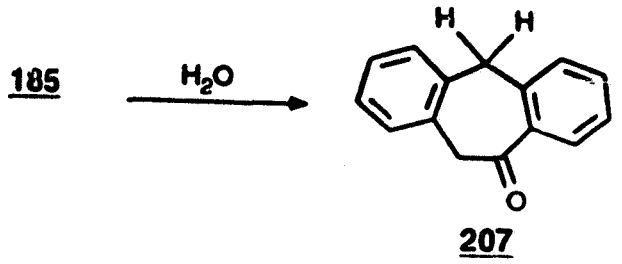

(3.6)

of carbanion a similar photolysis of **186** in 50%H_2O-CH_3CN also resulted in the formation of **206** (~6%) (eq 3.7).

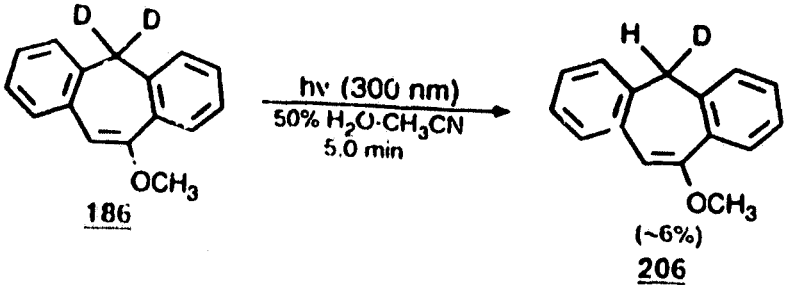

(3.7)

Photolysis of **189** in 50% D_2O-CH_3CN gave monodeuterated **208** (42%) and **190** (8%) (eq 3.8). A similar photolysis of suberene (**37**) resulted in significantly

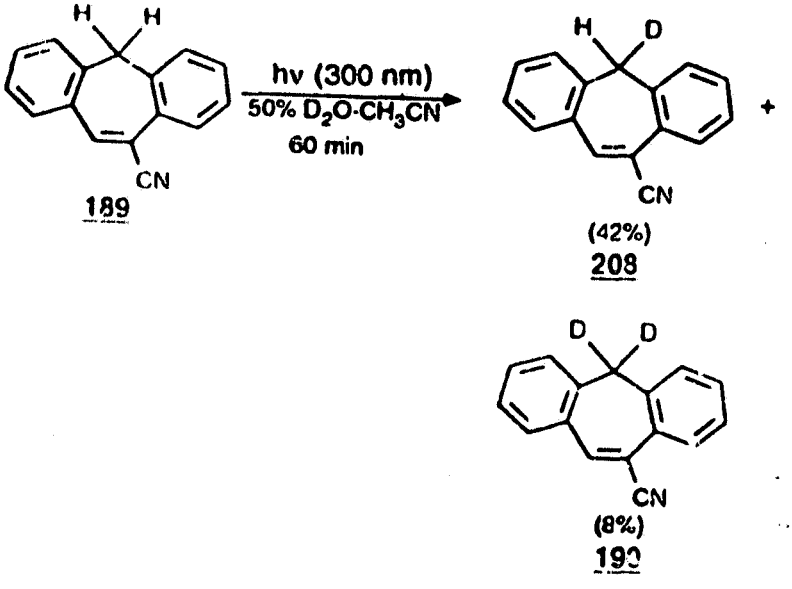

(3.8)

lower amounts of deuterium incorporated photoproducts, viz.,monodeuterated **37-*d*** (35.5%) and dideuterated **37-d_2** (5%). The increased amount of deuterium incorporation in **189** suggests that the presence of the cyano group at the 10-position increases the C-H ionization rate of **189**. This is understandable since the intermediate carbanion **209** is stabilized by the cyano group which will enhances the C-H bond ionization rate. This observation further supports the intermediacy

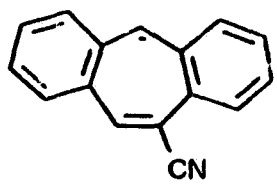

209

of carbanion intermediates in the deuterium exchange reactions of suberene (**37**) and its derivatives.

3.2.3 Photolysis of 10-Bromosuberene (187)

Deuterium exchange studies of **187** proved to be difficult because of its efficient photodebromination and photohydrolysis in aqueous CH_3CN. Thus, photolysis of **187** in 50% H_2O-CH_3CN resulted in the formation of **37** (~ 12%) and ketone **207** (~ 15%) (eq 3.9). In the absence of irradiation, a very slow thermal solvolysis of **187** (to give ketone **207**) was observed. It has been shown that photolysis of vinyl bromides results in the C-Br bond homolysis to generate a radical pair.[58] Rapid electron transfer within the radical pair results in the

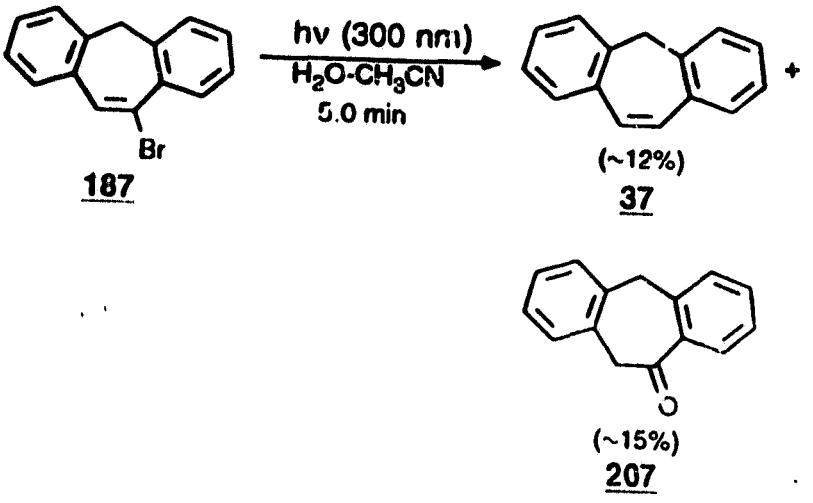

(3.9)

formation of vinyl cation which is subsequently trapped by solvent to give solvolysis products. A similar mechanism is proposed to operate in the case of **187**. That is, photolysis of **187** results in the vinylic C-Br bond homolysis, to give

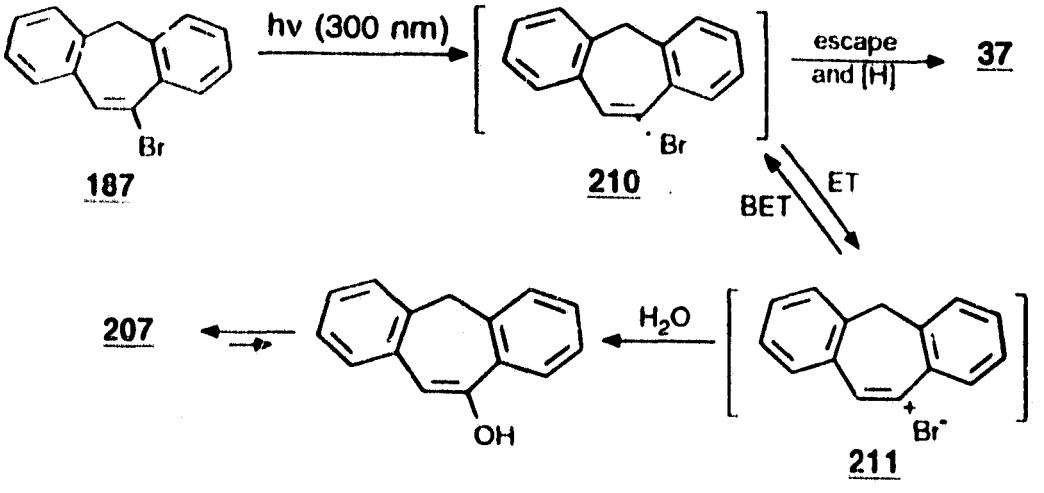

Scheme 3.6

the radical pair **210** in a solvent cage. Electron transfer (ET) within the caged

radical pair **210** generates the ion pair **211**, which is subsequently trapped by water to yield ketone **207** (Scheme 3.6). Escape of radical pair **210** from the solvent cage followed by hydrogen abstraction from the solvent generates **37**. Formation of carbocation **211** was shown by photolyzing **187** in 100% MeOH which resulted in the formation of the corresponding methyl ether **185** (~ 30%) (eq 3.10). The notion that the primary photochemical event is the vinylic C-Br bond homolysis is supported by the fact that when **187** was photolyzed in 100% CH_3CN (dry), only **37** was formed (eq 3.11).

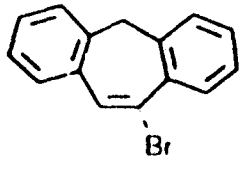

187

$$\xrightarrow[100\%\ MeOH]{h\nu\ (300\ nm)} \underline{185} \qquad (3.10)$$

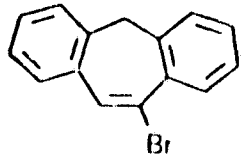

187

$$\xrightarrow[100\%\ CH_3CN]{h\nu\ (300\ nm)} \underline{37} \qquad (3.11)$$

3.2.4 Photolysis of Tribenzosuberene (193) and 8*H*-Furo[3,4d]-dibenzo[b,f]suberene (196)

Photolysis of **193** and **196** in 50% D_2O-CH_3CN did not result in deuterium

exchange and the starting materials were recovered. However, photolysis of **193** in 50% 1 M NaOD-EtOD resulted in the formation of **212** (~15%) and **194** (~3%) (eq 3.12). A similar photolysis of **193** in 100% EtOD did not result in any reaction. The amount of exchange photoproduct **212** increased with the concentration of

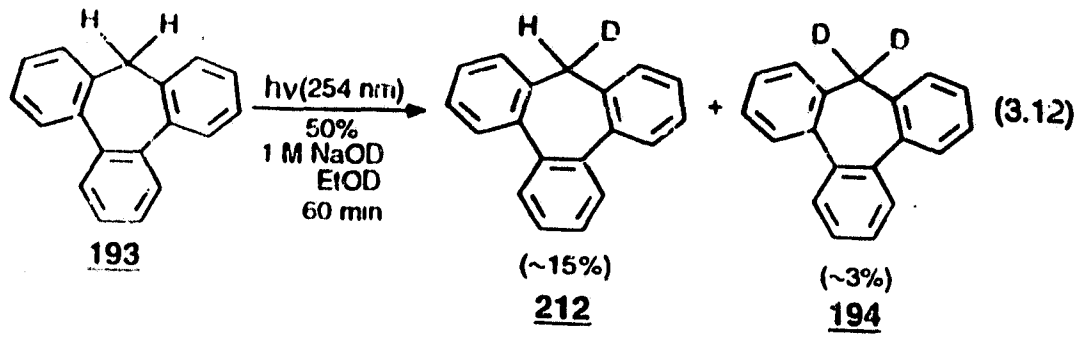

NaOD suggesting that it was the deprotonating base.

Photolysis of **194** in the presence of amine bases resulted in substantially higher amount of exchange. Thus, photolysis of **194** in the presence of 1 M ethanolamine solution in CH_3CN resulted in the formation of **212** (26%) and **193** (7%) (eq 3.13). Similarly, photolysis of **197** in the presence of 0.5 M ethanolamine

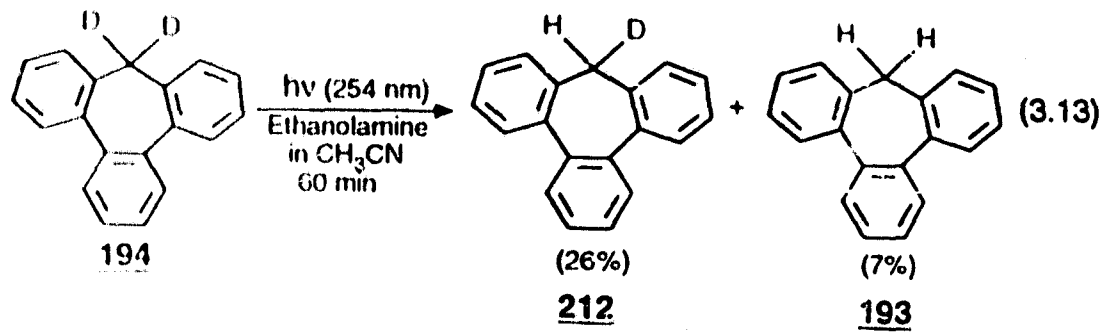

solution in CH_3CN also resulted in the deuterium exchange to give monodeuterated **214** (~23%) and **196** (~7%) (eq 3.14). Photolysis of **194** and **197**

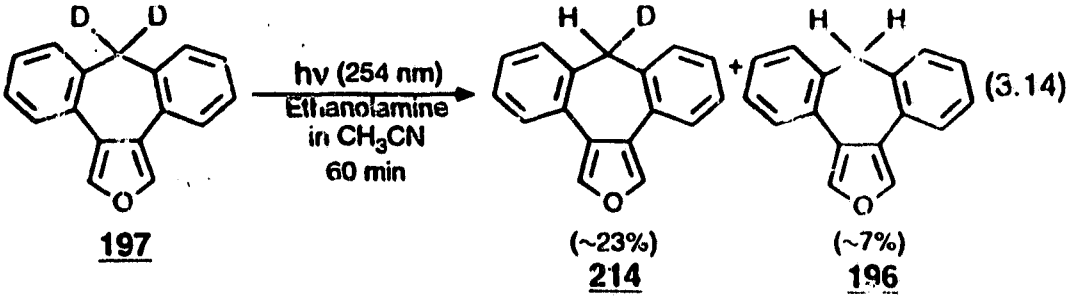

197 (~23%) **214** (~7%) **196** (3.14)

in 100% CH_3CN did not result in any observable exchange, suggesting that ethanolamine was the deprotonating base. This is further supported by the fact that when the concentration of ethanolamine in CH_3CN was increased, the amount of exchange product **212** also increased.

3.2.5 Photolyses of 3,4-Benzotropilidine (201) and 1,2-Benzotropilidine (202)[158]

Possibility of deuterium exchange in less rigid systems (compared to suberene) **201** and **202** was also explored. It has been shown earlier that photoexcitation of **201** and **202** in cyclohexane results in the formation of

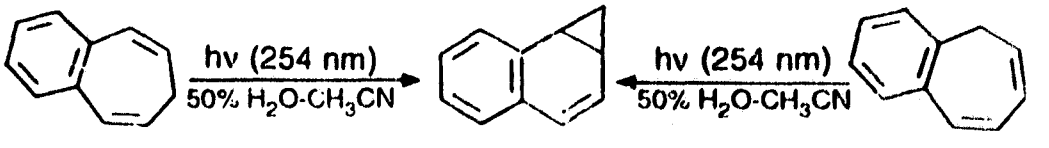

201 **215** **202** (3.15)

benzonorcaradiene (215) (eq 3.15).[156] The mechanism of the rearrangement has been shown to involve initial 1,7-hydrogen shift followed by electrocyclic ring closure to give 215.[156,157] Photolysis of both 201 and 202 in 100% CH_3CN or 50-70% D_2O-CH_3CN gave 215 as the only product (eq 3.15), with no evidence for deuterium incorporation in recovered substrates or 215 as determined by ^1H NMR and GC/MS analyses. The rearrangement to 215 was a very efficient process and only short photolysis times were required to convert 201 or 202 to 215. Thus it would appear that in the excited state C-H bond ionization cannot compete with efficient molecular rearrangement for these more flexible systems, although they possess the correct incipient 8π electron carbanion ring system to undergo C-H bond ionization.

3.3 Quantum Yields

Quantum yields (Φ) for deuterium incorporation in 180 (i.e., formation of 203) and protium incorporation in 181 (i.e., formation of 203) were measured on an optical bench at λ_{ex} = 280 nm. Quantum yields of deuterium/protium incorporation in other substituted suberene derivatives viz., 185, 186, 189, 190, 193, 194, 197, were also measured. Conversions to exchange photoproducts were kept between 12-20% and measured by GC/MS analyses.

Table 3.1 shows the quantum yields (Φ's) of deuterium incorporation in 180 on photolysis in deuterated solvents. For the purpose of comparisons, the quantum yields of deuterium incorporation into 37 are also presented in Table 3.1.

Table 3.1 Quantum Yields (Φ) for Monodeuterium Incorporation into 180 in Various Solvents.[a]

Solvent Mixture[b]	Φ	
	180	37[d]
100% CD_3CN[c]	0.000	0.000
70% D_2O-CH_3CN	0.0079 ± 0.0005	0.029 ± 0.004
50% D_2O-CH_3CN	0.0071 ± 0.0004	0.030 ± 0.004
20% D_2O-CH_3CN	0.0046 ± 0.0002	0.021 ± 0.001

a) Determined by mass spectral analyses; errors quoted are standard deviation in amounts of deuterium incorporation calculated by 2-3 independent mass spectral analyses.
b) For solubility reasons CH_3CN was used as cosolvent.
c) NMR solvent used without further treatment.
d) Obtained from ref. 48.

Table 3.2 presents the quantum yields (Φ's) of monoprotium incorporation in **181** in a variety of solvent mixtures. It is clear from Table 3.1 that aqueous CH_3CN is the best solvent mixture to observe exchange. Furthermore, Φ's of exchange in H_2O-CH_3CN and D_2O-CH_3CN for **180** and **181**, respectively (Tables 3.1 and 3.2), were essentially same (no significant isotope effect), even though the initial process required to observe exchange involves C-H bond ionization in **180** vs C-D bond ionization in **181**.

Table 3.2 Quantum Yields (Φ) for Protium Incorporation into 181 in Various Solvents.[a]

Solvent Mixture[b]	Φ	
	181	**37-d_2**[d]
100% CH_3CN[c]	0.000	0.000
70% H_2O-CH_3CN	0.011 ± 0.002	0.045 ± 0.006
50% H_2O-CH_3CN	0.0076 ± 0.0004	0.035 ± 0.006
20% H_2O-CH_3CN	0.0050 ± 0.0004	0.024 ± 0.003
70% MeOH-CH_3CN	0.0023 ± 0.0004	0.012 ± 0.002
70% EtOH-CH_3CN	0.0012 ± 0.0004	0.008 ± 0.001

a) Determined by mass spectral analyses; errors quoted are standard deviation in amounts of deuterium calculated by 2-3 independent mass spectral analyses.
b) For solubility reasons CH_3CN was used as co-solvent.
c) Dry CH_3CN used without further treatment.
d) Obtained from ref. 48.

Quantum yields (Φ) for exchange of **181** were also measured in aqueous EtOH or CH_3CN solutions where the acidity or basicity of the aqueous portion was varied (Table 3.3). It was found that the exchange efficiency was reduced in acidic solutions and enhanced in aqueous NaOH solutions.

The quantum yields (Φ's) of deuterium incorporation (Table 3.1) in **180** are lower compared to suberene (**37**). This is in accord with the destabilizing effect

Table 3.3 Quantum Yields (Φ) for Protium Incorporation into 181 in Acidic and Basic Solutions.[a]

Solvent Mixture[b]	Φ 181
70% H_2O-CH_3CN	0.012 ± 0.004
70% 1.25 M H_2SO_4-EtOH	0.0028 ± 0.0003
70% 2.5 M H_2SO_4-EtOH	0.0012 ± 0.0004
50% 0.5 M NaOH-EtOH	0.0124 ± 0.0004
50% 1.0 M NaOH-EtOH	0.017 ± 0.003
50% 2.0 M NaOH-EtOH	0.020 ± 0.002

a) Determined by mass spectral analyses; errors quoted are standard deviation in amounts calculated by mass spectral analyses.
b) For solubility reasons CH_3CN and EtOH were used as cosolvents.

of methoxy groups on the incipient carbanion intermediate **204**. In contrast, the cyano group stabilizes the carbanion intermediate **209**. This is manifested in the higher quantum yields of exchange for **189** and **190** compared to **37** (Table 3.4).

Table 3.4 Quantum yields of deuterium incorporations in 185 and 189 and protium incorporation in 186 and 190.[a]

Solvent Mixture	Φ[b]		Φ[b]	
	185	186	189	190
70% D_2O-CH_3CN	0.036		0.035	
70% H_2O-CH_3CN		0.027		0.046

a) Determined by mass spectral analyses.
b) errors are ± 10% of the quoted values.

Quantum yields (Φ's) of protium incorporation for **194** and **197** were measured in NaOH-EtOH solution and in the presence of ethanolamine in CH_3CN (Table 3.5). The exchange process in **194** and **197** was sluggish at lower ethanolamine concentrations and no exchange took place in the absence of the base (NaOH or ethanolamine).

Table 3.5 Quantum Yields for Protium Incorporation in 194 and 197 in Various Solvents.[a]

Solvent Mixture	Φ[c]	
	194	**197**
1.0 M Ethanolamine[b]	0.0086	0.017
2.0 M Ethanolamine[b]	0.016	0.023
50% 3.0 M NaOH-EtOH	0.0015	
70% H_2O-CH_3CN	0.000	0.000
100% CH_3CN	0.000	0.000
95% EtOH	0.000	0.000

a) Measured by GC/MS analyses of reaction mixtures.
b) Ethanolamine solutions in dry CH_3CN
c) Errors are ± 10% of the quoted values.

The quantum yield (Φ) for rearrangement of **201** has been measured by Swenton and coworkers[15e] to be ≈0.9 in cyclohexane (λ_{ex} = 330 nm). Using this reaction as the secondary actinometer, quantum yields for rearrangement of **201** and **202** (to **215**) were measured in a number of additional solvents (Table 3.6).

In all cases, the rearrangement quantum yields were very high, with no apparent retarding effect by added water.

Table 3.6 Quantum Yields of Rearrangement of 201 and 202 in Various Solvents.

	201[a]	202[a]
100% CH_3CN	0.84	
95% EtOH	≥ 0.7	
50% H_2O-CH_3CN	≥ 0.7	≈0.7
C_6H_{12}	0.87[b]	0.7 ± 0.1

a) Measured relative to the known quantum yield of **201** in C_6H_{12} (Φ = 0.87);[159] λ_{ex} = 254 nm.
b) From ref. 156.

3.4 Steady-State Fluorescence Studies

3.4.1 General Spectral Characteristics and Fluorescence Quantum Yields

The fluorescence emission spectra of all suberene derivatives, viz., **160**, **185** and **189**, displayed spectral characteristics similar to the parent suberene[48] (**37**). The absorption and emission spectra of tribenzosuberene (**193**) and 8*H*-furo[3,4d]dibenzo[b,f]suberene (**196**) however, were blue shifted compared to the parent system.

The fluorescence quantum yields (Φ_f's) of substituted suberenes were measured in 100% CH_3CN, relative to the parent suberene (**37**) (Φ_f = 0.86 ± 0.05

in CH_3CN)[48], and are presented in Table 3.7. The fluorescence quantum yields

Table 3.7 Photophysical Parameters of Substituted Suberenes in CH_3CN.

Molecule	Φ_f[a]	τ (ns)[d]	λ_{max} (emission)
180	0.47 ± 0.05[b]	5.10 ± 0.05[e]	410 nm
185	0.0051 ± 0.0004[b]	3.55 ± 0.05[e]	390 nm
189	0.0048 ± 0.0005[b]	4.36 ± 0.05[e]	385 nm
193	0.18 ± 0.02[c]	3.21 ± 0.04[f]	325 nm
196	0.24 ± 0.03[c]	2.21 ± 0.05[f]	340 nm

a) Errors are ± 10% of the quoted values.
b) Measured relative to suberene (37) (Φ_f = 0.86 in CH_3CN)[48].
c) Measured relative to biphenyl ether (Φ_f = 0.03 in cyclohexane)[135].
d) Measured by single photon counting.
e) λ_{ex} = 280 nm.
f) λ_{ex} = 260 nm.

(Φ_f's) of the substituted suberenes were considerably lower than the parent 37 (Table 3.7). The reduced emission yields (Φ_f's) of substituted suberenes is due to the presence of substituents which open additional pathways for radiationless deactivation of S_1.

3.4.2 Fluorescence Quenching.

The emissions of suberene derivatives **180**, **185** and **189** and their deuterated analogues, viz., **181**, **186** and **190**, in CH_3CN were quenched on addition of H_2O. A representative case of emission quenching of **185** in CH_3CN

by added H_2O is shown in Figure 3.2.

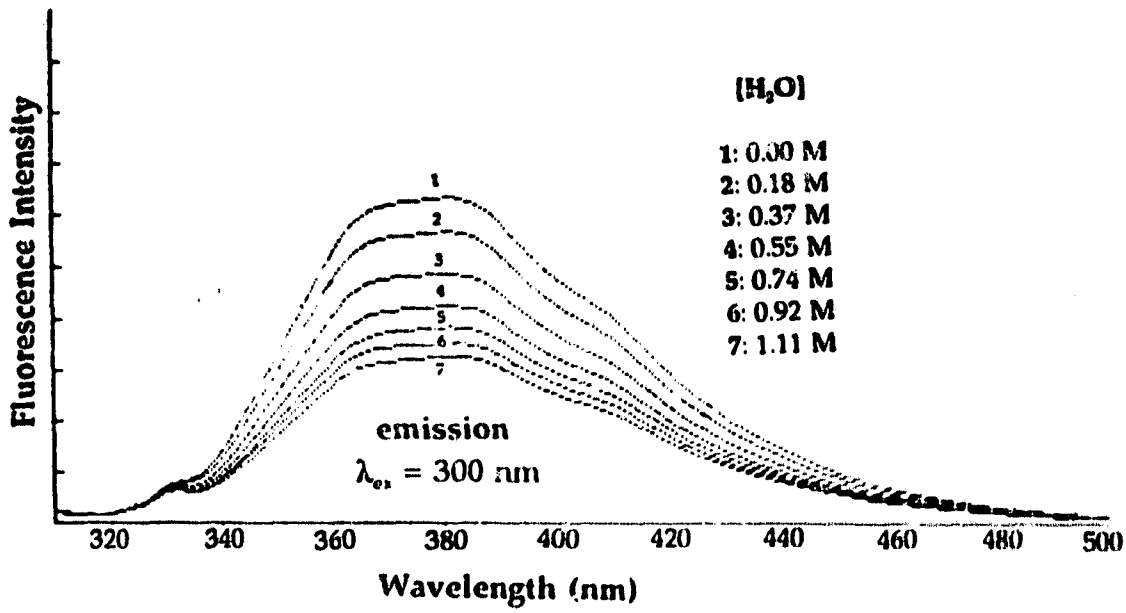

Figure 3.2 Fluorescence quenching of **185** in CH_3CN by added H_2O.

Quenching rate constants (k_q's) were calculated by standard Stern-Volmer analysis and are presented in Table 3.8. For the sake of comparison the fluorescence quenching rate constants for parent **37** and **37-d_2** are also presented in Table 3.8. The fluorescence quenching rate (kq) of **180** by H_2O was lower than the suberene (**37**), whereas the cyano substituted **190** was quenched at a slightly higher rate (Table 3.8). The fluorescence quenching rate constants (k_q's) for dideuterated **181**, **186** and **191** were smaller than the diprotiated molecules, viz., **180**, **185** and **190**, corresponding to a primary kinetic isotope effect of $(k_H/k_D)_q$ = 2.20-3.00 (Table 3.8). These isotope effects are consistent with the C-H vs C-D bond ionization in S_1, with H_2O acting as the deprotonating base.

Table 3.8 Fluorescence Quenching Rate Constants (k_q's) of Substituted Suberenes in CH_3CN by Added H_2O.[a]

Molecule	$k_q(H_2O)$ M^{-1} s^{-1}	k_H/k_D
180	$(1.53 \pm 0.06) \times 10^7$	3.00 ± 0.40
181	$(0.51 \pm 0.05) \times 10^7$	
185	$(1.81 \pm 0.07) \times 10^8$	2.51 ± 0.20
186	$(0.72 \pm 0.05) \times 10^8$	
189	$(2.05 \pm 0.08) \times 10^8$	2.47 ± 0.30
190	$(0.83 \pm 0.04) \times 10^8$	
37[b]	$(1.68 \pm 0.08) \times 10^8$	2.75 ± 0.40
37-d_2[b]	$(0.61 \pm 0.06) \times 10^8$	

a) Rate constants (k_q's) obtained by standard Stern-Volmer analysis of quenchings; λ_{ex} = 280 nm.
b) Obtained from ref. 48.

To study the effect of medium acidity or basicity on fluorescence efficiency, the fluorescence emission intensity of **180** was monitored by varying the aqueous portion of the solution from 1 M NaOH (pH 14) to ca. 10% H_2SO_4 (Figure 3.3). The emission intensity of **180** stays relatively constant over the pH 7-10 region. However, the emission intensity of **180** was substantially enhanced on increasing the acidity, from pH 6 to pH 4. In solutions of higher acidities, the fluorescence intensity drops off. This intensity drop off in stronger acids is probably due to some thermal reaction of substrate since, **180** could not be recovered unchanged from these solutions of higher acidities. However, emission behaviour of **180** in

acidic solutions of pH < 5 suggests that we are observing fluorescence titration of the excited state carbon acid **180** (Figure 3.3). That is, on increasing the

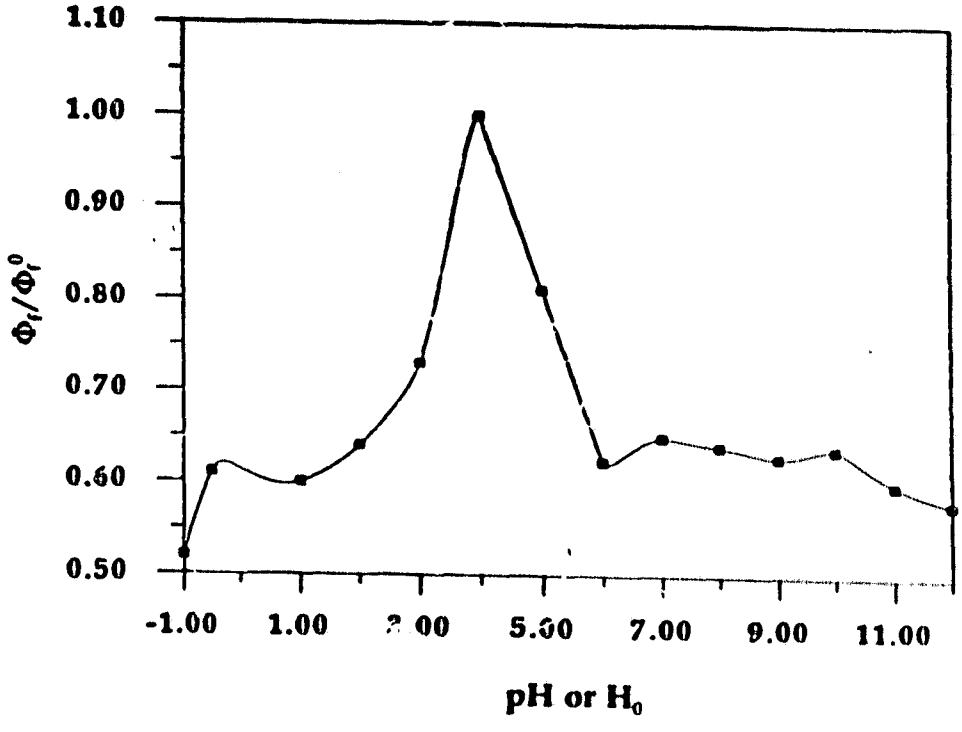

Figure 3.3 Fluorescence emission intensity of **180** vs pH or H_0 (30% EtOH co-solvent).

solution acidity, the medium basicity is decreased, thus reducing the rate of deprotonation. This argument is further supported by the fact that the quantum yields of exchange of **180** decrease in the same acidity region. Similar behaviour has also been observed for the suberene (**37**).[46] Fluorescence of **180** was quenched in basic (pH > 12) aqueous solutions which suggests the base catalysis of deprotonation process. The enhanced quantum yields (Φ's) for exchange measured for **180** in basic aqueous solutions also support this notion (Table 3.3).

Consistent with their reactivity, fluorescence emission of tribenzosuberene (**193**) and **196** in CH_3CN was not quenched by added H_2O. However, the emission of **193**, **194** and **196** in CH_3CN was quenched by added ethanolamine. A representative case of fluorescence quenching of **193** in CH_3CN by added ethanolamine is shown in Figure 3.4. The calculated fluorescence quenching rate constants (k_q's) for **193**, **194** and **197** are shown in Table 3.9.

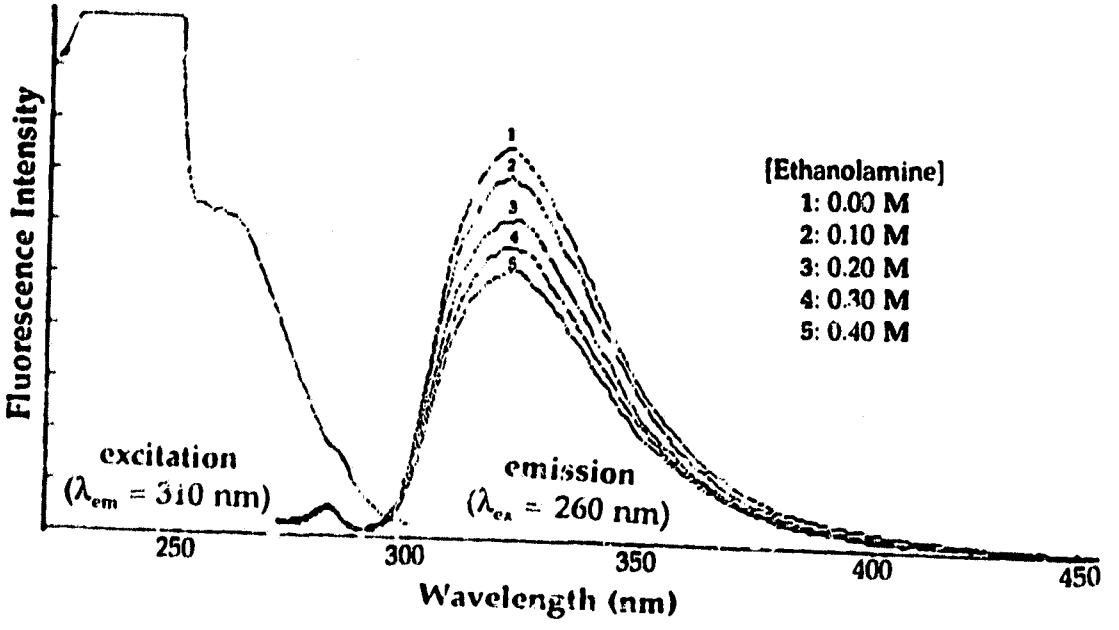

Figure 3.4 Fluorescence excitation and emission spectra of 193 in 100% CH_3CN, with overlay of fluorescence quenching of 193 by ethanolamine in CH_3CN.

Table 3.9 Fluorescence Quenching Rate Constants (k_q's) of 193, 194 and 196 in CH_3CN by Added Ethanolamine.[a]

Molecule	k_q M^{-1} s^{-1}	k^H/k^D
193	$3.50 \pm 0.07 \times 10^8$	1.65 ± 0.20
194	$2.12 \pm 0.05 \times 10^8$	
196	$9.09 \pm 0.09 \times 10^8$	

a) Quenching rate constants (k_q's) obtained by standard Stern-Volmer analyses of quenchings; λ_{ex} = 260 nm.

3.5 Mechanism of Proton and Deuteron Exchange in Suberenes

The results of the product and fluorescence studies are consistent with an ionic mechanism of exchange in S_1. The proposed mechanism for exchange in the case of **180** is shown in Scheme 3.7 . In this simple carbon acid mechanism, **180** is deprotonated by D_2O in S_1, to give the intermediate carbanion **204** (which is presumed to be hydrogen bonded to the departing hydronium ion). The deprotonated proton may rebond to the carbanion **204**, thus resulting in no net exchange (internal return). However, exchange of the departing proton with deuterons from D_2O, and subsequent deuteration of the carbanion **204** results in an overall exchange at the 5-position. An estimate of the percentage internal return can be made as follows. The fluorescence quantum yield (Φ_f) of **180** in the nonreactive solvent CH_3CN is 0.47 ± 0.05. In 70% D_2O-CH_3CN, Φ_f drops to ≈0.16.

The observed exchange quantum yield in this solvent is 0.0079 ± 0.0005. Assuming that the decrease in Φ_f is mostly due to reaction via deprotonation of the benzylic C-H bond, then out of about 30 deprotonated molecules only 1 undergoes exchange.

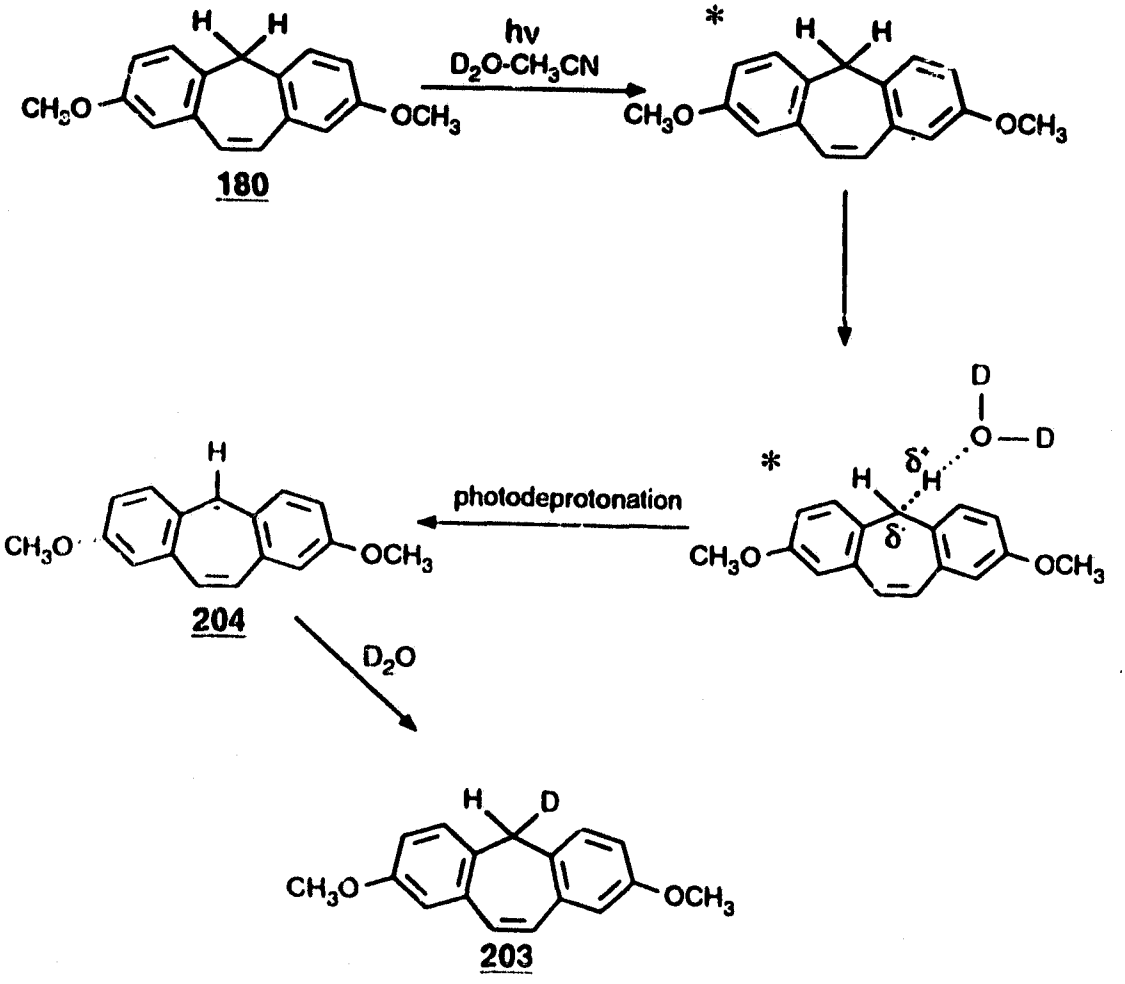

Scheme 3.7

Fluorescence quenching rates of **180** and **181** by H_2O in CH_3CN show a significant isotope effect, $(k_H/k_D)_q = 3.00 \pm 0.40$, which is consistent with the cleavage of C-H vs C-D bond in the key primary step in S_1. However, primary isotope effect on the exchange quantum yields in L_2O-CH_3CN (L = H or D) (Tables 3.1 and 3.2) is significantly smaller (Φ_H/Φ_D = 1.1-1.4). That is, the primary isotope effect which arises from C-H vs C-D bond cleavage is not manifested in exchange quantum yields. This is understandable, since the overall exchange requires the protonation of the intermediate carbanion **204** in a second step (Scheme 3.7). This second step has associated with it a primary isotope effect (protonation from L_2O) which compensates for the initial isotope effect (due to C-H vs C-D bond cleavage). The small isotope effect observed for the exchange quantum yields further underscores the significance of internal return in these photogenerated carbanions. Because, if every deprotonation resulted in exchange, a large isotope effect (equal to $(k_H/k_D)_q$) would have been observed in the exchange quantum yields. Results obtained for other suberene derivatives, viz., **185** and **189**, are also consistent with the mechanism presented in the Scheme 3.7.

Scheme 3.7 also explains the observed exchange of **193** and **196** in the presence of base (NaOH or ethanolamine). Increase in exchange quantum yields (Table 3.5) of **194** and **197** with increasing ethanolamine concentration is consistent with the notion that ethanolamine acts as the deprotonating base in S_1. Furthermore, the fluorescence quenching rates for **193** and **194** in CH_3CN by ethanolamine exhibits a moderate isotope effect, $(k^H/k^D)_q = 1.65 \pm 0.20$, which is

consistent with the C-H vs C-D bond ionization in S_1.

The excited state carbon acid behaviour of substituted suberenes (**180**, **185** and **189**) is similar to the parent suberene **37**. However, the stability of the intermediate carbanions, viz., **204** and **207**, is significantly different from the parent suberenyl carbanion **35**. The fluorescence titration of **180** indicates $pK(S_1) = 4$ (Figure 3.3), which is significantly higher than that of **37** ($pK(S_1) \approx -1$)[48] obtained by similar method. This reduced acidity of **180** in S_1 is attributable to the reduced stability of carbanion **204**. The lower exchange quantum yield (Φ) of **180** compared to suberene (**37**) (Tables 3.1 and 3.2), is consistent with the notion that the reduced stability of intermediate carbanion **204** retards the rate of C-H bond cleavage of **180** in S_1. This is manifested in the lower fluorescence quenching rate (k_q) of **180** ($1.53 \pm 0.06 \times 10^7$ M^{-1} s^{-1}) by H_2O compared to **37** ($1.68 \pm 0.08 \times 10^8$ M^{-1} s^{-1}). Assuming that these measured k_q's for fluorescence quenching of **180** by H_2O are equatable to the rates of C-H bond ionization in S_1, the difference in reactivity of **180** vs **37** are easily understood by application of the Hammond postulate to S_1. Thus, the lower rate of deprotonation of **180** implies that the transition state of C-H bond cleavage in S_1 occurs late along the C-H stretch reaction coordinate compared to **37**. That is, the activation energy required to cleave C-H bond of **180** is higher than that of suberene (**37**). This is because the methoxy groups destabilize the developing negative charge on the incipient carbanion intermediate **204** in the transition state. This situation is diagrammatically presented in the Figure 3.5. On the other hand, the cyano

group stabilizes the incipient carbanion **209**, and the deprotonation rate of **189** (k_q = 2.05 ± 0.08 x 10^8 M^{-1} s^{-1}) is faster than **37**, suggesting that the transition state of C-H bond cleavage occurs earlier in S_1 (lower activation barrier compared to **37**) along the C-H bond stretch reaction coordinate (Figure 3.5).

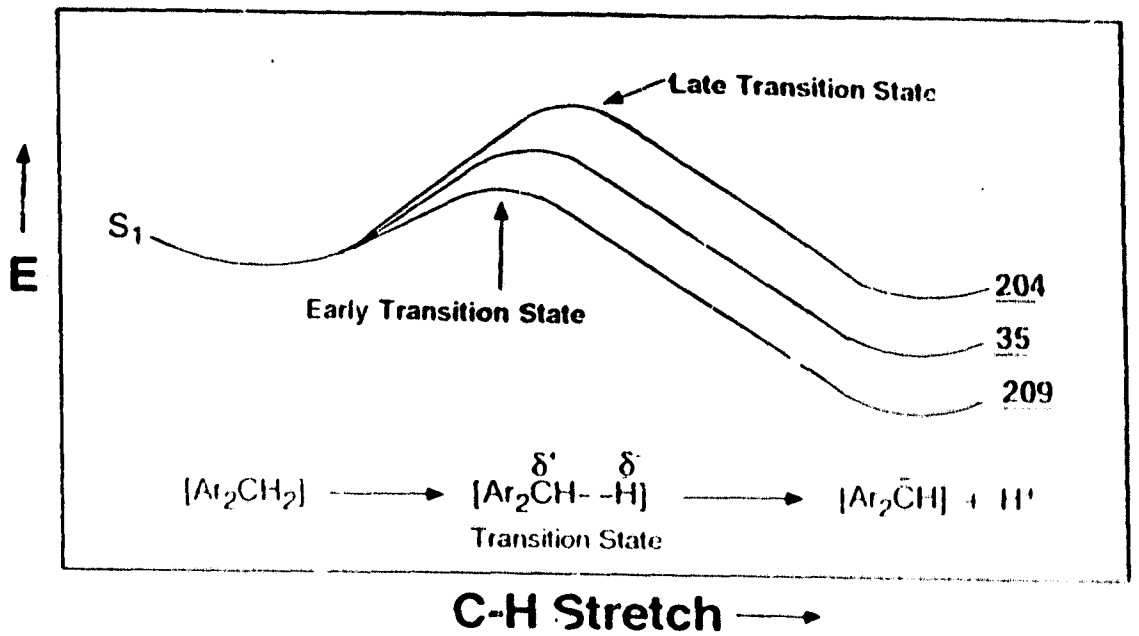

Figure 3.5 Generalized potential energy surfaces for the C-H bond ionizations of suberenes in S_1. Carbanion **204** is less stable than **35** and hence the transition state of C-H bond ionization for **180** occurs late along the reaction coordinate. In contrast, carbanion **209** is more stable than **35** and hence the early transition state for the C-H bond ionization in **189**.

The requirement of a stronger base (viz., ethanolamine) to induce the C-H bond cleavage in **193** implies that it is less acidic than simple suberenes in S_1. The

MMX (PCMODEL force field) calculations indicate that in S_0 **193** has a highly bent structure ("saddle shape") (Figure 3.6) which prevents an extensive π-orbital

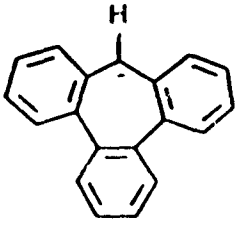

213

overlap. As a consequence, the negative charge in the incipient tribenzosuberenyl carbanion **213** in the transition state is less stabilized compared to simple suberenyl carbanions (e.g., **35**).

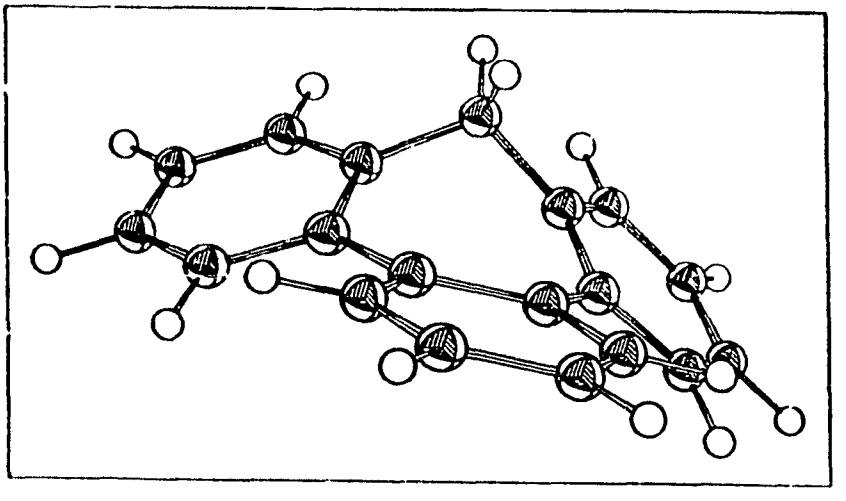

Figure 3.6 Minimum energy structure for **193** predicted from PCMODEL.

CHAPTER FOUR

PHOTOGENERATION AND REACTIONS OF THIOXANTHENIUM AND XANTHENIUM CATIONS

4.1. Product Studies of Electron Transfer to Photoexcited Xanthenium and Thioxanthenium cations in S_1 in Aqueous Acid Solution

4.1.1 Product Studies

9-Phenylxanthen-9-ol (**98**), and 9-xanthenol (**216**) were purchased from Aldrich and purified by recrystallization from hexane. 9-Phenylthioxanthen-9-ol (**219**) was prepared by adaption of reported procedures.[159] 9,9'-Bisxanthene (**128**) was made according to a literature method, by photolysis of 9*H*-xanthene (**125**) followed by purification using preparative thin layer chromatography (eq 2.9).[117] 9-Phenylxanthene (**133**), 9-phenylthioxanthene (**139**) and 9*H*-thioxanthene (**136**) were prepared via $LiAlH_4/AlCl_3$ reduction of the corresponding alcohols and purified by recrystallization from $EtOH/H_2O$. Bis(xanthen-9-yl)peroxide (**217**) was made by adaptation of reported method,[160] via the oxidation of **216** with H_2O_2 and purified by recrystallization from petroleum ether (eq 4.1).

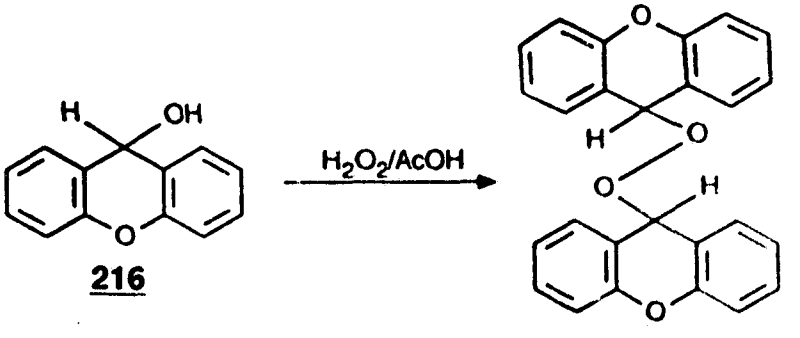

216 **217** (4.1)

4.1.1.2 Photolysis of 9-Phenylxanthenium Cation (99)

Acidification of a CH_3CN solution of 9-phenylxanthenol (98) (pK_{R+} = 1.0 ± 0.5 in aq. H_2SO_4)[92] by 10% (w/w) H_2SO_4 readily afforded the cation 99 (eq 4.2).

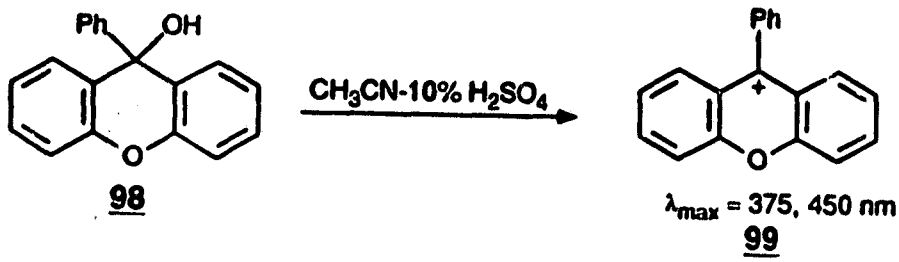

98

λ_{max} = 375, 450 nm

99

(4.2)

The cation 99 had a strong absorption band at approximately 375 nm and a broad weaker band at 450 nm giving rise to a characteristic yellow solution. Photolysis of 10^{-2} M solutions of 99 for 30-60 min at 350 nm in 1:1 CH_3CN-10% (w/w) H_2SO_4 resulted in no significant reaction and the alcohol precursor 98 could be recovered after neutralizing the solution. However, when the above solution of 99 was photolyzed in the presence of 10^{-2} M 1,3-dimethoxybenzene (1,3-DMB), a brown precipitate was observed to be forming after only 2 min of photolysis. After 30 min photolysis, the precipitate was filtered, washed with water and dried (yield ≈ 10 mg). The ^1H NMR of the precipitate was not very informative and showed no significant peaks between δ 1-7 region indicating that the precipitate contained no 1,3-DMB fragment. The mass spectrum (CI) of this precipitate showed a significant peak at m/z 257 which corresponded to the 9-phenylxanthenyl fragment. On the other hand, when the filtrate was neutralized and extracted with CH_2Cl_2 it yielded recovered 98 and 1,3-DMB.

Only the cation **98** absorbs at the irradiation wavelength of 350 nm. In addition, there was no reaction observed when the reaction mixture was left in the dark or when irradiated in the absence of 1,3-DMB. Thus it is clear that the chemistry observed is due to photoexcited **99** in the presence of 1,3-DMB. Formation of precipitate was also seen when irradiation was carried out in the presence of 1,2-, 1,4-DMB and 1,3,5-TMB instead of 1,3-DMB. However, irradiation of **99** in the presence of benzonitrile did not result in the formation of the precipitate and **98** was recovered unchanged after photolysis.

Since the ^{1}H NMR and mass spectral analyses of the precipitate were not particularly informative it was decided to make the use of X-ray crystallography to elucidate the nature of the precipitate. The precipitate was crystallized from CH_2Cl_2/hexanes to obtain yellowish crystals. The ^{1}H NMR of the re-crystallized material was identical to the spectrum observed before re-crystallization reassuring that crystallization process did not change the structure of the photoproduct, or at least any change that could be detected by ^{1}H NMR. The structure of the crystal was solved by X-ray crystallography (Table 4.1 and Figure 4.1) and found to be bis(9-phenylxanthen-9-yl) peroxide (**218**) (eq 4.3). It is

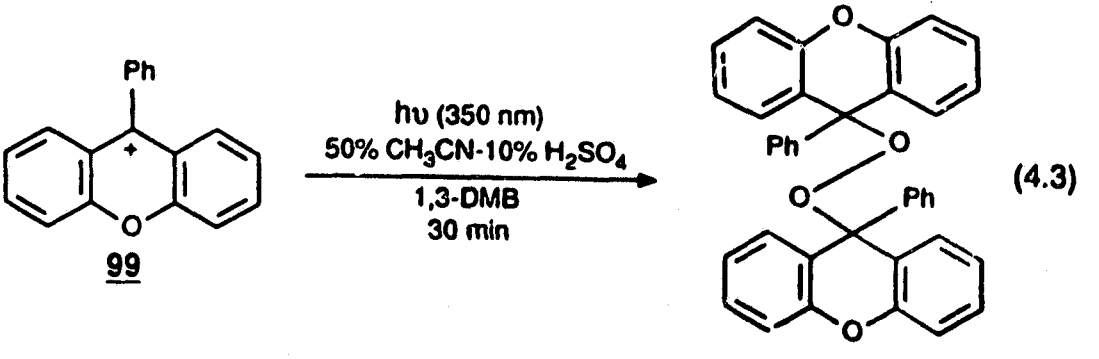

(4.3)

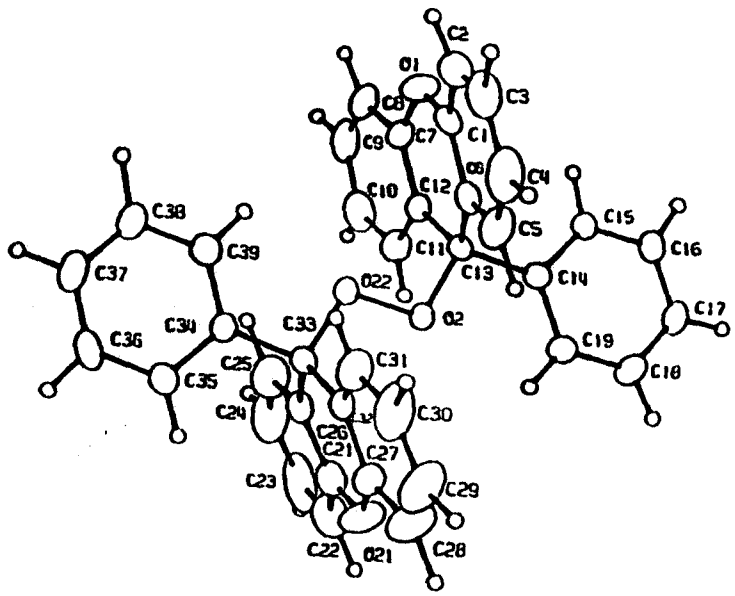

Figure 4.1 X-Ray structure of **218**.

Table 4.1 Summary of Crystallographic Data for 218.

Formula	$C_{38}H_{26}O_4$
mol wt	546.62
crystal system	monoclinic
space group	$p2_1/n$
cell dimensions	
a, Å	8.461(1)
b, Å	16.870(4)
c, Å	19.847(3)
α, deg	90
θ, deg	95.80(1)
γ, deg	90
V, Å^3	2822.3
Z	4
T	20 °C
λ	Mo Kα(0.71069)
ρ_{obsd}, g cm^{-1}	1.281
ρ_{obsd}, g cm^{-1}	1.286
$R(F_0)$	0.0753
$R_w(F_0)$	0.0707

evident from the structure of **218** the anti arrangement of the xanthene and phenyl rings with respect to the O-O bond, relieves a significant amount of the steric interaction. The compound **218** has been previously reported in the literature. It has been made via the oxidation of 9-phenylxanthene (**133**)[161] and via reduction of **99** with VCl_2[162] but its crystal structure has not been reported.

The formation of **218** suggests the formation of 9-phenylxanthenyl radical (**113**) which, in principle, could either react with another radical to give rise to a dimer or, undergo a bimolecular reaction with O_2 to yield **218**. The presence of bulky phenyl groups induces unfavourable steric interactions and prevents the possibility of dimerization of radical **113** and hence the only observed photoproduct is **218**. The possibility that the excited carbocation **99** itself could react with O_2 to give rise to **218** is ruled out since the photolysis of **99** in the absence of 1,3-DMB did not lead to any reaction (eq 4.4). Moreover, it has been shown that **99** reacts slowly (compared to aromatic donors) with O_2 ($k_q^{O2} \sim 10^9\ M^{-1}\ s^{-1}$).[163] This is mainly because the cation **99** being electron deficient, the charge transfer interaction with O_2 is absent. Additionally, the fact that an incipient

$$\underline{\mathbf{99}} \quad + \quad O_2 \xrightarrow[1{:}1\ H_2SO_4\text{-}CH_3CN]{h\nu} \text{no reaction} \qquad (4.4)$$

dication-anion pair would be formed in the course of charge-transfer makes the latter unfavourable on the basis of intramolecular columbic attraction.[163]

Formation of 9-phenylxanthenyl radical **113** was further evident in the

course of photolysis of **99** in 2-propanol. Photolysis of **99** in 1:1 2-PrOH-10% (w/w) H_2SO_4 for 60 min failed to give any precipitate and **98** could be recovered

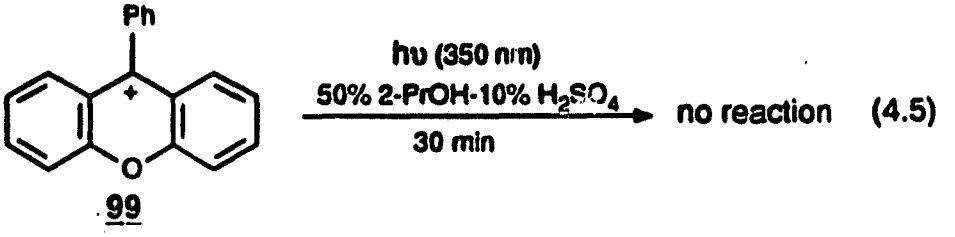

after work up of the reaction mixture (eq 4.5). However, when the photolysis of such a solution was carried out in the presence of 1,3-DMB, the only product observed was 9-phenylxanthene (**133**) (≈ 30%), by comparison with an authentic

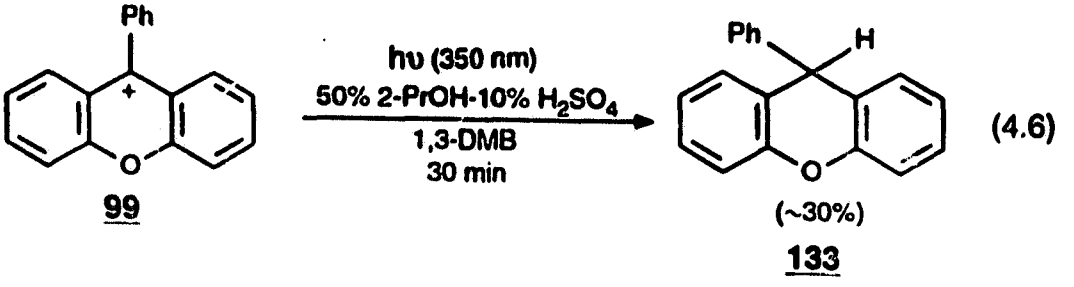

sample (eq 4.6). These observations are consistent with the formation of the 9-phenylxanthenyl radical (**113**) as an intermediate in the photoreaction.

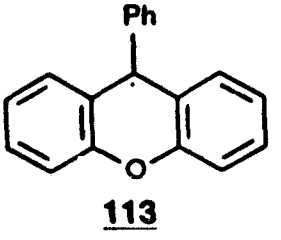

Moreover, **133** was only formed in the presence of dimethoxy benzenes, viz., 1,2-, 1,4- and 1,3-DMB.

4.1.1.3 Photolysis of Xanthenium Cation (114)

The parent xanthenium cation (**114**) was generated from 9-xanthen-9-ol (**216**) in 1:1 CH_3CN-30% (w/w) H_2SO_4 (eq 4.7). Lower H_2SO_4 concentration failed to produce the cation on dissolution of the alcohol **216** signifying that the pK_{R+} is

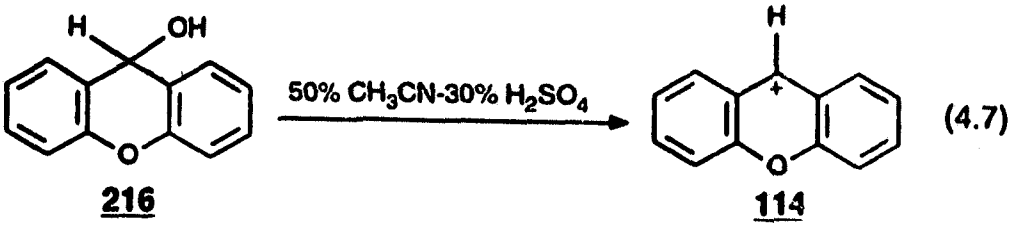

216 **114** (4.7)

significantly lower (= -0.84 in aq H_2SO_4).[164] The cation **114**, similar to **99**, had a strong absorption band at ≈ 374 nm and a much weaker broad band at ≈ 450 nm giving rise to its characteristic yellow colour.

Photolysis of a solution **114** in 1:1 CH_3CN-30% (w/w) H_2SO_4 in the presence of 1,3-DMB produced a yellow precipitate. This yellow precipitate upon isolation gave an ^1H NMR spectrum with singlets at δ 5.8 and 4.2 indicative of two methine signals as well as aromatic signals characteristic of xanthone (**144**). In the absence of 1,3-DMB, photolysis of **114** did not yield any precipitate. However, upon work up of such a solution, the ^1H NMR spectrum of the reaction mixture showed formation of an equal amount of 9-xanthone (**144**) and 9*H*-xanthene (**125**). This mixture was also observed in a dark control reaction and therefore is attributed to a thermal reaction: a hydride transfer from the methine of **216** to the carbocationic centre of **114** (eq 4.8).

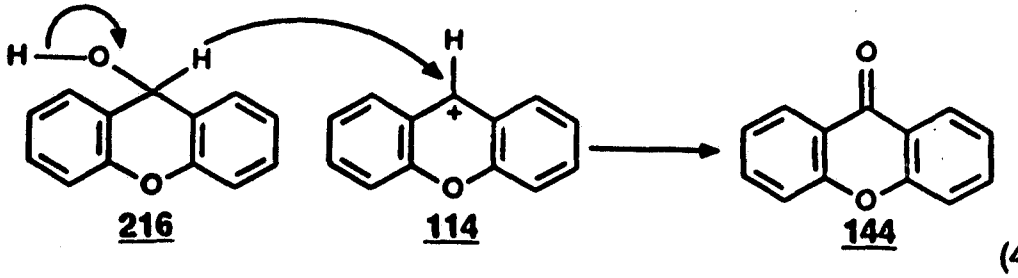

216 114 144 (4.8)

144 : 125 = 1:1

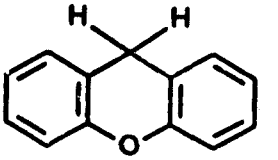

125

It was not possible to grow crystals from the photochemical product mixture that were suitable for X-ray crystallography. Therefore, the structure of the products, obtained on the photolysis of **114** in the presence of 1,3-DMB, were assigned by comparison with ^{1}H NMR spectra of authentic samples. The singlet at δ 4.2 was assigned to 9,9'-bisxanthene (**128**), by comparison to an authentic sample prepared independently.[117] The other singlet at δ 5.8 was assigned to

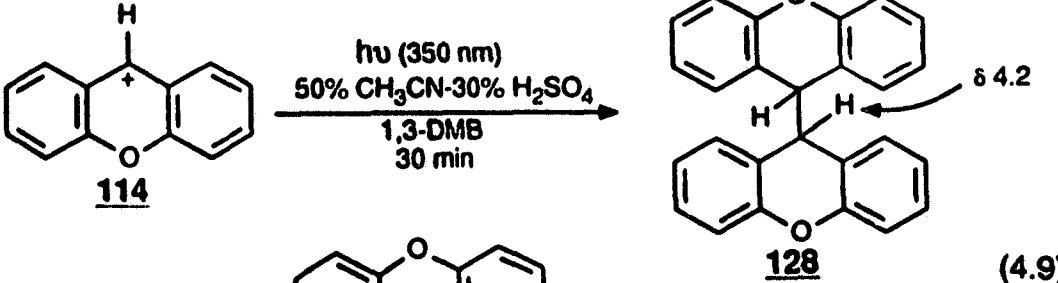

114 128 (4.9)

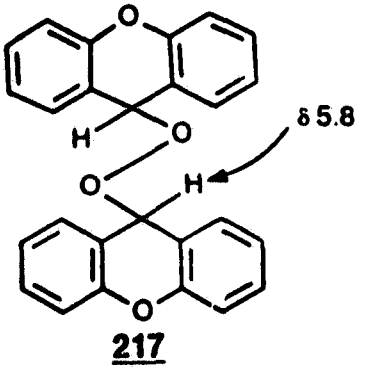

217

bis(xanthen-9-yl) peroxide (**217**), by comparison with an authentic sample made via H_2O_2 oxidation of **216** (eq 4.9).[160] In a separate experiment when **217** was dissolved in aqueous H_2SO_4 (≈ 5% (w/w)) it readily decomposed to yield 9-xanthone (**144**). Thus, 9-xanthone (**144**) observed in the reaction mixture is probably due to reaction of **217** in water. Because, if **144** were formed in a thermal reaction, an equal amount of **125** should also have been observed (*vide supra*).

4.1.1.4 Photolysis of 9-Phenylthioxanthenium Cation (220)

The 9-phenylthioxanthenium cation (**220**) was generated by acidifying acetonitrile solution of the precursor 9-phenylthioxanthene-9-ol (**219**) with 30% (w/w) H_2SO_4 (eq 4.10). The cation **220** showed strong absorption band at ~ 385

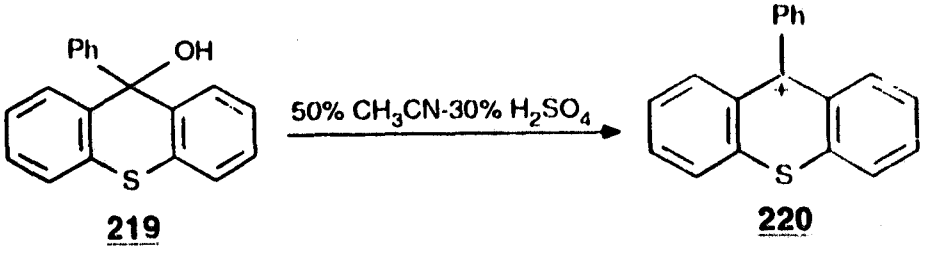

219 **220** (4.10)

nm as well as a weak long wavelength band at 500 nm, giving it a characteristic orange-red colour. Photolysis of a solution of **220** in 1:1 CH_3CN-30% H_2SO_4 (λ_{ex} 350 nm) did not result in any observable reaction and alcohol **219** could be recovered unchanged after work-up of the reaction mixture. Photolysis as above but in the presence of 1,3-DMB also did not show any reaction and **219** could be

recovered unchanged after work-up (eq 4.11). Use of 1,2-, 1,4-DMB and 1,3,5-TMB also did not result in any observable reaction. This apparent lack of

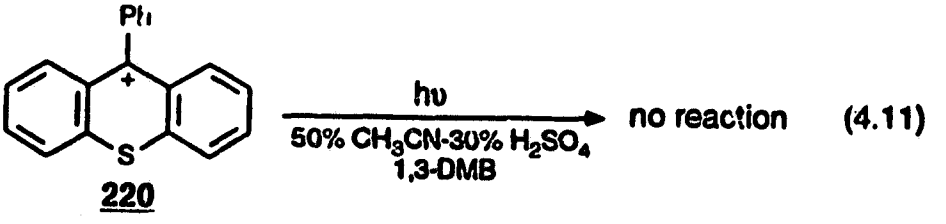

220 (4.11)

reactivity of cation **220** was intriguing because under similar conditions photolysis of 9-phenylxanthenium cation (**99**) results in the formation of peroxy compound **218** via 9-phenylxanthenyl radical **113**. It is possible that in the case of **220** the

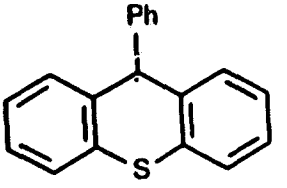

221

the corresponding radical **221** is formed but does not undergo any further reaction with O_2. If the radical **221** is formed it could be reduced in the presence of a good hydrogen donating solvent like 2-propanol to yield the hydrocarbon **139**. However, when a solution of **220** in 1:1 2-propanol-30% H_2SO_4 along with 1,3-DMB was irradiated as above, it did not result in the formation of 9-phenyl-9*H*-thioxanthene (**139**).

4.2 Quantum Yield Measurement

Since it was not possible to directly monitor the appearance of **218** in any quantitative fashion (GC, NMR), quantum yields for the loss of **99** (Φ_L) in 8:2 1.25 M H_2SO_4-CH_3CN were measured instead. The measurements were carried out in the presence of 10^{-2} M 1,3-DMB and followed by UV-Vis spectrophotometry (λ_{ex} = 375 nm). Potassium ferrioxalate actinometery was employed to monitor the light intensity. Both the substrate and actinometer solutions were purged with a stream of argon prior to and during the photolysis. The $\Phi_L \approx 0.0007$ was obtained for the loss of **99**. The low Φ_L indicates that the reaction of excited **99** is extremely inefficient.

4.3 Steady-state Fluorescence and Lifetime Quenching Studies

The fluorescence behaviour of variety of xanthenium and thioxanthenium cations has been previously examined by several groups.[163,105a] Most of these cations fluoresce strongly and have relatively long (except **220**) singlet liftimes. Relevant fluorescence lifetimes (τ's) and quantum yields (Φ_f) data in 8:2 1.25 M H_2SO_4-CH_3CN for the cations examined in this work are collected in Table 4.2.

Table 4.2 Photophysical Parameters of Carbocations in Aqueous H_2SO_4 Solution.[a]

Carbocation	Φ_f[b]	τ_f (ns)	ε_{max} (10^3 M^{-1} cm^{-1})
99	0.077 ± 0.004	4.25 ± 0.02[c]	39.00 ± 0.07[f]
114	0.057 ± 0.003	6.22 ± 0.02[d]	21.80 ± 0.05[g]
221	0.015 ± 0.003	0.85 ± 0.05[e]	16.50 ± 0.05[h]

a) Standard 2.5 N H_2SO_4 solutions with 20% CH_3CN (v/v) as co-solvent.
b) Φ_f's measured relative to quinine bisulfate (Φ_f = 0.55 in 1 N bH_2SO_4)[177].
c) λ_{ex} 372 nm/λ_{em} 520 nm. d) λ_{ex} 370 nm/λ_{em} 540 nm. e) λ_{ex} 385 nm/λ_{em} 580 nm.
f) At λ_{max} = 374 nm. g) At λ_{max} = 375 nm. h) At λ_{max} = 384 nm.

The fluorescence of 9-phenylxanthenium cation (**99**) and xanthenium cation (**114**) in 8:2 H_2SO_4-CH_3CN were found to be easily quenched by di- and trimethoxybenzenes. This was evident in terms of both progressive decrease in steady-state emission intensity and gradual shortening of observed lifetimes. A representative case of steady-state fluorescence quenching of emission of **99** by added 1,3-DMB is shown in Figure 4.2. Figure 4.3 shows the effect of added benzonitrile on the emission of **99**.

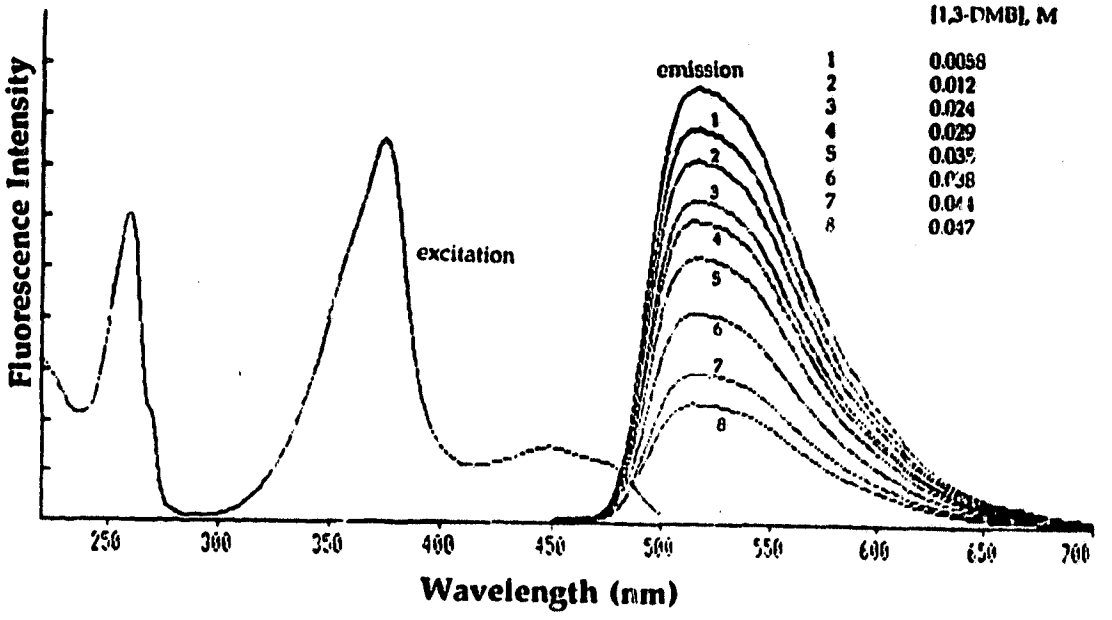

Figure 4.2 Fluorescence quenching of cation 99 by added 1,3-DMB in 8:2 1.25 M H_2SO_4-CH_3CN solution (λ_{ex} = 375 nm).

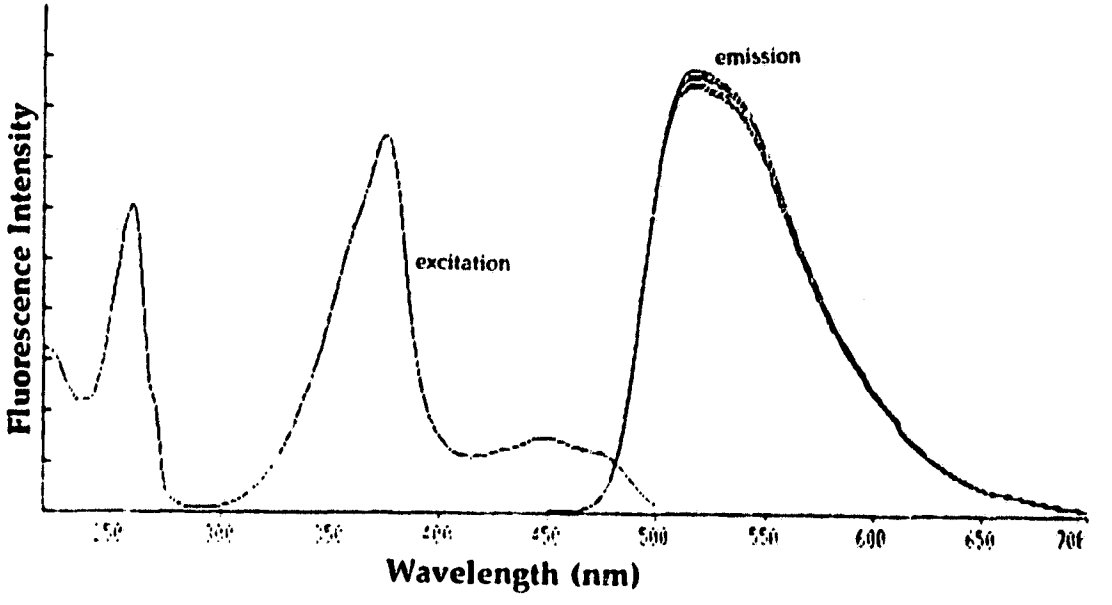

Figure 4.3 Fluorescence quenching of cation 99 by added benzonitrile in 8:2 1.25 M H_2SO_4-CH_3CN solution (λ_{ex} = 375 nm). Note the lack of any significant quenching using the same concentration of benzonitrile as 1,3-DMB used in Fig. 4.2.

The quenching rate constants from steady-state fluorescence quenching (k_q^{ss}) and lifetime quenching (k_q^{τ}) were calculated by standard Stern-Volmer analyses of the quenching process and are presented in Table 4.3. The good

Table 4.3 Fluorescence Quenching Rate Constants (k_q's) for 99 and 114 in 8:2 1.25 M H_2SO_4-CH_3CN Solution.[a]

	k_q (M^{-1} s^{-1})[b]			
	99		114	
Quencher	Steady-State	Lifetimes[c]	Steady-State	Lifetimes[c]
1,2-DMB	7.0×10^9	1.4×10^{10}	6.3×10^9	6.18×10^9
1,3-DMB	5.0×10^9	4.9×10^9	-	-
1,4-DMB		1.4×10^{10}	-	-
1,3,5-TMB	7.9×10^9	7.8×10^9	7.3×10^9	7.12×10^9

a) Calculated by standard Stern-Volmer analysis of quenching.
b) Errors in k_q's are ± 10% of the quoted values.
c) Measured by single photon counting.

agreement seen between the two rate constants (steady-state and lifetimes) signifies that the quenching is a dynamic process, and that the fluorescence quenching observed is not due to some ground state complexation of the cation and the quencher. Moreover, no ground state complexation between carbocations and the quencher(s) was indicated in the absorption spectra of the carbocations in the presence of the quenchers at the highest concentrations used.

Previous studies have shown that the fluorescence of cations 99, 114 and

220 is readily quenched by aromatics (e.g., benzene) by predominantly electron-transfer mechanism in which the excited carbocations act as electron acceptors.[105a,163] The products derived from electron transfer, viz., radical cations (from aromatic quenchers) and radicals (from carbocations) have also been observed in nanosecond laser flash photolysis studies. The thermodynamics of photochemical electron transfer are governed by the Rhem-Weller equation (eq 4.12).[165] Using eq 4.12, the electron transfer from variety of substituted benzenes

$$\Delta G_{ET} = -E_s - E^{red}_{1/2}\text{(carbocation)} + E^{ox}_{1/2}\text{(donor)} \qquad (4.12)$$

to these cations has been shown to be an exothermic process.[163] For example, the free energy of electron transfer (ΔG_{ET}) from anthracene ($E_{1/2}$ = 0.84 V) to S_1 of **99** ($E_{1/2}$ = -0.374 V; in sulfolane/3-methylsulfolane vs silver/silver nitrate; glassy carbon electrode) has been calculated to be -32 kcal/mol.[163] Although the $E_{1/2}$ values of the various quenchers (e.g., 1,2- and 1,3-DMB) used in this work are not known, the results of steady-state emission quenching and product studies strongly indicate that di- and trimethoxybenzenes quench S_1 of carbocations via electron transfer with rates indicated by the fluorescence quenching rates (k_q's). Laser flash photolysis studies of electron transfer from aromatic donors to **99** have revealed that the yield of such electron transfer as a result of S_1 quenching is very small *ca.* ≤ 0.02.[163a] These low yields suggest that the back electron transfer in the photogenerated singlet radical-ion/radical pairs is predominant over their

dissociation. This small yield of electron transfer also explains the low yield for loss (Φ_L) of **99** obtained in the product studies.

4.1.4 Mechanism of Formation of Peroxy Products

A mechanism for the reaction of **99** in the presence of electron donor 1,3-DMB is shown in Scheme 4.1. Electron transfer from 1,3-DMB gives the radical

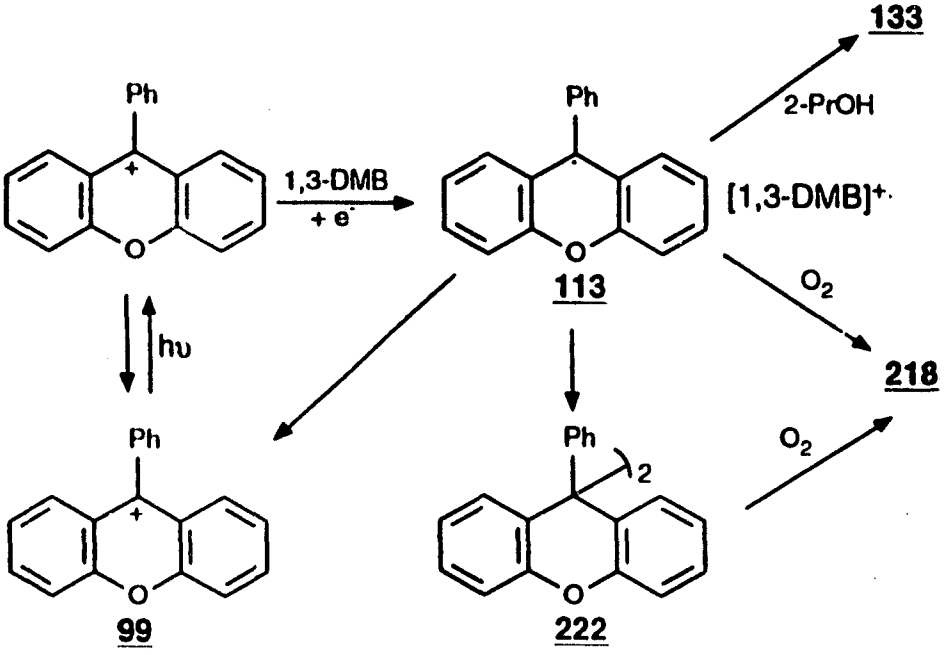

Scheme 4.1

113/1,3-DMB radical ion pair, most of which reverts back to regenerate **99** (and 1,3-DMB) via back electron transfer. In the presence of 2-propanol (2-PrOH), reduction of **113** to give **133** is the only observed reaction in competition with the back electron transfer. In the absence of 2-PrOH, **113** reacts with the residual

oxygen in the solution to generate **218**. Alternatively, dimerization of radical **113** gives bis(9-phenylxanthen-9-yl) (**222**), which is unstable and known to react with oxygen to give **218**. The possibility that the initial precipitate observed on the photolysis of **99** is in fact **222** (or an isomer), which upon subsequent

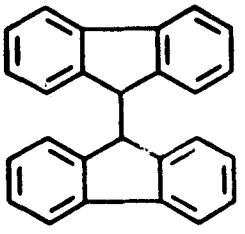

223

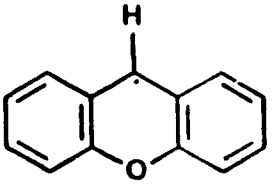

131

crystallization and contact with air gives **218** has not been ruled out. There is literature precedent to indicate that this pathway is plausible. In fact, it has been reported that bis(9-phenylfluoren-9-yl) dimer (**223**) slowly absorbs oxygen to give the corresponding peroxide. In any event, results of this study clearly indicate that 9-phenylxanthenyl radical (**113**) is the primary intermediate formed on photolysis of **99** in the presence of an electron donor.

In the case of reaction of **114**, a similar mechanistic scheme applies. However, there is an important subtle difference: dimer **128** is formed and more significantly, **128** is not a precursor to peroxide **217** as indicated by an independent photolysis of **128**. This implies that **217** is formed via reaction of the free radical or the radical/radical ion pair with oxygen. The lack of reactivity of 9-bisxanthene (**128**) suggests that the photogenerated radical pair from this dimer preferentially undergoes geminate recombination as opposed to reaction with

oxygen or escape out of the solvent cage.

The steady-state fluorescence quenching of **220** by 1,3 DMB (k_q = (1.92 ± 0.04) x 10^{10} M^{-1} s^{-1}) indicates that the electron transfer to the cation **220** in S_1 is thermodynamically allowed and does take place. The observation of 9-phenylthioxanthenyl radical (**221**) in the LFP of **220** in the presence of other aromatic donors (e.g., benzene, naphthalene) confirms this.[105a] However, as indicated by the results obtained in the product studies, further reaction of the radical does not take place to yield any observable product. An efficient back electron transfer in the photogenerated radical/radical ion pair to regenerate **220** seems to be the dominant reaction pathway.

4.2 Adiabatic Photogeneration of Thioxanthenium Cations in Neutral Aqueous Solution

4.2.1 Product Studies

Thioxanthenols **226-229** and **219** were prepared from the corresponding commercially available ketones **224** and **225** (Aldrich), by $NaBH_4$ reduction or by reaction with the appropriate Grignard reagent. The alcohols were purified by recrystallization from warm (~ 35 °C) hexanes/ether. The ^1H NMR spectra were all consistent with their assigned structures. The alcohols slowly decomposed via

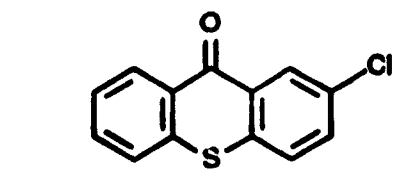

225

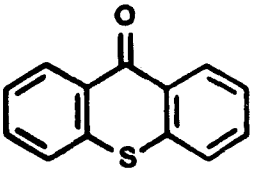

224

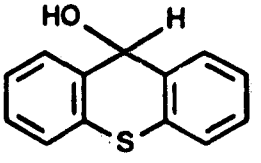

226

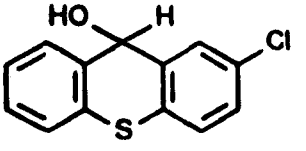

227

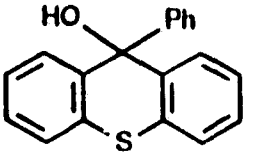

219

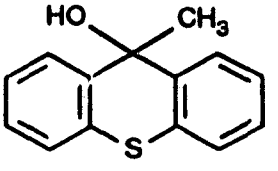

228

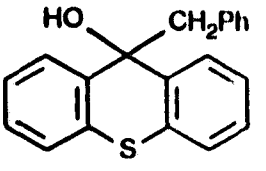

229

a disproportionation pathway, to give the corresponding thioxanthone **224** (or **225**), and the corresponding 9,9'-disubstituted (with R) thioxanthene. This decomposition pathway was most significant when R = H and CH_3 (i.e., alcohols **226**, **227**, and **228**). The purified alcohols were used as soon as possible after recrystallization or stored in the cold under an inert atmosphere. Because these alcohols also decomposed on the GC column (via the same pathway described above), purity checks were carried out by high field (250 MHz) ^{1}H NMR. The absence of characteristics peaks of **224** and **225** at δ 8.7 (peri protons on the ring) was used as an indication of alcohol purity.

Photodehydroxylation of the thioxanthenols was carried out in aqueous MeOH (typically 50% (v/v) MeOH-H_2O; pH 7) and 100% MeOH solutions. On

photolysis many of these alcohols were converted to their corresponding methyl ethers, thus the overall process is photosolvolysis. The methyl ethers thus produced were themselves photochemically reactive, producing secondary photoproducts, particularly at higher conversions.

4.2.1.1 Photolysis of Thioxanthen-9-ol (226) in Aqueous Methanol

Photolysis of **226** in 50% H_2O-CH_3OH (pH 7) at 254 nm resulted in the formation of corresponding methyl ether **230** (≈40%) (eq 4.13), as indicated by

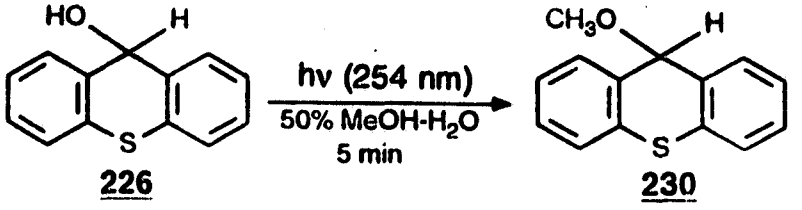

226 **230** (4.13)

the characteristic methoxy resonance at δ 3.2 in ^1H NMR spectra of the reaction mixture. The formation of methyl ether **230** in the photosolvolysis of **226** is consistent with the intermediacy of carbocation **231**. However, the yield

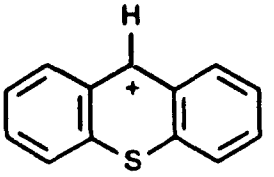

231

of methyl ether **230** is only a lower limit of the yield of carbocation formation, because a certain portion of carbocation is trapped by H_2O and therefore

regenerates the starting material. Previous studies have shown that the photodeydroxylation of aryl and diaryl alcohols is catalyzed by acids.[87,88,90,96] In the case of photodehydroxylation of **226** it was not possible to address the question acid catalysis because of efficient thermal dehydroxylation of **226** even in mildly acidic solutions (*ca.* pH 6).

4.2.1.2 Photolysis of 226 with External Nucleophiles

In order to substantiate the intermediate 9-thioxanthenium cation **231**, attempts were made to trap it using nucleophiles other than solvent (MeOH). Previous studies in our laboratory have shown that cyanide ion (0.25 **M** NaCN in aqueous CH_3CN) is capable of trapping the incipient cation generated in the photolysis of 2,6-dimethoxybenzyl alcohols.[88] Thus, photolysis of **226** in 50%

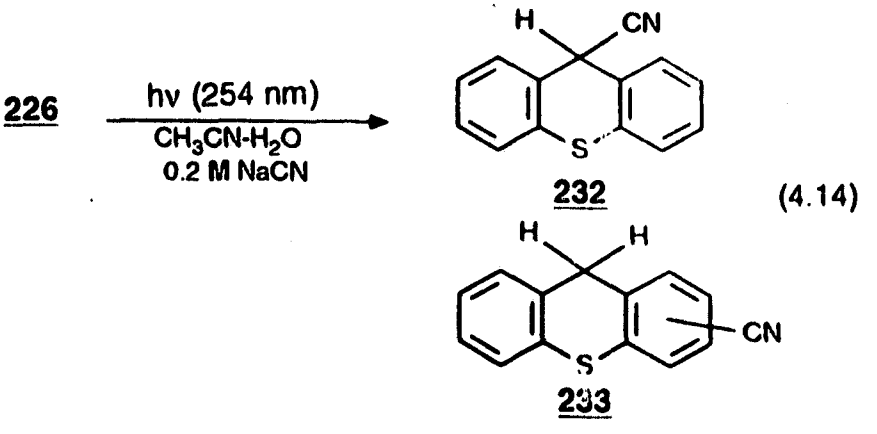

(4.14)

CH_3CN-H_2O (0.2 **M** NaCN) for 10 min resulted in the formation of two trapping products, 9-cyanothioxanthene (**232**) (≈30%). and a ring substituted cyanothioxanthene **233** (≈10%) (eq 4.14).

4.2.1.3 Photolysis of Alcohols 227, 228, 229 and 219 in Aqueous Methanol

Photolysis of alcohols **227**, **228** and **219** in 50% MeOH-H_2O (pH 7) also resulted in the formation of the corresponding methyl ethers (yields 25-35%) as indicated by the ^1H NMR spectra of the reaction mixtures (eq 4.15). However, a

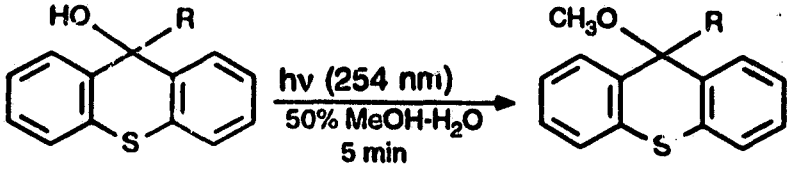

(4.15)

228 R = CH_3
219 R = Ph

similar photolysis of **229** gave only a trace of methyl ether, the major product being alkene **234** (≈20%) (eq 4.16). The alkene **234** is believed to arise by the loss

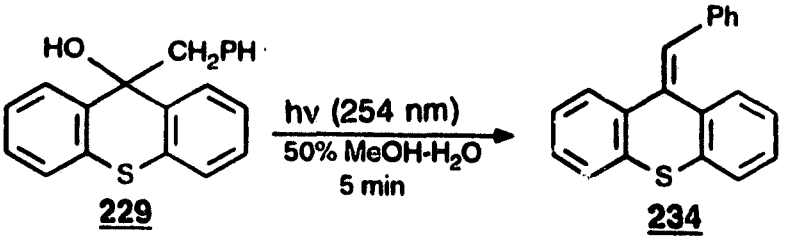

229 **234**

(4.16)

of proton from the intermediate cation via a formal E1 elimination.

4.2.2 Steady-State and Transient Fluorescence Studies

Fluorescence emission spectra of alcohols **219** and **226-229** recorded in dry

CH_3CN gave only emission from the corresponding alcohols (λ_{max} ≈ 340-350 nm), with no longer wavelength emitting species. A representative fluorescence excitation and emission spectra of **226** in CH_3CN (dry) is shown in Figure 4.4.

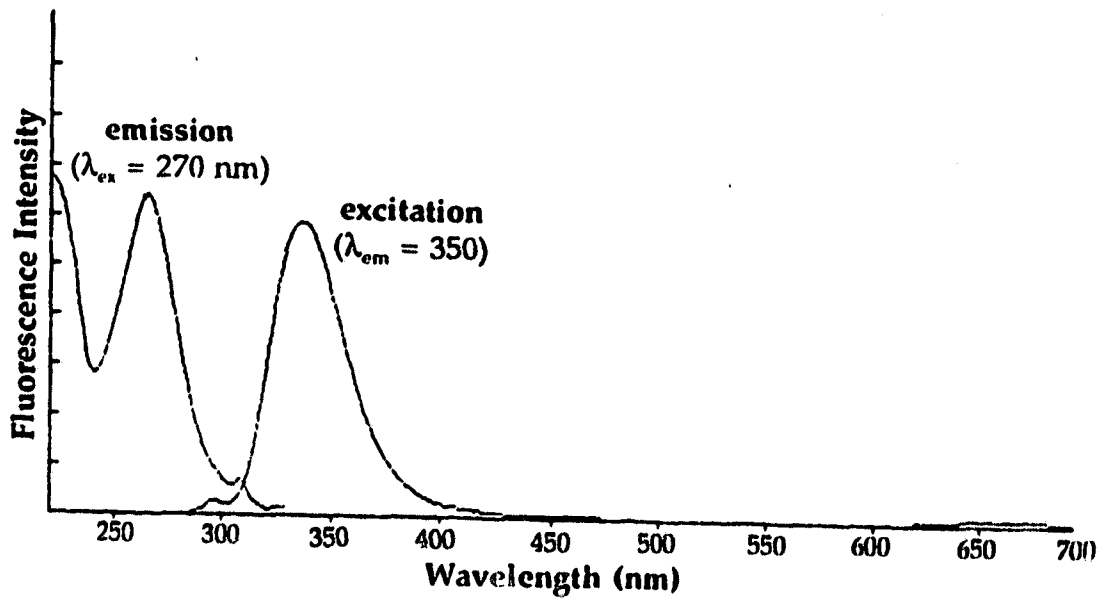

Figure 4.4 Fluorescence excitation and emission spectra of **226** in CH_3CN.

However, emission spectra recorded in aqueous solutions (100% H_2O; pH 7 buffer), showed two additional bands at 450 and 550 nm. The relative intensity of these two new emission bands depended on the nature of the alkyl group in alcohols **226-229**. Figure 4.5 shows such an emission spectrum for **226** (λ_{ex} = 250 nm). The emission band at 450 nm was identified to be due to ketone **224**, by comparison with its authentic emission. The excitation spectrum of 450 nm band

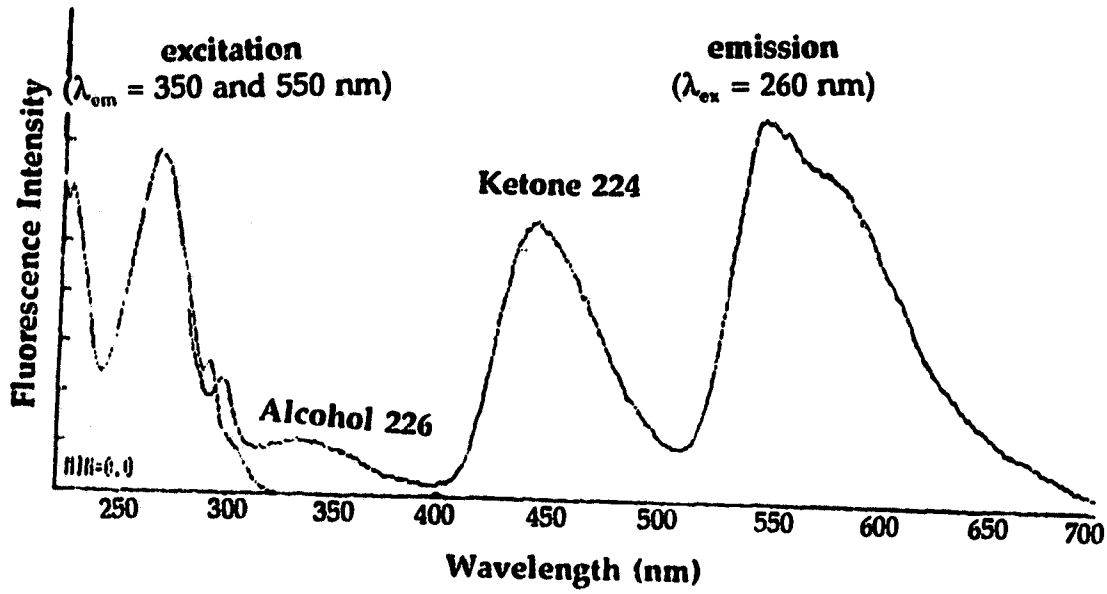

Figure 4.5 Fluorescence excitation and emission spectra of **226** in pH 7 Buffer.

resembled the absorption spectrum of the ketone **224** indicating that it arises from the trace quantities of **224** present in the sample and it is not generated via excitation of the alcohol precursor. The ketone **224** is believed to be formed thermally via a disproportionation pathway described above, which takes place to some extent upon dissolution of alcohol in aqueous solutions.

The emission band at 550 nm had the same excitation spectrum as the emission at 340 nm and was identical in appearance to the authentic emission of thioxanthenium cation **231** (generated in 10% H_2SO_4). Therefore, this band at 550 nm was assigned to adiabatically generated **231** (Scheme 4.2). There is essentially

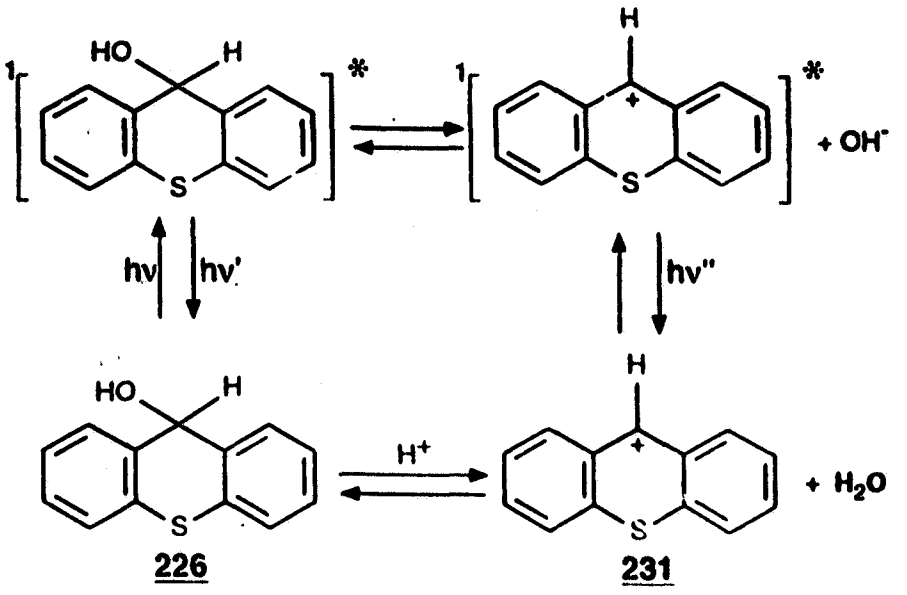

226 **231**

Scheme 4.2

no cation present in the ground state at pH 7. To further confirm this, excitation of the sample at 375 or 450 nm (where only the cation absorbs strongly) gave no detectable emission peaks. Similar observations were made for alcohols **227-229** and **219**. However, in the cases of alcohols **229** and **219** much less emission was observed from the ketone **224**. These two compounds also gave the weakest emission due to the corresponding adiabatically generated cations. Figure 4.6 shows the excitation and emission spectra of **219** recorded in aqueous solution (ph 7 buffer).

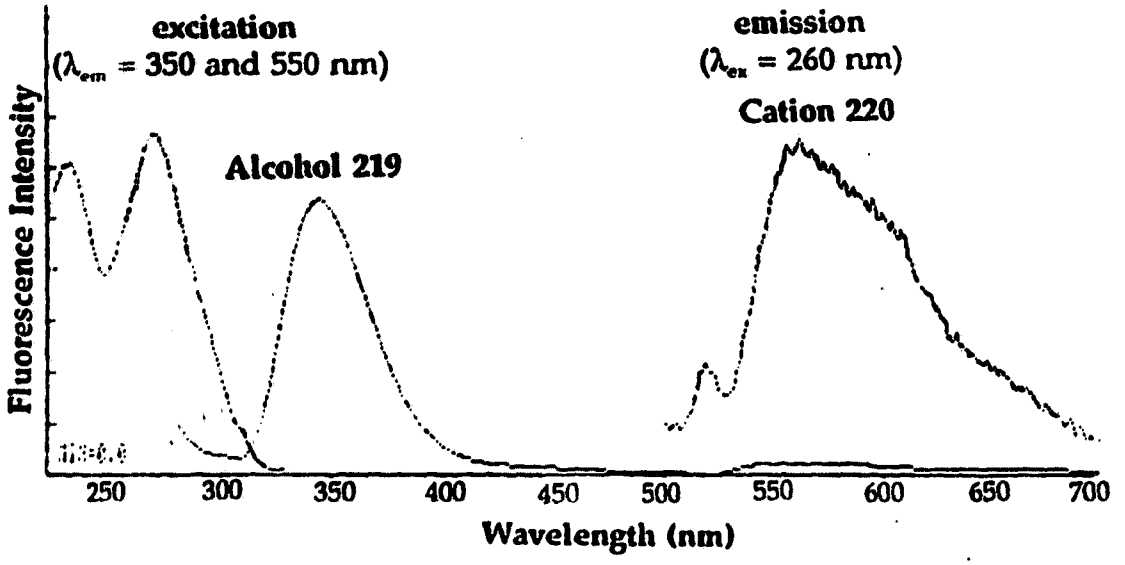

Figure 4.6 Fluorescence excitation and emission spectra of 219 in pH 7 buffer (inset x 50).

Figure 4.7 presents a generalized look at the potential energy surfaces for the adiabatic photodehydroxylation of thioxanthenols. These energy surfaces give

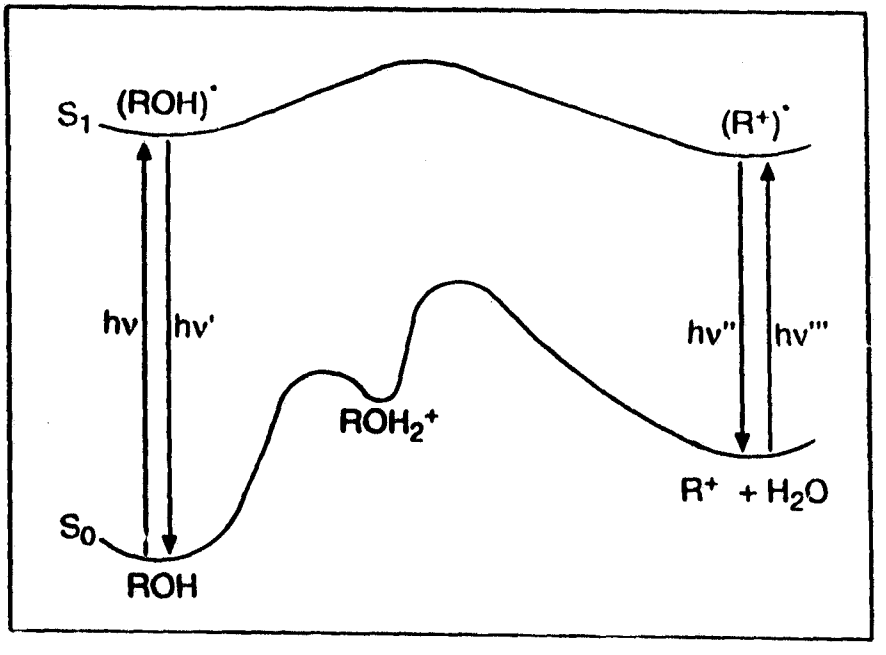

Figure 4.7 Generalized excited state potential energy surface, relative to the ground state, for the adiabatic photodehydroxylation of thioxanthenols (e.g., 226) in H_2O.

us a clue regarding the nature of the excited state energy surface in relation to the ground state energy surface for photodehydroxylation process. Since the photogenerated thioxanthenium cations exhibit fluorescence emission the energy minimum for excited cation $(R^+)^*$ must be nearly or directly situated above the energy minimum for R^+ of the ground state surface.

The relative emission intensities of 345 nm and 550 nm bands were affected by use of H_2O/D_2O. For the 345 nm emission (due to alcohol **226**), the ratios of emission intensities in H_2O vs D_2O $((\Phi_f^H/\Phi_f^D)_{345})$ was 0.82 ± 0.06. For the 550 nm emission (due to cation **231**) an inverted ration $((\Phi_f^H/\Phi_f^D)_{550} = 1.38 \pm 0.04)$ was observed. Both of these experiments were carried out in 100% L_2O (L = H and D) at a pH of 7.0 ± 0.2), without any added buffer. These isotope effects are consistent with a reaction mechanism involving product-determining proton transfer from the solvent to the incipient leaving hydroxide ion of photoexcited **226**, to give thioxanthenium cation **231**. It also suggests that the protonation of excited **226** is irreversible. That is, since the rate of photodehydroxylation is greater in H_2O than in D_2O (due to primary solvent isotope effect), a proportionately larger amount of cation **231** is formed in H_2O than in D_2O, thus resulting in the observed decrease in fluorescence emission intensity relative to D_2O at 345 nm (due to photoexcited **226**). Because the rate of reaction is faster in H_2O, $(\Phi_f^H/\Phi_f^D)_{550} = 1.38 \pm 0.04$ is found for the 550 nm emission of the carbocation **231**. Furthermore, this latter observation supports the photodehydroxylation mechanism involving product determining proton transfer from the solvent (H_2O)

in the primary step of the reaction. Catalysis of photodehydroxylation process by added hydronium ions could not be tested because 226 (and other alcohols as well) ionizes in the ground state even in solutions of moderate acidity (pH 6.0).

Adiabatic reactions of large organic molecules are in general not common.[166] Concerted or stepwise structural isomerization reactions are known to take place adiabatically.[166] However, adiabatic photoreactions involving heterolytic bond cleavages are not common. The most common adiabatic reactions are simple excited state proton transfer reactions. The first example of adiabatic photodehydroxylation was shown in the case of 9-phenylxanthenol (98).[92] It has been shown that 9-phenylxanthenol (98) undergoes adiabatic photodehydroxylation in aqueous solution to give 9-phenylxanthenium cation (99) in S_1.[92] Laser flash photolysis[93-95] of this reaction confirm that the primary photochemical step in this reaction is the loss of the hydroxide ion. However, it was also noted that only a small fraction (≈ 1%) of the photodehydroxylation occurs adiabatically.

Fluorescence quantum yields (Φ_f's) of the adiabatically generated thioxanthenium cations in H_2O (pH 7 buffer) were measured using quinine bisulphate as a secondary standard and are presented in Table 4.4. Corrected fluorescence spectra of thioxanthenols and quinine bisulfate were utilized for the measurement of Φ_f's. These fluorescence quantum yields are the lower limits for

Table 4.4 Photophysical Parameters of Adiabatically Photogenerated Thioxanthenium Cations.[a]

Alcohol	λ_{max} (emission)	Φ_f[b]	τ[c] (ns)
226	549 nm	0.038 ± 0.004	21.20 ± 0.04
227	549 nm	0.014 ± 0.002	16.40 ± 0.04
228	555 nm	0.035 ± 0.002	18.70 ± 0.05
229	550 nm	0.0015 ± 0.0004	≈0.3
220	555 nm	0.0014 ± 0.0004	0.80 ± 0.04

a) In wholly aqueous solutions (pH 7 phosphate buffers); λ_{ex} = 250 nm.
b) Measured relative to quinine bisulfate (Φ_f = 0.546 in 0.05 M H_2SO_4)[177].
c) Measured via single photon counting; λ_{ex} = 260 nm.

the quantum yield of the adiabatic step for each substrate. For example, substrate **226** reacts via the adiabatic pathway with at least 0.038 quantum efficiency. This is in contrast to the results obtained for 9-phenylxanthenol (**98**) which reacts with about 1% efficiency via the same pathway.[93-95] Also presented in Table 4.4 are the fluorescence lifetimes (τ's) in H_2O of adiabatically generated thioxanthenium cations. Unlike adiabatically photogenerated xanthenium cations, all of the thioxanthenium cations have lifetimes that were measurable using single photon counting (H_2 lamp). The parent (**226**) and methyl substituted (**228**) alcohols exhibited the highest adiabatic fluorescence emissions, with significant quantum yields. Phenyl or benzyl groups, **219** and **229**, lower the emission quantum yields and lifetimes, probably due to enhanced internal conversion rates due to the

bulkier groups at the 9-position.

The possible factor responsible for the enhanced adiabatic fluorescence emission yields (Φ_f's) of the thioxanthenols systems is that the corresponding excited state thioxanthenium cations are less prone to the nucleophilic attack by water, and hence are not deactivated as readily as the xanthenol systems. Boyd and coworkers[167] have shown that the fluorescence lifetimes of xanthenium cations are very sensitive to the presence of H_2O in acid solutions, indicating that they are probably efficiently quenched by nucleophilic attack by H_2O. To test the proposal that the present thioxanthenium cation excited singlet states are less prone to nucleophilic attack by H_2O, fluorescence lifetimes of 231 were measured in a range of acidities (Table 4.5). Interestingly, the lifetime (τ = 21.25 ns) of

Table 4.5 Lifetimes (τ) of Thioxanthenium Cation (231) in Various Solvents.[a]

Solvent	τ (ns)
H_2O (pH 7 buffer)[b]	21.25 ± 0.04
10% H_2SO_4	22.07 ± 0.04
20% H_2SO_4	22.12 ± 0.04
30% H_2SO_4	22.61 ± 0.05
CF_3CH_2OH[b]	28.42 ± 0.05

a) Measured by single photon counting.
b) Adiabatically generated; λ_{ex} 250 nm/λ_{em} 540 nm.

adiabatically photogenerated cation **231** in pH 7 is not very different from the

lifetimes (τ 22 ± 1 ns) of cation **231** generated thermally in 10-30% H_2SO_4 solutions. In the H_2SO_4 solutions, the lifetimes were measured by direct excitation of the cation **231** at 375 nm. In the highly ionizing medium 100% CF_3CH_2OH, the lifetime of adiabatically generated **231** was 28.42 ns. Thus it is clear from the lifetimes (Table 4.4) that the excited state of **231** is not prone to quenching by H_2O. For the same reasons the adiabatically photogenerated thioxanthenium cations exhibit relatively strong emissions (high Φ_f's) in H_2O (pH 7 buffer).

Though the emission from photogenerated thioxanthenium cations is not greatly affected by H_2O, interestingly, addition of MeOH quenched the fluorescence emission when added to the aqueous samples. Stern-Volmer analysis of fluorescence quenching of adiabatically generated **231** by MeOH gave

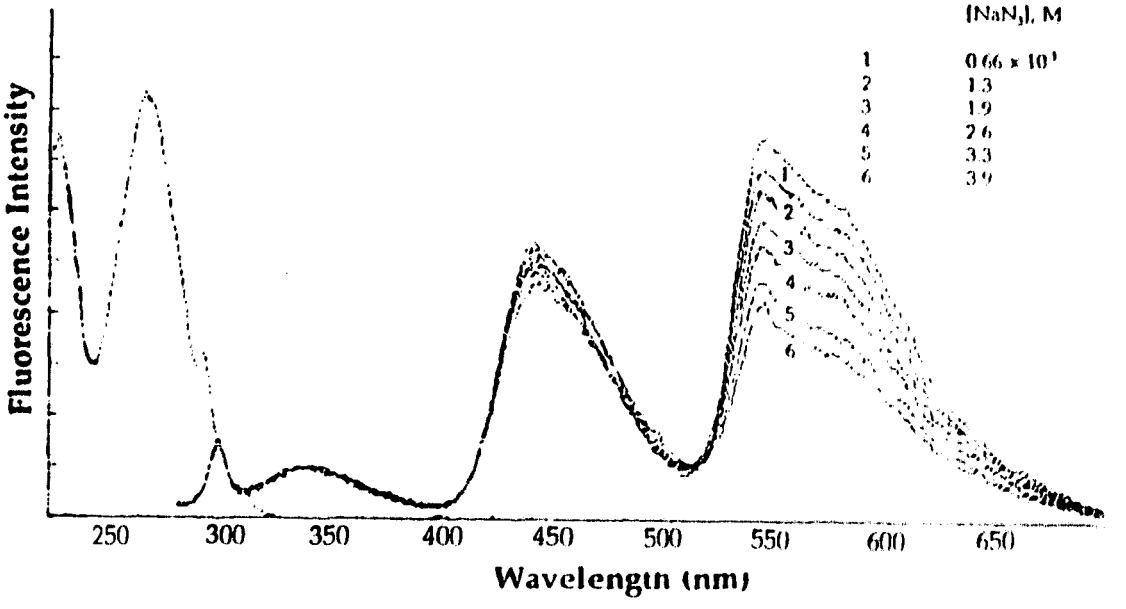

Figure 4.8 Quenching of adiabatically photogenerated cation **231** by NaN_3 in pH 7 buffer (λ_{ex} = 270 nm; 20% (v/v) CH_3CN used as co-solvent).

rate constant k_q = (4.10 ± 0.07) x 10^7 M^{-1} s^{-1}, suggesting that MeOH is more nucleophilic towards 231 in H_2O than water itself. Addition of other nucleophiles, viz., N_3^- and ^-CN also quenched the emission of cation 231 in H_2O. Figure 4.8 shows the fluorescence emission quenching of adiabatically photogenerated 231 in H_2O by added N_3^-. Note that the emission due to ketone 224 (450 nm) is not significantly quenched. Quenching rate constants (k_q's) for 231 by N_3^- and ^-CN were obtained by standard Stern-Volmer analyses of quenching processes and are collected in Table 4.6.

Table 4.6 Fluorescence Quenching Rate Constants (k_q's) for Adiabatically Photogenerated Thioxanthenium Cation (231) in Water (pH 7 buffer).[a]

Quencher	k_q M^{-1} s^{-1}
MeOH[b]	4.10 ± 0.07 x 10^7
^-CN[c]	1.34 ± 0.05 x 10^9
N_3^-	1.47 ± 0.05 x 10^{10}

a) Rate constants (k_q's) obtained by standard Stern-Volmer analysis of quenching.
b) k_q obtained by lifetimes (τ) quenching of cation 231 by added MeOH.

The possibility that the observed quenching is due to initial electron transfer from nucleophile to the excited state carbocation needs to be addressed. It has been shown earlier that excited state of xanthenium and thioxanthenium cations act as very good electron acceptors in the presence of variety of

donors.[105,163] Direct evidence for an electron transfer mechanism would be isolation of radical coupling products such as 9,9'-bis(thioxanthene), which were not observed in this study. Furthermore, attempts to trap any photogenerated 9-thioxanthenyl radical with 2-propanol were of no avail. Thus, if any electron transfer mechanism was operative, the subsequent coupling of the geminate radicals pairs is very fast. In such a case, it would be mechanistically indistinguishable from simple direct nucleophilic attack, at least with the probes at our disposal.

CHAPTER FIVE

SUMMARY AND CONCLUSIONS

In photoreactions of a series of structurally related dibenzannelated systems, it was demonstrated that the driving force inherent in many of their reactions is the attainment of an 4n π-electron system or intermediate in S_1. For example, in the photolysis of 9*H*-xanthene (**125**) and 9*H*-thioxanthene (**136**) in basic solution, it was demonstrated that the driving force for the C-H bond cleavage in S_1 was the formation of 8π-electron cyclically conjugated carbanions **130** and **137**, respectively. Intermediacy of carbanions in these reaction was demonstrated by deuterium incorporation in photoproducts when these compound were irradiated in deuterated solvents. Additional support for the C-H bond cleavage in S_1 was provided by the fluorescence studies of these molecules. Fluorescence quenching of **125** in CH_3CN by added ethanolamine gave a linear Stern-Volmer plot, with $k_q = (2.52 \pm 0.04) \times 10^7\ M^{-1}\ s^{-1}$. The calculated k_q was equated to the rate by which ethanolamine deactivates S_1 of **125** via C-H bond ionization. Consistent with this, the fluorescence quenching rates (k_q's) of **125** and **123** by ethanolamine in CH_3CN showed a substantial kinetic isotope effect. A systematic quenching study of **135** was not possible because of its very weak fluorescence. The 9-phenyl analogue **139** did not exhibit excited state C-H bond ionization, possibly because of the presence of phenyl group which prevents the C-H bond ionization by the base.

The enhanced stability of 8π-electron carbanions was further evident in the

efficient photodecarboxylation of diarylacetic acids **142**, **145**, **147** and **148**. Photolysis of these acids in aqueous solution led to the photogeneration of the corresponding carbanion intermediates. The involvement of carbanions in these reactions was demonstrated by deuterium incorporation experiments. Fluorescence behaviour of the diarylacetic acids showed considerable solvent and pH dependency, which is consistent with reaction via the carboxylate ion. Interestingly, the presence of a 9-phenyl group in **145** and **148** had no significant effect on the reactivity of these acids, and they decarboxylated with the same facility as the parent acids.

Additional support for the excited state stability of 4n systems came from the studies of **155**. The steady-state fluorescence studies of **155** demonstrated that photoexcitation of bent **155** results in the change of its conformation to give planar **155** in S_1. The driving force for the planarization of **155** in S_1 was shown to be the attainment of a 8π-electron internal cyclic array.

Product studies of **140** showed that it does not exhibit excited state C-H bond ionization even though it is isoelectronic to **125** and **136**. However, it was shown that photolysis of **140** in aqueous solution results in its dimerization, to give **141**. The mechanism of this process was investigated in detail by laser flash photolysis studies and was shown to involve one-electron ionization of **140** in S_1, to form radical cation **140**$^{\cdot+}$. The major pathway for the reaction of photogenerated **140**$^{\cdot+}$ was shown to be deprotonation of one of the benzylic protons, to generate radical **140**$^{\cdot}$, which subsequently dimerizes to give **141**.

The question of structure-reactivity in the excited state carbon acid behaviour of suberene (37) was also addressed. Results obtained in the photolysis of substituted suberene derivatives showed that the efficiency of C-H bond cleavage in S_1 was greatly affected by the nature of the substituent present in the molecule. The results of these studies were consistent with the involvement of carbanions in the C-H bond ionization in S_1. The methoxy groups in **180** retarded the C-H bond ionization in S_1, whereas the cyano substituted **189** was shown to react more efficiently than the parent suberene (**37**). These differences in reactivities of **180** and **189** compared to **37** were correlated to the differences in the relative stabilities of the photogenerated carbanion intermediates **204** and **209** vs **35** in S_1. It was also shown that the highly annelated molecules **193** and **197** exhibit reduced carbon acid behaviour in S_1, because of the lower stability (due to non-planarity) of the photogenerated carbanion intermediates.

In the study of 9-phenylxanthenium (**99**) and xanthenium (**114**) cations it was shown that S_1 of these cations acts as an excellent electron acceptor from di- and trimethoxybenzenes. The kinetics of electron transfer to excited **99** and **114** was followed by steady-state fluorescence quenching of **99** and **114** in aqueous H_2SO_4 solution by added di- and trimethoxybenzenes. It was also shown that the radical intermediates formed in these reactions undergo an irreversible reaction with dissolved oxygen to give isolable peroxides, viz., **217** and **218** respectively.

Lastly it was shown that thioxanthenols undergo efficient adiabatic photodehydroxylation in aqueous solution to give thioxanthenium carbocations

in the S_1 state. The adiabaticity of this process was demonstrated by the steady-state fluorescence studies. A lower limit of 5% adiabatic efficiency was observed for the more reactive derivatives, although it is believed that the carbocation is still generated predominantly via a diabatic step. The adiabatically generated thioxanthenium cations exhibited substantially higher emission yields than the corresponding xanthenium cations. This is believed to be due to the low reactivity of the excited thioxanthenium cations with water, as demonstrated by the lack of fluorescence quenching by water.

CHAPTER SIX

EXPERIMENTAL METHODS

6.1 Instrumentation

^{1}H NMR spectra were recorded on a Perkin-Elmer R32 (90 MHz), Bruker WM-250 (250 MHz). or Bruker AMX (360 MHz) instrument in, $CDCl_3$ unless otherwise noted. Tetramethylsilane was used as an internal standard in the recording of 90 MHz spectra. UV spectra were recorded on a Perkin-Elmer Lambda 4B or a Pye-Unicam 800 spectrophotometer. IR spectra were recorded on a Perkin-Elmer 283 instrument. Mass spectra were obtained on a Finnigan 3300 instrument. High resolution mass spectra (HRMS) were recorded on a Kratos Concept 1H instrument. Melting points were determined on a Koefler hot stage microscope and are uncorrected. Gas chromatography was performed on a Varian 3700 instrument with a Hewlett Packard 3390A integrator. Measurements of pHs were carried out on a Corning pH meter 140. Photolyses were carried out in Suprasil quartz cuvettes or 100/200/600 ml quartz tubes using a Rayonet RPR 100 photochemical reactor (254, 300, or 350 nm lamps). An Oriel 200 W Hg light source and an Applied Photophysics monochromator on an optical bench were employed in the quantum yield determinations. Fluorescence lifetimes were measured using time correlated single photon counting on a Photon Technology International (PTI) LS-1 instrument in lifetime mode.

6.2 Common Laboratory Reagents

Dichloromethane (Van Waters and Rogers Ltd.) was distilled before use. Other solvents (A.C.S. reagent grade) were used in reactions, for extraction or for column chromatography without further purification. Deuterated solvents used for NMR spectroscopy were $CDCl_3$ (Aldrich gold label) and acetone-d_6 (MSD Isotopes). The D_2O used for solvent isotope studies, preparatory photolysis and NMR spectroscopy was 99.9% D (MSD Isotopes). Standard buffer solutions (Fisher Scientific), were used for product quantum yield experiments and fluorescence spectrophotometry work. Solvents for fluorescence studies were of the highest available purity and checked for spurious emission before use.

6.3 Materials

The following compounds were purchased from Aldrich Chemical Co. for use in synthetic preparations: benzosuberone (**198**); *m*- methylanisole; 1,2-dimethoxy benzene (1,2-DMB); 1,3-dimethoxybenzene (1,3-DMB); 1,4-dimethoxy benzene (1,4-DMB); 1,3,5-trimethoxybenzene (1,3,5-TMB); benzonitrile; 9-xanthone (**144**); 9-phenylxanthen-9-ol (**98**); thioxanth-9-one (**224**); xanthene-9-ol (**216**); xanthene-9-carboxylic acid (**142**); *trans*-10,11-dibromodibenzosuberone (**182**); *N*-methylacridone; *N*-methylacridinium iodide (**172**); iminostilbine (**170**). The following compounds were used as secondary standards for fluorescence quantum yield experiments: quinine bisulfate (recrystallized); biphenylether (recrystallized); dibenzofuran; fluorene (**36**); and suberene (**37**; recrystallized).

6.3.1 9*D*-Xanthene (123)

To a stirred suspension of $LiAlD_4$ (0.047 g; 1.3 mmol) in diethyl ether (200 mL; dry) at -4 °C, $AlCl_3$ (0.35 g;2.6 mmol) was slowly added under an inert atmosphere. The mixture was stirred for 10 min at 0 °C and then 9-xanthone (144) (0.2 g; 0.7 mmol) was introduced into the cold reaction mixture. The reaction mixture was allowed to attain the room temperature and then refluxed for 12 hours. At the end of reflux, the reaction was cooled in an ice bath and carefully quenched with water (100 mL) followed by the addition of sufficient amount of 10% HCl solution to dissolve the suspension. The organic layer was separated and the aqueous layer was extracted with CH_2Cl_2 (2 x 100 mL). The combined organic layers were dried over anhydrous $MgSO_4$, and CH_2Cl_2 removed to yield 0.18g of the crude **123** as a white solid (yield > 95%), which was purified by recrystallization from 95% $EtOH/H_2O$; mp 102-104 °C; ^1H NMR (90 MHz, $CDCl_3$) δ 7.10-7.50 (m, 8H, arom.); mass spectrum (CI) (m/z) 185 (M^++1).

6.3.2 9*D*,9*H*-Xanthene (124)

Treatment of xanthen-9-ol (216) with $LiAlD_4/AlCl_3$ in dry THF afforded a white solid which was purified by recrystallization from $EtOH/H_2O$ to obtain pure **124**; mp 103 °C; ^1H NMR (250 MHz, $CDCl_3$) δ 4.05 (t, 1H, J ≈ 1.6 Hz, Ar_2CHD), 7.0-7.4 (m, 8H, arom.); mass spectrum (CI) (m/z) 184 (M^++1).

6.3.3 9*H*-Xanthene (125)

Treatment of 9-xanthone (**144**) (0.4 g; 0.14 mmol) with $LiAlH_4$ (0.094 g; 2.6 mmol)/$AlCl_3$ (0.70 g; 5.2 mmol) in dry THF (200 ml) at -4 °C in a manner described earlier afforded 9*H*-xanthene (**125**) as a white solid (yield > 95%), which was purified by recrystallization from $EtOH/H_2O$; mp 100-101 °C [lit.[168] mp 100.5 °C]; ^1H NMR (90 MHz, $CDCl_3$) δ 4.0 (s, 2H, $ArCH_2Ar$), 7.10-7.50 (m, 8H, arom.); mass spectrum (CI) (m/z) 183 (M^++1).

6.3.4 9-Phenyl-9*D*-xanthene (132)

A solution of commercially available 9-phenylxanthen-9-ol (**98**) in dry THF on treatment with $LiAlD_4/AlCl_3$, in a manner described earlier, afforded crude **132** as a white solid (yield > 95%), which was purified by recrystallization from 95% $EtOH/H_2O$; mp 144-145 °C; ^1H NMR (90 MHz, $CDCl_3$) 6.95-7.30 (m, 13H, arom.); mass spectrum (EI) (m/z) 259 (M^+).

6.3.5 9-Phenyl-9*H*-xanthene (133)

Treatment of 9-phenylxanthen-9-ol (**98**) with $LiAlH_4/AlCl_3$ in dry THF in usual manner afforded crude **147** which was purified by recrystallization from $EtOH/H_2O$ to obtain **147** as a white crystalline solid (yield > 95%); mp 144 °C [lit.[169] mp 145 °C]; ^1H NMR (90 MHz, $CDCl_3$) δ 5.25 (s, 1H, Ar_3CH), 6.95-7.30 (m, 13H, arom.); mass spectrum (EI) (m/z) 258 (M^++1).

6.3.6 9*D*-Thioxanthene (134)

Treatment of 9-thioxanthone (**224**) with $LiAlD_4/AlCl_3$ in dry THF afforded **134** as a white solid (yield > 93%), which was purified by recrystallization from $EtOH/H_2O$; mp 147-148 °C; ^1H NMR (90 MHz, $CDCl_3$) δ 7.10-7.50 (m, 8H, arom.); mass spectrum (CI) (m/z) 201 (M^++1).

6.3.7 9*D*,9*H*-Thioxanthene (135)

Treatment of thioxanthen-9-ol (**226**) with $LiAlH_4/AlCl_3$ in dry THF afforded **135** which was further purified by recrystallization from $EtOH/H_2O$; mp 146 °C; ^1H NMR (250 MHz, $CDCl_3$) δ 3.82 (t, 1H, J ≈ 2 Hz, Ar_2CHD), 7.1-7.5 (m, 8H, arom.); mass spectrum (CI) (m/z) 200 (M^++1).

6.3.8 9*H*-Thioxanthene (136)

Treatment of 9-thioxanthone (**224**) with $LiAlH_4/AlCl_3$ in dry THF in the procedure described earlier afforded a white solid (yield > 90%), which was purified by recrystallization from $EtOH/H_2O$; mp 127-128 °C [lit.[170] mp 128 °C]; ^1H NMR (90 MHz, $CDCl_3$) δ 3.85 (s, 2H, $ArCH_2Ar$), 7.10-7.50 (m, 8H, arom.); mass spectrum (CI) (m/z) 199 (M^++1).

6.3.9 9-Phenylthioxanthene-9-ol (219)

To the stirred solution of 9-thioxanthone (**224**) (1.0 g, 4.72 mmol) in dry THF (125 mL) at 0 °C, 2.0 **M** solution of PhLi (2.5 **M**, 5.0 mmol; Aldrich) was

introduced slowly with the aid of a syringe. The reaction mixture was stirred at room temperature for 12 hours and then carefully quenched with water. The organic layer was separated out and the aqueous layer was extracted with CH_2Cl_2 (3 x 75 mL). The combined organic layers were washed with water (3 x 75 mL), dried over $MgSO_4$ and CH_2Cl_2 removed to afford a pale yellow solid which was recrystallized from warm hexane/ether mixture to give **219** as a white crystalline solid; mp 107 °C [lit.[179] mp 109 °C]; ^1H NMR (90 MHz, $CDCl_3$) δ 2.30 (s, 1H, -OH), 6.90-7.50 (m, 11H, arom.), 7.90-8.10 (m, 2H, peri arom. Hs); mass spectrum (CI) (m/z) 291 (M^++1).

6.3.10 9-Phenyl-9D-thioxanthene (138)

Treatment of 9-phenylthioxanthen-9-ol (**219**) (2.0 g, 6.9 mmol) with $LiAlD_4/AlCl_3$ in dry THF (175 mL) in a manner described earlier afforded a white solid (1.8 g; yield > 93%), which was purified by recrystallization from $EtOH/H_2O$ to obtain **138** as a white crystalline solid; mp 100-101 °C; ^1H NMR (90 MHz, $CDCl_3$) 7.90-7.55 (m, 13H, arom.); mass spectrum (CI) (m/z) 276 (M^++1).

6.3.11 9-Phenyl-9*H*-thioxanthene (139)

Treatment of 9-phenylthioxanthen-9-ol (**98**) (2.0 g, 6.9 mmol) in usual manner with $LiAlH_4/AlCl_3$ in dry THF yielded **150** as a white solid (1.8 g; yield > 93%), which was purified by recrystallization from $EtOH/H_2O$; mp 99-100 °C [lit.[171] mp 99 °C]; ^1H NMR (90 MHz, $CDCl_3$) δ 5.25 (s, 1H, Ar_3CH), 6.90-7.55 (m,

13H, arom.); mass spectrum (CI) (m/z) 275 (M^++1).

6.3.12 9-Phenylxanthen-9-carboxylic Acid (145)

To a stirred solution of 9-phenyl-9*H*-xanthene (147) (2.0 g, 7.76 mmol) in dry THF at -100 °C (diethyl ether/dry ice), a solution of *n*-BuLi (2 M, 8 mL, 16 mmol) was slowly added under an inert atmosphere. The colour of the reaction mixture turned to dark brown immediately after the addition of *n*-BuLi. The reaction mixture was allowed to warm up to the room temperature (*ca.* 22-25 °C) and refluxed for an additional 4 hours. The reaction mixture was cooled down to -100 °C and a stream of dry CO_2 gas was bubbled into it for approximately 1 hour. The reaction was warmed up to the room temperature and refluxed with continuous bubbling of CO_2 gas for another 5 hours. The reaction was cooled down in an ice bath and carefully quenched by adding a 15% HCl solution (200 mL). The organic layer was separated and the aqueous layer was extracted with CH_2Cl_2 (3 x 100 mL). The organic layers were combined and extracted with a 1 M NaOH solution (5 x 50 mL). Careful neutralization of the combined base extract with conc. HCl solution (≈ 10 M) afforded a white precipitate. The precipitate was filtered out and recrystallized from 95% EtOH to yield **145** as a white crystalline solid (1.2 g; yield 55%); mp 168-169 °C; ^{1}H NMR (90 MHz, acetone-d_6) δ 5.35 (s, 1H, -CO_2H), 7.0-7.40 (m, 13H, arom.); IR (KBr, cm^{-1}) ν 3450 (broad, O-H str.), 1690 (strong, C=O str.), 1266 (strong, C-O str.); mass spectrum (CI) (m/z) 303 (M^++1); HRMS (EI) 302.3321 (calc. 302.3323).

6.3.13 9*H*-Thioxanthen-9-carboxylic Acid (147)

Treatment of 9*H*-thioxanthene (**136**) (2.0 g; 10 mmol) in dry THF (175 mL) with *n*-BuLi (2 M, 7 mL, 14 mmol) and CO_2, in a manner described earlier, yielded crude **148** as a white solid (1.64 g; yield > 65%). The crude material was purified by recrystallization from 95% EtOH to afford **147** as a white crystalline material; mp 224-226 °C [lit.[180] mp 227 °C]; ^{1}H NMR (90 MHz, acetone-d_6) δ 5.10 (s, 1H, Ar_2CH), 5.20 (s, 1H, -CO_2H), 7.20-7.60 (m, 8H, arom.); IR (KBr, cm^{-1}) ν 3400-3200 (broad, O-H str.), 1698 (strong, C=O str.), 1254 (strong, C-O str.); mass spectrum (CI) (m/z) 243 (M^++1).

6.3.14 9-Phenylthioxanthen-9-carboxylic Acid (148)

Treatment of 9-phenyl-9*H*-thioxanthene (**139**) (3.0 g, 10.1 mmol) in dry THF (200 mL) with *n*-BuLi (2 M, 7 mL, 14 mmol) and CO_2(g), in a manner described earlier, afforded crude **149** as a light pink solid (1.75 g, yield > 50%), which on recrystallization from 95% EtOH yielded pure **149** as a white crystalline solid; mp 162 ± 1 °C; ^{1}H NMR (90 MHz, acetone-d_6) δ 4.85 (s, 1H, -CO_2H), 6.95-7.50 (m, 13H, arom.); IR (KBr, cm^{-1}) ν 3400-3200 (broad, O-H str.), 1700 (strong, C=O str.), 1260 (strong, C-O str.); mass spectrum (CI) (m/z) 319 (M^++1); HRMS 318.3967 (calc. 318.3969).

6.3.15 Xanthene-9-methanol (154)

To a stirred solution of xanthene-9-carboxylic acid (**142**; Aldrich) (5.0 g,

22.12 mmol) in dry THF (250 mL) at 0 °C, $LiAlH_4$ (0.84 g, 22.0 mmol) was slowly added under an inert atmosphere. The reaction was warmed up to the room temperature and refluxed for 12 hours. At the end of reflux, the reaction was quenched with cold saturated NH_4Cl solution and the organic layer was separated out. The aqueous layer was extracted with CH_2Cl_2 (3 x 75 mL) and the combined organic layers were washed with water, dried over $MgSO_4$ and solvent removed on a rotary evaporator to afford a yellow coloured oil, which on trituration with cold hexanes gave a white solid. The crude product was recrystallized from hexanes to yield **154** as a white crystalline material (3.5 g; yield ≈ 75%); ^1H NMR (90 MHz, $CDCl_3$) δ 1.52 (s, 1H, -OH), 3.6 (d, 2H, J = 2.7 Hz, $-CH_2-$), 4.0 (t, 1H, J = 2.7 Hz, Ar_2CH-), 6.95-7.40 (m, 8H, arom.).

6.3.16 Dibenz[*b,f*]oxepin (155)[130]

To a stirred solution of **154** (4.0 g, 19.0 mmol) in benzene (200 mL), P_2O_5 (30 g, 22.0 mmol) was slowly added and the reaction mixture was boiled under reflux for 15 minutes. The reaction mixture was cooled and filtered through a sintered funnel and the residual solid washed with benzene (2 x 20 mL). The combined benzene extracts were washed with saturated brine solution, dried over $MgSO_4$ and benzene removed to afford a white solid (3.0 g; yield ≈ 85%), which upon recrystallization from 95% EtOH gave **155** as a white crystalline solid; mp 107-108 °C [lit.[130] mp 107 °C]; ^1H NMR (90 MHz, $CDCl_3$) δ 6.65 (s, 2H, -CH=CH-), 7.0-7.32 (m, 8H, arom.); mass spectrum (EI) (m/z) 194 (M^+).

6.3.17 10,11-Dihydrodibenzo[*b,f*]oxepin (156)[130]

A mixture of **155** (2.0 g, 10.21 mmol) and 5% palladium-on-charcoal (0.30 g) in 100 mL ethyl acetate was hydrogenated at 25 psi H_2 pressure. When the hydrogen uptake was complete, the solution was filtered and solvent removed to afford a colorless oil (1.8 g; yield ≈ 89%). Distillation under reduce pressure gave **156** as colourless viscous oil (**Caution:** *this material is extremely light sensitive; store in a cool dark place*); ^{1}H NMR (90 MHZ, $CDCl_3$) δ 3.1 (s, 4H, -CH_2CH_2-), 7.0-7.3 (m, 8H, arom.) [lit.[130] ^{1}H NMR δ 3.1 (s, 4H, -CH_2CH_2-), 7.0-7.3 (m, 8H, arom.); mass spectrum (EI) (m/z) 196 (M^+).

6.3.18 10-Hydroxy-10,11-dihydrodibenz[*b,f*]oxepin (157)

To a cold stirred solution of **155** (1.5 g, 7.73 mmol) in THF (dry; 100 mL) at ~ -4 °C (dry ice/acetone), a solution of BH_3-THF (2.5 M) was slowly added (ca. 30 min) under an inert atmosphere. The reaction was allowed to stir for an additional 15 minutes at -4 °C and then warmed to room temperature and refluxed for 4 hours. At the end of reflux the reaction mixture was cooled to -4 °C and 100 mL of water was added dropwise into it (**CAUTION:** *some foaming occurs at this stage which could be avoided by changing the rate of addition of water*). The reaction was stirred for 15 minutes and then 40 mL of 30% H_2O_2 followed by 40 mL of 3 M NaOH solution was introduced into the reaction mixture.[131] The reaction was stirred for another 3 hours at 30-40 °C and then quenched by pouring it over crushed ice (500 g). The organic layer was separated out and the

aqueous layer was extracted with CH_2Cl_2 (3 x 50 mL). The combined organic layers were washed with water, dried over $MgSO_4$ and CH_2Cl_2 removed to afford a pale yellow oil (yield ≥ 90%), which on distillation under reduced pressure yielded **157** as a colourless viscous oil; ^1H NMR (90 MHz, $CDCl_3$) δ 2.0-2.2 (s, 1H, OH), 3.3 (q, J = 6Hz; 2H, $-CH_2-$), 5.03 (dd, J ≈ 2 Hz, 1H, -CH-), 6.9-7.5 (m, 8H, arom.); mass spectrum (CI) (m/z) 213 (M^++1).

6.3.19 10-Hydroxysuberane (10-Hydroxydibenz[*a,d*]cycloheptene) (158)

Treatment of a solution of suberene (**37**) in dry THF with a solution of BH_3-THF, followed by addition of 30% H_2O_2 and 3 M NaOH solutions, in a manner described earlier, yielded a colorless oil (yield ≈ 90%), which on purification by column chromatography (neutral alumina, CH_2Cl_2) gave **158** as a colourless viscous oil; ^1H NMR (90 MHz, $CDCl_3$) δ 3.65 (m, 2H, $-CH_2-$), 2.65 (s, 1H, -OH), 4.05 (q, J = 10 Hz; 2H, Ar_2CH_2), 5.0-5.2 (m, 1H, -CH-), 7.1-7.6 (m, 8H, arom.); mass spectrum (CI) (m/z) 211 (M^++1).

6.3.20 Thioxanthene-9-methanol (159)

To a stirred solution of 9*H*-thioxanthene-9-carboxylic acid (**148**) (1.0 g 4.2 mmol) in 150 mL dry THF at 0 °C, a cold solution of BH_3-THF was slowly added under an inert atmosphere. The reaction mixture was refluxed for 18 hours and then quenched with water. The organic layer was separated out and the aqueous layer was extracted with CH_2Cl_2 (2 x 75 mL). The combined organic layers were

washed with water, dried over $MgSO_4$, and removed to afford a white solid (yield ~ 80%), which on recrystallization from hexanes gave **159** as a white crystalline solid; ^1H NMR (90 MHz, $CDCl_3$) δ 1.75 (s, 1H, -OH), 3.7 (d, 2H, J = 2.7 Hz, $-CH_2-$), 4.2 (t, 1H, J= 2.7 Hz, Ar_2CH-), 7.1-7.5 (m, 8H, arom.); mass spectrum (CI) (m/z) 229 (M^++1).

6.3.21 Dibenz[*b,f*]thiepin (160)

Treatment of **159** in benzene with P_2O_5, in a manner described earlier, yielded a white solid (yield 90%), which upon recrystallization from hexanes afforded **160** as a white crystalline material; mp 76 °C [lit.[172] mp 73-75 °C); ^1H NMR (90 MHz, $CDCl_3$) δ 7.0 (s, 2H, -CH=CH-), 7.2-7.6 (m, 8H, arom.); mass spectrum (EI) (m/z) 210 (M^+).

6.3.22 Dibenzocycloöctatetraene (163)[132]

A mechanically stirred mixture of *ortho*-xylylene bis(triphenylphosphonium bromide) (**162**) (18.1 g, 23 mmol) and *ortho*-phthaldehyde (**161**) (3.0 g, 22 mmol) in 400 mL of dry DMF was heated to 90 °C under an atmosphere of N_2. A solution of lithium ethoxide (59 mmol) in 100 mL absolute ethanol was added to the reaction mixture with rapid stirring over a period of 30 hours. Addition of the base gave a deep orange solution which persisted for 20 hours. After the addition of base was complete, the reaction mixture was diluted with 500 mL water. A precipitate came out of the solution which was separated by decantation. The precipitated material was extracted with diethyl ether (5 x

50 mL) and the ethereal extracts were washed with water, dried over $MgSO_4$ and removed to obtain a dark brown oil. The oil was extracted with boiling petroleum ether to effect separation of triphenylphosphine oxide. Evaporation of petroleum ether gave ~5.0 g of an orange coloured oil which was chromatographed on a silica gel column (2.5 cm diameter, 20 cm long, first 10 fractions 25 mL each). Elution with petroleum ether gave 1.0 g of a pale yellow oil which was again chromatographed on silica gel column (1.0 cm diameter, 40 cm long) using petroleum ether. The first six fractions were collected and the solvent was removed to afford **163** as a white solid (yield ≈ 1%); mp 107-108 °C [lit.[132] 106.8-108.1 °C]; ^{1}H NMR (250 MHz, $CDCl_3$) δ 6.74 (s, 4H, -CH=CH-), 7.03 (m, 4H, arom), 7.12 (m, 4H, arom.) [lit.[173] δ 6.74 (s, 4H, -CH=CH-), 7.03 (m, 4H, arom.), 7.12 (m, 4H, arom.)]; mass spectrum (CI) (m/z) 205 (M^++1).

6.3.23 N-methylacridan (140)[140]

To a stirred solution of *N*-methylacridinium iodide (4 g, 12.5 mmol) in 150 mL 2-propanol, $NaBH_4$ (0.5 g, 15.0 mmol) was added at room temperature. The reaction was refluxed for 6 hours and worked up by pouring into a dilute $NaHCO_3$ solution (200 mL) to obtain a white precipitate (yield ≥ 90%), which was recrystallized from 95% EtOH to afford **140** as white crystalline solid; mp 93-94 °C [lit.[140] mp 94 °C); ^{1}H NMR (90 MHz, $CDCl_3$) δ 3.3 (s, 3H, N-CH_3), 3.85 (s, 2H, Ar_2CH_2), 6.75-7.3 (m, 8H, arom.); mass spectrum (CI) (m/z) 196 (M^++1).

6.3.24 *m*-Bromomethyl-*p*-bromoanisole (176)[174]

A mixture of *m*-methylanisole (15 g, 122.95 mmol) and *N*-bromosuccinimide (13.3 g, 75.59 mmol) in 50 mL CCl_4 was stirred under reflux for 24 hours. The mixture was cooled, filtered and CCl_4 was removed to yield crude *p*-bromo-*m*-methylanisole[174] as a red coloured oil which was taken to the next step without further purification (yield 23 g, 93%).

Treatment of *p*-bromo-*m*-methylanisole (20 g, 99.50 mmol), with *N*-bromosuccinimide (20.2 g, 114.77 mmol) and benzoyl peroxide (0.20 g) in refluxing CCl_4 (ca. 20 hours), yielded crude **176** as a reddish brown solid. Recrystallization of crude material from boiling petroleum ether (30-60°) yielded pure **176** as yellow needle shaped crystals (yield 15 g, 54%); mp 91 °C [lit.[174] mp 91-92 °C); ^{1}H NMR (90 MHz, $CDCl_3$) δ 7.5 - 6.6 (m, 3 H, arom.); 4.52 (s, 2 H, Ar-CH_2-); 3.74 (s, 3 H, -OCH_3)

6.3.25 2,8-Dimethoxydibenzosuberone (178)[149]

m-Bromomethyl-*p*-bromoanisole (14 g, 50 mmol) was dissolved in dry THF (325.0 mL) and hexane (100 mL, dry) in a 1 L two necked flask and was cooled to -100° (CO_2-Et_2O slurry). *n*-BuLi (50 mmol) was added at such a rate that the temperature of the reaction mixture did not rise above -99°. After 1 hour at -100°, a stream of CO_2 gas was bubbled through the reaction mixture for 1.5 hours at -100° to -80°. After this, the cooling bath was removed and the temperature was allowed to rise to 25° (approx. 2 h). A stream of argon was bubbled through the

reaction mixture for ~1.5 hours to get rid of the excess of CO_2. The reaction mixture was again cooled to -100° and *n*-BuLi (30 mmol, 30% excess) added into it at such a rate that the temperature never exceeded -98°. The reaction mixture was stirred for 30 min at -100°, then allowed to warm to 25°, and stirred for 6 hours at 25°. The reaction was quenched by pouring into 5% HCl solution and the organic layer was separated and the aqueous layer was extracted with CH_2Cl_2 (3 x 150 mL). The combined organic layers were washed with 5% NaOH (w/w) solution and dried over anhydrous $MgSO_4$. Removal of CH_2Cl_2 yielded 2.0g of the crude product which upon recrystallization from CH_2Cl_2/MeOH (1:1) afforded slightly yellow needle like crystals of **178** (yield 1.3g); mp 121 °C (lit.[149] mp 119-121 °C); ^{1}H NMR ($CDCl_3$) δ 3.12 (s, 4H, -CH_2.CH_2-); 3.85 (s, 6H, -OCH_3); 6.60- 8.20 (m, 6H, arom.).

6.3.26 2,8-Dimethoxydibenzosuberenone (179)

A mixture of 2,8-dimethoxydibenzosuberone (**178**) (1.3 g, 4.80 mmol), *N*-bromosuccinimide (0.87 g, 5.0 mmol) and benzoyl peroxide (0.1 g) in CCl_4 (50 mL) were stirred with reflux for 36 hours. The reaction mixture was cooled to room temperature and filtered through a sintered funnel and filtrate washed with water (2 x 100 mL). The combined organic layers were dried over anhydrous $MgSO_4$ and CCl_4 removed to afford 1 g of the crude product. This crude product was analyzed to be a mixture of 10,11-dibromo-2,8-dimethoxydibezosuberone and 10,10'-dibromo-2,8-dimethoxydibenzosuberenone by ^{1}H 90 MHz NMR. The

mixture was separated by competitive recrystallization from 95% EtOH/ H_2O (1:1). The dibromo compound crystallized out first as long yellow crystals and were filtered out. On further cooling of the filtrate white crystals of 10,10'-dibromo-2,8-dimethoxydibenzosuberone came out of the solution.

The dibromo compounds (0.4 g) were dissolved in 15 mL of 2,4,6-trimethylpyridine (collidine) and refluxed for 24 hours. The reaction mixture was cooled in an ice bath and quenched with an excess of 20% HCl and extracted with CH_2Cl_2 (2 x 100 mL). The combined CH_2Cl_2 layers were washed with water (2 x 50 mL), dried over anhydrous $MgSO_4$ and removed to yield 0.25g of **180**; mp 119-121 °C; ^1H NMR (90 MHz, $CDCl_3$) δ 3.75 (s, 6H, -OCH_3); 6.90 (s, 2H, -CH=CH-); 6.8-7.25 (m, 6H, arom.); IR (KBr, cm^{-1}) υ 1690 (strong, C=O stretch), 1645 (medium, vinylic C=C stretch), 1600 and 1460 (medium, arom. C=C stretch); mass spectrum (EI) (m/z) 266 (M^+).

6.3.27 2,8-Dimethoxydibenzosuberene (180)

To a stirred suspension of $LiAlH_4$ (0.047 g; 1.3 mmol) in diethyl ether (200 mL; dry) at -4 °C, $AlCl_3$ (0.35 g; 2.6 mmol) was slowly added under an inert atmosphere. The mixture was allowed to stir for additional 10 min at 0 °C and then **179** (0.2 g; 0.7 mmol) was introduced into it. The reaction mixture was allowed to attain the room temperature and refluxed for 4 hours. At the end of reflux the reaction was cooled in an ice bath and carefully quenched by addition of water (~ 75 mL), followed by the addition of a sufficient amount of 10% HCl

to dissolve the suspension. The organic layer was separated and the aqueous layer was extracted with CH_2Cl_2 (2 x 100 mL). The combined organic layers were washed with water, dried over anhydrous $MgSO_4$, and CH_2Cl_2 removed to yield 0.18g of the crude product. Recrystallization of crude material from 50% EtOH/ H_2O afforded 0.17g of pure **180** as white crystalline solid; mp 185-187 °C; ^{1}H NMR (90 MHz; $CDCl_3$) δ 3.75 (s, 6H, -OCH_3), 3.60 (s, 2H, Ar.CH_2.Ar), 6.90 (s, 2H, -CH=CH-); 6.8-7.25 (m, 6H, arom.); mass spectrum (EI) (m/z) 252 (M^+); HRMS 252.3153 (calc. 252.3154).

6.3.28 5-Deuterio-2,8-Dimethoxydibenzosuberone (181)

Treatment of **179** with $LiAlD_4/AlCl_3$ in dry THF afforded **181**, which was purified by recrystallization from EtOH/H_2O to give pure **181** as a white crystalline solid (yield > 93%); mp 188-189 °C; ^{1}H NMR (90 MHz; $CDCl_3$) δ 3.75 (s, 6H, -OCH_3), 6.90 (s, 2H, -CH=CH-), 6.80-7.25 (m, 6H, arom.); mass spectrum (EI) (m/z) 254 (M^+);

6.3.29 10-Bromodibenzo[*a,e*]cyclohepten-5-one (183)

trans-10,11-dibromodibenz[*a,e*]cyclohepten-5-one (**182**) (5 g, 13.6 mmol; Aldrich) was dissolved in a 3 M methanolic solution of KOH (22.25 g KOH in 125.0 ml CH_3OH) and refluxed with stirring for one hour (**Caution:** *only one hour! longer reflux results in much lower yields*) to give a yellow coloured solution. The hot reaction mixture was filtered through a sintered funnel (to remove the

precipitated KBr) and the filtrate cooled in an ice bath for 2 hours to afford crude **183**. The crude product was recrystallized from warm hexanes to yield 10-bromodibenz[*a,e*]cyclohepten-5-one (**183**) as pale yellow crystalline solid (yield 80%); mp 116-117 °C [lit.[152] 117 °C]; ^{1}H NMR (90 MHz, $CDCl_3$) δ 7.8 (s, ArCH=CBr-), 7.0-7.7 (m, 8H, arom.); mass spectrum (CI) (m/z) 286 (M^++1).

6.3.30 10-Methoxydibenz[*a,e*]cyclohepten-5-one (184)

A mixture of 10-bromodibenz[*a,e*]cyclohepten-5-one (**183**) in a methanolic solution of KOH (3 M, 250 mL) was refluxed with stirring for 16 hours. At the end of reflux the reaction mixture was allowed to stand at 0 °C for 24 hours to afford yellow crystals of **184**; mp 132 °C; ^{1}H NMR (90 MHz, $CDCl_3$) δ 3.9 (s, 3H, -OCH_3), 6.4 (s, 1H, -CH=C-), 7.4-8.2 (m, 8H, arom.); mass spectrum (CI) (m/z) 237 (M^++1).

6.3.31 10-Methoxysuberene (10-Methoxy-5H-dibenz[*a,e*]cycloheptene) (185)

Reduction of **184** with $LiAlH_4/AlCl_3$ in dry THF, in a manner described earlier, yielded **185** which was purified by recrystallization from hexanes to afford pure **185** as a white crystalline solid; mp 146 °C; ^{1}H NMR (90 MHz, $CDCl_3$) δ 3.9 (s, 3H, -OCH_3), 3.7 (s, 2H, $ArCH_2Ar$), 6.3 (s, 1H, -CH=C-), 7.2-7.8 (m, 8H, arom.); mass spectrum (CI) (m/z) 223 (M^++1).

6.3.32 10-Methoxy-5*D*-suberene (10-Methoxy-5*D*-dibenz[*a,e*]cycloheptene) (186)

Reduction of **184** with $LiAlD_4/AlCl_3$ in dry THF, in a usual manner, yielded crude **186** which was purified by recrystallization from hexanes to afford pure **186** as a white crystalline solid; mp 147 °C; ^1H NMR (90 MHz, $CDCl_3$) δ 3.9 (s, 3H, $-OCH_3$), 6.3 (s, 1H, -CH=CR-), 7.2-7.8 (m, 8H, arom.); mass spectrum (CI) (m/z) 225 (M^++1).

6.3.33 10-Bromo-5*H*-suberene (10-Bromo-5*H*-dibenz[*a,e*]cycloheptene) (187)

Reduction of 10-bromosuberone (**183**) with $LiAlH_4/AlCl_3$ in dry THF afforded **187** which was purified by column chromatography (silica gel, hexanes) and recrystallized from 95% EtOH to afford **187** as white crystalline solid; mp 62 °C; ^1H NMR (90 MHz, $CDCl_3$) δ 3.70 (s, 2H, $ArCH_2Ar$), 7.10-7.35 (m, 7H, arom.), 7.65 (s, 1H, -CH=CBr-), 7.70-7.85 (m, 1H, ArH next to Br); mass spectrum (EI) (m/z) 271 (M^+); (CI) (m/z) 272 (M^++1).

6.3.34 10-Bromo-5*D*-suberene (10-Bromo-5*D*-dibenz[*a,e*]cycloheptene) (188)

Reduction of 10-bromodibenzosuberone (**183**) with $LiAlD_4/AlCl_3$ in dry THF afforded crude **188** which was purified by column chromatography (silica gel, hexanes) and recrystallized from 95% EtOH to give pure **188** as white solid; mp 55-58 °C; ^1H NMR (90 MHz, $CDCl_3$) δ 7.10-7.35 (m, 7H, arom.), 7.65 (s, 1H, -CH=CBr-), 7.70-7.80 (m, 1H, ArH closest to Br); mass spectrum (CI) (m/z) 274 (M^++1).

6.3.35 10-Cyano-5*H*-suberene (10-Cyano-5*H*-dibenz[*a*,*e*]cycloheptene) (189)

A stirred mixture of 10-bromosuberene (**187**) (0.2 mmol) and CuCN (0.4 g, 6 mmol) were dissolved in 1-methyl-2-pyrrolidinone (100 mL) and refluxed for 36 hours at 180 °C. The reaction mixture was cooled to 100 °C and poured into a 1:1 NH_3/H_2O solution (300 mL) and stirred at room temperature for 12 hours. The solution was then filtered through a celite pad, and the filtrate was extracted with CH_2Cl_2 (3 x 100 mL). The combined organic layers were dried over $MgSO_4$ and evaporated to yield a yellow oil. The oil was dissolved in 1:2 Et_2O/H_2O (500 mL) mixture and stirred overnight at room temperature. The ether layer was separated, dried and removed to yield the crude **189** which on purification by column chromatography (silica gel, CH_2Cl_2) afforded pure **189** as a white solid; mp 97-99 °C; ^{1}H NMR (90 MHz, $CDCl_3$) δ 3.80 (s, 2H, $ArCH_2Ar$), 7.10-7.75 (m, 8H, arom.), 7.80 (s, 1H, -CH=C-); IR (KBr, cm^{-1}) ν 2220 (medium, CN str.), 1606 (strong, vinyl C=C str.), 1480 (medium, arom. C=C str.); mass spectrum (CI) (m/z) 218 (M^++1); HRMS 217.2723 (calc. 217.2724).

6.3.36 10-Cyano-5*D*-suberene (10-Cyano-5*D*-dibenz[*a*,*e*]cycloheptene) (190)

Treatment of 10-bromo-5*D*-dibenzosuberene (**188**) with CuCN in 1-methyl-2-pyrrolidinone, afforded **190** as white solid which was purified by column chromatography (silica gel; CH_2Cl_2); mp 98-100 °C; ^{1}H NMR (90 MHz, $CDCl_3$) δ 7.10-7.75 (m, 8H, arom.), 7.80 (s, -CH=C-); mass spectrum (CI) (m/z) 220 (M^++1).

6.3.37 10,13-Epoxy-10,13-dihydro-tribenzo[*a,c,e*]cyclohepen-5-one (191)[152]

To a stirred mixture of 10-bromodibenz[*a,e*]cyclohepten-5-one (**183**) (3.8 g, 13.33 mmol) and potassium *t*-butoxide (3 g, 13.33 mmol) in THF (150 ml, dry) at 0 °C, freshly distilled furan (50 mL) was added under an inert atmosphere. The reaction mixture immediately turned to a brick-red colour. The reaction was allowed to stir at room temperature for additional 18 hours after which it was poured over an ice cold solution of 10% HCl. The organic layer was separated and the aqueous layer was extracted with CH_2Cl_2 (4 x 75 mL). The combined organic layers were washed with water, dried over $MgSO_4$ and the solvent was removed to yield a yellow coloured solid. The crude material was recrystallized from petroleum ether (40-60 °C) to yield **191** as yellow coloured prism like crystals (yield 2.86 g, 79%); mp 205-206 °C [lit.[152] mp 203-207 °C]; ^{1}H NMR (90 MHz, $CDCl_3$) δ 6.0 (s, 2H, -CH=CH-), 7.35 (s, 2H, -CH-O-CH-), 7.42-8.25 (m, 8H, arom.); mass spectrum (CI) (m/z) 273 (M^++1).

6.3.38 Tribenzosuberone (Tribenzo[*a,c,e*]cyclohepten-5-one) (192)

To a stirred solution of **191** (1.5 g, 5.86 mmol) in benzene (70 mL), $Fe_2(CO)_9$ (9.0 mmol) was added and the mixture was refluxed for 4 hours. The rection was cooled and filtered through a celite pad. The filtrate was washed with brine solution (2 x 50 mL), dried over $MgSO_4$ and benzene was evaporated to yield a pale yellow solid which on recrystallization from hexanes afforded **192** as yellow crystalline solid; mp 175-176 °C [lit.[152] mp 176.5-177.5 °C]; ^{1}H NMR (90 MHz,

$CDCL_3$) δ 7.32-7.80 (m, 12 H, arom.); mass spectrum (CI) (m/z) 257 (M^++1); (EI) (m/z) 228 (M^+).

6.3.39 Tribenzosuberene (5*H*-Tribenzo[*a,c,e*]cycloheptene) (193)

To a stirred suspension of $LiAlH_4$ (0.06 g; 1.5 mmol) in THF (dry; 150 mL) at -4 °C (CO_2/acetone), $AlCl_3$ (0.4 g, 3.0 mmol) was slowly added under an inert atmosphere. Tribenzosuberone (**192**) (1.0 g, 4.4 mmol) was introduced into the reaction mixture at -4 °C and the reaction was allowed to warm up to the room temperature and refluxed for 5 days. The reaction was carefully quenched with an ice cold 5% HCl solution and the aqueous layer was extracted with CH_2Cl_2 (4 x 50 mL). The combined organic layers were washed with water (2 x 100 mL), dried over $MgSO_4$ and solvent evaporated to yield a white solid. The crude solid was purified by column chromatography (silica gel, CH_2Cl_2) to afford pure **193** which on recrystallization from EtOH gave **193** as a white crystalline solid; mp 107-108 °C [lit.[176] mp 105-115 °C]; ^{1}H NMR (90 MHz, $CDCl_3$) δ 3.65 (s, 2 H, $ArCH_2Ar$), 7.1-7.8 (m, 12 H, arom.); mass spectrum (CI) (m/z) 243 (M^++1); (EI) (m/z) 242 (M^+).

6.3.40 5*D*-Tribenzosuberene (5*D*-Tribenzo[*a,c,e*]cycloheptene) (194)

Reduction of **192** with $LiAlD_4/AlCl_3$ in dry THF (7 days) afforded crude **194** which was purified by column chromatography (silica gel, CH_2Cl_2) to obtain pure **194** as a white solid; mp 108 °C; ^{1}H NMR (90 MHz, $CDCl_3$) δ 7.1-7.8 (m, 12

H, arom.); mass spectrum (CI) (m/z) 245 (M^++1); (EI) (m/z) 244 (M^+).

5.3.41 Furo-[3,4d]dibenzo[b,f]suberone (195)

To a well stirred solution of adduct **191** (0.5 g, 1.84 mmol) in $CHCl_3$ (70 mL), an equivalent amount of 3,6-di(pyridin-2'-yl)-s-tetrazine[155] was added at room temperature. The reaction was stirred for 12 hours (22-25 °C) and $CHCl_3$ removed to obtain a orange coloured crude product. The crude material was purified by column chromatography (silica gel, CH_2Cl_2) to get pure **195** as yellow crystalline solid; mp 153-155 °C; ^{1}H NMR (250 MHz, $CDCl_3$) δ 7.37-7.63 (m, 6H, arom.), 7.81 (m, 2H, peri arom. Hs), 7.89 (s, 2H, -CH-O-CH-); mass spectrum (CI) (m/z) 247 (M^++1); HRMS 246.2680 (calc. 246.2680).

6.3.42 8*H*-Furo[3,4*d*]dibenzo[*b,f*]suberene (196)

Reduction of ketone **195** with $LiAlH_4/AlCl_3$ in THF (dry) in usual manner afforded **196** which was purified by column chromatography (silica gel, CH_2Cl_2); mp 76-77 °C; ^{1}H NMR (250 MHz, $CDCl_3$) δ 3.86 (s, 2H, $ArCH_2Ar$), 7.2-7.44 (m, 8H, arom.), 7.76 (s, 2H, -CH-O-CH-); mass spectrum (CI) (m/z) 233 (M^++1); HRMS 232.2844 (calc. 232.2846).

6.3.43 8*D*-Furo[3,4*d*]dibenzo[*b,f*]suberene (197)

Treatment of ketone **195** with $LiAlD_4/AlCl_3$ in THF afforded **197** which was purified by column chromatography (**Caution:** *light sensitive!*); mp 75-77 °C; ^{1}H

NMR (250 MHz, $CDCl_3$) 7.2-7.44 (m, 8H, arom.), 7.76 (s, 2H, -CH-O-CH-); mass spectrum (CI) (m/z) 235 (M^++1).

6.3.44 5-Bromobenzosuberone (199)

A well stirred mixture of benzosuberone (198) (10 g, 60.0 mmol), N-bromosuccinimide (12.0 g, 66.0 mmol) and benzoylperoxide (0.025 g) in CCl_4 (200 mL) was refluxed for 8 hours. At the end of reflux the reaction mixture was cooled and filtered through a sintered funnel. The filtrate was washed successively with water (2 x 100 mL) and brine solution (1 x 100 mL) and CCl_4 was evaporated to yield 5-bromo-benzosuberone (199) as a yellow coloured oil, which was taken to the next step without any further purification.

6.3.45 2,3-Benzocyclohepta-2,4-dienone (200)[156]

5-Bromobenzosuberone (199) (12.8 g; 53.0 mmol) was dissolved in 2,4,6-collidine (30 mL) and stirred under reflux for 18 hours. The reaction was cooled and quenched by pouring into ice-cold 5% HCl solution (150 mL) and extracted with CH_2Cl_2 (3 x 75 mL). The combined CH_2Cl_2 layers were washed with 10% HCl (2 x 50 mL), dried over $MgSO_4$ and CH_2Cl_2 was evaporated to yield cr e 200 as a dark red coloured oil. The crude product was distilled under reduced pressure to yield pure 200 (yield > 50%); bp 85-87 °C, 5 mm Hg [lit.[156] bp 83-86 °C; 5 mm Hg].

6.3.46 3,4-Benzotropilidine (201)[156]

A mixture of **200** (4.33 g, 27.4 mmol), tosylhydrazide (5.9 g, 32.8 mmol) in methanol (100 mL) in the presence of a catalytic amount of conc. HCl (1.0 mL) was refluxed for 2 hours. The solvent was evaporated to yield a yellow oil which solidified on trituration with Et_2O. The solid was recrystallized from C_2H_5OH-H_2O to yield the corresponding hydrazone of **200** as yellow crystalline material; mp 155 °C [lit.[156] 155-156 °C].

To a stirred solution of the hydrazone (3.0 g) in THF (dry; 150 mL) at 0 °C, CH_3Li (1.2 M, 20 mL) was slowly added for over 30 minutes under an inert atmosphere. The reaction mixture was allowed to attain the room temperature, and stirred for an additional 1 hour. The reaction was quenched by water and the aqueous layer was extracted with CH_2Cl_2 (3 x 75 mL). The combined organic layers were washed with water (150 mL), dried over $MgSO_4$ and solvent was removed to yield a dark red oil. The crude oil was distilled under reduced pressure to afford 3,4-benzotropilidine (**201**) as a colourless oil; ^1H NMR (90 MHz, $CDCl_3$) δ 2.5 (t, J = 7 Hz, $-CH_2-$), 5.85 (dt, J = 10, 7 Hz, $ArCH=CHCH_2-$), 6.6 (d, J = 10 Hz, ArCH=), 7.1-7.5 (m, 4 H, arom.); mass spectrum (EI) (m/z) 142 (M^+).

6.3.47 1,2-Benzotrpilidene (202)[157]

3,4-Benzotropilidine (**201**) (0.28 g, 2.0 mmol) was dissolved in a mixture of *t*-BuOH-*t*-BuOK^+ and refluxed for 3 hours. The reaction was quenched with water and extracted with CH_2Cl_2 (3 x 50 mL). The combined organic layers were

washed with 10% HCl solution, dried over $MgSO_4$ and solvent evaporated to afford 1,2-benzotropilidene (**202**) as a colorless oil which was further purified by distillation under reduced pressure; ^{1}H NMR (90 MHz, $CDCl_3$) δ 3.05 (d, *J* = 7 Hz, $ArCH_2$-), 5.6-6.2(m, 2 H, ArCH=CHC<u>H</u>$_2$-), 6.5 (dd, J = 7, 10 Hz, ArCH=CH-), 7.1 (d, J = 10 Hz, ArCH=), 7.1-7.4 (m, 4 H, arom.); mass spectrum (EI) (m/z) 142 (M^+).

6.3.48 Bis(xanthen-9-yl)peroxide (217)

A solution of xathene-9-ol (**216**) (1.0 g) in diethyl ether (20 mL), was stirred for 4 hours with 30% hydrogen peroxide (20 mL). Addition of petroleum ether to the reaction mixture gave a precipitate which was recrystallized from a mixture of Et_2O/petroleum ether yielded xathene hydroperoxide as colorless crystalline solid (mp 122 °C [lit.[160a] mp 123-124 °C]); ^{1}H NMR (90 MHz) δ 6.0 (s, 1H, Ar_2CH), 7.1-7.7 (m, 8H, arom.).

A stirred solution of xanthene hydroperoxide (0.5 g), obtained above, in glacial acetic acid (10 mL) was warmed in a water bath to 50 °C for 1 hour. The reaction mixture was poured over crushed ice (50 g) to afford crude **217** as a white solid which was recrystallized from 95% EtOH; mp 152 °C [lit.[160b] mp 152-153 °C]; ^{1}H NMR (90 MHz) δ 5.71 (s, 2H, ArCH-O-O-CHAr), 7.0-7.7 (m, 16H, arom.).

6.3.49 Thioxanthen-9-ol (226)

A stirred mixture of thioxanthen-9-one (224) (5.0 g, 23.6 mmol) and $NaBH_4$ in 2-propanol (200 mL) was refluxed for 5 hours. The reaction was cooled down to room temperature and poured over 500 g of crushed ice and allowed to stand for 30 minutes. A white precipitate was obtained, which was recrystallized from warm hexane/ether to get pure 226; mp 91 °C; ^{1}H NMR (90 MHz, $CDCl_3$) δ 2.41 (d, J = 8 Hz, 1H, -OH), 5.48 (d, J = 8 Hz, 1H, Ar_2CH-), 7.2-7.7 (m, 8H, arom.); mass spectrum (CI) (m/z) 215 (M^++1).

6.3.50 2-Chlorothioxanthen-9-ol (227)

A mixture of 2-chlorothioxanthen-9-one (225) (1.0 g, 4.1 mmol) and $NaBH_4$ (5.0 mmol) in 2-propanol was refluxed for 5 hours and then cooled to room temperature. The cold reaction mixture was poured over 500 g of crushed ice to afford a white precipitate (yield ~ 78%), which was recrystallized from warm hexane/ether to give pure 227; mp 90-91 °C; ^{1}H NMR (90 MHz, $CDCl_3$) δ 2.41 (d, J = 8 Hz, 1H, -OH), 5.45 (d, J = 8 Hz, 1H, Ar_2CH-), 7.1-7.7 (m, 7H, arom.); mass spectrum (CI) (m/z) 249 (M^++1).

6.3.51 9-Methylthioxanthen-9-ol (228)

To a cold (0 °C) stirred solution of thioxanthen-9-one (244) (1 g, 4.7 mmol) in THF (dry, 100 mL), CH_3MgCl was slowly (*ca.* 5 min) introduced with the aid of a syringe. The reaction was allowed to warm to the room temperature and

refluxed for 6 hours. The reaction was cooled and quenched with cold water and aqueous layer extracted with CH_2Cl_2 (2 x 75 mL). The combined CH_2Cl_2 layers were washed with water, dried over $MgSO_4$, and CH_2Cl_2 removed to afford a pale yellow solid (yield ≈ 65%), which upon recrystallization from warm hexane/ether mixture gave **228** as a white crystalline solid; mp 88 °C; ^1H NMR (90 MHz, $CDCl_3$) δ 1.52 (s, 3H, $-CH_3$), 2.35 (s, 1H, -OH), 7.1-7.45 (m, 6H, arom.), 7.8-8.0 (m, 2H, peri Hs); mass spectrum (CI) (m/z) 227 (M^++1).

6.3.52 9-Benzylthioxanthen-9-ol (229)

To a stirred solution of thioxanthen-9-one (**224**) (3.0 g, 14 mmol) in THF (dry, 150 mL) benzyl magnesium chloride (15.5 mmol) was introduced, with the aid of a syringe, at room temperature. The reaction was refluxed for 12 hours then quenched by pouring into 200 mL of ice cold water. The organic layer was separated out and the aqueous layer extracted with CH_2Cl_2 (3 x 50 mL). The combined organic layers were washed with water, dried, and CH_2Cl_2 removed to afford a white solid (yield ~ 85%), which was recrystallized from hexanes; mp 113 °C; ^1H NMR (90 MHz, $CDCl_3$) δ 2.5 (s, 1H, -OH), 3.05 (s, 2H, $PhCH_2$-), 6.6-7.7 (m, 13H, arom.); mass spectrum (CI) (m/z) 305 (M^++1).

6.3.53 9-Benzylidienethioxanthene (234)

A solution of 9-benzylthioxanthen-9-ol (0.20 g, 0.66 mmol) dissolved in acetonitrile (50 mL) was treated with an equal volume of 20% (v/v) H_2SO_4 and

stirred at room temperature for 2 hours. The reaction was quenched by pouring into 100 mL water (pH ~ 12) and extracted with CH_2Cl_2 (3 X 50 mL). The organic layers were combined, washed with water, dried, and CH_2Cl_2 removed to afford a white solid (yield ≥ 90%), which was recrystallized from 95% EtOH-H_2O mixture; mp 109 °C; ^{1}H NMR (90 MHz, $CDCl_3$) δ 6.9 (s, 1H, Ph-CH=C-), 7.0-7.8 (m, 13H, arom.); mass spectrum (CI) (m/z) 287 (M^++1).

6.4 Excited State Carbon Acid Behaviour of 9*H*-Xanthene (125) and 9*H*-Thioxanthene (136)

6.4.1 Product Studies

6.4.1.1 Dark Reactions of Xanthenes 123, 125, 133 and thioxanthenes 134, 136 and 138 in Various Solvents

None of the xanthenes (**123** and **125**) and thioxanthenes (**134** and **136**) or their 9-phenyl analogues (**132** and **138**) exhibited any tendency to undergo deuterium/protium exchange thermally (22 ± 2 °C) with the solvent L_2O (L = H or D), under the reaction conditions where their photochemical behaviour was being investigated. Thermally, these compounds did not show any sign of deuterium and/or protium exchange even at higher basicities (*ca.* up to 6.0 M NaOH and 5.0 M ethanolamine). In preparative scale dark reactions, ~70 mg of substrate was dissolved in an appropriate solvent mixture, viz., 50% (v/v) 1-4 M NaOH-EtOH (175 mL) or in a 1-2 M solution of ethanolamine in CH_3CN, and left stirring in dark for 1-2 hours. The reaction mixture was then worked up in an appropriate manner and samples were analyzed by GC/MS and ^{1}H NMR.

6.4.1.2 Photolysis of 123/125 and 134/136 in Aqueous Solutions

In a typical preparative scale photolysis ~70 mg of the substrate was dissolved in 75 mL of CH_3CN and diluted by adding 75 mL of H_2O or D_2O to a total volume of 150 mL. The solution was then transferred into a quartz tube equipped with a cooling finger and deaerated with a continuous stream of argon. The solution was then irradiated at 300 nm in a Rayonet RPR 100 photochemical reactor for an appropriate period of time. After photolysis the reaction was worked up by adding a saturated solution of NaCl, and extracting with CH_2Cl_2 (3 x 30 mL). The combined organic layers were washed with water, dried over $MgSO_4$, and CH_2Cl_2 removed on a rotary evaporator. The photolysate was examined by ^1H NMR (250 MHz) and GC/MS analyses. The photoproducts were identified by comparisons with the ^1H NMR spectra of the authentic materials and conversions to photoproducts calculated by ^1H NMR integration and GC/MS.

Photolysis of **125** and **134** in 50% D_2O-CH_3CN (ca. 60 min) did not result in the formation of deuterium incorporated products as determined by the GC/MS (CI mode) analyses of the reaction mixtures. However, photolysis of **125** (λ_{ex} 300 nm; 60 min) in 50% H_2O-CH_3CN results in its isomerization to yield **126**, **127**, **128** and **129**. These products were identified by comparison with the ^1H NMR spectra of the authentic samples. The GC/MS analysis of the recovered **125** did not show any sign of deuterium incorporation. Photolysis of **135** under similar conditions also did not result in the formation of deuterium exchanged products. No isomerization of **135** takes place under these reaction conditions.

6.4.1.3 Photolysis of 123/125 and 134/136 in Aqueous Ethanol Solutions

Photolysis of **123** and **134** in 50% NaOH-EtOH solution resulted in deuterium incorporation at the benzylic position to yield monodeuterated **124** and **135** respectively. A similar photolysis of **125** and **136** in 50% NaOD-EtOD also resulted in the formation of **124** and **135**. The preparative scale photolysis were carried out by dissolving ~75 mg of substrate in 75 mL of 95% EtOL (L = H or D) and diluted by 75 mL of aqueous 1 M NaOL (L = H or D) solution. The solution was then irradiated at 300 nm in a quartz vessel for an appropriate period of time. After photolysis the reaction mixture was worked up by saturating with NaCl and neutralizing it by a careful addition of 10% HCl solution. The aqueous layer was then extracted with CH_2Cl_2 (3 x 75 mL), and the combined organic layers were washed with saturated brine solution (2 x 50 mL), followed by water and dried over $MgSO_4$. The photsolyate was analyzed by ^1H NMR (250 MHz) and photoproducts identified by comparison with the ^1H NMR spectra of the authentic samples prepared separately (*vide supra*). The conversions to exchange photoproducts were determined both by ^1H NMR integration and GC/MS (CI mode) analyses. For example, photolysis of **134** in 50% 1 M NaOH-EtOH for 30 min results in the formation of **135** (~18%) and **136** (~7%) as calculated by the integration of ^1H NMR (250 MHz) spectrum of the photolysate (Figure 2.3). No attempts were made to isolate these photoproducts.

6.4.1.4 Photolyses of 123 and 133 in Solutions of Ethanolamine in CH_3CN

Photolyses of **123** and **133** in the presence of ethanolamine in CH_3CN also resulted in the formation of exchange products. In general, 75-80 mg of the substrate was dissolved in 175 mL solution of ethanolamine in CH_3CN (0.5-2 M concentration) and irradiated in a quartz tube at 300 nm. The reaction mixture, after photolysis, was poured into a flask and cooled in an ice bath, and carefully quenched with 10-15% HCl solution. The aqueous layer was then extracted with CH_2Cl_2 (3 x 50 mL), and the combined CH_2Cl_2 layers were washed successively with 5% HCl solution and water, dried over $MgSO_4$, and removed to obtain the product mixture. Photolysis of both **123** and **134** in the presence of ethanolamine in CH_3CN resulted in the deuterium incorporation at the benzylic position. The photoproducts (**124** and **135**) were identified by comparison with the ^1H NMR spectra of authentic samples. The percentage exchanged product was calculated by ^1H NMR and GC/MS (CI mode) analyses.

6.4.2 Thermal Generation of 9-Xanthenide Carbanion (130)

The ground state 9-xanthenide carbanion (**130**) was generated in THF solution by deprotonating 9*H*-xanthene (**125**) with excess of *n*-BuLi under N_2. The reaction was slow and required heating to reflux for 10-30 min, which gave a deep orange black solution. That the carbanion was indeed generated was shown by quenching the solution with CO_2(g), which gave xanthene-9-carboxylic acid (**142**) in >75% yield. The absorption spectrum of **130** was obtained by transferring

a portion (200-500 μL) of the solution to a quartz cuvette containing 2.5 mL of dry THF in a glove bag. The absorption spectrum showed a strong band at λ_{max} ≈590 nm. This band disappears on exposure of the solution to moisture.

6.4.3 Quantum Yields Measurements

Quantum yields (Φ's) of monodeuterium incorporation in **123**, **125**, **133**, and **136** were measured in a variety of solvent mixtures on an optical bench using an Oriel 200W Hg lamp and an Applied physics monochromator set at λ_{ex} = 280 nm with slits of 7.0 nm. Samples were prepared by taking 50 μL of stock solution (~ 10^{-4} - 10^{-3} M) of substrate and diluting it to 3.00 mL with the appropriate solvent mixture in a suprasil quartz cuvette. The concentration of the each substrate in the cuvette solutions were such that they had an absorbance ≥ 2.0 at the excitation wavelength (λ_{ex} = 280 nm). The solutions were purged with a stream of argon for 5 min prior to and during the photolysis (usually 30-45 min). The irradiation time was so adjusted as to keep the conversions to photoproducts between 10-15% in all cases. After irradiation the photolysate was transferred to a test tube, saturated with NaCl, acidified to pH ≈ 7 by adding 5% HCl, and extracted with CH_2Cl_2 (4 x 5 mL). The organic fractions were combined and washed with H_2O (pH ~ 1; 2 x 10 mL), dried over $MgSO_4$, and evaporated to yield the photolysate. The photolysate was then analyzed by GC/MS (CI mode) to determine the percent deuterium/protium exchanged products formed. For example, photolysis of **134** (1.5 x 10^{-6} moles) in 50% 1 M NaOH-EtOH for 30 min upon work up gave

a mixture whose mass spectrum (CI mode) showed molecular ion peaks at M^+ = 201 (due to **134**), M^+ = 200 (due to **135**) and M^+ = 199 (due to **136**). The percentage **135** (16.8%) formed was calculated from the mass spectrum after correcting for the natural abundance of D and ^{13}C. Only trace amount of **136** (< 1%) was formed in this photolysis. The percentage conversion to **135** in conjunction with the knowledge of number of moles of starting material used and the intensity of light at 280 nm (*vide supra*) gave the quantum yield of exchange. Similar method was employed to measure the quantum yields of exchange for **123**,**125**, and **136** in other solvent mixtures.

Since all photolysis were carried out on 3.0 mL of solution, the light intensity in einstein/min was measured before each photolysis by employing potassium ferrioxalate ($K_3Fe(C_2O_4)_3$; PF) actinometry [118] When solutions of PF in dilute H_2SO_4 are irradiated, Fe^{3+} is efficiently reduced to Fe^{2+} with the simultaneous oxidation of oxalate ion. Quantum yields for this reaction range from 1.25 to 0.90 over the wavelength range 250-500 nm.[118] The relatively small dependence of these quantum yields on reactant and product concentration, intensity of the incident light, and temperature makes this a convenient actinometer. The Fe^{2+} is transparent to the incident radiation and is analyzed by forming the highly coloured $Fe(phen)^{2+}$ complex (where phen = 1,10-phenanthroline).

A solution of 0.0060 M PF in 0.05 M H_2SO_4 (250 mL) was prepared in the dark along with a 2% by weight solution of 1,10-phenanthroline in distilled water

(to be used later). All subsequent solution transfers were carried out under a red photographic light. To determine the light intensity at 280 nm, 3.0 mL (V_1) solution of PF was pipetted into two quartz cuvettes. One of these was then irradiated on the optical bench at 280 nm for the appropriate time (Δt was typically 5 min at this wavelength) under a stream of argon purging which served to stir and purge the solution. The other cell was handled under the safelight for the same duration and served as a blank. Both solutions were the worked up as follows: 1.0 mL (V_2) of reaction mixture was pipetted from the cuvette into a 10 mL (V_3) volumetric flask. To this was added 2.0 mL of a 2% (weight) solution of 1,10-phenanthroline in water and 0.5 mL of a buffer solution (prepared from 41.0 g $NaOAc.3H_2O$ and 5.0 mL H_2SO_4 in 1 L). The volume was adjusted to 10 mL with distilled water and the solutions were mixed and allowed to stand in dark for 30 min. The absorbance of the irradiated and blank solutions was then measured at 510 nm and the difference (ΔA) was used in eq 6.1 to calculate the number of Einsteins of incident light (where $\varepsilon = 1.11 \times 10^4\ M^{-1}\ cm^{-1}$ and $\Phi(Fe^{2+})$

$$\text{einstein/min} = \Delta A\ V_1\ V_3/\varepsilon\ \Phi(Fe^{2+})\ V_2\ \Delta t \qquad (6.1)$$

= 1.25 at 280 nm).[118] The absorbance of the blank (O.D at 510 nm < 0.05) was used to check the quality of the stock solution of PF with respect to photodecomposition. Using this procedure the average intensity of light at 280 nm (7 nm slit width) was measured to be 4.67×10^{-7} einstein/min.

6.4.4 Steady-state Fluorescence and Lifetime Measurements

Steady-state fluorescence spectra (uncorrected, including those used for measuring Φ_f) were taken in 3.0 mL Suprasil quartz cuvettes at $\approx 10^{-4}$ M using a Perkin Elmer MPF-66 spectrophotometer at ambient temperature. Solutions were purged for 5.0 min with a stream of argon prior to measurements. Lifetimes were measured using a Photon Technology International (PTI) LS-1 instrument with a H_2 lamp. All decays were first-order by analysis using software supplied by PTI. Figure 6.1 shows a representative lifetime decay of **125** in 100% CH_3CN. The

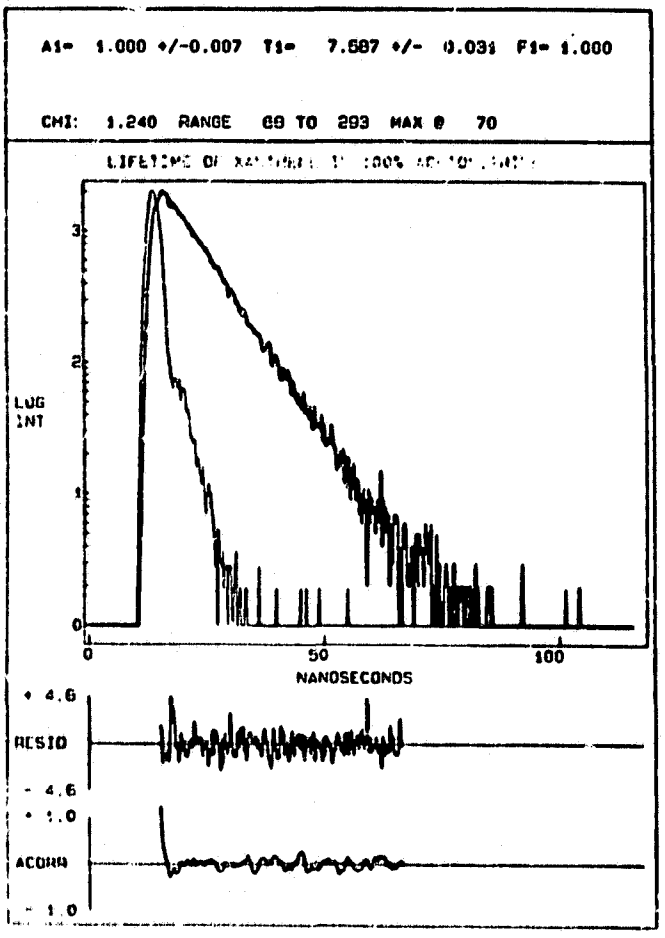

Figure 6.1 Representative fluorescence lifetime decay curve of **125** in 100% CH_3CN, τ = 7.59; χ^2 = 1.24.

lifetime (τ) was generated by mathematical deconvolution procedure that separates the lamp profile from the sample (125) decay function. The value of χ^2, was taken as a measure of agreement between the calculated line and experimental data. The weighted residuals and autocorrelation functions were also utilized in judging the quality of the calculated curve (in other words τ), and are shown in Figure 6.1.

Fluorescence quantum yields (Φ_f) were determined by comparing the integrated emission bands of the substrates with those of a secondary standards according to eq 6.2,[177]

$$\Phi_f^u = \Phi_f^s \, (I_f^u \, \eta_u^2 / I_f^s \, \eta_s^2) \qquad (6.2)$$

where I_f^u and I_f^s are the total fluorescence intensities of the unknown samples and a standard, η is the refractive index of the solvent, and Φ_f^s is the fluorescence quantum yield of the standard. In measuring the fluorescence quantum yields the solutions (O.D. < 0.1) of substrate and standard were absorption matched at the exciting wavelength. Standards were chosen to maximize their spectral overlap with the emission band of the samples. Dibenzofuran was the standard of choice for 9*H*-xanthene (125) whereas suberene (37) provided a better spectral overlap with the emission band for 9*H*-thioxanthene (136). All solutions were purged with argon for at least 5 min prior to measurements.

6.5 Photodecarboxylation of Xanthene and Thioxanthene Carboxylic Acids in Aqueous Solution

6.5.1 Product Studies

6.5.1.1 Dark Reactions

None of the xanthene- and thioxanthene-9-carboxylic acids studied in this work showed any tendency to decarboxylate thermally under the conditions employed to investigate their photochemistry. In preparative scale dark reactions a solution of ~100 mg of acid was dissolved in 30 mL CH_3CN and diluted with 70mL H_2O. The pH of the solution was adjusted to pH ≥ 8 by adding a stock solution of 1 M NaOH and using a pH meter. The reaction mixture was then stirred at room temperature (22 ± 3 °C) in dark for one hour. The reaction mixtures were quenched with dilute acid (~ 5% HCl solution) and extracted with CH_2Cl_2. After removal of solvent, analysis of the reaction mixtures by ^1H NMR (90 MHz) did not shown any sign of reaction (i.e., no new product was formed).

6.5.1.2 Preparative photolyses of 142, 145, 147 and 148 in CH_3CN-H_2O mixtures

In preparative scale studies, ~70 mg of the acid was dissolved in 30 mL CH_3CN and then diluted with 70 mL H_2O. The solutions were adjusted to pH ≥ 8 with the aid of a pH meter, by dropwise addition of a stock solution of ≈ 1 M NaOH. The solution was then transferred to a quartz vessel fitted with a cooling finger and deaerated with a continuous stream of argon. The solution was irradiated at 254 nm in a Rayonet RPR 100 photochemical reactor for an

appropriate period of time. After photolysis the solution was worked up by saturating with NaCl, acidifying to pH ≈ 1 with 10% HCl, and extracting with CH_2Cl_2 (3 x 75 mL). The photoproducts formed in each case were characterized by comparison with the ^1H NMR spectra of authentic samples, and conversions to products determined by the ^1H NMR integration (relative to the benzylic proton of the starting material). In the case of **145** (and **148**), the percentage conversion to product was determined by ^1H NMR using suberene (**37**) as an external standard. All acids investigated in this study photodecarboxylated cleanly giving rise to only one photoproduct (except **142** which gave two products, viz., **125** and the dimer **128**).

6.5.1.3 Preparative Photolyses of 142, 145, 147 and 148 in CH_3CN-D_2O mixtures

In preparative scale studies, ~55 mg of the acid was dissolved in 30 mL CH_3CN and diluted with 80 mL of D_2O. After adjusting the pD ≥ 8 with ≈ 1 M NaOD, the solutions were photolyzed at 254 nm and worked up in the usual manner. Conversions to monodeuterated products were determined by ^1H NMR (90 MHz) integrations (in the case of **142** and **147**) and mass spectral analyses (in the case of **145** and **148**). The monodeuterated products, viz., **124**, **132**, **135** and **138** were isolated by extracting the crude reaction mixtures with bicarbonate solution, and characterized by comparison of their ^1H NMR and mass spectra with the authentic samples.

6.5.1.4 Preparative photolysis of 142, 145, 147 and 148 in oxygen saturated solutions

Photolysis were carried out as before but under continuous stream of oxygen instead of argon. The conversions were determined by ^{1}H NMR analysis of the crude reaction mixtures. In all cases, except **142**, only the corresponding decarboxylated product was formed. The ketone **144** formed in the case of **142** was identified by comparison of its ^{1}H NMR and GC retention time with an authentic sample. The ratios of ketone **144** to **125** were determined by integration of appropriate ^{1}H NMR signals (**144**: δ 8.4 and **125**: δ 4.0).

6.5.2 Steady-State and Transient Fluorescence Behaviour

Fluorescence quantum yields were measured on a MPF-66 instrument employing appropriate secondary standard of known fluorescence quantum yield (eq 6.2).[177] Biphenyl ether[135] was employed as a secondary standard for xanthene carboxylic acids **142** and **145**. Solutions (≈10^{-5} M) of acids and the reference were matched for the absorbance (O.D. < 0.08) at λ_{ex} = 260 nm and deaerated with a fine stream of argon for 5 min prior to measurements. Because of the better spectral overlap suberene (**37**) was chosen as the fluorescence standard for acids **147** and **148**. Fluorescence lifetimes of **142** and **145** were measured in 80% H_2O-CH_3CN (pH 7) by time correlated single photon counting method on a PTI LS-1 instrument. Solutions of the substrate (O.D. < 0.2) were deaerated with argon before measurements. Lifetimes of **147** and **148** in 80% H_2O-CH_3CN could not be measured accurately because of their weak fluorescence.

6.5.3 Ground State pK_a Estimation of 142 145 and 147

The pK_a's of diarylacetic acids were estimated under an inert (N_2) atmosphere by titrating a 10^{-3} M solution of substrate dissolved in 80% H_2O-CH_3CN (deionized H_2O) with a standardized NaOH solution (1.0070 M). A standard glass electrode with Ag/AgCl reference was employed for the hydronium ion concentrations. End points were determined by a curve-fitting procedure, and the pK_a was taken as the pH at half-neutralization.

6.5.4 Product Quantum Yields

Quantum yields of formation of the corresponding decarboxylated products for **142**, **145**, **147** and **148** were measured in a variety of solvent mixtures on an optical bench (λ_{ex} = 280 nm). In general, 0.6 mL of a stock solution of substrate in CH_3CN (5×10^{-4} M) was transferred to a quartz cuvette and diluted with 2.4 mL of H_2O (of appropriate pH). The concentration of the each substrate in the cuvette solutions were such that they had an absorbance ≥ 2.0 at the excitation wavelength. The solutions were purged with a stream of argon for 5 min prior to and during the photolysis (usually 1-10 min). The irradiation time was so adjusted as to keep the conversions to products between 10-15% in all cases. After irradiation the photolysate was transferred to a test tube, saturated with NaCl, acidified to pH ≈ 1 by adding 5% HCl, and extracted with CH_2Cl_2 (4 x 5 mL). The organic fractions were then combined and washed with H_2O (pH ~ 1; 2 x 10 mL), dried over $MgSO_4$ and filtered. Each solution was then injected with

50 μL of a stock solution of an external standard of appropriate molarity (viz., suberene (**37**) in the case of **142** and **147** ; 9-phenyl-9*H*-thioxanthene (**139**) in the case of 9-phenylxanthene carboxylic acid (**145**); and 9-phenyl-9*H*-xanthene (**133**) in the case of 9-phenylthioxanthene carboxylic acid (**148**)) and evaporated to *ca.* 200 μL before being injected into a GC capillary column (programmed with initial temperature at 150 °C with temperature increment of 10 °C/min up to 250 °C) for analyses. The number of moles of product (**125**, **133**, **136** and **139**) formed were determined by comparing integrated peak areas of the product and the external standard and employing a correction factor to compensate for the GC detector response. Correction factor in each case were generated by injecting solution of the authentic sample of photoproduct and external standard in known molar ratios and checking the responses. In the case of **142** both **125** and **128** are formed however, the measured product quantum yields (Φ_p) of this substrate refer to the formation of **125** only. This was because of the long retention time of **128** on the GC column which prevented the determination of the percentage **128** formed. Light intensity at 280 nm was determined to be 1.0687×10^{-7} Einstein/min/3 mL according to the method of Hatchard and Parker[118] described earlier (*vide supra*).

6.6 Conformational Studies of Dibenz[b,f]oxepin (155) and Related Systems

6.6.1 Product Studies

6.6.1.1 Photolysis of Dihydrodebenz[b,f]oxepin (156) in CH_3CN

In a preparative scale photolysis, 100 mg of **156** was dissolved either in

100% CH_3CN or 50% CH_3CN-H_2O and the colourless solution was then transferred into a quartz tube fitted with a cooling finger and deaerated with continuous stream of argon and irradiated at 254 nm (Rayonet RPR 100 photochemical reactor) for 10 min. After irradiation the yellow reaction mixture was worked-up and photolysate analyzed by ^1H NMR (90 and 250 MHz) and TLC. The ^1H NMR spectrum of the reaction mixture showed a complicated set of multiplets between δ 2.0-3.0 and 6.0-7.0. The TLC (silica gel, CH_2Cl_2) of the reaction mixture showed the formation of one major product (R_f = 0.14). Preparative thin layer chromatography was employed to isolate this material as a yellow solid. The ^1H and ^{13}C NMR spectra of the purified material are shown in Figure 6.2. Crystals of the pale yellow solid were grown in CH_2Cl_2/hexanes. The results of preliminary X-ray crystallographic analysis indicated that this solid was adduct **166**. The ^{13}C NMR which showed the presence of 28 distinct carbons was consistent with the structure of **166**.

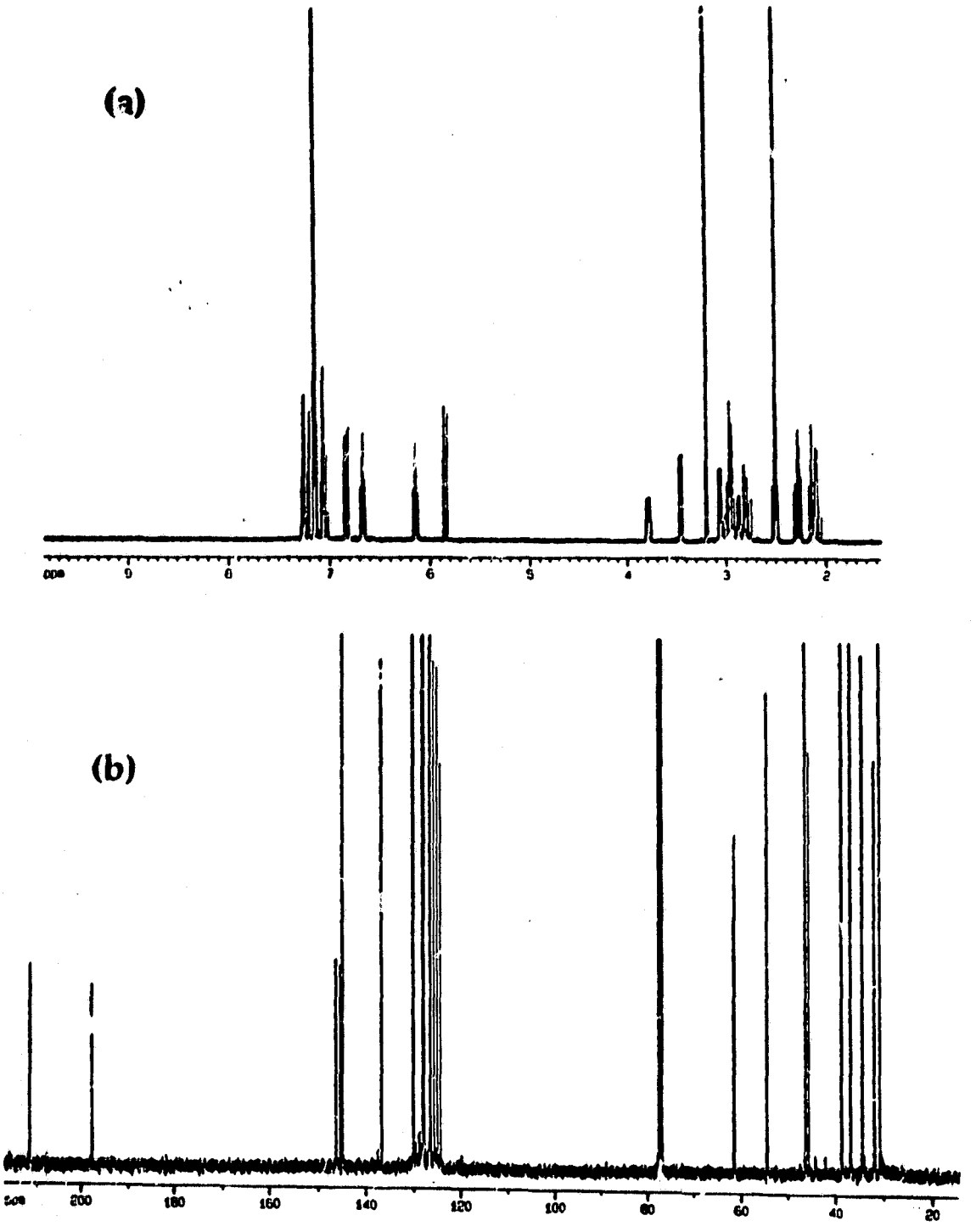

Figure 6.2 ^{1}H (360 MHz) (a) and ^{13}C (b) NMR spectra of 16

6.6.1.2 Preparative scale photolyses of 155 and 37 in CH_3CN solution of Et_3N

In a typical run ~80 mg of **155** or **37** was dissolved in 0.5 M solution of Et_3N in CH_3CN and irradiated at 254 nm (*ca.* 30 min). After irradiation the reaction mixture was quenched by adding a cold aqueous solution of 15% (v/v) HCl, and extracted with CH_2Cl_2 (3 x 40 mL). The organic layers were combined and washed with 10% HCl solution and water, dried over $MgSO_4$, and CH_2Cl_2 was removed and the photolysate examined by ^1H NMR. In each case the only product formed was the corresponding reduced hydrocarbon, viz., **156** and **49**. Preparative scale thin layer chromatography (silica gel, CH_2Cl_2) was employed to isolate these photoproducts from the reaction mixture and identified by comparison with the ^1H NMR spectra of authentic samples.

6.6.1.3 Preparative Scale Photolyses of 155 and 37 and 157 and 158 in Aqueous CH_3CN Solution

In preparative scale experiments the substrate (~80 mg) was dissolved in 80 mL of CH_3CN and diluted with an equal amount of buffer solution of appropriate pH. In the case of photolysis in the presence of sulfuric acid, the CH_3CN solution of the substrate (75 mL) was diluted with an equal amount of 10-20% (w/w) H_2SO_4 solution. After irradiation of these solutions at 300 nm (in the case of **155** and **37**) or 254 nm (in the case of **157** and **158**) for an appropriate period of time the reaction mixture was worked up by adding a saturated brine solution, neutralizing with an aqueous NaOH solution and extracting the aqueous

layer with CH_2Cl_2 (3 x 30 mL). The organic layers were combined and washed with water, dried over $MgSO_4$ and CH_2Cl_2 removed. The photolysate was examined by ^1H NMR (90 MHz) and photoproducts identified by comparison with the ^1H NMR spectra of the authentic materials.

6.6.2 Steady-State Fluorescence Studies

Fluorescence spectra were measured in 1.00 cm Suprasil quartz cuvettes at 10^{-5}-10^{-4} M after 10 min of argon purging. Fluorescence lifetimes were measured by single photon counting at optical densities of 0.03-0.08 at the exciting wavelength (details of the single photon counting discussed later, *vide infra*). Fluorescence quantum yield (Φ_f) of **155** was measured relative to quinine bisulfate (Φ_f = 0.55 in 1 N H_2SO_4)[177] according to eq 6.? (*vide supra*).

6.7 Photoionization of *N*-methylacridan (140)

6.7.1 Product Studies

6.7.1.1 Dark Reactions of 140

N-methylacridan (**140**) did not show any reactivity in the dark under the conditions employed to study its photochemistry. Control experiments were performed by treating ≈ 60 mg of substrate in exactly the same manner as the photolyzed sample except that they were stirred in dark for 30-60 min. The samples were then worked up in a usual manner and analyzed by ^1H NMR (90 MHz).

6.7.1.2 Preparative Scale Photolysis of *N*-methylacridan (140)

In a typical preparative study 100 mg of **140** was dissolved in 200 mL of solvent (e.g., CH_3CN, Et_2O etc.) and irradiated at 254/300 nm for 60 min. The solvent was then evaporated on a rotary evaporator and photolysate analyzed by ^1H NMR (90 MHz, $CDCl_3$) for the product bis(*N*-methylacridyl) (**141**) formed. The percentage conversion to bis(*N*-methylacrdyl) (**141**) (mp 238 ± 2 °C) was determined by integrating the *N*-CH_3 signals of the product **141** (δ 2.95 (s, 6H)) with respect to that of starting material **140** (δ 3.31 (s, 3H)).

6.7.2 Product Quantum Yields

Quantum yields (Φ_L) for loss of **140** were measured in number of solvents on an optical bench (λ_{ex} = 302 nm). In a typical experiment 0.5 mL of a stock solution of **140** in CH_3CN (2×10^{-3} M) was transferred to a quartz cuvette and diluted with 2.5 mL of the appropriate solvent in which the quantum yield was being measured. The solutions were purged with a stream of argon for 10 min prior to and during the photolysis (usually 1-10 min). Conversions to product were kept below 15% in all solvents. After irradiation the photolysate was transferred into a round bottomed flask and solvent was evaporated under reduced pressure to *ca.* 100 μL. In case of photolysis in 1:1 CH_3CN-H_2O, the photolysate was transferred to a test tube, saturated with NaCl, and extracted with CH_2Cl_2 (3 x 5 mL). The organic fractions were combined, dried over $MgSO_4$ and filtered, and solvent removed to ca. 100 μL. Each solution was then injected

with 50 μL of a stock solution of 9*H*-xanthene (**125**) before being injected into the GC capillary column (180 °C) for analysis. Since the retention time of the product bis(*N*-methylacridyl) (**141**) was very long, loss of starting substrate **140** was measured instead to measure the number of moles of products formed. This was achieved by comparing the integrated peak areas of external standard xanthene (**125**) and *N*-methylacridan (**140**). The respective peak areas were corrected for the differences in the GC detector response. Correction factors were generated independently by injecting solutions of the **125** and **140** in known molar ratios and checking the response. Light intensity measurement were made by employing potassium ferrioxalate actinometery according to the method of Hatchard and Parker described earlier (*vide supra*).[118]

6.8 Excited State Carbon Acid Behaviour of Substituted Suberenes

6.8.1 Product Studies

6.8.1.1 Preparative Scale Photolyses of 180, 181, 185, 186, 187, 188, 189, 190, 193, 194, 196 and 197 in Aqueous CH_3CN

In general ~ 60-75 mg of substrate was dissolved in the 75 mL of CH_3CN and then diluted with an equal amount of L_2O (L = H or D), and transferred to a 200 mL quartz tube. The solution was cooled to ≈ 14 °C with an internal cooling finger and purged with a stream of argon for 5 min before photolysis at 300 nm inside a Rayonet RPR 100 photochemical reactor. Photolyzed solutions were worked up by first saturating the solution with NaCl, extracting with CH_2Cl_2 (3 x 50 mL), and then evaporating the solvent on a rotary evaporator. The

photoproducts formed in each case were identified by ^1H NMR (250 MHz) and conversion to deuterium/protium exchange photoproducts were calculated by ^1H NMR integration and GC/MS analyses.

6.8.1.2 Preparative scale photolysis of 194 and 197 in Ethanolamine solution

In these experiment ~ 50 mg of the substrate (194 or 197) was dissolved in 100 mL solution of ethanolamine (*ca.* 0.2-0.5 M) in CH_3CN. The solution was transferred into a quartz tube and purged with argon for 5 min, and irradiated at 254 nm. After photolysis, the reaction mixture was carefully quenched with a 10% HCl solution and extracted with CH_2Cl_2 (3 x 30 mL). The CH_2Cl_2 layers were combined and washed with water, dried over $MgSO_4$ and evaporated on a rotary evaporator. The photolysate was then examined by ^1H NMR (250 MHz) and conversions to deuterium exchanged photoproducts were calculated by GC/MS.

6.8.2 Quantum Yields Measurements

Quantum yields (Φ's) of monodeuterium and monoprotium incorporation were measured in a variety of solvent mixtures on an optical bench (λ_{ex} = 280 nm). Potassium ferrioxalte actinometry was employed to determine the light intensity at 280 nm (4.7632-4.7732 x 10^{-7} Einstein/min/3 mL) (*vide supra*). In general, 3 mL solution (~ 10^{-3} - 10^{-4} M) of substrate in an appropriate solvent mixture was transferred to a quartz cuvette. The concentrations of the each

substrate in the cuvette solutions were such that they had an absorbance ≥ 2.2 at the excitation wavelength (λ_{ex} = 280 nm). The solutions were purged with a stream of argon for 5 min prior to and during the photolysis (usually 30-60 min). The irradiation time was so adjusted as to keep the conversions to photoproducts between 10-12% in all cases. After irradiation the photolysate was transferred to a test tube, saturated with NaCl, acidified to pH ≈ 7 by adding 5% HCl, and extracted with CH_2Cl_2 (4 x 5 mL). The organic fractions were then combined and washed with H_2O (pH ~ 1; 2 x 10 mL), dried over $MgSO_4$ and filtered. The photolysate was then analyzed by GC/MS (CI mode) to calculate the percentage deuterium incorporation (after correcting for the natural abundance of D and ^{13}C) in photoproducts. A representative case of percentage conversion of **181** to **203** in various solvent mixtures is shown in Table 6.1.

Table 6.1 Percentage Conversion to 203 in the Photolysis of 181 at 280 nm in Various Solvent Mixtures

Molecule	Solvent Mixture	Photolysis Time	% 203
181	70% H_2O-CH_3CN[a]	30 min	10.74 ± 0.03
	70% 1.25 M H_2SO_4-EtOH[b]	120 min	8.87 ± 0.04
	50% H_2O-CH_3CN[a]	45 min	10.47 ± 0.05
	50% 1.0 M NaOH-EtOH[b]	30 min	13.96 ± 0.03
	50% 2.0 M NaOH-EtOH[b]	20 min	11.50 ± 0.05

a) Number of moles of **181** photolyzed: 1.60 x 10^{-6}; light intensity at 280 nm: 4.77 x 10^{-7} einstein/min.
b) Number of moles of **181** photolyzed: 1.74 x 10^{-6}; light intensity at 280 nm: 7.76 x 10^{-7} einstein/min.

Table 6.2 shows the conversion of 180 to 203 on photolysis in D_2O-CH_3CN solutions. Only trace amounts of 181 (< 1%) were formed in these photolysis.

Table 6.1 Percentage Conversion to 203 in the Photolysis of 180 at 280 nm in Various Solvent Mixtures[a]

Molecule	Solvent Mixture	Photolysis Time	% 203
180	70% D_2O-CH_3CN	45 min	9.73 ± 0.03
	50% D_2O-CH_3CN	60 min	11.33 ± 0.05
	20% D_2O-CH_3CN	75 min	9.85 ± 0.03
	CD_3CN	60 min	0.00

a) Number of moles of 180 photolyzed: 1.74×10^{-6}; light intensity at 280 nm: 4.76×10^{-7} einstein/min.

6.8.3 Steady-State Fluorescence Studies

Fluorescence quenching studies of 180, 181, 185, 186, 189, and 190 were performed on a Perkin-Elmer MPF-66 spectrophotometer using H_2O as the quencher. A dilute sample ($\approx 10^{-5}$ M) of the substrate in CH_3CN (dry) was prepared and its fluorescence spectrum recorded. No fluorescence was observed form the distilled H_2O or CH_3CN used in these experiments. The photostability of the samples over time was determined by monitoring the samples fluorescence intensity for ≈30 min. Little variation in the fluorescence intensity was observed.

For systematic fluorescence quenching studies, a series of substrate solutions in CH_3CN (dry) with varying concentration of H_2O were prepared in Suprasil quartz cuvettes. Three samples were prepared at each concentration of H_2O. The fluorescence intensity was measured for each and an average of three values was taken. These values of fluorescence intensities over the range of H_2O concentration were then used in Stern-Volmer analysis to obtain quenching rate constants (k_q). Fluorescence of **194** and **197** in CH_3CN was not quenched by added H_2O. However, fluorescence of these molecules was efficiently quenched by added ethanolamine. A representative case of such fluorescence quenching of **193** in CH_3CN by ethanolamine is shown in Figure 3.4 (Chapter Three).

Fluorescence quantum yields (Φ_f) of various suberene derivatives, viz., **180**, **185** and **189**, in CH_3CN were measured relative to suberene (**37**) using eq 6.2. For these purposes each set of solution (sample and **37**) were absorption matched at λ_{ex} = 280 nm (O.D. = 0.019-0.025). Excitation of each compound was then done at 280 nm and the resulting fluorescence spectrum recorded. The area of the integrated emission band of sample relative to **37** was then used in eq 6.2 to calculate the Φ_f of the substrate. Because of the better spectral overlap biphenyl ether was chosen as the secondary fluorescence standard for **193** and **196**.

6.9 Product Studies of Electron Transfer to Photoexcited Xanthenium and Thioxanthenium Cation in S_1 in Aqueous Acid Solution

6.9.1 Product Studies

6.9.1.1 Photolysis of 99 in aqueous H_2SO_4

The cation 99 was generated by dissolving ≈ 250 mg of 9-phenylxanthenol (98) in 100 mL of CH_3CN and diluting the solution with 100 mL of 10% (w/w) H_2SO_4. A bright yellow solution was obtained indicating the formation of cation 99. The solution was transferred into a pyrex tube and purged with Argon for 5 min prior to its photolysis at 345 nm (Rayonet RPR 100 photochemical reactor; ≈ 14 °C) for 30 min. The reaction was worked up by neutralizing it with a solution of NaOH (*ca.* 0.5 M) and extracting several times with CH_2Cl_2. The combined CH_2Cl_2 layers were washed with water and CH_2Cl_2 was removed on a rotary evaporator. The photolysate was then examined by ^1H NMR (90 MHz).

6.9.1.2 Photolysis of 99 in aqueous H_2SO_4 in the presence of 1,3-DMB

The cation 99 was generated in 1:1 CH_3CN-10% (w/w) H_2SO_4 and ≈ 300 mg of 1,3-DMB was added into the solution. Irradiation of such a solution at 345 nm for 30 min resulted in the formation of a off-white precipitate. The precipitate was filtered out and washed with water. The filtrate was then neutralized and extracted with CH_2Cl_2. The ^1H NMR analysis of the filtrate showed it to be the mixture of 98 and 1,3-DMB. The crystals of the precipitate were grown in CH_2Cl_2/hexane and its structure was solved by X-Ray crystallography (Figure 4.1).

6.9.1.3 Photolysis of 99 in 2-PrOH in the presence of 1,3-DMB

In preparative scale experiment the cation 99 was generated in 1:1 2-PrOH-

10% H_2SO_4 and ~ 200 mg of 1,3-DMB was added into it. The solution was photolyzed at 345 nm for 30 min and the reaction mixture worked up by neutralizing with an aqueous solution of NaOH and extraction with CH_2Cl_2. The photolysate was then examined by ^1H NMR (90 MHz) and the photoproduct **133** formed characterized by comparison with the ^1H NMR spectrum of an authentic sample. A similar photolysis of **99** in the presence of 1,2- and 1,4-DMB also resulted in the formation of **133** as indicated by the ^1H NMR spectrum of the reaction mixtures. In the absence of 1,3-DMB (or 1,2- and 1,4-DMB) no **133** was formed.

6.9.1.4 Photolysis of 114 in aqueous H_2SO_4 in the presence of 1,3- and 1,4-DMB

The cation **114** was generated by dissolving ~ 200 mg of xanthenol in 100 mL of CH_3CN and diluting the resulting solution with an equal amount of 30% (w/w) H_2SO_4. A deep yellow coloured solution of cation **114** was formed. To this solution of cation **114**, ~ 200 mg of 1,3-DMB was added and the solution was transferred into a pyrex tube and irradiated at 345 nm for 30 min. A yellow coloured precipitate was formed after the photolysis. The precipitate was filtered out and washed with water. The ^1H NMR (90 MHz) of the precipitate showed it be a mixture of **128** (δ 4.20) and **217** (δ 5.71) by comparison with the ^1H NMR spectra of the authentic samples. Same products (**128** and **217**) were obtained when 1,4-DMB was used instead of 1,3-DMB.

6.9.5 Quantum Yield Measurement

Quantum yield for the loss of cation **99** in the presence of electron donors, viz., 1,3-, 1,2-, and 1,4-DMB was measured using UV-visible spectrophotometry. In a typical experiment the cation **99** was generated in 8:2 1.25 M H_2SO_4-CH_3CN and a solution of 1,3-DMB (10^{-2} M) was into it. The solution was transferred into a quartz cuvette and the absorbance of the cation **99** measured at 375 nm (ε = 39000 M^{-1} cm^{-1}). The solution was then irradiated on an optical bench at 358 nm under a fine stream of argon for 30-45 min. At the end of photolysis, the absorbance of the cation **99** at 375 nm was measured again. The change in the absorbance (ΔA) of cation **99** at 375 nm before and after photolysis was noted, and the quantum yield for loss of substrate was calculated using eq 6.3,

$$\Phi_L = \Delta A_\lambda / (10^3 \varepsilon_\lambda \Delta I_a) \qquad (6.3)$$

where ΔA_λ is the change in absorbance at 375 nm, ε_λ is the corresponding extinction coefficient and ΔI_a is the moles of photons absorbed during the photolysis time. The concentration of **99** so set that its absorbance at irradiation wavelength (358 nm) was greater than 1.75, ensuring absorption of more than 95% of the exciting light.

6.10 Adiabatic Photogeneration of Thioxanthenium Cations in pH 7 Buffer

6.10.1 Product Studies

6.10.1.1 Preparative Scale Photolysis in Methanol

In a typical experiment 75 mg of alcohol was dissolved in 75 mL of MeOH and then diluted with an equal amount of H_2O (pH ~7). The solution was transferred to a quartz tube and purged with argon for 5 min prior to photolysis. The solution was then irradiated at 254 nm (Rayonet RPR 100 photochemical reactor; ≈ 15 °C; 5-10 min). After photolysis, the solution was saturated with NaCl, and extracted with CH_2Cl_2 (3 x 40 mL). The combined CH_2Cl_2 layers were washed with water, dried over $MgSO_4$ and evaporated on a rotary evaporator. The photolysate was then examined by ^1H NMR. Photolysis of **226**, **219**, **227** and **228** alcohols in 50% MeOH-H_2O resulted in the formation of corresponding methyl ethers. The ^1H NMR data of the corresponding methyl ethers formed are presented below:

9-Methoxythioxanthene

^1H NMR (90 MHZ, $CDCl_3$) δ 3.28 (s, 3H, OCH_3), 5.10 (s, 1H, Ar_2CH), 7.1-7.7 (m, 8H, arom.).

9-Methoxy-9-phenylthioxanthene

^1H NMR (90 MHz, $CDCl_3$) δ 3.10 (s, 3H, OCH_3), 6.9-8.1 (m, 13H, arom.).

9-Methoxy-2-Chlorothioxanthene

^1H NMR (90 MHz, $CDCl_3$) δ 3.3 (s, 3H, OCH_3), 5.15 (s, 1H, Ar_2CH), 7.1-7.7 (m, 7H, arom.).

9-Methoxy-9-Methylthioxanthene

^1H NMR (90 MHz, $CDCl_3$ δ 2.45 (s, 3H, CH_3), 3.0 (s, 3H, OCH_3), 7.1-7.9 (m, 8H,

arom.).

6.10.1.2 Preparative scale photolysis of 226 in aqueous NaCN

60 mg of **226** was dissolved in 50 mL of CH_3CN and diluted with an equal amount of 0.2 M aqueous NaCN solution. The solution was transferred into a quartz tube and photolyzed at 254 nm with continuous purging with argon. The reaction was worked up by saturating with NaCl, and extracting the aqueous layer with CH_2Cl_2 (4 x 40 mL). The photolysate was examine by ^1H NMR and GC/MS. The GC/MS analyses indicated the formation of two isomeric cyano substituted thioxanthenes, viz., **232** and **233**. Thioxanthenes **232** and **233** were separated by preparative thin layer chromatography (Silica gel; CH_2Cl_2), and characterized by ^1H NMR:

9-Cyano-9*H*-thioxanthene (232)

^1H NMR (90 MHz, $CDCl_3$) δ 4.80 (s, 1H, Ar_2CH), 7.2-7.8 (m, 8H, arom.); IR (Nujol) 2250 cm^{-1} (weak, CN stretch); GC-mass spectrum (CI) (m/z) 224 (M^++1).

9*H*-Cyanothioxanthene 233

^1H NMR (90 MHz, $CDCl_3$) δ 4.10 (s, 2H, Ar_2CH_2), 7.3-7.8 (m, 8H, arom.); IR (Nujol) 2235 cm^{-1} (weak, CN stretch); GC-mass spectrum (CI) (m/z) 224 (M^++1).

6.10.2 Steady-state Fluorescence Studies of Thioxanthenols

Fluorescence excitation and emission spectra of thioxanthenols were recorded on a Perkin-Elmer MPF-66 instrument at room temperature (22 ± 3 °C)

and are uncorrected. Solutions of thioxanthenols were prepared in pH 7 buffer (*ca.* 10^{-4} M) in a quartz cuvette, by injecting a known volume (*ca.* 50 μL) of the substrate dissolved in 100% CH_3CN (dry). The solution in the cuvette was vigorously shaken and purged (*ca.* 3-5 min) with a fine stream of Argon prior to recording of the fluorescence spectrum. Because the adiabatically generated thioxanthenium cations in pH 7 buffer fluoresce between 400-700 nm region, second-order effects (i.e., 2 x excitation wavelength) become important. To eliminate these, a 290 nm band-pass filter was placed in front of the excitation monochromator. This effectively cuts-out the 2 x 260 nm (= 520 nm) second-order scattering due to the exciting wavelength. It also eliminates the second-order band of the Raman scattering peak of the excitation wavelength. The fluorescence quantum yields (Φ_f's) of the cations were measured using emission of quinine bisulfate in 1 N H_2SO_4 as the reference ($\Phi_f = 0.55$)[177] (eq 6.2 *vide supra*). For these purposes, the corrected fluorescence spectra of thioxanthenols and quinine bisulfate were utilized.

6.10.3 Fluorescence Lifetime Measurement of Thioxanthenium Cations

Fluorescence lifetimes of thioxanthenium cations (ground state and adiabatically photogenerated) were measured by time-correlated single photon counting (SPC) (PTI LS-1 instrument) in argon saturated solutions with optical densities of 0.20-0.30 at the exciting wavelength.

The time correlated SPC method measures the time delay between the

absorption and emission of individual photons in a fluorescent sample. The key components of a SPC consists of a high repetition rate, low intensity pulsed excitation source (e.g., low pressure H_2 lamp), a start photomultiplier tube (PMT), a stop PMT, a time-to-amplitude convertor (TAC), and a multichannel analyzer (MCA). The triggering of the excitation source is detected optically by start PMT that generates an electrical signal correlated to the excitation pulse. This signal travels to a discriminator and then to TAC, thus initiating the charging of a capacitor resulting in a voltage ramp which is linear with time. On detection of the emitted photon (by stop PMT) the ramp is halted and the voltage output of the TAC is given a value by the analog to digital convertor and a count is stored in the appropriate channel of the MCA corresponding to the delay of the emitted photon with respect to the excitation pulse. With the high frequency of detected events a statistical distribution of the fluorescence emission is quickly accumulated that corresponds to the time dependence of the intensity of fluorescence from which the lifetime information can be obtained.

The SPC traces are generally recorded using the semilogrithmic graphics. A representative case of such a fluorescence decay of thioxanthenium cation **231** in CF_3CH_2OH recorded on LS-1 SPC instrument is presented in Figure 6.3. Note that the ordinate is logarithmic such that the single exponential decay function give rise to a straight line. The LS-1 SPC instrument also records the instrument response function (or the lamp profile). The IRS was collected by using a scattering solution (milk/water solution) and recording the temporal data as it

was done for the sample. The LS-1 SPC automatically alternates between the sample and scattering solutions during the course of the data acquisition. Both the observed decay and IRF are down-loaded and stored on a microcomputer

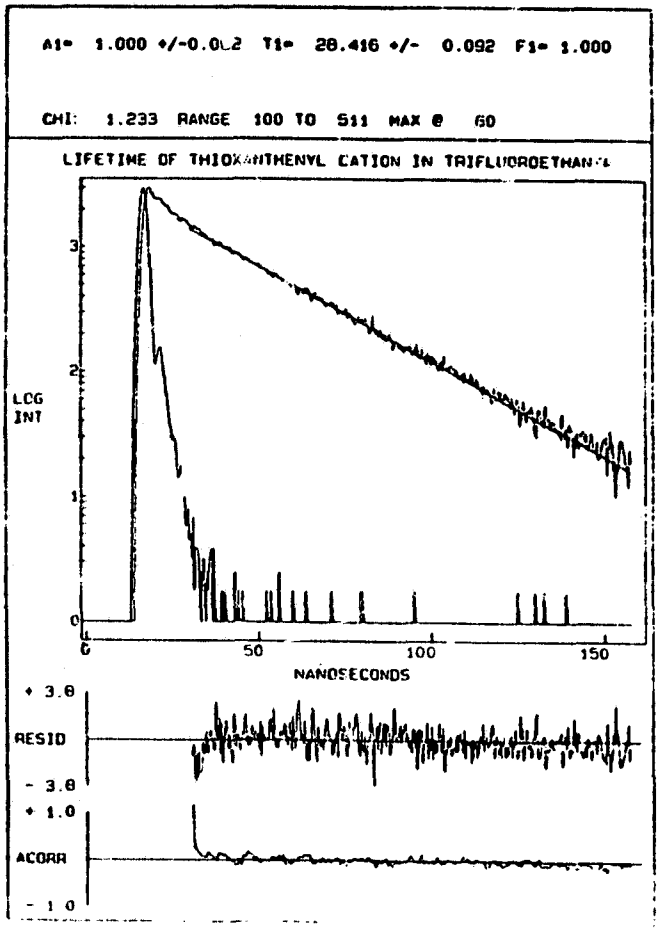

Figure 6.3 Representative fluorescence lifetime decay curve of adiabatically photogenerated thioxanthenium cation **231** in CF_3CH_2OH. τ = 28.42; χ^2 = 1.23.

(NEC 8086 processor). The lifetime of the sample is then extracted from the above data by an iterative reconvolution procedure.[181] In this method the measured IRF, described by R(t) is fixed and convoluted along with a variable

G(t) function to give a simulated decay function S(t) (eq 6.4).

$$S(t) = {}_0\int^t R(t)\, G(t-t')dt \qquad (6.4)$$

The simulated decay, S(t), is then compared to the measured decay, I(t), and the chi-squared (χ^2) value is calculated using eq 6.5

$$\chi^2 = \Sigma_{i=n1}^{n2} [I(t_i) - S(t_i)]^2 / I(t_i) \qquad (6.5)$$

where n_1 (channel with maximum counts) and n_2 (channel where the count reach a background level) are the limits of the analysis range. In the iterative reconvolution process the parameters in G(t) are varied and optimized to achieve a minimum value in χ^2, the point by point deviation between experimental and simulated decay curves. For correct calculated function χ^2 value between 0.9-1.3 is acceptable (e.g., in Figure 6.3 χ^2 = 1.23). The χ^2 parameter, however, contains no information on the error distribution within the analyzed range of data points. A plot of the weighted residuals $r(t_i)$ (eq 6.6) may be used to visualize the error distribution where,

$$r(t_i) = I(t_i) - S(t_i) / [I(t_i)]^{1/2} \qquad (6.6)$$

In this context the autocorrelation function, C(j), is useful. It describes the correlation between the residuals $r(t_i)$ and $r(t_{i+j})$ and is defined by eq 6.7,

$$C(j) = 1/m \sum^{n1+m-1}_{i=n} r(t_i)\, r(t_{i+j}) \,/\, i/n_3 \sum [r(t_i)]^2 \qquad (6.7)$$

where $n_3 = n_2-n_1+1$, $j = n_3/2$, and $m = n_3-j$. For good fits, the autocorrelation plots should show an initial value of 1.0 and random dispersion of the residuals around the $C(j) = 0$ line (see at the bottom of Figure 6.3). A poor fit is demonstrated by sigmoidal distribution around $C(j) = 0$ or a plot that fails to cross this line.

REFERENCES

1. Calvert, J. G.; Pitts, Jr., J. N., *Photochemistry*; John Wiley and Sons Inc.: New York, 1966, pp. 22-23.
2. Streitwieser, Jr., A., *Solvolytic Dispiacement Reactions*; McGraw Hill Book Co.: New York, 1962, p. 42.
3. Margerum, J. D.; Miller, L. J.; Saito, E.; Brown, M. S.; Mosher, H. S.; Hardwick, R., *J. Phys. Chem.*, **1962**, *66*, 2434.
4. Wettermark, G., *Nature*, **1962**, *194*, 677.
5. Wettermark, G., *J. Am. Chem. Soc.*, **1962**, *84*, 3658.
6. Wettermark, G., *J. Phys. Chem.*, **1962**, *66*, 2560.
7. Wettermark, G.; Ricci, R., *J. Chem. Phys.*, **1963**, *39*, 1218.
8. Langmuir, M. E.; Dogliotti, L.; Black, E. D.; Wettermark, G., *J. Am. Chem. Soc.*, **1969**, *91*, 2204.
9. Burlinson, N. E.; Sitzman, M. E.; Kaplan, L. A.; Kayser, E., *J. Org. Chem.*, **1979**, *44*, 3695.
10. Craig, B. B.; Atherton, S. J., In *Application of Laser Chemistry and Diagnostics, SPIE, Vol. 482*, Harvey, A. B. (ed.), **1984**, 96.
11. Atherton, S. J.; Craig, B. B., *Chem. Phys. Letters* **1986**, *127*, 7.
12. Chattopadhyay, S. K.; Craig, B. B., *J. Phys. Chem.*, **1987**, *91*, 323.
13. McClelland, R. A.; Steenken, S., *Can. J. Chem.*, **1987**, *65*, 353.
14. Mathew, T.; Ramaiah, D., Joshua, C. P.; Weir, D.; George, M. V., *J. Photochem. Photobiol., A*, **1993**, *70*, 245.

15. Morrison, H.; Migdalof, B., *J. Org. Chem.*, **1965**, *30*, 3996.

16. Craig, B. B.; Atherton, S. J., *J. Chem. Soc., Perkin Trans. 2*, **1988**, 1929.

17. Frakas, L.; Wansbrough-Jones, O. H., *Z. Phys. Chem. B*, **1932**, *18*, 124.

18. Budac, D.; Wan, P., *J. Photochem. Photobiol., A: Chem.*, **1992**, *67*, 135.

19. Margerum, J. D.; Petrusis, C. T., *J. Am. Chem. Soc.*, **1969**, *91*, 2467.

20. Stermitz, F. R.; Huang, W. H., *J. Am. Chem. Soc.*, **1971**, *93*, 3427.

21. Epling, G. A.; Lopes, A., *J. Am. Chem. Soc.*, **1977**, *99*, 2700.

22. Craig, B. B.; Weiss, R. G.; Atherton, S. J., *J. Phys. Chem.*, **1987**, *91*, 5906.

23. Givens, R. S.; Matuszewski, B.; Levi, N.; Leung, D., *J. Am. Chem. Soc.*, **1977**, *99*, 1896.

24. Meiggs, T. D.; Grossweiner, L. I.; Miller, S. I., *J. Am. Chem. Soc.*, **1972**, *94*, 7981.

25. Steenken, S.; Warren, C. J.; Gilbert, B. G., *J. Chem. Soc., Perkin Trans. 2*, **1990**, 335.

26. Meiggs, T. O.; Miller, S. I., *J. Am. Chem. Soc.*, **1972**, *94*, 1989.

27. (a) Wan, P.; Xu, X., *Tetrahedron Lett.*, **1990**, *31*, 2809. (b) Xu, X., M.Sc. Thesis, University of Victoria, Victoria, British Columbia, Canada, 1990.

28. Stermitz, F. R.; Huang, W. H., *J. Am. Chem. Soc.*, **1970**, *92*, 1446.

29. Defoin, A.; Defoin-Straatmann, R.; Hildenbrand, K.; Bittersmann, E.; Kreft, D.; Kuhn, H. J., *J. Photochem.*, **1986**, *33*, 237.

30. Kuhn, H. J.; Görner, H., *J. Phys. Chem.*, **1988**, *92*, 6208.

31. McAuley, I.; Krogh, E.; Wan, P., *J. Am. Chem. Soc.*, **1988**, *110*, 600.

32. (a) Krogh, E.; Wan, P., *J. Am. Chem. Soc.*, **1992**, *114*, 705. (b) Krogh E., Ph.D Thesis, University of Victoria, 1991. (c) Feldman, M. R.; Thame, N. G., *J. Org. Chem.*, **1979**, *44*, 1863.

33. Wan, P.; Muralidharan, S., *J. Am. Chem. Soc.*, **1988**, *110*, 4336.

34. Steenken, S.; McClelland, R. A., *J. Am. Chem. Soc.*, **1989**, *111*, 4967.

35. Iwamoto, N.; Okamoto, Y.; Takamuku, S., *Bull. Chem. Soc. Jpn.*, **1986**, *59*, 1505.

36. Okamoto, Y.; Iwamoto, N.; Takamuku, S., *J. Am. Chem. Soc., Chem. Commun.*, **1986**, 1516.

37. Okamoto, Y.; Iwamoto, N.; Toki, S.; Takamuku, S., *Bull. Chem. Soc. Jpn.*, **1987**, *60*, 277.

38. Wayner, D. D. M.; Gravelle, L., *Tetrahedron Lett.*, **1988**, *29*, 431.

39. Shi, M.; Okamoto, Y.; Takamuku, S., *Bull. Chem. Soc. Jpn.*, **1990**, *63*, 453.

40. Vander Donckt, E.; Nasielski, J.; Thiry, P., *Chem. Commun.*, **1969**, 1249.

41. Manoharan, R.; Dogra, S. K., *J. Photochem. Photobiol., A*, **1988**, *43*, 81.

42. Grellmann, K. H.; Heilbronner, E.; Seiler, P.; Weller, A., *J. Am. Chem. Soc.*, **1968**, *90*, 4238.

43. Stewart, R., *The Proton: Application to Organic Chemistry*; Academic Press: Orlando, **1985**.

44. Kresge, A. J., *Acc. Chem. Res.*, **1975**, *8*, 354.

45. Brauman, J. I.; Schwartz, J.; van Tamleen, E. E., *J. Am. Chem. Soc.*, **1968**, *90*, 5328.

46. Schwartz, J. J., *J. Chem. Soc., Chem. Commun.*, **1969**, 833.

47. Wan, P.; Krogh, E.; Chak, B., *J. Am. Chem. Soc.*, **1988**, *110*, 4073.

48. Budac, D.; Wan, P., *J. Org. Chem.*, **1992**, *57*, 887.

49. Wan, P.; Budac, D.; Krogh, E., *J. Chem. Soc., Chem. Commun.*, **1990**, 255.

50. Wan, P.; Yates, K., *J. Org. Chem.*, **1983**, *48*, 136.

51. Wan, P.; Yates, K., *J. Chem. Soc., Chem. Commun.*, **1981**, 1023.

52. Wan, P.; Yates, K., *Can. J. Chem.*, **1986**, *64*, 2076.

53. Wan, P.; Muralidharan, S.; McAuley, I.; Babbage, C. A., *Can. J. Chem.*, **1987**, *65*, 1775.

54. Olah, G. A., *Angew. Chem. Int. Ed. Engl.*, **1973**, *12*, 173.

55. Olah, G. A.; Schleyer, P. V. R., *Carbonium Ions, Vols. 1-5*; Wiley Interscience: New York, 1976.

56. Deno, N. C.; Grover, P. J.; Pittman, Jr., C. U.; Waack, R.; Doran, M., *J. Am. Chem. Soc.*, **1966**, *88*, 2331.

57. Brouwer, D. M.; Hogeveen, H., In *Progress in Physical Organic Chemistry, Vol. 9*, Streitwieser, A. and Taft, R. W. (ed.); Wiley Interscience: New York, 1972.

58. Cristol, S. J.; Bindel, T. H., *Org. Photochem.*, **1983**, *6*.

59. Das, P. K., *Chem. Rev.*, **1993**, *93*, 119.

60. Lifschitz, J.; Joffe, C. L., *Z. Physik. Chem.*, **1921**, *27*, 426.

61. Weyde, E.; Frankenburger, *Trans. Faraday Soc.*, **1931**, *27*, 561.

62. (a) Holmes, E. O., *J. Phys. Chem.*, **1957**, *61*, 434; (b) Holmes, E. O., *J. Phys.*

Chem., **1958**, *62*, 884.

63. Herz, M. L., *J. Am. Chem. Soc.*, **1975**, *97*, 6777.

64. Peters, L. E.; Manring, K. S., *J. Phys. Chem.*, **1984**, *88*, 3516.

65. Cremers, D. A.; Cremers, T. L., *Chem. Phys. Lett.*, **1983**, *94*, 102.

66. Alonso, E. O.; Johnston, L. J.; Scaiano, J. C.; Toscano, V. G., *J. Am. Chem. Soc.*, **1990**, *112*, 1270.

67. Bart, J.; Steenken, S.; Mayr, H.; McClelland, R. A., *J. Am. Chem. Soc.*, **1990**, *112*, 6918.

68. McClelland, R. A.; Kanagasabapathy, V. M.; Banait, N. S.; Steenken, S., *J. Am. Chem. Soc.*, **1989**, *111*, 3966.

69. Zimmerman, H. E.; Sandel, V. R., *J. Am. Chem. Soc.*, **1963**, *85*, 915.

70. Zimmerman, H. E.; Somasekhara, S., *J. Am. Chem. Soc.*, **1963**, *85*, 922.

71. Cristol, S. J.; Schloemen, G. C., *J. Am. Chem. Soc.*, **1972**, *94*, 5916.

72. (a) Lillis, V.; McKenna, J.; McKenna, J. M.; Smith, M. J.; Taylor, P. S.; Williams, J. H., *J. Chem. Soc., Perkin Trans. 2.*, **1980**, 80.; (b) Lillis, V.; McKenna, J.; McKenna, J. M.; Smith, M. J.; Taylor, P. S.; Williams, J. H., *J. Chem. Soc., Chem. Commun.*, **1974**, 474.

73. (a) Jaeger, D. A., *J. Am. Chem. Soc.*, **1975**, *95*, 102.; (b) Jaeger, D. A.; Angelos, G. H., *Tetrahedron Lett.*, **1981**, 803.

74. Maycock, A. L.; Berchtold, G. A., *J. Org. Chem.*, **1970**, *35*, 2532.

75. Appleton, D. C.; Bull, D. C.; Givens, R. S.; Lillis, V.; McKenna, J.; Mckenna, J. M.; Thackery, S.; Walley, A. R., *J. Chem. Soc., Perkin Trans. 2*, **1980**, 77.

76. Appleton, A. L.; Brocklehurst, B.; McKenna, J.; McKenna, J. M.; Thackery, S.; Walley, A. R., *J. Chem. Soc., Perkin Trans. 2*, **1980**, 87.

77. Arnold, B.; Donald, L.; Jurgens, A.; Pincock, J. A., *Can. J. Chem.*, **1985**, *63*, 3140.

78. Slocum, G. H.; Kaufman, K.; Schuster, G. B., *J. Am. Chem. Soc.*, **1981**, *103*, 4625.

79. Cristol, S. J.; Mahfuza, B. A.; Sankar, J. V., *J. Am. Chem. Soc.*, **1989**, *111*, 8207, and references cited therein.

80. Morrison H., *Rev. Chem. Int.*, **1987**, *8*, 125, and references cited therein.

81. Jaeger, D. A., *J. Am. Chem. Soc.*, **1976**, *98*, 6401.

82. Miller, G. C.; Mille, M. J.; Crosby, D. G.; Sontum, S.; Zepp, R. G., *Tetrahedron*, **1979**, *35*, 1797.

83. Shukla, D.; Wan, P., *Trends in Organic Chemistry (India)*, **1991**, *2*, 143.

84. Rosenfeld, T.; Alchalal, A.; Ottolenghi, M., *Chem. Phys. Lett.*, **1972**, *20*, 291.

85. Pienta, N. J.; Kesseler, R. J., *J. Am. Chem. Soc.*, **1992**, *114*, 2419.

86. Lin, C. I.; Singh, P.; Ullman, E. F., *J. Am. Chem. Soc.*, **1976**, *20*, 671.

87. Wan, P., *J. Org. Chem.*, **1985**, *50*, 2583.

88. Wan, P.; Chak, B., *J. Chem. Soc., Perkin Trans. 2*, **1986**, 1751.

89. Wan, P.; Chak, B.; Krogh, E., *J. Chem. Soc., Perkin Trans. 2*, **1989**, *46*, 49.

90. Hall, B.; Wan, P., *J. Photochem. Photobiol., A*, **1991**, *56*, 35.

91. Turro, N. J.; Wan, P., *J. Photochem.*, **1985**, *50*, 93.

92. Wan, P.; Yates, K.; Boyd, M., *J. Org. Chem.*, **1985**, *50*, 2881.

93. Das, P. K.; Minto, R. E., *J. Am. Chem. Soc.*, **1989**, *111*, 8858.

94. McClelland, R. A.; Banait, N.; Steenken, S., *J. Am. Chem. Soc.*, **1989**, *111*, 2929.

95. Okuyama, T.; Ueno, K.; Morishima, Y.; Kamachi, M.; Fueno, T., *Chem. Lett.*, **1990**, 1129.

96. (a) Wan, P.; Krogh, E., *J. Am. Chem. Soc.*, **1989**, *111*, 4887.; (b) Wan, P.; Krogh, E., *J. Chem. Soc., Chem. Commun.*, **1985**, 1627.

97. Mecklenburg, S. L.; Hilinski, E. F., *J. Am. Chem. Soc.*, **1989**, *111*, 5471.

98. McClelland, R. A.; Mathivanan, N.; Steenken, S., *J. Am. Chem. Soc.*, **1990**, *112*, 4857.

99. (a) Blazek, A.; Pungente, M.; Krogh, E.; Wan, P., *J. Photochem. Photobiol., A*, **1992**, *64*, 315.; (b) Krogh, E.; Wan, P., *Can. J. Chem.*, **1990**, *68*, 1725.

100. Rehm, D.; Weller, A., *Isr. J. Chem.*, **1970**, *8*, 259.

101. (a) Fox, M. A., *Chem Rev.*, **1979**, *79*, 253.; (b) Tolbert, L. M., *Org. Photochem.*, **1983**, *6*, 177.; (c) Tolbert, L. M., *Acc. Chem. Res.*, **1986**, *19*, 268.; (d) Tolbert, L. M., In *Comprehensive Carbanion Chemistry, Part C*; Buncel, E.; Durst, T., (eds.), Elsevier: Amsterdam, **1987**, chapter 4.; (e) Krogh, E.; Wan, P., *Topics Curr. Chem.*, **1990**, *156*, 93.

102. (a) van Tamelen, E. E.; Cole, T. M.; Greely, R. H.; Schumacher, H., *J. Am. Chem. Soc.*, **1968**, *90*, 1372.; (b) van Tamelen, E. E.; Cole, T. M., *J. Am. Chem. Soc.*, **1970**, *92*, 4123.; (c) van Tamelen, E. E.; Cole, T. M., *J. Am. Chem. Soc.*, **1971**, *93*, 6158.; (d) van Tamelen, E. E.; Greely, R. H.; Schumacher, H., *J.Am.*

Chem. Soc., **1973**, *93*, 6151.

103. Al-Ekabi, H.; Kawata, H.; de Mayo, P., *J. Org. Chem.*, **1988**, *53*, 1471.

104. Takahashi, Y.; Sankararaman, S.; Kochi, J. K., *J. Am. Chem. Soc.*, **1989**, *111*, 2954.

105. (a) Johnston, L. J.; Wong, D. F., *J. Phys. Chem.*, **1993**, *97*, 1589.; (b) Johnston, L. J.; Kanigan, T., *J. Am. Chem. Soc.*, **1990**, *112*, 1271.

106. Azarani, A.; Berinstain, A. B.; Johnston, L. J.; Kazanis, S., *J. Photochem. Photobiol., A*, **1991**, *57*, 175.

107. Faraday, M., *Phil. Trans. Roy. Soc.*, **1825**, *115*, 440.

108. (a) Kekulé, A., *Bull. Soc. chim. Fr.*, **1965a**, *3*, 98.; (b) Kekulè, A., *Bull. Acad. R. Belg.*, **1865b**, *19*, 551.; (c) Kekulé, A., *Liebigs Ann.*, **1866**, *137*, 129.

109. Lewis, D.; Peters, D., *Facts and Theories of Aromaticity*; Macmillan Press: London, 1975.

110. (b) Hückel, E., *Z. Physik*, **1931**, *70*, 204. (b) Hückel, E., *Z. Physik*, **1931**, *72*, 310.

111. Glukhovtsev, M. N.; Simkin, B. Ya.; Minkin, V. I., *Russian Chemical Reviws*, **1985**, *54*, 54.

112. (a) Jug, K.; Padma Malar, E. J., *J. Mol. Struc.*, **1987**, *153*, 221.; (b) Padma Malar, E. J.; Jug, K., *Tetrahedron*, **1986**, *42*, 417.

113. (a) Lipp, E. D.; Seliskar, C. J., *J. Mol. Spectrosc.*, **1981**, *87*, 242.; (b) Grabowska, A., *J. Mol. Spectrosc.*, **1966**, *20*, 96.

114. Aihara, J., *Bull. Chem. Soc. Jpn.*, **1978**, *51*, 1788.

115. Padma Malar, E. J.; Jug, K., *Tetrahedron*, **1986**, *42*, 417.

116. Chak, B.; Dingle, T., unpublished results.

117. Huang, C.-G; Shukla, D.; Wan, P., *J. Org. Chem.*, **1991**, *56*, 5437.

118. Hatchard, C. G.; Parker, C. A., *Proc. R. Soc. London, Ser. A*, **1956**, *235*, 518.

119. Lakowicz, J. R., *Principles of Fluorescence Spectroscopy*; Plenum Press: New York, 1983.

120. Turro, N. J., *Modern Molecular Photochemistry*; University Science Books, Mill Valley: California, 1991, pp. 47-48 and 185-195.

121. Cram, D. J., *Fundamentals of Carbanion Chemistry*; Academic Press: New York, 1965, pp. 1-15.

122. Ireland, J. F.; Wyatt, P. A. H., *Adv. Phys. Org. Chem.*, **1976**, *12*, 131.

123. Ceccon, A.; Gambaro, A.; Pizzato, L.; Romanin, A.; Venzo, A., *J. Chem. Soc., Chem. Commun.*, **1982**, 907.

124. (a) Anastassiou, A. G.; Kasami, H. S.; Saadein, M. R., *Tetrahedron Lett.*, **1980**, *21*, 3743.; (b) Anastassiou, A. G.; Kasami, H. S., *Angew. Chem. Int. Ed. Engl.*, **1980**, *19(1)*, 43.; (c) Anastassiou, A. G.; Kasami, H. S.; Saadein, M. R., *Angew. Chem. Int. Ed. Engl.*, **1981**, *20(1)*, 115.

125. Garratt, P. J., *Aromaticity*; McGraw Hill: London, **1971**, pp. 118-135.

126. (a) Zimmerman, H. E., *Acc. Chem. Res.*, **1971**, *4*, 272.; (b) Dewar, M. J. S., In *Aromaticity- An International Symposium*; The Chemical Society: London, 1967, pp. 177-215; (c) Dewar, M. J. S., *Angew. Chem. Int. Ed. Engl.*, **1971**, *10*, 761.; (d) Woodward, R. B.; Hoffmann, R., *The Conservation of Orbital*

Symmetry; Verlag-Chemie: Weinhiem, 1970.

127. March, J., *Advanced Organic Chemistry (Edition Two)*; McGraw-Hill: New York, 1977, pp. 160-165, and references cited therein.

128. Lowry, T. H.; Richardson, K. S., *Mechanism and Theory in Organic Chemistry*; Harper and Row: New York, 1987, p. 212-217.

129. (a) Shukla, D.; Wan, P., *J. Am. Chem. Soc.*, 1993, *115*, 2990.; (b) Shukla, D.; Wan, P.; Dingle, T. W., unpublished results.

130. Hess, B. A. Jr.; Bailey, A. S.; Bartusek, B.; Boekelheide, V., *J. Am. Chem. Soc.*, 1969, *91*, 1665.

131. Zweifel, X ; Brown, H. C., *J. Am. Chem. Soc.*, 1964, *86*, 393.

132. Griffin, C. E.; Peters, J. A., *J. Org. Chem.*, 1963, *28*, 1715.

133. Budac, D.; Wan, P., unpublished results.

134. (a) Werner, T. C., in *Modern Fluorescence Spectroscopy*, Vol. 2; Wehry, E. L., Ed.; Plenum Press: New York, 1976; (b) Berlman, I. B., *J. Phys. Chem.*, 1970, *74*, 3085.

135. Berlman, I. B., *Handbook of Fluorescence Spectra of Aromatic Molecules*, 2nd ed.; Academic Press: California, 1971.

136. Drake, J. A. G.; Jones, D. W., *Acta Crystallogr.*, 1982, *B38*, 200.

137. (a) Wagner, P. J., *J. Am. Chem. Soc.*, 1967, *89*, 2820. (b) Zimmerman, H. E.; Crumrine, D. S., *J. Am. Chem. Soc.*, 1972, *94*, 498. (c) Imamura, A.; Hoffmann, R., *J. Am. Chem. Soc.*, 1968, *90*, 5379. (d) Takei, Y.; Yamaguchi, T.; Osamura, Y.; Fuke, K.; Kaya, K., *J. Phys. Chem.*, 1988, *92*, 577.

138. (a) Dewar, M. J. S.; Trinajstic, N., *Tetrahedron*, **1970**, *26*, 4269. (b) Hess, Jr., B. A.; Schaad, L. J.; Holyoke, Jr., C. W., *Tetrahedron*, **1972**, *28*, 3657.

139. Shukla, D.; de Rege, F.; Wan, P.; Johnston, L. J., *J. Phys. Chem.*, **1991**, *95*, 10240.

140. Colter, A. K.; Saito, G.; Sharom, F. J., *Can. J. Chem.*, **1977**, *55*, 2741.

141. Fukuzumi, S.; Ishikawa, M.; Tanaka, T., *J. Chem. Soc., Perkin Trans. 2*, **1989**, 1037.

142. Barltrop, J. A.; Coyle, J. D., *Excited States in Organic Chemistry*; John Wiley and Sons: New York: 1975, p. 143.

143. (a) Murov, S L., *Handbook of Photochemistry*; Marcel Dekker: New York, 1973. (b) Carmichael, I.; Hug, G. L., In *Handbook of Organic Photochemistry*; Scaiano, J. C., Ed.; CRC Press: Boca Ration, FL, 1989; Vol. 1.

144. (a) Fukuzumi, S.; Mochizuki, S.; Tanaka, T., *J. Phys. Chem.*, **1990**, *94*, 722. (b) Fukuzumi, S.; Mochizuki, S.; Tanaka, T., *Chem. Lett.*, **1988**, 1983. (c) Fukuzumi, S.; Mochizuki, S.; Tanaka, T., *J. Am. Chem. Soc.*, **1989**, *111*, 1497. (d) Ishikawa, M.; Fukuzumi, S.; Goto, T.; Tanaka, T., *Bull. Chem. Soc. Jpn.*, **1989**, *62*, 3754. (e) Fukuzumi, S.; Kitano, T.; Mochida, K., *J. Am. Chem. Soc.*, **1990**, *112*, 3246. (f) Fukuzumi, S.; Kitano, T.; Ishikawa, M., *J. Am. Chem. Soc.*, **1990**, *112*, 5631. (g) Fukuzumi, S.; Kitano, T., *Chemm. Lett.*, **1990**, 1275. (h) Ishikawa, M.; Fukuzumi, S., *J. Am. Chem. Soc.*, **1990**, *112*, 8864. (i) Fukuzumi, S.; Mochizuki, S.; Tanaka, T., *J. Chem. Soc., Dalton Trans.*, **1990**, 695. (j) Fukuzumi, S.; Koumitsu, S.; Hironaka, K.; Tanaka, T., *J. Am. Chem.*

Soc., **1987**, *109*, 305. (k) Fukuzumi, S.; Chiba, M.; Ishikawa, M.; Ishikawa, K.; Tanaka, T., *J. Chem. Soc. Perkin Trans. 2*, **1989**, 1417. (l) Fukuzumi, S.; Tanaka, T., In *Photoinduced Electron Transfer*, Fox, M. A., Channon, M., Eds.; Elsevier: Amsterdam, 1988; Part C.

145. Peters, K. S.; Pang, E.; Rudzki, J., *J. Am. Chem. Soc.*, **1982**, *104*, 5335. (b) Manring, L. E.; Peters, K. S., *J. Am. Chem. Soc.*, **1983**, *105*, 5708. (c) Manring, L. E.; Peters, K. S., *J. Am. Chem. Soc.*, **1985**, *107*, 6452.

146. Rahn, R.; Schroeder, J.; Troe, J., *J. Phys. Chem.*, **1989**, *93*, 7841.

147. Hapiot, P.; Moiroux, J.; Savéant, J.-M., *J. Am. Chem. Soc.*, **1990**, *112*, 1337.

148. Poulos, A. T.; Hammond, G. S.; Burton, M. E., *Photochem. Photobiol.*, **1981**, *34*, 169.

149. Reames, D. C.; Hunt, D. A.; Bradsher, C. K., *Synthesis*, **1980**, 454.

150. Parham, W. E.; Jones, L. D.; Sayed, Y., *J. Org. Chem.*, **1975**, *40(16)*, 2394.

151. Ashby, E. C.; Prather, J., *J. Am. Chem. Soc.*, **1966**, *88*, 729.

152. Tochtermann, W.; Oppenlander, K.; Walter, U., *Chem. Ber.*, **1964**, *97(5)*, 1318.

153. Iyer, V. S., personal communication.

154. King, R. B., *Organometallic Synthesis*; Academic Press: New York, 1965, p. 93.

155. Geldard, J. F.; Lions, F., *J. Org. Chem.*, **1965**, *30*, 318.

156. Burdett, K. A.; Shenton, F. L.; Yates, D. H.; Swenton, J. S., *Tetrahedron.*, **1974**, *30*, 2057.

157. Pomerantz, M.; Gruber, G. W., *J. Am. Chem. Soc.*, **1967**, *89*, 6799.

158. Wan, P.; Budac, D.; Earle, M.; Shukla, D., *J. Am. Chem. Soc.*, **1990**, *112*, 8048.

159. Davies, A. G.; Smiles, S. J., *J. Chem. Soc.*, **1910**, 1290.

160. (a) Davies, A. G.; Foster, R. V.; White, A. M., *J. Chem. Soc.*, **1954**, 2200. (b) Davies, A. G.; Foster, R. V.; Nery, R., *J. Chem. Soc.*, **1954**, 2204.

161. (a) Schönberg, A.; Mustafa, A., *J. Chem. Soc.*, **1945**, 655. (b) Schönberg, A.; Mustafa, A., *J. Chem. Soc.*, **1947**, 997. (c) Glover, S. A.; Goosen, C. E.; McClelland, B.; Talijaard, B.; Vogel, F. R., *S. Afr. J. Chem.*, **1984**, *37*, 164.

162. Conant, J. B.; Sloan, A. W., *J. Am. Chem. Soc.*, **1923**, *45*, 2466.

163. (a) Samanta, A.; Gopidas, K. R.; Das, P. K., *J. Phys. Chem*, **1993**, *97*, 1583. (b) Samanta, A.; Gopidas, K. R.; Das, P. K., *Chem. Phys. Lett.*, **1990**, *167*, 165.

164. Bethell, D.; Gold, V., In "*Carbonium Ions*"; Academic Press: New York, 1967.

165. (a) Rehm, D.; Weller, A., *Israel J. Chem.*, **1970**, *8*, 259. (b) Rehm, D.; Weller, A., *Ber. Bunsenges. Physik. Chem.*, **1969**, *73*, 834.

166. Turro, N. J.; McVey, J.; Ramamurthy, V.; Lechten, P., *Angew. Chem. Int. Ed. Engl.*, **1979**, *18*, 572.

167. Boyd, M. K.; Lai, H. Y.; Yates, K., *J. Am. Chem. Soc.*, **1991**, *113*, 7294.

168. Latif, N., *J. Org. Chem.*, **1962**, *27*, 846.

169. (a) Ungnade, H. E.; Kline, E. F.; Crandall, E. W., *J. Am. Chem. Soc.*, **1953**, *75*, 3333. (b) Hubacher, M. H., *J. Am. Chem. Soc.*, **1943**, *65*, 1655.

170. Graebe, C., *Justus Liebigs Ann. Chem.*, **1891**, *263*, 1.

171. (a) Maryanoff, B. E., *J. Am. Chem. Soc.*, **1975**, *97*, 2718. (b) Schönberg, A.;

Asker, W., *J. Chem. Soc.*, **1945**, 657.

172. Bergmann, E. D.; Rabinovitz, M., *J. Org. Chem.*, **160**, *25*, 828.

173. Buchanan, G. W.; McCarville, A. R., *Can. J. Chem.*, **1973**, *51*, 177.

174. Breslow, R.; Garrat, L.; Kaplan, L.; La Fallette, D., *J. Am. Chem. Soc.*, **1958**, *90*, 4051.

175. Barnard, R. A. B.; Leith, L. C., *Can. J. Chem.*, **1948**, *34*, 1464.

176. Bergman, E. D.; Klien, J., *J. Org. Chem.*, **1957**, *22*, 512.

177. Eaton, D. E., *Pure and Appl. Chem.*, **1988**, *60*, 1107.

178. Melhuish, W. H., *J. Phys. Chem.*, **1961**, *85*, 229.

179. Gomberg, V. M.; Cone, L. H., *Justus Liebigs Ann. Chem.*, **1910**, *376*, 201.

180. Burtner, R. R.; Cusic, J. W., *J. Am. Chem. Soc.*, **1943**, *65*, 1582.

181. O'Connor, D. V.; Phillips, D., *Time-Correlated Single Photon Counting*; Academic Press: Orlando, FL, 1984.